Wind Flow and Vapor Cloud Dispersion at Industrial and Urban Sites

A CCPS CONCEPT BOOK

Steven R. Hanna
Rex E. Britter

WIND FLOW AND VAPOR CLOUD DISPERSION AT INDUSTRIAL AND URBAN SITES

Steven R. Hanna

Hanna Consultants

Rex E. Britter

University of Cambridge

Center for Chemical Process Safety
of the
American Institute of Chemical Engineers
3 Park Ave., New York, NY 10016-5991

Library of Congress Cataloging-in-Publication Data

ISBN: 0-8169-0863-X

This book is available at a special discount when ordered in bulk quantities. For information, contact the Center for Chemical Process Safety at the address shown above.

PRINTED IN THE UNITED STATES OF AMERICA
10 9 8 7 6 5 4 3 2 1

Preface

For over 40 years the American Institute of Chemical Engineers (AIChE) has been involved with process safety and loss control in the chemical, petrochemical, hydrocarbon process and related industries and facilities. The AIChE publications are information resources for the chemical engineering and other professions on the causes of process incidents and the means of preventing their occurrences and mitigating their consequences.

The Center for Chemical Process Safety (CCPS), a Directorate of the AIChE, was established in 1985 to develop and disseminate information for use in promoting the safe operation of chemical processes and facilities and the prevention of chemical process incidents. With the support and direction of its advisory and management boards, CCPS established a multifaceted program to address the need for process safety technology and management systems to reduce potential exposures to the public, the environment, personnel and facilities. This program entails the development, publication and dissemination of *Guidelines* relating to specific areas of process safety; organizing, convening and conducting seminars, symposia, training programs, and meetings on process safety-related matters; and cooperating with other organizations and institutions, internationally and domestically to promote process safety. Within the past several years CCPS extended its

publication program to include a "Concept Series" of books. These books are focused on more specific topics than the longer, more comprehensive *Guidelines* series and are intended to complement them. With the issuance of this book, CCPS has published almost 80 books.

CCPS activities are supported by the funding and technical expertise of over 80 corporations. Several government agencies and nonprofit and academic institutions participate in CCPS endeavors.

In 1989 CCPS published the landmark *Guidelines for the Technical Management of Chemical Process Safety*. This book presents a model for process safety management built on twelve distinct, essential and interrelated elements. The Foreword to that book states:

> For the first time all the essential elements and components of a model of a technical management program have been assembled in one document. We believe the *Guidelines* provide the umbrella under which all other CCPS Technical Guidelines will be promulgated.

This Concept Series Book supports several of the twelve elements of process safety enunciated in the landmark *Guidelines for the Technical Management of Chemical Process Safety* including process risk management, incident investigation, process knowledge and documentation, and enhancement of process safety knowledge. The purpose of this book is to assist designers and operators of chemical facilities to more realistically estimate the effects of on-site and nearby plant structures, process equipment, buildings and other "obstacles" on the transport and dispersion of releases of hazardous materials.

This book should also be useful for emergence response and homeland safety and security personnel who must deal not only with accidental episodic releases but also with deliberate acts.

Acknowledgments

The American Institute of Chemical Engineers and the Center for Chemical Process Safety express their gratitude to all the members of the Vapor Cloud Modeling Subcommittee for their generous efforts and technical contributions in the preparation of this Concept Series Book.

Dr. Ronald J. Lantzy of Rohm and Haas Corporation initially chaired the Vapor Cloud Modeling Subcommittee. Mr. David Fontaine of Chevron Corporation assumed the chairmanship in June 2000. The other subcommittee members were: Gene K. Lee, Air Products & Chemicals Corporation; Donald J. Connolley, AKZO Nobel Chemicals, Incorporated; William J. Hague, Honeywell International Incorporated; Manny Vazquez, Honeywell International Incorporated, John T. Marshall, Dow Chemical Company; Wilfred K. Whitcraft, DuPont Company; Kenneth W. Steinberg, ExxonMobil R & E; Jeff Robertson, Numerical Applications, Incorporated; Malcolm L. Preston, Eutech; Martin Tasker, Eutech; Mr. Joseph R. Natale, ExxonMobil R & E; Daniel C. Baker, Equilon Enterprises LLC; Albert G. Dietz, Jr.,United States Department of Energy, Jawad Touma, United States Environmental Protection Agency; Breeda Reilly, United States Environmental Protection Agency; Jerry M. Schroy, Solutia, Incorporated; David McCready, Union Carbide Corporation;

Rashid Hamsayeh, Formosa Plastics Corporation, and Richard D. Siegel, Roy F. Weston, Incorporated. The contributions of Sanford G. Bloom, and Doug N. Blewitt are also acknowledged. Martin E. Gluckstein was the CCPS Staff Liaison and was responsible for the overall administration and coordination of the project.

Before publication, all CCPS books are subjected to a thorough peer review process. CCPS also acknowledges the thoughtful comments and suggestions of the peer reviewers John Woodward of Baker Engineering and Risk Consultants, Craig Matthiessen of the United States Environmental Protection Agency, and Jan Windhorst of Nova Chemicals.

Lastly, CCPS is grateful to the American Petroleum Institute for permitting the distribution of its copyrighted computer program, ROUGH, with this book in the interest of improved knowledge and safer facilities in the industry.

Dr. Steven Hanna and Dr. Rex Britter acknowledge the contributions of Dr. Pasquale Franzese, who prepared many of the tables and figures in this book, as well as the read-me files for the CD-ROM. They further acknowledge Linda Hanna of Hanna Consultants, who has been responsible for publication and distribution of the drafts sent to the AIChE Vapor Cloud Modeling subcommittee for review.

List of Symbols

A, B, C, D, E, F	The Pasquill stability class scheme, with A very unstable, B moderately unstable, C slightly unstable, D neutral, E slightly stable, and F very stable.
A	Constant in dispersion Eqs. (56) and (58)
A'	Constant in dispersion Eqs. (66) and (67)
A_f (m^2)	Vertical cross-section or frontal area of obstacle facing the wind.
A_p (m^2)	Horizontal or plan area of obstacle
A_T (m^2)	Total lot area of each obstacle
B and C_g	Often experimentally determined functions of the shape and geometric arrangement of the roughness elements (Schlichting, 1968, and Raupach et al., 1991).
$c_p = 1005$ J $kg^{-1}K^{-1}$	Specific heat of air at constant pressure
C (kg/m^3 or ppmv)	Concentration of pollutant
C/Q (s/m^3)	Normalized concentration
$C(z)$ (kg/m^3 or ppmv)	Height-variable concentration of pollutant in the cloud
C_y (kg/m^2 or ppmv-m)	Crosswind integrated concentration

d (m)	Displacement length
D	Constant in Eq. (14)
f (1/s)	Coriolis force or parameter
$g = 9.8$ m/s^2	Acceleration of gravity
G (m/s)	Free stream or geostrophic wind speed at the top of the boundary layer
h_e (m)	Effective height of plume above ground
H_r (m)	Height of obstacles
HS	Horizontal solidity or lack of porosity of an obstacle, ranges from 0.0 to 1.0
H_s (J/sm^2)	Surface heat flux $H_s = c_p \rho u^* \theta^*$
I	Flow interference constant in Eq. (21)
K (m^2/s)	Eddy diffusivity coefficient
L (m)	Monin–Obukhov length $L = -(u^{*3}/\kappa)/(gH_s/c_p \rho T)$
L (m)	Along-wind length of obstacle
ppmv	Concentration unit of parts per million volume
Q (kg/s)	Continuous source emission rate
Q_t (kg)	Instantaneous source emission
Ri	Richardson number
S_x (m)	Along-wind separation between obstacles
S_y (m)	Crosswind separation between obstacles
T (K)	Temperature
T' (K)	Fluctuation in temperature
T_I (s)	Integral time scale of turbulence
T_{Ix} (s)	Integral time scale of along-wind turbulence
T_{Iy} (s)	Integral time scale of lateral turbulence
T_{Iz} (s)	Integral time scale of vertical turbulence
u (m/s)	Wind speed
$u(z)$ (m/s)	height-variable wind speed
u_{avg} (m/s)	Average cloud speed over time of travel, t
u_c (m/s)	Characteristic wind speed in urban/industrial obstacles
u_e (m/s)	Effective cloud speed, u_e (m/s) $\int u(z)C(z)\,dz / \int C(z)\,dz$
u_{ref} (m/s)	Mean reference wind speed
u^* (m/s)	Friction velocity

u^*_{local} (m/s)	Local friction velocity observed at height z
u_o^* (m/s)	Friction velocity appropriate for flat area in between buildings but with buildings removed
u' (m/s)	Longitudinal wind speed fluctuation
VS	Vertical solidity or lack of porosity of an obstacle, ranges from 0.0 to 1.0
w^* (m/s)	Convective scaling velocity
w' (m/s)	Vertical wind speed fluctuation
W (m)	Crosswind width of obstacle
WD	Wind direction
x (m)	Downwind distance
x_o (m)	Along-wind position of center of puff
x_v (m)	Virtual source distance
y (m)	Crosswind distance from the plume centerline
y_o (m)	Lateral position of center line of plume or puff
z (m)	Height above ground
z_i (m)	Mixing depth
z_{ibl} (m)	Height of internal boundary layer
z_m (m)	Height of instrument above ground
z_o (m)	Surface roughness length
z_{ref} (m)	Reference height (typically between about 2 m and 10 m).
θ (K)	Potential temperature
θ^* (K)	Scaling potential temperature, about –0.1 K at night and 1.0 K in the day
κ	Von Karman constant (assumed to equal 0.4)
$\lambda_p = A_p/A_T$	Ratio of obstacle plan area to lot area
$\lambda_f = A_f/A_T$	Ratio of obstacle frontal area to lot area
ν	Kinematic molecular viscosity $\nu = 1.5 \times 10^{-5}$ m^2/s for air
ρ (kg/m^3)	Air density, equal to 1.2 kg/m^3 at sea level at a temperature of 293 K
σ_u (m/s)	Turbulent velocity fluctuations in the along-wind (x) direction
σ_v (m/s)	Turbulent velocity fluctuations in the lateral (y) horizontal direction

σ_w (m/s)	Turbulent velocity fluctuations in the vertical (z) direction
σ_x (m)	Along-wind dispersion component
σ_y (m)	Lateral dispersion component
σ_z (m)	Vertical dispersion component
τ_o (kg/m/s^2)	Surface stress

Contents

1

Introduction

1.1. Background

U.S. regulations require that the potential concentrations of toxic or flammable substances in the atmosphere must be calculated as part of health, environmental and safety assessments at and near industrial facilities. For example, these calculations may be part of planning studies, may be used in real-time hazard assessments, or may be part of submittals to regulatory agencies. Similar requirements are often set in other countries. The calculations are needed for routine emissions, such as combustion emissions from stacks, as well as for accidental episodic emissions. These issues are addressed using atmospheric transport and dispersion models, which require a variety of meteorological inputs, often including boundary layer scaling parameters such as surface roughness length, z_o, displacement length, d, friction velocity, u^*, and Monin–Obukhov length, L. Most of these models are being applied by technically trained individuals who are aware of but are not necessarily expert in dispersion phenomena. A need exists for a straightforward guidelines document that describes the meteorological variables of importance for calculating vapor and aerosol concentrations at industrial facilities where the buildings and structures influence the calculations. The basis for parameters such as the surface roughness

length needs to be described and methods included for how to estimate that parameter from readily available information such as site plans of industrial plants. It is important to account for the site roughness because the maximum ground level concentration for near-ground releases tends to decrease by about a factor of two for each order of magnitude increase in surface roughness length, z_o.

Practically all models currently available for dispersion calculations implicitly assume that the depth of any vapor cloud is considerably greater than the height of nearby buildings and obstacles. For releases near and within an industrial facility, this is unlikely to always be the case. The appropriateness of existing models for application to industrial facilities must be objectively assessed. For many actual scenarios, models do not currently exist. We have developed within this book a number of novel approaches that may be useful to dispersion calculations in real scenarios.

This book is written at a level so that it is useful to persons such as the *on-site engineer*, the *designer,* the *process hazards analysis (PHA) team member*, and *regulatory personnel*, as well as *fluid dynamicists and transport and dispersion modelers*. It is important to clearly define parameters and methods because this is a cross-discipline activity being carried out by engineers, meteorologists, chemists, economists and others. The book is intentionally short and descriptive, similar to the AIChE/CCPS documents by DeVaull et al. (1995) entitled *Understanding Atmospheric Dispersion of Accidental Releases,* or by Hanna et al. (1996) entitled *Guidelines for Use of Vapor Cloud Dispersion Models*. The book is intended to mesh closely with those related AIChE/CCPS documents.

The book concentrates on explaining dispersion enhancement resulting from industrial buildings, tanks, pipe structures, and other facilities. Emphasis is on simplified descriptions of the effects of roughness obstacles on the boundary layer and on dispersion. Differences between the effects of the obstacles on dispersion of pollutant clouds or plumes with depths less than and greater than the average obstacle height, H_r, are described. Methods of estimating surface roughness length are outlined. Several worked examples based on varied industrial scenarios are presented in the book. A comprehensive list of references, a glossary, and an index are included, so that the book can be more easily used by practicing engineers and other readers and so that they will be able to obtain more detailed technical discussions if they are interested.

Although the focus of the book is on industrial sites, the methods are also applicable to urban sites. In both cases, the enhanced roughness effects are due to the presence of obstacles, and the geometric shapes and spacings of the obstacles are similar at both types of sites. The same physical principles apply. Also, many of the concepts used in this book were derived from observations and scientific analyses whose emphasis was on urban sites.

After reading the book, a person should be more conversant with dispersion phenomena near industrial plants and in urban areas and should have acquired the basics to use gas dispersion models, estimate surface roughness lengths for industrial facilities and urban areas and their surrounding areas, better communicate with regulators and the public, and develop more realistic risk management plans. Another outcome would be improved emergency response planning and preparedness.

1.2. Objectives of This Book

The previous subsection discussed the general background for the book, characterized its intended audience, and provided a brief overview of its contents. The current subsection lists five specific objectives of the book.

Objective 1: *To describe how structures (such as buildings, tanks, and pipe racks) at an industrial or urban site affect dispersion and show how these effects can be parametrized in consequence models.* The results are to be applicable to a wide variety of industrial sites, such as a chemical processing plant or oil refinery, a brewery or food processing plant, or a steel mill, to name a few. The results are also to be applicable to urban areas surrounding the industrial site. We start with the general assumption that the concentration downstream from a source is most strongly influenced by wind speed (advection) and turbulence (diffusion). The roughness obstacles at the industrial or urban site affect both of these – *above* the roughness obstacles, *within* the roughness obstacles, and *downstream* of the roughness obstacles. In most cases the effects generally enhance the cloud dilution. It is assumed that these methods have broad applicability to other regions marked by enhanced roughness, such as residential areas, urban areas, warehouse complexes, and vegetative canopies.

Objective 2: *To explain surface roughness length, z_o, and displacement length, d, so the concepts are understandable to scientists and engineers with little or no meteorological background, such as chemical process plant engineers, safety managers, and other users.* Relate the meteorological concepts to the concept of skin friction coefficients, which may be more familiar to engineers.

Objective 3: *To present criteria for when the structures should be considered broadly as roughness elements or when they should be considered from the viewpoint of their wake effects.* If one takes the "broad" view, there is no need to consider the details of the obstacles and they can be treated in a gross manner; this is desirable and simplifies the dispersion calculations. However, if some isolated large obstacles are present and there is a desire to consider the flow and dispersion near to these obstacles, a more detailed specific investigation may be necessary. Even when adopting the "broad" view, the specific approach may be quite different, depending on the ratio of cloud height to the roughness obstacle heights.

Objective 4: *To assure that the suggested formulas are applicable to a wide range of scenarios and give continuous solutions for values of input variables on the boundary between two regimes, such as rural and urban regions.* It is undesirable to have discontinuities between regimes where solutions are nonexistent or uncertain or where alternate formulas give divergent answers.

Objective 5: *To show how the methods for estimating the surface roughness length can provide inputs to transport and dispersion models that apply to a variety of initial cloud or plume buoyancies, including positively buoyant plumes, negatively buoyant (dense) gas plumes, and neutrally buoyant clouds and momentum jets.* However, in the examples of transport and dispersion models given in Section 4, emphasis is on neutrally buoyant plumes with minimal initial momentum. It is not the intent of this book to suggest specific transport and dispersion model algorithms for buoyant or dense plumes and/or momentum jets in congested areas.

1.3. Overview

The book is organized into several chapters, such that the story is told in a sequence beginning with meteorology and definitions, and ending

with specific examples and worked scenarios. Detailed references are provided.

In Chapter 2, an overview is given of the basic physics of meteorology and dispersion modeling in general, consistent with other CCPS books. Definitions are given and methods of estimating the effects of surface roughness obstacles are provided. The proposed simplified algorithms are related to concepts familiar to engineers such as the surface skin friction coefficient, and it is shown how z_o can be written in terms of that coefficient. The relations between plume dispersion coefficients and atmospheric turbulence are summarized, including the effects of ambient atmospheric stability. The current state-of-the-art concerning relevant experiments and available roughness estimation methods is briefly reviewed. In particular, the many fluid model experiments on flow and dispersion around obstacle arrays are discussed and references given so the readers can obtain the data. Methods by which recently developed dispersion models parametrize the roughness length, z_o, are outlined. For example, the U.S. Environmental Protection Agency's (EPA's) model, AERMOD, uses an estimate of z_o (Cimorelli et al., 1998). The reliability and limitations of models and data are summarized.

The third chapter of the book provides details concerning methods of estimating the surface roughness length, z_o, and the related displacement length, d. Several optional methods for estimating these parameters are presented, such as land use category tables, wind profile methods, and obstacle geometry (morphological) methods. The general characteristics of working models for estimating surface roughness length and displacement length are described (e.g., the Petersen, 1997, method and the Macdonald et al., 1998, method). The importance of the friction velocity, u^*, is emphasized and formulas are included for its estimation based on a wind speed observation and a knowledge of z_o. It is shown how the turbulent velocity components are directly related to u^*. Formulas are also suggested for the variation of wind speed below and above the obstacle heights.

Chapter 4 includes a comprehensive set of equations for estimating transport and dispersion of pollutant clouds at industrial and urban sites. Differences between the two situations when most of the cloud is located at heights less than or greater than the roughness element height are described. The types of problems that are covered include a release within the obstacle array (i.e., the group of buildings, tanks and

other structures), which may be at high elevation (above ground level) and which is carried downwind and mixes down to the ground, and a release at low elevation which mixes up through and above the obstacle array while being advected downwind. The formulas recommended for estimating surface obstacle roughness are used to suggest some practical guidelines for dispersion models for a variety of scenarios. Simplified models are proposed for the different scenarios and criteria outlined for deciding which model to use, as well as methods for interpolating between model options.

In Chapter 5, seven worked examples are given based on realistic scenarios. The scenarios include a range of types of industrial plants and urban areas, including a small section of a refinery, a group of wide and flat warehouses, a large refinery, a Chicago residential area, a moderate-sized industrial plant in an urban area, a moderate-sized industrial plant on a peninsula, and a large industrial plant in a remote flat desert.

1.4. Definition of Scenarios and Modeling Scales

Prior to beginning any modeling activity, one should first decide upon the scenario that is to be modeled and the time and space scales that need to be considered. This decision is driven by the emissions scenario and by the health, safety, or environmental effects being investigated. For example, if the question is whether a flammable cloud of propane will burn or explode, then the relevant time scale is a few seconds. Short time scales will also be of interest for transient emissions which are released over only a few minutes. On the other hand, if the issue concerns health effects of toxic pollutants such as ammonia or SO_2, the relevant averaging time scale depends on how the health standards are written. If the emissions are fairly continuous (e.g., routine releases of benzene from a short stack over a period of years) and the primary risk is a one-year dosage, then the modeling methods will be quite different than if the primary risk is a 10-minute maximum concentration. The emissions scenario and the health criteria or pollutant standards should be known beforehand.

The modeling approach is more straightforward if the release is continuous and is one of the pollutants (e.g., SO_2) regulated according to the EPA's National Ambient Air Quality Standards (NAAQS). In

these cases, the EPA prescribes the transport and dispersion model to be used, the types of input data and output data, and the procedures to be followed in the analysis. The EPA also prescribes the averaging time (1-hour minimum), with options of 3, 8, and 24 hours, and annual averages for some NAAQS pollutants.

The distances of interest are not well-known unless the scenario is similar to another scenario that has already been modeled. Otherwise, it is advisable to apply a simple screening model to the scenario in order to determine the worst-case concentrations that will occur at various downwind distances. If the concentrations are expected to be high only in the region around the building or other structure, a detailed study of the flow and dispersion around the structure may be necessary. If the concentrations drop down to levels of little concern at a distance of, say, 300 m from the source, then a simple Gaussian-type model may be sufficient. However, if the concentrations are still above some lower limit of toxicity at a downwind distance of 10 or 20 km, then a variable puff-trajectory model that accounts for time and space variations in meteorological conditions may be more appropriate. Some detailed analysis is obviously required in order to settle on an appropriate scenario and relevant time and distance scales.

2

Overview of Meteorology and Atmospheric Dispersion

This overview is intended to be consistent with similar sections in other CCPS books such as DeVaull, King, Lantzy and Fontaine (1995) and Hanna, Drivas and Chang (1996). It explains basic meteorological concepts and describes how the average obstacle height, H_r, the surface roughness length, z_o, and the displacement length, d, are important in the calculation of atmospheric transport and dispersion. The terms in this section conform to definitions and derivations in standard atmospheric boundary layer textbooks such as Garratt (1992) and Stull (1997) and in standard atmospheric dispersion textbooks such as Arya (1999), Hanna, Briggs and Hosker (1982), and Pasquill and Smith (1983). More detailed discussions of many of these topics will be given in subsequent chapters.

It is first important to stress that, at low concentrations, nearly all gases, vapors, and small aerosols or particles are transported and dispersed through the atmosphere in the same way and can be treated using the same physical concepts, including basic boundary layer formulations. Consequently the concepts discussed below are generic and are not specific to any particular chemical. The effects of the boundary layer (i.e., u^*, z_o, and d) on the cloud can be treated using universal relations.

2.1. Definitions of Concepts and Terms

This section introduces several key concepts and terms relative to meteorology and atmospheric dispersion. The key concepts and terms are highlighted by italics and underlines, and a few sentences of explanation are provided.

The *atmospheric or planetary boundary layer* (abl or pbl) is the layer about 1000 m deep next to the ground that is strongly affected by diurnal variations in surface conditions such as ground temperature. This distinction is made because there is another class of atmospheric transport and dispersion models that is used for elevated clouds of pollutants from volcanoes, forest fires, and other types of sources where the cloud is initiated or rises to elevations greater than 1000 m. In this book, we are concerned only with pollutant clouds released at the ground or at relatively low elevations such that the cloud remains in the lowest 1000 m. The lower part of the pbl is the surface boundary layer, which is 50 to 100 m deep. The roughness sublayer (rsl) is the range of heights defined by plus or minus about a factor of two about the average obstacle height, H_r. The roughness canopy layer is defined as the layer below about 0.5 H_r.

An *atmospheric transport and dispersion model* follows the movement and dilution of a pollutant after it is released into the atmosphere (Hanna et al., 1982). The model requires the location, geometric size, physical and chemical characteristics, magnitude, and time variation of the emissions source. It also requires information on the meteorological conditions (e.g., wind speed and stability variation in space and/or time) and the characteristics of the underlying surface (e.g., industrial plant, wheat field, water, desert, mountains and valleys). From this information, the transport and dispersion model is used to calculate the gas concentration as a function of three-dimensional position (i.e., height, lateral position, and downwind distance) and time. Although some fundamental three-dimensional grid models predict the detailed time variation of concentration, most models predict the concentration averaged over some time period (usually a few minutes to an hour). Based on the resulting calculations of the concentration at any position (and possibly as a function of time), other types of calculations can be made, such as the *average concentration* over some time period, the *dose* (i.e., the time-integrated concentration) or the *deposition* (i.e., the rate at which material accumulates on a surface). The exact nature of these

calculations depends on what is required to determine health or environmental effects. For example, toxicologists could take the outputs of the transport and dispersion model and use them to estimate health effects to individuals or to populations. As another example, engineers could take the information about a flammable cloud (location and mass) and make further calculations of the explosion or flammable effects as described by Woodward (1998).

Cloud, Puff, and Plume: The term *cloud* refers to all types of releases. A *plume* is a continuous but not necessarily steady release. A *puff* is an instantaneous or short duration release.

Types of Transport and Dispersion Models: There are several types of transport and dispersion models available, as summarized by Hanna et al. (1982 and 1996). A few are briefly mentioned below:

- The simplest and the most frequently used are *Gaussian models*, which assume that the distribution of pollutant concentration has a Gaussian or normal shape [e.g., $\exp(-y^2/2\sigma_y^2)$], where y is the lateral crosswind distance from the center of the plume or puff. The dispersion coefficients such as σ_y (lateral component), σ_z (vertical component), and σ_x (along-wind component) are measures of the size of the cloud and can be specified by empirical methods or theoretical formulas.
- A few dispersion models are based on solving the pollutant conservation equation using *gradient transport or K theory*. The eddy diffusivity coefficient K is expressed as an empirical function of scaling parameters. The solution can be obtained analytically for some simple cases but must be solved numerically for more general cases. This model is most useful when the size of the cloud is greater than the dominant turbulent length scales.
- Some recent advanced models make use of *Lagrangian Particle Dispersion Models* (LPDM), where the individual trajectories of thousands of "particles" are tracked by the computer and the particle's motion is determined by a mean flow velocity plus a correlated turbulent velocity and a random turbulent velocity. Because the method makes use of turbulent velocities and time scales, it agrees with the Gaussian plume model for simple scenarios.
- For estimating transport and dispersion at distances ranging from a few kilometers to 100 kilometers, intermediate-scale *mesoscale puff models* are often used. The pollutant release is mod-

eled as a series of puffs, which are allowed to have curved trajectories to account for space and time variations in meteorology.

- Close to buildings or other obstacles, the flow and dispersion can be calculated using *building downwash models* or *vent models*. These simplified models account for the presence of displacement zones and recirculating cavities. In most cases, these models are based on the results of fluid modeling experiments
- With advances in computer power, it is possible to use *Computational Fluid Dynamics* (CFD) models to predict very highly resolved three-dimensional time-dependent distributions of wind flows and material concentrations. These models generally use very small grid spacings and time steps and are computer-intensive.

When discussing model applications, the terms "near-field" and "far-field" are often used. The *near-field* is defined as the area within a few hundred meters downwind of the source where there is possible influence of local structures, source geometry, and initial plume momentum and buoyancy effects. For the purposes of this book, a *very near-field* could also be defined very close to the source where the specific geometry of one or two individual obstacles influences the flow and dispersion. The *far-field* is defined as the area beyond the influence of local structures and plume buoyancy effects. Typically the far-field begins at about 1000 m from the source.

The initial behavior of the pollutant cloud is often dominated by internal cloud buoyancy effects. The *cloud buoyancy* must be distinguished from the ambient or environmental boundary layer buoyancy. The ambient boundary layer buoyancy is usually defined by the ambient Richardson number, Ri, or the ambient Monin–Obukhov length, L. The internal cloud buoyancy is a measure of whether the in-cloud density is greater than or less than the ambient or environmental density. If the cloud density is greater than the ambient density, the cloud is called "*dense*" and may need to be treated by special models that account for the gravity spreading of the cloud. Dense gases can occur due to the high molecular weight, the cold temperature, and/or the presence of aerosols in the emissions. Several options for dense gas clouds and examples of field experiments are discussed by Hanna, Drivas, and Chang (1996). If the in-cloud density is less than the ambient density, the cloud is called "*buoyant*" and may rise as much as several hundred

meters for power plant stack plumes. Buoyant clouds usually result from the emissions of hot gases or materials with low molecular weights. Briggs' plume rise equations for buoyant plumes are summarized in Hanna, Briggs, and Hosker (1982). If the in-cloud density is equal to the ambient density, there is no positive or negative buoyancy force, the cloud is considered "*neutral*," and the cloud trajectory is determined by the initial cloud momentum and the boundary-layer meteorology.

The *effective transport speed*, u_e, of a pollutant cloud is defined as the vertical integral of the concentration-weighted wind speed:

$$u_e = \frac{\int u(z)C(z)\,dz}{\int C(z)\,dz} \tag{1}$$

where z is the height above ground, $C(z)$ is the height-variable concentration of pollutant in the cloud, and $u(z)$ is the height-variable wind speed. The effective transport speed, u_e, is also known as the cloud advective speed. As the cloud disperses upward from a ground-based release, it encounters stronger wind speeds and the cloud accelerates as it moves downwind. For puffs or for strongly transient (time-varying) releases, the wind speed determines the time lag between the release of a pollutant and its arrival at any downwind location, which is approximately equal to the distance divided by the wind speed. The speed and direction of travel of the pollutant cloud obviously depend on knowledge of the time-varying, three-dimensional wind field, and can be estimated either from observations or from the outputs of a meteorological model.

The wind speed also affects the *dilution* of a continuous release. For example, for a continuous release of a nonbuoyant (neutral or passive) gas at a given emission rate with no plume rise, the predicted concentration at the plume center is approximately inversely proportional to the wind speed. Therefore, the concentration at a given distance will be twice as large for a wind speed of 2 m/s as for a wind speed of 4 m/s.

The *turbulent dispersion* [i.e., rate of spread in the vertical (z), lateral (y), or downwind (x) directions] of the pollutant cloud about its center of mass depends on the atmospheric turbulence in the atmosphere, which itself depends on the *surface roughness conditions*, the *wind speed*, and the *stability* (i.e., day or night). Maximum concentrations generally decrease as the amount of turbulent dispersion increases, since the cloud volume is increased by turbulent dispersion. Even though the

cloud centerline maximum concentration may be decreased by enhanced dispersion caused by atmospheric turbulence, the geographic area covered by the cloud will be increased, thus possibly affecting a larger population.

Atmospheric turbulence determines the rate of turbulent dispersion or spread of the cloud. For this purpose, atmospheric turbulence is typically expressed by the *turbulent velocity* (averaging about 1 m/s), which is the standard deviation of rapid fluctuations in wind speed (σ_u refers to fluctuations in the along-wind (x) direction, σ_v refers to fluctuations in the lateral (y) horizontal direction, and σ_w refers to fluctuations in the vertical (z) direction). Like most large-scale engineering flows, the atmosphere is nearly always turbulent. The turbulent velocity is primarily determined by the wind speed, by the relative roughness of the underlying surface and by the time of the day (that is, the *stability*). *Turbulence intensity* is defined as the ratio of the turbulent velocity to the mean wind speed (e.g., σ_u/u). The atmospheric turbulence can be of two types, depending on the generating mechanism: mechanical turbulence and/or buoyant turbulence. In most cases, σ_u, σ_v, σ_w are proportional to the friction velocity, u^*.

Mechanical turbulence is generated by the wind speed variations and the surface roughness elements, and can be thought of as simple mechanical mixing or stirring of the air. Therefore, the larger the roughness obstacles, the more turbulence is generated, due to the increased mechanical mixing generated by the obstacles. Transport and dispersion models characterize the effect of roughness obstacles by many different alternate methods; for example, most of the older EPA models, such as the Industrial Source Complex (ISC) model, have two roughness categories—rural and urban. The turbulent dispersion or rate of spread of the cloud with distance is proportional to the turbulent velocity. The cloud maximum concentration is approximately inversely proportional to each component of the turbulent velocity.

Buoyant turbulence is generated by heating of the ground surface by the sun and is suppressed by cooling of the ground surface at night. Surface heating leads to the formation of buoyant thermal bubbles from the warm ground surface on sunny afternoons. The opposite effect happens during clear nights, when the surface cooling causes the suppression of turbulence.

The term *stability* refers to the ratio of the suppression of turbulence by thermal effects to the generation of turbulence by mechanical effects

such as wind shears. Transport and dispersion models characterize the effect of stability through use of one or more dimensionless stability parameters, such as the Monin–Obukhov length, L, defined below, or the Pasquill stability class used later in Table 1 (see page 23).

Monin–Obukhov similarity theory is used in many transport and dispersion models (e.g., the EPA's new AERMOD model, described by Cimorelli et al., 1998) to estimate winds, temperatures, and turbulence in the atmospheric boundary layer. This theory, summarized in every atmospheric boundary layer textbook (e.g., Stull, 1997), states that the mean wind and temperature profiles and turbulent velocities in the boundary layer are completely determined by three scaling lengths (z_o, d, and L) and a scaling velocity (u^*), as defined below:

- The *surface roughness length,* z_o, is a measure of the amount of mechanical mixing introduced by the surface roughness elements and, as a rough rule of thumb, is equal to about 0.1 times the average height, H_r, of the roughness elements (Section 2.2 further describes the concept and Chapter 3 gives detailed formulas). In practice, when the wind speed is observed at heights greater than ten times the height of the roughness obstacles, z_o can be estimated by plotting wind speed, u, observations as a function of $\ln z$ (where z is height) and fitting a straight line to the points near the ground. The straight line intercepts $u = 0.0$ at a height z_o. The appropriate wind profile formula for nearly neutral conditions is:

$$u/u^* = (1/\kappa) \ln(z/z_o) \tag{2a}$$

  where κ is the von Karman constant (assumed to equal 0.4), and the friction velocity, u^*, is defined below. This equation is valid over relatively smooth surfaces and/or at heights much greater than the obstacle height, H_r, where the displacement length, d, can be ignored. The next paragraph discusses the case where d must be accounted for. Figure 1 illustrates the calculated wind profiles for several assumed z_o values, for constant free stream (i.e., geostrophic) wind speed, G, at the top of the boundary layer (about 12 m/s in the figure). As $\ln z$ increases, the straight lines given by Eq. (2a) begin to curve as all profiles approach the speed, G.

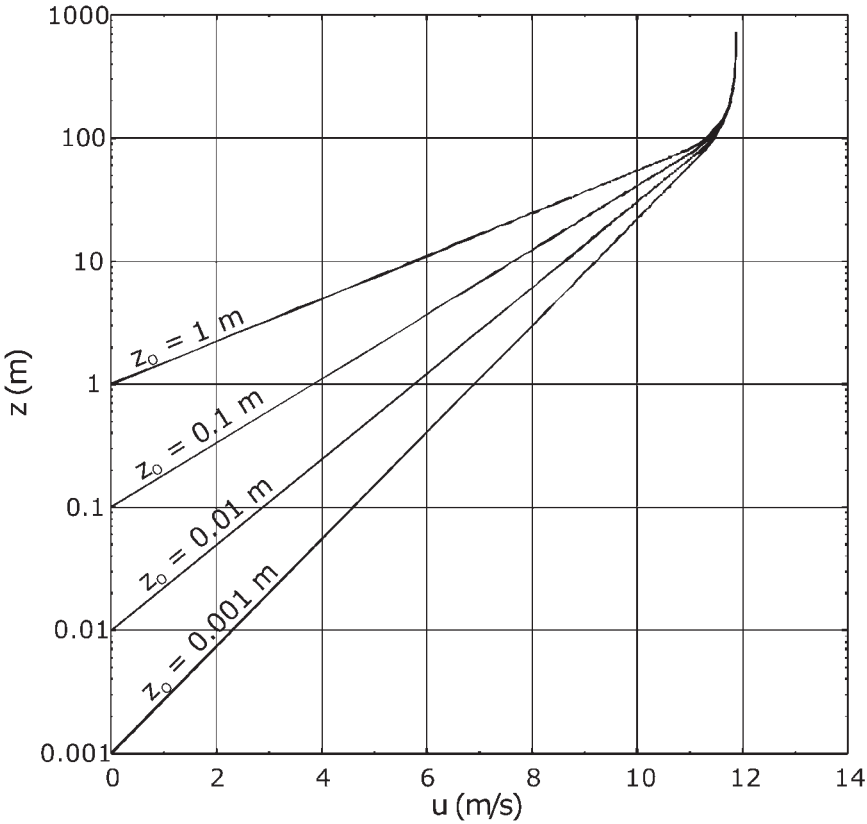

FIGURE 1. Vertical profiles of wind speed in the atmospheric boundary layer, plotted as ln *z* on the vertical axis and as arithmetic *u* on the horizontal axis. Neutral ambient stability is assumed. A constant free-stream or geostrophic wind speed is assumed at the top of the boundary layer (i.e., at an elevation of about 1000 m above ground level). Straight lines, given by Eq. (2a), are seen near the ground for four typical surface roughness lengths, covering three orders of magnitude.

- The *displacement length*, d, is a scaling length that becomes important for describing the wind profile at elevations close to the average roughness obstacle height, H_r, for densely packed roughness obstacles. It describes the vertical displacement (from the ground surface) of the effective ground level and is approximately equal to 0.5 H_r for obstacle types such as urban centers, tall crops, and forests. The displacement length, d, equals about 0.1 or 0.2 H_r for more loosely packed obstacles such as residential developments

and industrial processing plants. The applicable wind profile formula is

$$u/u^* = (1/\kappa)\ln[(z - d)/z_o] \tag{2b}$$

which is most valid at $(z - d)/z_o > 10$. Chapter 3 contains detailed formulas for estimating z_o and d based on the geometric characteristics of the obstacles.

- The *friction velocity, u**, is the fundamental scaling velocity and equals the square root of the surface stress, τ_o, divided by the air density, ρ. Note that $\rho = 1.2\ \text{kg/m}^3$ at sea level at a temperature of 293 K. The surface stress can be observed by special instruments that directly observe the drag at the surface, or by fast response turbulence instruments using the definition

$$\tau_0 = \rho\langle -u'w'\rangle = \rho u^{*2} \tag{2c}$$

where u' is the longitudinal wind speed fluctuation, w' is the vertical wind speed fluctuation, and the average is over about a one-hour time period. The variable, u^*, can also be estimated from wind observations by making use of Eq. (2b). As suggested by Eq. (2b), when u is plotted on the abscissa versus $\ln(z - d)$ on the ordinate, the slope of the best-fit straight line is inversely proportional to u^*. A rough rule of thumb is that the ratio u^*/u is about 0.05 to 0.1, where u is the wind speed at a height of about 10 m, which is the standard measurement height at airports around the world. In order to avoid the effects of local flows around the roughness obstacles, the height of the wind observation should be more than about two times the average height of the obstacles, H_r. The friction velocity u^* has typical values ranging from about 0.05 m/s in light winds to about 1 m/s in strong winds. The stress, τ, decreases by only about 10% in the lowest 50 or 100 m, leading to the assumption of a *constant stress layer* or *constant u* layer* near the ground. Turbulent velocities are proportional to u^* in this layer. For example, the lateral, longitudinal, and vertical turbulent velocities in the boundary layer are equal to about $1.9u^*$, $2.4u^*$, and $1.25u^*$, respectively (Stull, 1997). This layer, of depth 50 to 100 m, is also known as the *surface boundary layer*.
- The friction velocity, u^*, defined in the above paragraph is the fundamental definition and relates to the wind stress or drag at

the surface. It is also possible to define a *local friction velocity*, u^*_{local}, which can be calculated from the local wind shear at some height, z. By taking the derivative of Eq. (2a) with respect to z, we can express u^*_{local} by the formula:

$$u^*_{\text{local}} = \kappa z \, (\partial u / \partial z) \tag{2d}$$

An alternate u^*_{local} can be calculated by taking local measurements of u' and w' and calculating the square root of the one-hour average of their product:

$$u^*_{\text{local}} = \langle -u' w' \rangle^{1/2} \tag{2e}$$

These local values of u^* can be quite different from the surface u^* in regions with variations in surface conditions, such as an urban area located on a large bay.

- The *Monin–Obukhov length, L*, accounts for the effects of stability and is proportional to u^{*3} divided by the turbulent heat flux, H_s, to or from the ground surface:

$$L = -\frac{u^{*3}/\kappa}{g H_s / c_p \rho T} \tag{3a}$$

where g = 9.8 m/s^2 is the acceleration of gravity, c_p = 1005 J kg^{-1}K^{-1} is the specific heat of air at constant pressure, and T is the air temperature (in K). The friction velocity, u^*, in this formula is based on the surface stress, τ_o. H_s (in Watts/m^2) is positive during the day and negative at night. H_s can be measured by fast response turbulence instruments using the identity

$$H_s = c_p \rho \langle w' T' \rangle \tag{3b}$$

where w' is the fluctuation in vertical wind speed and T' is the fluctuation in temperature, and the average is taken over about one hour. A typical value of H_s in the daytime is about 200 w/m^2 (J/sm^2) and in the night-time is about –20 W/m^2. It is found that H_s is proportional to u^* and therefore L becomes proportional to u^{*2} showing how L is so strongly dependent on wind speed. According to Monin–Obukhov similarity theory, L completely determines the effects of atmospheric stability on the wind speed profile. The dimensionless ratio z/L indicates the ratio of the tur-

bulence suppression by ambient buoyancy to the turbulence generation by mechanical wind shear. Over flat rural terrain, L is relatively small and negative (about –10 to –50 m) during sunny days with light winds, is relatively large and negative (about –50 to –1000 m) during windy or cloudy days, is relatively large and positive during windy or cloudy nights (about 50 to 1000 m), and is relatively small and positive during clear nights with light winds (about 10 to 50 m). For very light winds (less than 1 m/s), the magnitude of L can approach 1m or less. For very strong winds (greater than 10 m/s) the magnitude of L is very large and the boundary layer is said to be neutral.

Assuming that the boundary layer is stationary (does not vary in space or time), it follows from Monin–Obukhov similarity theory that there are general dimensionless functional relations that apply such that, for example, u/u^* is a general function of z/z_o, z/d, and z/L.

For areas with relatively large roughnesses such as urban areas and industrial sites, the Monin–Obukhov length, L, is relatively large because the surface drag is larger and therefore the u^{*3} term is larger in the numerator of Eq. (3a), which defines L. As discussed by Hanna and Chang (1992), the heat flux, H_s, can be assumed to equal $c_p \rho u^* \theta^*$, where θ^* is the scaling temperature, which is observed to have typical values of about –0.1 K at night and 1.0 K in the day. Because θ^* is observed to be relatively constant in the boundary layer, it follows from Eq. (3a) that L is approximately proportional to u^{*2} since the u^{*3} in the numerator is divided by a u^* in the denominator. This result for urban and industrial sites is a reflection of the large amounts of surface drag and mechanical turbulence generated by the roughness obstacles (e.g., buildings and storage tanks), which cause L to be dominated by u^{*2}. As a result, L is large and stabilities are more often nearly neutral at urban or industrial sites than at rural sites. During the night, a tendency toward stable conditions over urban and industrial sites is suppressed by the heat that is generated as a result of man's activities and industrial processes.

In reality, the ground surface usually varies with space due to the presence of a patchwork of fields, forests, lakes, industrial areas, residential areas, and so on. When the wind encounters a change in the underlying surface (e.g., when the flow passes from a sandy desert surface over an oil refinery or from a bay over a chemical plant), the

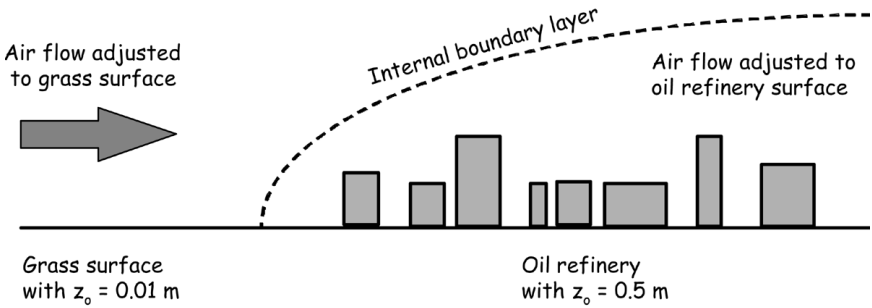

FIGURE 2. Schematic drawing of the growth of the internal boundary layer, at height z_{ibl}, downwind of a change in surface roughness, z_o.

boundary layer adjusts itself to the new surface from the bottom up. Figure 2 illustrates this phenomenon for a typical urban or industrial site (an oil refinery in this case) surrounded by another type of surface. There is an upward-sloping *internal boundary layer*, at height z_{ibl} on the figure, separating the air below, which has adjusted to the new surface, from the air above, which is still influenced by the old upwind surface. The local friction velocity, u^*_{local}, could be significantly different above and below the internal boundary layer.

The internal boundary layer has an average slope of about 1/10. It follows that, if we are interested in whether a 100 m deep layer has thoroughly adjusted itself to the new surface, an upwind distance of about 100 m/(1/10) = 1000 m is required over the new surface. It also follows that, if the centerline of a pollutant cloud released at the edge of the new surface is at an elevation of 50 m, this cloud centerline will cross through the internal boundary layer at a distance of 500 m from the edge of the new surface. Most models gloss over these effects by assuming a single representative surface roughness for the entire problem, while other models account for transitions via abrupt changes in dispersion coefficients at the edge of the new surface. However, since many industrial sites are located by the coast or are surrounded by rural areas, the internal boundary layer may often be important.

Urban/Industrial Heat Island: Because of heat generated by man's activities, including industrial processes, an urban or industrial area is often several degrees warmer than its surroundings. This is called a heat island and many examples are listed by Oke (1987). The surface energy budget for urban or industrial obstacles, including the thermal input from home-heating or from industrial processes, has been analyzed in

several studies (e.g., Masson, 2000). These heat fluxes are typically of order 10 to 100 W/m^2, or the same order as the natural boundary layer daytime heat flux, H_s. If these variable heat fluxes are well-known, they can be used as inputs to mesoscale meteorological models of thermodynamic conditions and flow around urban or industrial areas. The heat island can cause the boundary layer to be often nearly neutral or unstable over the urban or industrial area, with relatively few occurrences of stable conditions. Sometimes, during nearly calm conditions, the upward heat flux from the industrial stacks and processes can cause an inflow of winds around the boundaries of the facility (Brown, 2000).

Differential Heating of Obstacles by Sun: Local thermal circulations can be set up by the sun's heating of one side of a street canyon or obstacle, while the other side remains in the shade. The thermal effects would drive local flow circulations since the flow would tend to be upward on the heated side of a street and downward on the shaded side of a street. These phenonema have been observed in several cities, but have not yet been incorporated in applied transport and dispersion models.

Inversions: In the air quality literature (e.g., Pasquill and Smith, 1983), a commonly used term is "inversion," which refers to a situation when the actual temperature gradient is positive (i.e., the temperature increases with height). An inversion typically occurs near the ground surface during a clear night, when the ground surface is cooled due to the escape of thermal energy by long-wave radiation. An inversion is associated with stable conditions with little vertical turbulence and mixing. During calm and clear nights, the ground-based inversion can be as much as 100 or 200 m deep, causing inhibition of vertical growth of pollutant clouds. This type of inversion is eliminated and replaced by a neutral or unstable layer in a few hours by strong solar heating of the surface in the morning, which causes an upward heat flux, H_s. Another type of inversion occurs aloft, at an elevation of about 1000 m, and marks the top of the layer of air subjected to strong vertical mixing during the day. This latter inversion is called the "*capping inversion*" and also inhibits vertical growth of pollutant clouds. The height of this layer is often referred to as the *mixing depth,* z_i. Still another type of inversion aloft is a persistent "synoptic inversion" caused by subsiding air associated with a large-scale weather system such as a stagnant high-pressure system.

About 20 years after the introduction of the Monin–Obukhov similarity theory in the early, 1950s, it was found that the *convective scaling velocity, w*,* should be used as an additional scaling velocity in combination with Monin–Obukov similarity parameters during light-wind daytime conditions with strong surface heating (Deardorff, 1970). The convective scaling velocity w^* is proportional to the cube root of the product of the heat flux, H_s, and the *mixing depth,* z_i. During such convective conditions the turbulent velocities are found to scale more closely with w^* than with u^*. The magnitude of w^* is usually about 1 to 2 m/s.

Atmospheric stability categories used to describe turbulence. In order to estimate the transport and dispersion of a pollutant, it is best to observe turbulent velocities directly at a site and then express the cloud or plume crosswind spread as the product of the turbulent velocity and the time of travel, multiplied by a dimensionless function of the ratio of the travel time to the turbulent integral time scale, T_I (Pasquill, 1961). Unfortunately we seldom have the luxury of on-site observations of turbulence and therefore have to parametrize the turbulent velocities and the cloud crosswind spread. There is a wide variety of ways used by dispersion models to do this. The most commonly used alternative method was suggested by Pasquill (1961), who devised a six-category *stability class* scheme that is based on time of day, wind speed, cloudiness, and sun's intensity. The six stability classes are denoted by the letters A through F, with A being very unstable, D being neutral, and F being very stable. Given the stability class, the method proposes simple formulas for the growth of plume crosswind spread with downwind distance. Table 1 contains an example of the simplified formulas for plume crosswind spread suggested by Briggs (see Hanna, Briggs, and Hosker, 1982) that fit the Pasquill (1961) dispersion curves for rural terrain and that also fit the so-called McElroy–Pooler (1968) dispersion curves for urban terrain. Note that σ_y refers to the crosswind lateral dispersion and that σ_z refers to the crosswind vertical dispersion. To calculate σ_y and σ_z for the urban categories in Table 1, the stability class for urban areas is calculated using the standard criteria for rural areas. The criteria for defining stability class include wind speed, cloudiness, and time of day and year. The simple but practical Pasquill stability class method is still in use in many operational models today (e.g. the EPA (1995) ISC3 model).

The term *neutral stability*, which is associated with Pasquill Class D in Table 1, implies that there is minimal influence of daytime convection or nighttime temperature inversions. It also corresponds to a Monin–Obukov length, L, that is very large (i.e., near-zero heat flux). It is important to recognize a special characteristic of the atmosphere that is well-known to meteorologists but sometimes not immediately obvious to persons outside that discipline: because a rising parcel of air expands as its pressure decreases, it does work and therefore loses internal energy (i.e., temperature). This process is a simple adiabatic expansion. As a result, in a neutral atmosphere the temperature decreases with height at a rate of about 1 C/100 m. The vertical gradient of *potential temperature*, $d\theta/dz$, is defined such that it equals the vertical gradient of actual temperature, dT/dz, plus 1 C/100 m. Therefore, in a neutral atmosphere, the vertical gradient of potential temperature is 0.0 C/100 m.

TABLE 1
Formulas for Lateral and Vertical Dispersion Coefficients, σ_y (x) and σ_z (x), as a Function of Downwind Distance, x (m), for Rural and Urban Conditions[a]

Pasquill Stability Class	σ_y (m)	σ_z (m)
	Rural	
A	$0.22x\,(1 + 0.0001x)^{-1/2}$	$0.20x$
B	$0.16x\,(1 + 0.0001x)^{-1/2}$	$0.12x$
C	$0.11x\,(1 + 0.0001x)^{-1/2}$	$0.08x\,(1 + 0.0002x)^{-1/2}$
D	$0.08x\,(1 + 0.0001x)^{-1/2}$	$0.06x\,(1 + 0.0015x)^{-1/2}$
E	$0.06x\,(1 + 0.0001x)^{-1/2}$	$0.03x\,(1 + 0.0003x)^{-1}$
F	$0.04x\,(1 + 0.0001x)^{-1/2}$	$0.016x\,(1 + 0.0003x)^{-1}$
	Urban	
A-B	$0.32x\,(1 + 0.0004x)^{-1/2}$	$0.24x\,(1 + 0.001x)^{1/2}$
C	$0.22x\,(1 + 0.0004x)^{-1/2}$	$0.20x$
D	$0.16x\,(1 + 0.0004x)^{-1/2}$	$0.14x\,(1 + 0.0003x)^{-1/2}$
E-F	$0.11x\,(1 + 0.0004x)^{-1/2}$	$0.08x\,(1 + 0.0015x)^{-1/2}$

[a]Briggs' (1973) Curves as Reported in Hanna, Briggs, and Hosker (1982).

Such relatively large decreases of temperature with height are found in the lowest 1000 m of the atmosphere on a windy and/or sunny day.

Many persons consider the Pasquill stability classification system and dispersion curves to be outdated because they represent 1960s technology. Several new models have been proposed that employ the so-called "*continuous*" *stability categorization method* based on the Monin–Obukhov length, L (Arya, 1999). In new models such as the AERMOD model (Cimorelli et al., 1998) and the ADMS model (CERC, 1998), the observed wind speed and cloudiness are combined with information about the sun's elevation angle and the ground surface conditions (e.g., z_o, d, sun's reflectivity, and soil moisture) in order to describe the wind speed profile, the turbulent velocities, the surface heat flux, and the mixing depth. Then the dispersion parameters σ_y and σ_z are calculated directly using simple theoretical relations. It is obvious that the information in this book will be valuable for models such as AERMOD and ADMS, which can make use of inputs of surface roughness length, z_o.

Removal by settling, deposition, washout, and chemical reactions: Material can be removed from the atmosphere by a variety of processes (Hanna et al., 1982). Aerosols and particles with sizes greater than about 10 μm will have appreciable *gravitational settling velocities* (about 10 cm/s for an aerosol diameter of about 50 μm and about 100 cm/s for an aerosol diameter of about 200 μm, assuming an aerosol density approximately equal to the density of water, or about 1000 kg/m^3). For example, most of a cloud of 200-μm aerosols released near the ground will settle to the ground in a few minutes. Particles with sizes less than about 10 μm have gravitational settling velocities so small that the ambient turbulence tends to keep them suspended. However, aerosols with very small sizes and gases may deposit on the ground if they are chemically reactive with the ground surface. This is called *dry deposition*. In many cases, this process is a function of the ability of a vegetative leaf to absorb the substance once the substance passes through the openings in the leaf surface. For most materials, a dry deposition velocity of about 1 cm/s can be assumed and the deposition to the surface (mass per unit area per unit time) can be assumed to equal the dry deposition velocity times the concentration. Removal of aerosol pollutants is also accomplished by rain or cloud droplets. This "wash-out" or *wet deposition* effect is generally parametrized by assuming that the pollutant concentration in the air decreases exponentially with time, with a "wash-out" time scale

that is determined by the substance and by the rain rate but is typically assumed to equal about 30 minutes (i.e., about 90% of the pollutant is "washed out" of the air in about one hour). Volatile materials (including up to the nonane range) evaporate out of the rain about as fast as they are absorbed, but heavier components such as insecticides tend to stay washed out and not evaporate. The deposition rate of the washed-out pollutant on the ground is then assumed to equal the vertically integrated removal rate. Finally, *chemical reactions* are another effective method for removing pollutants from the air. However, although one pollutant may be removed by the chemical reaction, another pollutant may be generated. Recent research has expanded this concern to heterogeneous reactions involving both gases and particles.

Most of the removal processes discussed in the above paragraph are not significant in the near-field (distances less than about 1000 m), since their time scales are on the order of one hour. There are a few exceptions, such as the reaction of SO_3 with water vapor to form H_2SO_4, or the gravitational settling of large particles with diameters of 1000 μm. In most cases, the realistic conservative assumption can be made that removal effects are negligible.

2.2. Engineering Background

Readers of this book will have diverse backgrounds including, in particular, meteorologists and engineers. Because fundamental physical processes are often described differently by different disciplines, here we present some jargon and concept conversions which should be useful to the reader. The focus of this section is on explaining how boundary layer formulas familiar to engineers are related to boundary layer formulas familiar to meteorologists.

Engineering fluid dynamics notes that the fluid viscosity requires there to be a "no-slip" condition at any surface. When there is a fluid flow over a surface, there will be a surface shear stress imposed on the surface by the fluid, and a profile of average speed increasing from zero at the surface and extending into the fluid. For flows with Reynolds numbers relevant to this book, the flow will always be turbulent. Thus there will also be profiles of velocity fluctuations or turbulence which have maxima very close to the surface and then decline away from the surface.

The surface stress, τ_o, arises through direct viscous stress and through the pressure asymmetry around roughness elements on the surface (sometimes called form or pressure drag). In atmospheric flows, the pressure asymmetry dominates over direct viscous stresses and it produces a drag force, commonly called the drag, on the roughness elements. See the discussions of τ_o from an atmospheric boundary layer perspective in Section 2.1 in the paragraph after Eq. (2b).

The engineer frequently addresses two types of flows: internal flows such as flow in a pipe and external flows such as flow around an air foil. In the first type, the engineer often speaks of a *fully developed* flow in, say, a long, constant area pipe in which the mean velocity profiles are independent of position along the pipe. In the pipe the surface shear stress is balanced by the longitudinal gradient of static pressure in the pipe (the "pressure gradient"). In the second type, the engineer often speaks of a *boundary layer* (which is the region over which the fluid velocity is influenced by the no-slip condition at the wall) that extends from the surface to the free-stream velocity. This boundary layer increases in thickness ("grows") downstream (that is, in space). For a "zero pressure gradient" boundary layer the surface shear stress is balanced by the "growth rate" of the boundary layer. For a boundary layer growing in a nonzero pressure gradient, as would be found on flow over curved surfaces, a more complex balance comes into play.

The *atmospheric boundary layer* is a complex flow including aspects of the two engineering flow types above with additional complications such as the earth's rotation.

However, in the two engineering examples of types of flow described above and in the atmospheric boundary layer, the descriptions of the flow are the same at positions "close" to the surface. This is the region in which the dispersion processes described in this book take place.

From the engineering perspective, the profile of mean velocity close to the surface is given by a mathematically derived (using a classical asymptote matching approach) and experimentally confirmed formula known as "the law of the wall." This has two forms, depending upon whether the surface is aerodynamically (or hydraulically if you are a civil engineer) smooth or rough.

For an aerodynamically smooth surface, the profile of mean velocity near the surface is given by Schlichting (1955) as

$$u/u^* = 5.75 \log(zu^*/\nu) + 5.5 \tag{4a}$$

where ν (1.5×10^{-5} m^2/s for air) is the kinematic molecular viscosity and log is the logarithm to base 10. For large zu^*/ν, this can be approximated by

$$u/u^* = \kappa^{-1} \ln[z/(0.11\nu/u^*)] \tag{4b}$$

where $\kappa = 0.4$ is the von Karman constant [as in Eq. (2a)] and ln is the natural logarithm (to base e). For the time being, the displacement length, d, is assumed to be negligible, which is a valid assumption for heights much greater than the average obstacle height, H_r, and/or for widely spaced obstacles.

The atmospheric boundary layer is, in nearly all cases, a turbulent flow over an aerodynamically rough surface. Under these conditions, the engineering "law of the wall" for the profile of mean velocity is given by

$$u/u^* = 5.75 \log(z/H_r) + B = \kappa^{-1} \ln(z/H_r) + B \tag{5}$$

which for our current purposes can be rewritten as

$$u/u^* = \kappa^{-1} \ln(z/C_g H_r) \tag{6}$$

where B and C_g are (often experimentally determined) functions of the shape and geometric arrangement of the roughness elements (Schlichting, 1968; Raupach et al., 1991).

These profiles of mean velocity are also commonly called the "logarithmic velocity profiles" or "log-laws."

Equation (6) is similar in form, as it must be, to the velocity profile used by meteorologists for positions close to the surface (see equation 2a) where the (often experimentally determined) surface roughness length, z_o, is used in the denominator of the ln term.

An alternative view of the connection between the engineering and meteorological approaches is to note that z_o is no more than an integration constant in many derivations of the profile of mean velocity. It is not, in itself, a physically relevant or transparent variable. We typically use Eq. (2a) in meteorology by inputting the mean reference wind speed, u_{ref}, observed at a given reference height, z_{ref} (typically between about 2 m and 10 m). For a given u_{ref} at z_{ref}—for example, 5 m/s at 10 m height—increasing the "roughness" does two things. It increases the surface shear stress (and thereby u^*) and it increases z_o. Both these effects are accepted and often tabulated. However, these two effects are manifestations of the same thing and, as we shall see, are linked by Eq. (2a).

Rewriting Eq. (2a), we find that z_o is equivalent to

$$z_o = z_{ref} \exp(-\kappa u_{ref}/u^*) \tag{7}$$

Therefore, z_o is just another way of writing u^*/u_{ref}. Its attractiveness is that it does not rely on specifying z_{ref}, u_{ref}, and u^*, and can be estimated from the surface geometrical characteristics. But u^*/u_{ref} is still the more physically relevant and fundamental variable. The use of a surface roughness length, z_o, also allows mechanical and thermal effects in the atmospheric boundary layer to be kept distinct.

The displacement length, d, describes the vertical displacement from the ground plane of the effective zero plane for the wind speed profile. If d is a significant fraction of z_{ref}, then z_{ref} in Eq. (7) should be replaced by $(z_{ref} - d)$.

Engineers are far more used to writing $2(u^*/u_{ref})^2$, which is a nondimensional local surface shear stress coefficient. The factor 2 is retained by convention. This nondimensional coefficient, commonly denoted by c_f, is referred to by the jargon terms "skin friction coefficient" or "friction factor" and is seen to be directly related to the roughness length z_o by

$$c_f = \frac{\tau_0}{0.5\rho_a u_{ref}^2} = \frac{2u^{*2}}{u_{ref}^2} = 2\left[\frac{\kappa}{\ln[(z_{ref} - d)/z_0]}\right]^2 \tag{8a}$$

or, alternatively, by

$$z_o = (z_{ref} - d) \exp[-\kappa(c_f/2)^{-1/2}] \tag{8b}$$

However, here a difference occurs in the implementation of these two equations by meteorologists and engineers. For the calculation of the transport and dispersion of material released near the ground, the meteorologist adopts reference positions (and corresponding velocities) that are relatively close to the surface and thus can be easily measured. And it is important to note that in the above development it has been assumed that z_{ref} is close enough to the surface that the "law of the wall" holds. Otherwise, more complex but explicit expressions result.

Moreover, the engineer will use the pipe radius or the boundary layer thickness as the reference position and the average velocity in the pipe or the free stream velocity outside the boundary layer as the reference velocity. Of course, the logarithmic velocity profile does not

extend throughout the pipe or boundary layer and, as a consequence, care is required in converting engineering based c_f values to the meteorological parametrization z_o.

Nevertheless, the engineering "skin friction coefficient," c_f, is traditionally tabulated in engineering texts. It is sometimes given as a function of surface type and ratio of roughness element height to pipe or boundary layer thickness. Often it is implicitly presented through the classic Moody diagram (Schlichting, 1968), which covers aerodynamically smooth and rough surfaces over a comprehensive range of Reynolds numbers including laminar, transitional and turbulent flows.

Thus, we see that, despite different jargon, the same fundamental physical problem is being addressed by the meteorologist and the engineer. In what follows in this book we retain the terminology of the meteorologist.

2.3. Survey of Currently Available Methods for Classifying Dispersion Coefficients for a Variety of Surface Types

The previous sections provided some basic background information on jargon, concepts, and definitions concerning atmospheric and engineering boundary layers and transport and dispersion within these boundary layers. The current section focuses on the effects of surface features on transport and dispersion.

2.3.1. Introduction to Discussion of Effects of Surface Features

The effects of surface features on transport and dispersion can be assessed in two ways—first, by attempting to resolve the flow around the individual surface obstacle, and second, by parametrizing the combined effect of groups of surface obstacles. The first approach is appropriate for pollutant clouds released near buildings or other obstacles where there is interest in assessing the effects in the immediate neighborhood of the obstacle and the cloud dimensions are smaller than the dimensions of the obstacle. The second approach is appropriate for clouds that have dispersed to a size greater than the height of the roughness obstacles. The second approach encompasses three situations.

Situation 1. The release is below the obstacle height, the cloud width is larger than the obstacle width, and the cloud depth is smaller than the obstacle height.

Situation 2. The release is below the obstacle height, the cloud width is larger than the obstacle width, and the cloud depth is greater than the obstacle height.

Situation 3. The release is above or near the tops of the obstacle arrays.

Situation 2 has been studied and Situation 1 less so and only very recently. Situation 3 has been very extensively studied, since it includes all tracer experiments over rural surfaces with small roughness. These scenarios are extensively discussed in Chapter 4, where Figures 15 and 16 illustrate typical cloud dispersion situations in obstacle arrays.

When resolving flow and dispersion around individual surface features, many models make use of simple parametrizations of dilution and dispersion within displacement zones and within recirculating cavities behind obstacles. When there is a release from a low velocity vent flush with the roof or side of a building, wind tunnel studies suggest that the concentration on the roof or side of the building is inversely proportional to the square of the distance from the vent (Wilson and Britter, 1982; Hanna et al., 1996). For releases into recirculating cavities or wakes behind buildings, EPA and NRC regulatory models such as ISC3 (EPA, 1995) make the simple assumption that the cloud of pollutants spreads across an initial area equal to the cross-sectional area of the structure facing the wind. Simplified models also exist for pollutant concentrations in street canyons and tunnel entrances. Furthermore, there is much research activity involving the use of detailed computational fluid dynamics (CFD) models to simulate flow around buildings and other obstacles, although such models are not yet widely used for routine applications (see Brown, 2000, for an overview).

For ground-level releases of neutrally buoyant (passive) gases with no plume rise, ground-level concentrations are usually reduced in the presence of enhanced roughness. However, it is possible in this scenario for ground-level concentrations to increase slightly with an increase in surface roughness length, z_o, in some special situations where the cloud depth is less than the average obstacle height, H_r. In this situation, the tendency toward an increase in concentration caused

by a decrease in wind speed below H_r more than compensates for the tendency toward a decrease in concentration due to the increase in turbulence. Section 2.3.2 further explains this phenomenon.

For elevated clouds or plumes or for near-ground releases with substantial plume rise, such that the cloud centerline height is above H_r, it is possible for the maximum ground-level concentrations to increase as H_r or z_o increases. This tendency is caused by the fact that the increased turbulence over the surface with larger z_o will cause the elevated cloud to disperse to the ground more quickly. Furthermore, the elevated cloud could be carried to the ground by the aerodynamic flows in the recirculating cavities behind individual roughness obstacles.

There is a rough rule of thumb that z_o is roughly equal to $\frac{1}{10}$ of the height of the obstacles, H_r, and d is roughly equal to $\frac{1}{2}$ H_r. Therefore, z_o would equal about 0.05 m for a grassy field where H_r is about 0.5 m, and about 1 m for an industrial area where H_r is about 10 m. Furthermore, d would equal about 0.25 m and 5 m for these surface types. In the advanced transport and dispersion models such as AERMOD (Cimorelli et al., 1998) and ADMS (CERC, 1998), the estimate of z_o is then combined with observations of wind speed, stability, and surface conditions in order to estimate the magnitude of the turbulent velocity components and calculate the variation of the wind speed with height. These advanced models usually do not require input of displacement length, d, because it is assumed that the centroid (mass-weighted mean) height of the cloud is at least several times larger than H_r.

Most EPA models, such as ISC3 (EPA, 1995), do not bother with such detailed boundary layer calculations and instead simply include options for dispersion coefficients for two alternate surface types—rural and urban.

2.3.2. *Use of a Simple Gaussian Dispersion Model to Understand the Effects of Roughness*

The effects of parametrizations of surface features in dispersion models can be understood through analysis of a simple transport and dispersion model. There are many available models, as briefly outlined in Section 2.1. The Gaussian plume model, which forms the basis for most applied models, is used to illustrate these principles. Note that we are using the terms cloud and plume interchangeably in this discussion. This model is called "Gaussian" because the crosswind distributions of

concentration are assumed to have a Gaussian (normal or bell-curve) shape [i.e., the Gaussian shape function, $\exp(-y^2/2\sigma_y^2)$ is used].

For a continuous nonbuoyant plume with emission rate, Q (kg/s), released at height, h_e (m), above ground, the ground-level concentration, C (kg/m^3), predicted by the Gaussian plume formula at some downwind distance, x, is:

$$C = \left(\frac{Q}{u\pi\sigma_y\sigma_z}\right)\exp\left(-\frac{y^2}{2\sigma_y^2}\right)\exp\left(-\frac{h_e^2}{2\sigma_z^2}\right) \tag{9}$$

where u (m/s) is wind speed at release height and y is crosswind distance from the plume centerline. It is assumed in deriving Eq. (9) that the trajectories of plumes follow a straight line and that conditions (e.g., wind speed and stability) are constant over the full path of the puff or plume. Formulas for σ_y and σ_z are given in Table 1 as a function of downwind distance, x, and can be used in Eq. (9). Concentration distributions can be calculated at ground-level as a function of downwind distance, x, and crosswind distance, y, thereby allowing population impacts to be estimated. Deposition could be calculated by multiplying C by the gravitational settling velocity or the dry deposition velocity.

In Eq. (9), the peak ground-level concentration at the center of the plume can be obtained by setting $y = 0.0$, thus forcing the "exp" term in y to equal 1.0 and therefore simplifying the solution. To simplify the analysis even further, assume that the release height is at the ground (i.e., $h_e = 0.0$), giving the following simple formula for the plume centerline normalized concentration:

$$C/Q = (\pi u\sigma_y\sigma_z)^{-1} \tag{10}$$

where the concentration, C, is normalized by the source emission rate, Q, and u should now be interpreted as the concentration-weighted wind speed [see Eq. (1)] at the mass-weighted mean height of the cloud. To show the dependence of C/Q on z_o and d, we can make the simple assumption in Eq. (10) that, for nearly neutral conditions close to the source, both σ_y and σ_z are proportional to u^*t or u^*x/u, where t is the travel time from the source to the distance x, and u is the average cloud speed over the trajectory (Hanna et al., 1996). The formulas in Table 1 are all seen to be linear in x at small distances. The proportionality factors are about 2 and 1.3 for σ_y and σ_z, respectively, since $\sigma_y = \sigma_v t$ and $\sigma_z = \sigma_w t$, and since $\sigma_v = 2u^*$ and $\sigma_w = 1.3u^*$ (Stull, 1997). We also

assume that the log wind profile law [Eq. (2b)] is valid. Consequently, Eq. (10) becomes:

$$\frac{C}{Q} = \frac{\ln[(z-d)/z_0]}{1.04\pi u^* x^2} \tag{11}$$

where z is the mass-weighted mean cloud height averaged over its trajectory. Because of the use of the log wind profile formula in Eq. (11), this solution is valid for situations where the plume depth is greater than the obstacle heights, H_r. For given values of wind speed observing height, z, and downwind distance, x, as z_o is increased in Eq. (11), the $\ln(z-d)/z_o$ term will decrease. At the same time, u^* will be larger for a larger z_o. Therefore the normalized concentration, C/Q, will decrease in Eq. (11) as z_o increases.

In situations when the plume dimension is less than the average obstacle height, H_r, Eq. (10) also reveals how it is possible, under certain conditions, for concentrations not to decrease as H_r increases. Because the wind speed is located in the denominator of Eq. (10), if the wind speed is markedly decreased down within the obstacles, the resulting decrease in dilution rate may sometimes dominate over the increase in dispersion due to increased turbulent velocities. In the latter situation, the predicted maximum normalized centerline concentration, C/Q, in Eq. (10) at a given distance, x, may not decrease and may even increase slightly as H_r increases. This scenario may occur in urban or industrial areas for relatively densely packed buildings at heights near street level.

2.3.3. *Situations Where Winds, Stability and Underlying Terrain Vary in Time and/or Space*

The simplified analysis given above is valid at relatively short distances from the source (say less than about 1 km). If the impact of the pollutant is expected to occur at distances no more than a few kilometers from the source emissions location, then it is reasonable to assume that the plume or puff travels in a straight line, that the meteorological conditions are steady in space and in time, and that the simplified boundary layer formulas and parametrizations apply. However, for some types of scenarios where longer distances and times are of interest (say distances greater than about 10 km and times of several hours) it may be important to account for time and space variations in meteorological condi-

tions and possible curvatures in cloud or plume or puff trajectories. Another complication occurs in mountainous terrain, where pollutant clouds may be diverted around or over hills or may impact hills. Some transport and dispersion modelers ignore these variations because it is often conservative (i.e., it leads to higher predicted concentrations at a fixed location) to assume a steady straight-line trajectory. However, there are several transport and dispersion models that can account for these variations, as long as the detailed observations are available for input to the models. These models include the SCIPUFF model (Sykes et al., 1998) and the CALMET/CALPUFF model (Scire et al., 1998). If the user is interested in the effects of the pollutant cloud on the population, it is important to account for the cloud trajectory curvature, since the curvature may cause the cloud to be diverted toward or away from a populated area.

The distance scales ranging from about 1 to 100 km are called "mesoscales" by meteorologists. At these scales, the scenarios satisfy the criterion that the cloud or plume dimension is larger than the dimensions of the roughness obstacles. This criterion will be satisfied even in urban areas with tall buildings, because the cloud or plume will mix over a layer several hundred meters deep after it has traveled a few kilometers. Therefore the primary conclusion following Eq. (11) will be valid in mesoscale regions: the concentration can be expected to be less in mesoscale regions if the surface roughness is greater.

2.3.4. Methods for Accounting for Surface Roughness Length and Displacement Length in Dispersion Models

In this subsection, we describe current methods for incorporating the effects of surface roughness into dispersion models. However, most discussions in Section 2.3 so far relate to the situation where the cloud depth is greater than the height of the roughness obstacles, H_r, thus allowing z_0 to be a relevant parameter. The case where the cloud depth is smaller than the height of the obstacles is not explicitly treated in the models mentioned so far. That special case, for small pollutant clouds located below H_r, may be more appropriately treated by resolving the flow and dispersion around the obstacles. We know of no publicly available comprehensive atmospheric transport and dispersion model that handles these situations in a smooth seamless manner. In Chapter 4, we will suggest a simple approach to such a comprehensive model.

Pasquill's (1961) original dispersion curves were intended only for rural surfaces (see the top part of Table 1). In fact, they were primarily applicable to grassy fields in England. Then, once field data started arriving from transport and dispersion experiments in urban studies in the 1960s and 1970s (e.g., the St. Louis data reported by McElroy and Pooler, 1968), urban dispersion curves (see the bottom part of Table 1) were included as an option in some applied models, such as the ISC3 model (EPA, 1995).

The EPA's determination of whether a region is rural or urban uses an objective quantitative method that is based on Auer's (1978) definitions of categories of land use. A few residential, industrial/commercial, and urban categories are included in Auer's (1978) land use tables. To briefly summarize the EPA method, the modeler is required to draw a circle with a radius of 3 km around an emissions source, and then assign Auer's land-use categories to portions of the circle. If more than 50% of the circle consists of land-use categories in the "urban" group, then the model is run in urban mode (i.e., using the urban dispersion curves). Otherwise it is run in rural mode (i.e., using the rural dispersion curves).

The EPA method described above satisfies their requirement that a method should yield consistent results when applied to the same scenario by several independent users. However, there are limitations resulting from the use of only two roughness types (rural and urban). From the start, there has been confusion about what to do about industrial plants surrounded by rural areas. The plant site itself can obviously be considered to be relatively rough, being covered by 10 to 20 m tall tanks, buildings, pipe racks, columns, and other obstructions. However, if the plant site area is less than 50% of the area of the circle with radius 3 km, the EPA method may assign a rural roughness type to the plant. The arbitrary determination of urban or rural dispersion curves can lead to significant differences in predicted ground level concentrations. For near-ground sources, where the cloud centerline is on the ground, predicted concentrations will be less if the urban curves are used, since there will be more dispersion in the lateral and vertical directions. For elevated stack sources, predicted concentrations may be greater if the urban curves are used, since the cloud will disperse down to the ground faster even though it is more dilute at locations on its centerline aloft.

As mentioned earlier, the EPA has proposed a new model, AERMOD (Cimorelli, 1998), which does not employ any arbitrary

roughness categories. Instead, the model contains a meteorological algorithm that allows for so-called "continuous" variations of roughness and stability. The user inputs a few basic observations (e.g., wind speed, cloudiness, time of day, mixing depth) and a few characteristics of the surface (e.g., roughness length, reflection of sun's radiation, soil moisture) and the model's meteorological preprocessor calculates all the required parameters for the dispersion model. If detailed observations of turbulence are taken or if there are vertical profiles of wind and temperature, the model will accept that additional information, too. It should be stated that AERMOD is not alone in its use of these "new" procedures, because several other models developed over the past 10 or 15 years also make use of these same principles. For example the ADMS model (CERC, 1998) and the SCIPUFF model (Sykes et al., 1998) use similar methods.

Although many transport and dispersion models still use the Pasquill stability classification categories (A, B, C, D, E, and F) and formulas such as listed in Table 1, most models for the accidental release of hazardous gases and aerosols employ "continuous" variations of roughness and stability. For example, HGSYSTEM (Witlox and McFarlane, 1994), DEGADIS (Havens and Spicer, 1985), and SLAB (Ermak, 1990) use some of the state-of-the-art approaches mentioned in the above paragraph. The roughness length and the Monin–Obukhov length, L, are input to these models, and the models then use state-of-the-art boundary layer theory to develop vertical profiles of wind speed and to estimate turbulent velocities. The displacement length is not an input to these models, since it is felt to be small (compared to H_r) at most oil refineries and chemical processing plants, where the roughness obstacles are not closely packed. However, these hazardous gas models differ from AERMOD in that they do not employ a surface energy balance equation to derive heat fluxes and L from basic principles; instead they rely on the modeler to input a correct value of L.

In most realistic scenarios, the characteristics of the surface vary with distance as the cloud is transported away from the source. Few of the models discussed so far allow variations of surface roughness with distance. Some mesoscale (i.e., 1 km to 100 km) transport and dispersion models such as CALPUFF (Scire et al., 1998) and SCIPUFF (Sykes et al., 1998) do allow roughness to vary. However, it is difficult to properly account for this effect in the context of the model equations. In particular, models such as CALPUFF and SCIPUFF cannot account

for the sloping internal boundary layer that marks the boundary between the layers influenced by different roughnesses; instead they account for the transition through the use of virtual sources and assumed abrupt transitions across the whole depth of the boundary layer.

It should be noted that, despite the fact that many models make use of the surface roughness length, z_o, and require this parameter as an input, there is little guidance for choosing z_o in the models' technical documents or user's guides. At best, a simple table may be provided in the model's technical document that lists z_o as a function of gross land-use category. Also, in most cases, d is not required as an input. The main purpose of this book is to improve upon this situation.

2.4. Survey of Experiments Showing Effects of Surface Roughness Obstacles on Dispersion

Because of recent increased interest in the effects of surface roughness obstacles on dispersion, there have been several field and fluid model experiments that have taken place in the past ten years. There was a lull in the 1980s after the intensive urban field experiments and wind tunnel experiments of the 1960s and 1970s. Much of the recent research has been driven by concerns about releases of toxic materials as part of military campaigns in urban areas and about accidental releases of hazardous chemicals at industrial plants. As discussed earlier, the discussions are presented separately for two cases: (1) situations where the cloud centroid (mass-weighted mean) height is larger than the surface obstacle heights, H_r, and the transport and dispersion over the obstacles can be characterized by Monin–Obukhov scaling parameters, and (2) situations where the cloud centroid height is less than H_r and the transport and dispersion around the individual obstacles can be estimated as a function of obstacle geometry. Note that the cloud centroid height can exceed H_r for sources that are elevated above H_r to begin with, or for ground-level sources that have dispersed upward above H_r.

2.4.1. Dispersion of Clouds with Mass-Weighted Mean Heights Greater Than the Roughness Obstacle Height, H_r

The first case of interest concerns clouds with mass-weighted mean heights larger than the average surface roughness element height, H_r,

such that the bulk of the cloud extends into the surface boundary layer. For these cases, the wind flow and the dispersion processes are explained by standard surface boundary layer theories such as Monin–Obukhov similarity theory (Stull, 1997). In neutral conditions, Eq. (2b) describes the wind profile. There is no need to resolve the flow around individual roughness obstacles and z_o and d are used to characterize the effects of the roughness obstacles.

For this scenario, the Gaussian plume model [Eq. (9)] was used in Section 2.3 to demonstrate the effects of variations in surface roughness length on the maximum ground-level concentration. It was seen that, for ground level sources, increases in z_o cause decreases in maximum normalized concentrations at ground-level at a given x, primarily due to the general increase in turbulence. For elevated sources, maximum ground level concentrations could increase or decrease as z_o increases, depending on the initial cloud or plume elevation, h_e. Some relevant experiments are summarized below:

2.4.1.1. Full-Scale Urban Tracer Experiments. The σ_y and σ_z formulas for urban areas in the lower part of Table 1 are derived directly from full-scale urban field experiments. These formulas indicate that, for a given stability class (determined from wind speed and sky conditions, and not taking the urban area into account) and for a given downwind distance, the σ_y and σ_z for urban conditions are consistently larger than those for rural conditions. The difference ranges from 20 to 30% during unstable conditions to a factor of five during stable conditions. The St. Louis urban tracer data showed this effect (McElroy and Pooler, 1968) and the resulting dispersion curves evolved into the urban dispersion formulas in Table 1. Data from other urban field experiments support this same conclusion (Ramsdell et al., 1982).

2.4.1.2. Small-Scale Field Experiment. The Kit Fox field experiments at the Nevada Test Site involved ground-level area source releases of CO_2 gas within a large array of roughness obstacles (Hanna and Steinberg, 2001; Hanna and Chang, 2001). The field experiment was about a 1/10 scale representation of the roughness typical at an industrial processing plant or oil refinery. Concentrations were observed on four monitoring lines at downwind distances of 25, 50, 100, and 225 m. The vertical extent of the cloud was always observed to be about equal to or larger than the height of the roughness obstacles. Several groups of releases of

about 20 and 120 seconds duration were made at ground level for three different surface roughness types, with z_o = 0.0002 m, 0.02 m, and 0.2 m. The z_o = 0.0002 m roughness length was associated with the flat desert. The z_o = 0.02 m roughness length was associated with the uniform roughness array (URA), which consisted of rectangular plywood boards with width, W = 0.8 m, and with height, H_r = 0.2 m. The z_o = 0.2 m roughness length was associated with the equivalent roughness pattern (ERP), which consisted of square plywood boards with $W = H_r$ = 2.4 m.

The maximum normalized ground-level concentrations, C/Q, for each of the three Kit Fox roughness types occurred during light-wind stable meteorological conditions for the continuous plume experiments. A very clear trend was seen in the observed C/Q values, which decreased by about a factor of four as roughness increased from 0.0002 m to 0.02 m, and decreased by another factor of four as roughness further increased from 0.02 m to 0.2 m. Therefore there was a factor of 15 to 20 decrease in C/Q as roughness increased from 0.0002 to 0.2 m. The simple power law, $C/Q \mu z_o^{-1/2}$, provides a good fit to the data and suggests that there is a factor of about three decrease in maximum C/Q for each order of magnitude increase in z_o (for sources near ground level). This decrease is approximately the same order as that suggested by the rough rule of thumb that there would be about a factor of two to four decrease in concentration for each order of magnitude increase in roughness (Pasquill and Smith, 1983).

Detailed wind profile and turbulence observations were also made during the Kit Fox experiments. It was found that, at heights above about 1½ times the obstacle height, H_r, the observed wind profiles conformed to log-law expectations [seeEq. (2b)] with the "best-fit" z_o agreeing with the estimated z_o on the basis of the roughness element heights and densities (see Chapter 3). It is important to include the displacement length, d, in the analysis for the ERP roughness obstacles, since the observation heights were close to H_r. The friction velocity, u^*, was also observed to be much larger for the larger roughness elements, again agreeing with quantitative predictions. Furthermore, the observed turbulent velocities increased for the larger roughness elements and followed scaling relations such as $\sigma_v = 2u^*$, again illustrating the importance of u^*. These effects are shown in Figure 3, where Kit Fox observed wind profiles on three separate towers are plotted for several concurrent time periods with relatively high wind speeds. The

dashed curves are drawn only between the measurement points. Tower 1 is in the flat desert with $z_o \geqslant 0.0002$ m. Tower 2 is in the URA roughness elements, where $H_r = 0.2$ m and $z_o \geqslant 0.02$ m. Tower 4 is 15 m downwind of the ERP roughness elements, where $H_r = 2.4$ m and $z \geqslant 0.2$ m. For Figure 3, periods with relatively high wind speeds are chosen to assure that the stability would be nearly neutral.

2.4.1.3. Fluid Model Experiments. Many fluid model (wind tunnel and water channel) experiments have been concerned with resolving flows around scale models of buildings and topography (e.g., see Hosker, 1984). However, there has been an increasing number of studies of flow and dispersion over arrays of roughness elements where the plume size exceeds the size of the roughness elements and therefore the elements can be parametrized through z_o. As examples of these wind tunnel studies, Dirkmaat (1981), Brighton (1989), Petersen and Ratcliff (1989), Britter et al. (1991), and Roberts et al. (1994) present results that confirm that the concentration would decrease as the roughness increases, for all other conditions the same. It is concluded from these studies that it is appropriate to parametrize the effects of an industrial area on dispersion by means of a surface roughness length, z_o.

2.4.2. Dispersion of Clouds with Mass-Weighted Mean Heights Less than the Roughness Obstacle Heights, H_r

The second case of interest concerns clouds with mass-weighted mean heights less than H_r. It should be mentioned that there is no firm guidance concerning where the switchover occurs between the cases of a cloud "above" and "below" H_r. A rough rule of thumb is that the switch-over would occur at a centroid height between about 1 and 2 H_r. Further experiments and theoretical analysis should shed light on this criterion. In the meantime, our proposed simplified models in Chapter 4 will suggest methods for interpolating between the two regimes.

For this case, the individual pollutant cloud will follow the streamlines and flow around the individual obstacles and accordingly the dispersion will depend on the local turbulence velocities. Therefore, for the initial trajectory, until the cloud grows to the size of the obstacles, there is a need to resolve the flow around individual obstacles.

The vertical profile of average wind speed at heights much less than the obstacle heights no longer follows the log-law [Eq. (2b)] that is

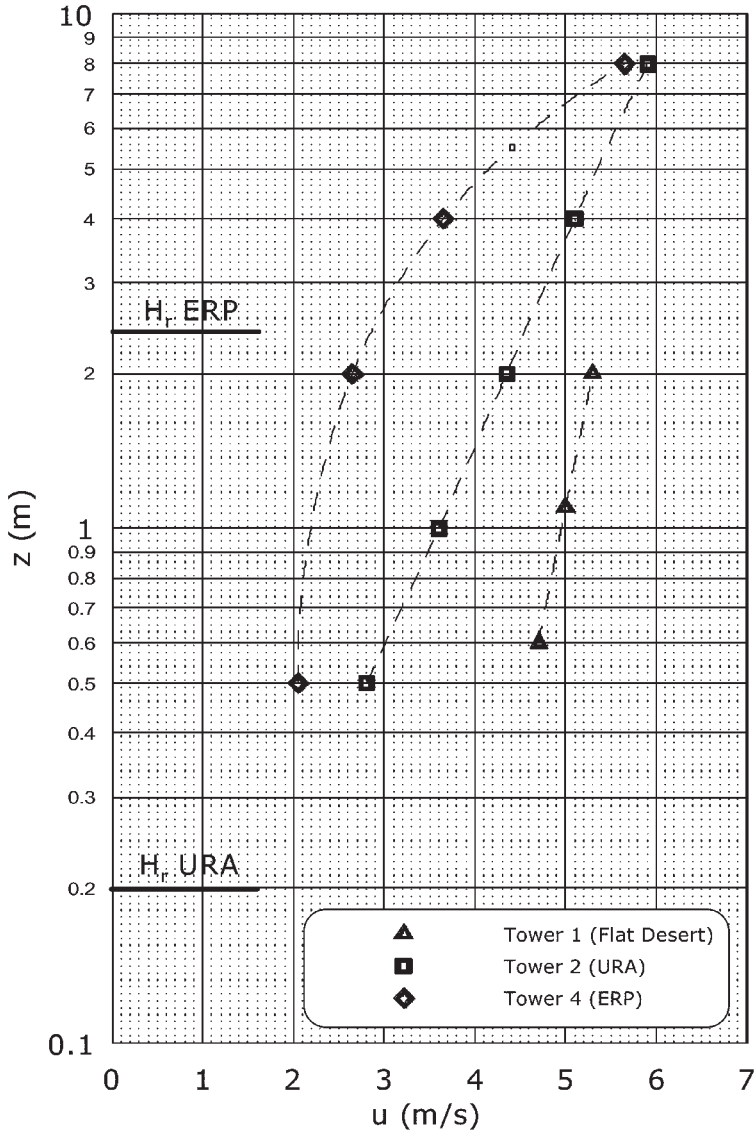

FIGURE 3. Observations of concurrent averaged wind profiles over three different roughness surfaces for high wind classes during the Kit Fox field experiments at the Nevada Test Site (Hanna and Chang, 2001). Tower 1 is on the flat desert with z_o = 0.0002 m. Tower 2 is within the URA roughness obstacles with H_r = 0.2 m and z_o = 0.02 m. Tower 4 is 15 m downwind of the ERP roughness obstacles with H_r = 2.4 m and z_o = 0.2 m. All towers are within about 100 m of each other. The dashed curves are drawn only between the measurement points.

appropriate in the boundary layer above the obstacles. Furthermore, at any specific location, an individual wind profile depends strongly on the closeness of nearby obstacles. The "average wind profile" must be determined by averaging over several positions (e.g., between obstacles, behind obstacles) The "average wind" as defined in this manner is observed to be roughly constant in most of the layer from the ground surface to the tops of the obstacles. Simplified exponential wind profile formulas have been proposed for vegetative canopies that are also valid for other types of surface obstacles (Cionco, 1965; Raupach et al., 1980; Brown, 2000; Macdonald, 2000). Section 3.4 suggests some straightforward formulas for estimating the wind speed at heights below the obstacle tops.

2.4.2.1 Full-Scale Field Experiments. Field experiments of flow and dispersion around full sized obstacles (e.g., buildings, storage tanks, nuclear reactor structures, street canyons, isolated hills) have necessarily involved very site-specific structures. A real industrial site or urban area consists of structures with different individual shapes and spacings, and never consists of the evenly spaced uniform square obstacles studied in wind tunnels and small-scale field studies. A summary of some of these field studies and suggestions for some simple scaling models are given in the review chapters by Johnson et al. (1976) and Hosker (1984). Generally the emphasis of field studies is on specific questions such as clouds in the recirculating wakes of single buildings or on pollutants from traffic in a street canyon. In these examples, the pollutant is diluted in the wake of the obstacle. However, it is possible for a cloud located slightly above the obstacle to downwash to the ground in the recirculating wake behind the obstacle. Because of the renewed interest in dispersion in urban areas, there are several new urban meteorology field experiments planned. The experimental designs suggest that sufficient wind profile locations will be used to allow the "average wind" in the urban area to be determined.

2.4.2.2. Small-Scale Field Experiments. With a smaller scale, the researcher has more control over the size and shape of the obstacles, and the setup of the experimental array is faster and can be easily changed. For example, movable cubes with dimensions of about 1.1 m have been employed to set up a variety of obstacle arrays, with different spacings and groupings, in a flat grassy field (Macdonald et al., 1997).

These experiments focused on the dispersion of a point source cloud or plume released at a height of 0.5 H_r (i.e., 0.55 m) and at a location about two H_r (i.e., 2.2 m) upwind of the array. Concentrations were observed at various points within the arrays. For comparison purposes, an identical experiment was carried out with no obstacles in place. The results showed little effect of the obstacles on the maximum ground-level concentration at a given downwind position within the obstacle arrays. For increased obstacle density, the cloud dispersion increased, thus tending to decrease the concentration, but at the same time, the wind speed decreased, tending to increase the concentration. The two effects roughly canceled out for this specific scenario involving a source location 2 H_r upwind of the obstacle array.

A similar small-scale field experiment, but with 2 m cubical-shaped obstacles, was reported by Davidson et al. (1995), who also used a source position about 2 H_r upwind of the array. They reached similar conclusions—that the maximum concentration at a given downwind position was little affected by changes in the obstacle arrays. Moreover, the cloud was observed to flow over and around the obstacle array, as if the entire array were a single barrier to the flow.

Both studies discussed here used source elevations equal to about 0.5 H_r and the source was located about 2 H_r upwind of the edge of the source array. This source position is clearly different from the ground-level area sources within the obstacle arrays in the Kit Fox experiments discussed in the previous section. Although the results of the Macdonald et al. (1997) and Davidson et al. (1995) experiments are consistent with expectations, it would be useful to have data for a wider range of scenarios, including ground-level releases within the arrays.

2.4.2.3. Fluid Model Experiments. As mentioned earlier, there are numerous wind tunnel and water channel studies of flow and dispersion around individual obstacles, and the results are summarized in review articles by, for example Meroney (1982), Hosker (1984), Brighton (1989), and Britter et al. (1991). The emphasis of these studies is generally on definition of the dimensions and other characteristics of the recirculating wake behind a single obstacle and estimation of concentrations within the wake and downwind of the wake due to a variety of point source locations relative to the obstacle.

Many experiments have concerned the related topic of maximum concentrations on the roof and sides of an individual structure due to

emissions from a vent or short stack on the roof or side of the structure. The cloud or plume can be a momentum jet. Suggestions have been made for simple conservative scaling formulas to be used to estimate the maximum concentrations on the roof and sides of structures (e.g., see Wilson and Britter, 1982).

More recently, there has been an increasing number of fluid modeling experiments concerning cloud releases within obstacle arrays. In particular, Hall et al. (1998) and Davidson et al. (1996) carried out wind tunnel experiments concerning dispersion in regularly spaced obstacle arrays, nearly exactly matching the geometry of the small-scale field experiments by these same groups (Macdonald et al., 1997, and Davidson et al., 1995, respectively). The small-scale field experiments were already described in the previous subsection. Not coincidentally, similar conclusions were reached, too—the presence of the obstacle arrays has little effect on the maximum ground-level concentration at a given downwind distance for pollutant clouds released 2 H_r upwind of the array at an elevation of 0.5 H_r.

The Hall et al. (1998) experiments also included some cases with cloud releases within the obstacle array. They found that lateral and vertical dispersion were enhanced in the first few obstacle rows after the release. However, after the cloud had passed by many (about 20) obstacle rows and was dispersing vertically above H_r, the rate of dispersion (e.g., $\partial\sigma_y/\partial x$) dropped back to that characteristic of the boundary layer above the obstacles. A set of best-fit formulas for the urban dispersion coefficients, σ_y and σ_z, was suggested by Hall et al. (1997) based on their wind tunnel and field experiments with arrays of obstacles, and has become the basis of the British Defence and Evaluation Research Agency (DERA) Urban Dispersion Model (UDM).

Another series of wind tunnel experiments involving cloud dispersion within and above uniform obstacle arrays of various heights was reported by Roberts et al. (1994). These scenarios included both cases of concern in this book—clouds with dimensions greater than the obstacle height and clouds with dimensions smaller than the obstacle height. Their findings confirm what has been concluded so far—for the first case (clouds with dimensions greater than the obstacle height), the dispersion can be modeled using z_o, and the maximum ground-level concentration at a given downwind distance for ground-level releases tends to decrease as surface roughness increases. For the second case (clouds with dimensions smaller than the obstacle height), the flow and

dispersion must be resolved for the specific case, and the maximum concentration at a given downwind distance may or may not decrease as the obstacle heights increase.

Nearly all of the fluid modeling experiments and small-scale field experiments have employed obstacle arrays with uniform heights. For real-world urban or industrial scenarios, the heights of individual obstacles will vary by a factor of two or more about the mean H_r.

The following chapters discuss these cases in more detail and make specific suggestions concerning straightforward formulas that can be used to study the problem.

3

Methods for Characterizing the Effects of Surface Roughness Obstacles on Flow

In this chapter, we discuss in more detail the effects of surface roughness obstacles on the flow and suggest some specific formulas for characterizing these effects. Generally, the rougher the surface, the lower the wind speed and the higher the turbulence intensity.

The effects of surface roughness obstacles on the flow above and below the elevations of the obstacles can be described by means of some simple geometric measures such as the surface roughness length, z_o, and the displacement length, d, which are related to the average height of the obstacles, H_r, and their geometric shapes and spacing. Thus, much of this chapter concerns the determination of these and related geometric measures. In Section 3.5 we summarize the results and recommendations and place them in an operationally useful format.

Chapter 4 will extend the study to describe methods for accounting for the roughness effects in transport and dispersion models.

Chapter 5 will provide worked examples of the estimation of z_o and d for seven typical urban and/or industrial scenarios.

3.1. Required Flow Characteristics for Input to Transport and Dispersion Models

It was shown in Chapter 2 that, no matter which type of source emissions scenario is being considered and which transport and dispersion model is being applied, there is a need to specify certain basic characteristics of the wind flow as inputs to the transport and dispersion model. Experimental evidence and theoretical derivations show that the surface roughness length, z_o, is a key scaling variable used in this specification.

Chapter 2 contained descriptions of several classes of transport and dispersion models and the types of variables that are required as inputs to the models. The following common variables are required as inputs or are estimated by all models:

- *Wind Speed (u) and Wind Direction (WD)*—The wind speed and direction at the mass-median height of the pollutant cloud are used to characterize the transport speed and direction of the cloud. The wind speed also is used to account for the dilution of material in continuously released plumes. It is important to note that the wind direction (WD) is defined to be the direction from which the wind is blowing rather than the direction toward which the wind is traveling.
- *Stability*—The stability can be estimated a number of ways. The most direct way is through on-site observations of turbulent heat and momentum fluxes by fast-response instruments. However, such observations are available only at special research sites and not at routine meteorological sites such as those in operation at industrial plants. The Pasquill (1961) stability class (see Table 1) is estimated from an observation of the wind speed and the sun's intensity and/or cloudiness, and is not a function of the type of surface. Intermediate methods are based on land-use data and solution of the surface energy-balance equation (e.g., Cimorelli et al., 1998; Hanna and Chang, 1992). It is noted that the industrial plant or urban area can affect the on-site stability because of the generation of additional mechanical turbulence and by the release of heat to the boundary layer.
- *Turbulent Velocities and Time Scales*—The three (x, y, z) components of the turbulent velocity (σ_u, σ_v, and σ_w) are used to characterize the turbulent dispersion of the cloud. Recall that x is the

downwind direction, y is the lateral crosswind direction, and z is the vertical direction. In addition, at large travel times (more than about 1000 seconds), it is important to also account for the effects of the turbulent integral time scales (T_x, T_y, and T_z) in the same three fundamental directions. These time scales may be thought of as the time periods of the dominant turbulent eddies. Section 3.3.2 suggests simple formulas for σ_u, σ_v, and σ_w, and Section 4.2.3 provides some estimates of integral time scales.

If the wind speed and direction and the turbulent velocities and time scales are known as a function of position (x, y, z) and time, then the solution to the transport and dispersion problem is completely determined. This is never the case. Usually all we have is a measure of the wind speed at one or two heights (perhaps not even at the site), an estimate of the land use or surface conditions, and a measure of the stability (for example, the cloudiness and time of day or the vertical temperature gradient). Fortunately, because of the applicability of scaling relations such as Monin–Obukhov scaling (see Chapter 2), the required wind and turbulence variables can be estimated using simple scaling variables such as the friction velocity, u^*, the surface roughness length, z_o, the displacement length, d, the height, z, and the Monin–Obukhov length, L. The effects of stability can also be estimated using simple methods based on routine observations. This chapter will describe how to estimate these scaling variables, with emphasis on z_o, d, and u^*. The effects of stability (i.e., L) can often be ignored when analyzing wind measurements at low heights over rough surfaces such as industrial sites, since the mechanical turbulence generated by the roughness obstacles is so dominant. To simplify the discussions below, it is assumed that the boundary layer over an urban or industrial site is nearly neutral for most applications. For stable or unstable boundary layers, see the suggested formulas for urban boundary layers given by Hanna and Chang (1992).

Even though the displacement length, d, has a role in the scaling analysis, it has historically not been required as an input by most transport and dispersion models. This is because the influence of d is minimal at $z \gg d$ [see Eq. (2b)] and because most observed wind profiles have enough scatter that they can be adequately fit using only z_o and ignoring d. Despite the lack of interest in d by most modelers, we include methods for estimating d, in anticipation that its use will become more widespread.

3.2. Consideration of Flow Above and Below the Tops of the Obstacles

For flat rural terrain with relatively small surface obstacles (e.g., a grass surface or a sand surface with obstacle heights, H_r, much less than about 1 m), the mass-weighted mean height of a pollutant cloud will always be much greater than the tops of the obstacles. In this situation, it is sufficient to simulate the transport of the cloud using the solution of the familiar logarithmic wind profile [Eq. (2b)].

Because of the substantial height of the roughness obstacles (H_r = 10 m or 20 m) at many industrial sites, in some cases the pollutant cloud may be constrained to elevations below the tops of the obstacles. A similar phenomenon can occur in urban areas, where the cloud may be initially located at street level, or in forested areas, where the cloud may be entirely below the canopy layer. However, at downwind distances beyond about 10 or 20 H_r, eventually these clouds will disperse to heights well above H_r (Hall et al., 1997). For these situations, it is necessary to be able to specify the flow both above and below H_r. The logarithmic wind profile given by Eq. (2b) applies at heights above the obstacle heights, a simplified wind profile (e.g., constant or linear) applies below the obstacle height, H_r, and a transition or blending region applies at intermediate heights.

The characteristics of wind flow around and above an array of surface roughness obstacles can be described by three different regimes of obstacle spacing, as discussed by Grimmond and Oke (1999), Oke (1987), and Robins and Macdonald (1999). The three regimes (isolated, wake interference, and skimming) are drawn schematically in Figure 4 and are seen to be determined primarily by the ratio of building or obstacle spacing, S_x, to building or obstacle height, H_r. The ratio S_x/H_r can be used to draw the boundaries between the regimes, which are based on the fact that the wake or recirculating cavity behind an obstacle has length about 3 to 5 H_r (Hosker, 1984). Figure 4 also shows that the regime boundaries are weak functions of the ratio of obstacle width, W, to height, H_r, since the length of the wake is observed to be slightly larger for obstacles with large W/H_r.

In general, if the obstacles are spaced more than 3 to 5 H_r apart, the wake from one obstacle will not interact significantly with the next downstream obstacle, and we have the "isolated obstacle" regime. At the extreme where the obstacles are spaced very far apart (say 100 H_r),

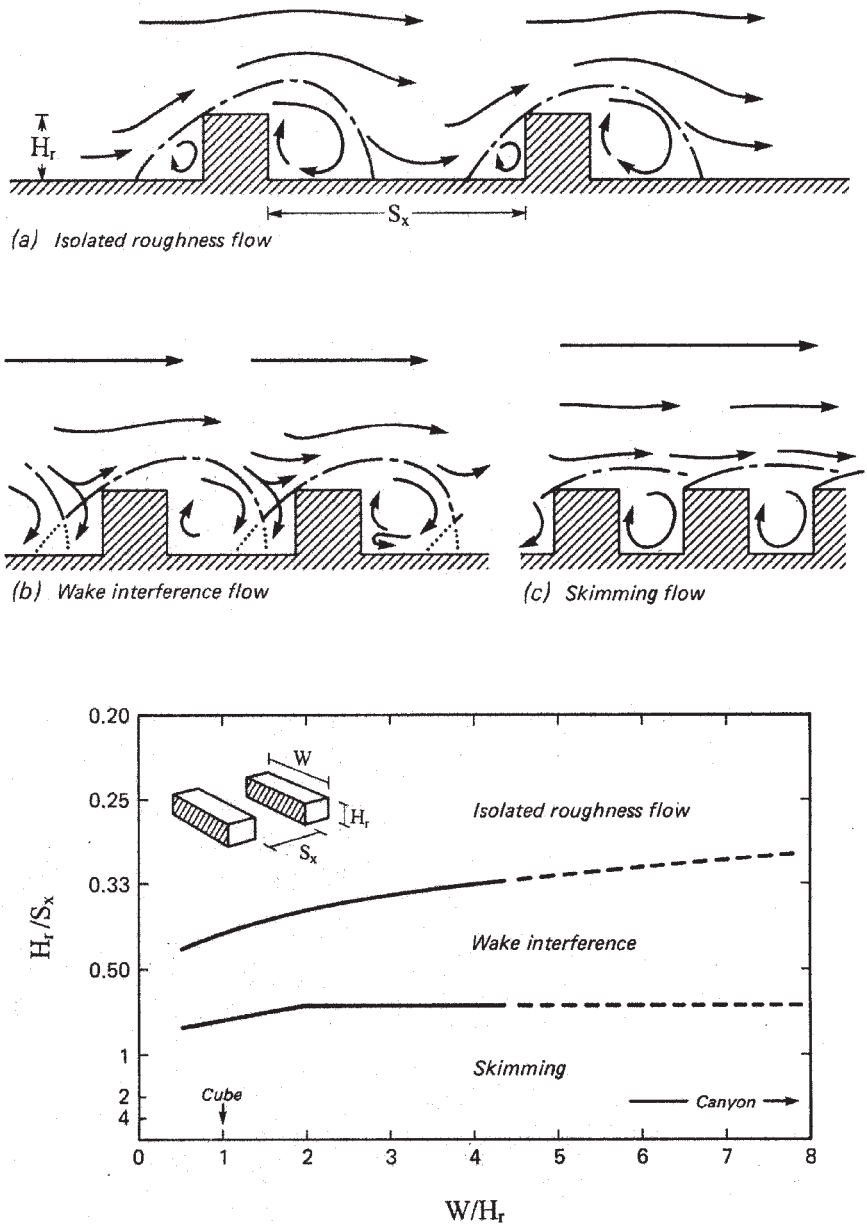

FIGURE 4. Schematic diagram from Oke (1987, with kind permission from Elsevier) showing the three regimes of flow over an obstacle array, the main flow features associated with each, and the ranges of inverse relative obstacle spacing, H_r/S_x, and relative obstacle width, W/H_r, to which each regime applies.

then the roughness is determined more by the ground surface between the obstacles rather than by the obstacles themselves.

If the obstacles are spaced about 1 to 3 H_r apart, then the wake from one obstacle will interact strongly with the next downstream obstacle. This is the "wake interference" regime and usually leads to the largest surface roughness for a given H_r.

If the obstacles are spaced less than about 1 H_r apart and the obstacles all have the same height, then there is so little space between the obstacles that the flow passes mostly over the obstacles, leading to the "skimming flow" regime. At the extreme where obstacle spacing approaches zero, and obstacle heights are all the same and have smooth roofs, a "new" surface will have been generated at height H_r and the roughness and flow will be a function only of the roughness of the flat tops (roofs) of the obstacles. This concept of a skimming flow is applicable only in limited situations in wind tunnel and small-scale field studies using uniform-shaped artificial cubes, which do have smooth tops. As Hall et al. (1997) point out, for real urban and industrial areas, the skimming flow will not be set up because the obstacles will not all have the same height. In fact, Hall et al. (1997) and Ratti et al. (2001) suggest that the typical standard deviation of the obstacle heights, σ_{H_r}, is about the same magnitude as the average H_r. In a comparison of five cities by Ratti et al. (2001), it was found that the ratio σ_{H_r}/H_r varied from 0.23 for a section of Berlin to 1.0 for a section of Los Angeles.

The observed wind profiles from the ground level up to and slightly above H_r exhibit variability because any single measurement location is influenced by peculiarities of flow around nearby obstacle corners and gaps between the obstacles. Figure 5 presents some examples of observed wind profiles in and above (i.e., $0 < z/H_r < 2$) seven different types of obstacles, most of which are vegetative canopies (Raupach et al., 1996). The wind speeds are normalized by the wind speed at H_r, or $u(H_r)$. It is seen that, in most cases, the wind speed, u, below about 0.5 H_r is nearly constant, with values ranging from about 0.1 to about 0.5 $u(H_r)$. The smallest wind speed ratios occur for the densest obstacle canopies (i.e., corn).

Sections 3.3 and 3.4 describe the flow above the obstacles and the flow below the obstacles, respectively. In each section formulas are suggested for the height regime of interest, and transition or blending formulas are suggested for extrapolating to the other regime.

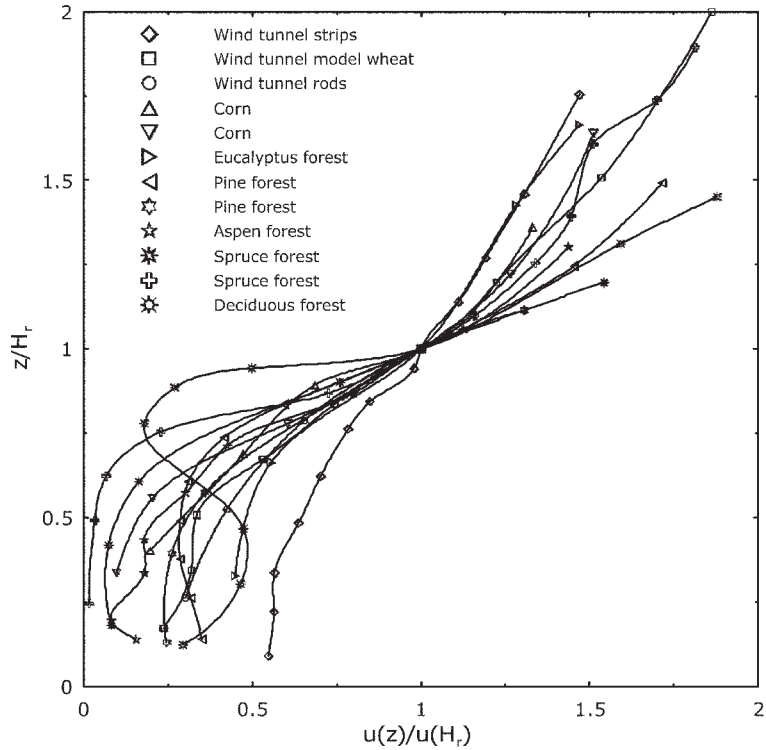

FIGURE 5. Observations of vertical profiles of normalized wind speed, $u(z)/u(H_r)$, through and above 12 real and simulated vegetative canopies, for wind-tunnel and atmospheric field data. From Raupach et al. (1996, with kind permission from Kluwer).

3.3. Flow above the Surface Roughness Obstacles

By definition, the logarithmic wind profile formula [Eq. (2b)] provides a solution (i.e., nonnegative wind speed estimates) at heights greater than $d + z_o$. The upper height limit for the formula is defined by the depth of the surface boundary layer, which is typically about 50 to 100 m. Since, as a rough approximation, $d \approx 0.5\ H_r$ and $z_o \approx 0.1\ H_r$, then it is clear that Eq. (2b) will give positive u values down to heights of about $0.6\ H_r$. However, as illustrated by the Kit Fox wind observations for Tower 4 in Figure 3, observed wind profiles at urban and industrial sites generally show departure from the logarithmic solution at heights less than about $1.5\ H_r$ to $2.0\ H_r$, due to the local effects of flows around individual obstacles. This section presents some approaches to estimation of flow near and above H_r.

3.3.1. Definition of Surface Roughness Length, z_o, and Displacement Length, d, as They Relate to Flow Characteristics Such as Wind Speed

Despite the fact that z_o is a key input required by state-of-the-art dispersion models such as AERMOD and ADMS (for neutrally buoyant gases) and DEGADIS and HEGADAS (for dense gases), z_o is not a tangible length that can be seen in the laboratory or the field or measured by a "z_o-meter-stick." Dispersion models do not usually require input of d, since it becomes important primarily for situations with densely packed obstacle arrays, such as urban areas and forested areas, and at heights less than about 2 H_r. The scaling lengths z_o and d exist only as constants within the context of Eq. (2b), as described in fundamental textbooks such as Arya (1999), Garratt (1992), Pasquill and Smith (1983), and Stull (1997).

The textbooks suggest that Eq. (2b) is valid for neutral boundary layers (i.e., the effects of boundary layer stability are ignored for the purposes of this section) at heights up to about 50 or 100 m, or for stable or unstable boundary layers as long as the height, z, is less than about 5 or 10 m. At heights above about 50 or 100 m, the wind speed gradually departs from the logarithmic formula and approaches the free stream or geostrophic wind speed, G, at a height of a few hundred meters (see Figure 1). The fundamental textbooks also point out that an additional limitation on Eq. (2b) is that it is valid only for elevations several times greater than the roughness obstacle height, H_r. However, we will present evidence and other references that support use of Eq. (2b) at heights down to about H_r.

Because of the 50 to 100 m height of the surface boundary layer, the z_o and d approach is most valid for obstacle heights less than about half of the surface boundary layer height, or about 25 to 50 m. Consequently these methods and z_o estimates are less useful for very tall buildings (skyscrapers) in downtown areas of cites such as New York, Chicago, or Atlanta, where H_r is greater than 20 or 30 m. In some of those applications the approach flow is deflected around the closely grouped tall buildings.

The scaling lengths z_o and d can be estimated in several ways, including use of wind speed vertical profile observations, use of obstacle size and shape (morphology), and use of land-use characterization. Specific recommendations are given in Section 3.5. This section focuses on the use of wind speed profiles.

Many books and papers exist that discuss the best way of estimating z_o and d using observations of wind speed at several levels on a meteorological tower (e.g., Businger, 1975; Garratt, 1992; Grimmond et al., 1998; Kondo and Yamazawa 1988; Lo, 1990; Stull, 1997; Weiringa, 1993). Typically a straight line is "best fit" through the points on a u versus $\ln(z-d)$ plot and z_o is then the value where the wind speed u would become zero on this best-fit line. Figure 1 gave several examples of straight lines for various z_o values, where it was assumed, as in Eq. (2a), that $d = 0.0$. Because there are two free parameters (z_o and d) in Eq. (2b), some iteration or optimization is usually required in order to select values that best fit the data. This would be the case for the observed wind profile for Tower 4 in Figure 3, where the line could be "straightened" by choosing an optimum value of d and then replotting the wind observations versus $\ln(z-d)$. However, this method can be uncertain and is dependent on the exact steps taken.

The z_o values estimated separately from concurrent wind, temperature, and water vapor profile observations on the same meteorological tower are usually different (Weiringa, 1993). In the case of temperature, T, and water vapor content, q, the values of $(T - T_o)$ or $(q - q_o)$ are plotted versus $\ln z$, where the subscript o indicates the observation at the lowest level of the tower, very near the ground. There are rational physical reasons for these differences. For our current purposes, however, we focus only on the wind profile observations, since they are more likely to be available, and since they allow a key model variable, u^*, to be estimated from the slope of the wind profile.

As it affects our study, the atmospheric wind field is a rough-walled boundary layer (atmospheric stability aside), for which Eq. (2b) is valid. We typically use this equation by inputting wind speed u observed at a given height, z (e.g., 2 or 10 m). With u given, increasing the "roughness" of the surface does two things: (1) it increases the surface stress, $\tau_o = \rho u^{*2}$ (this is intuitively obvious); and (2) it also increases z_o and d, which is a little less obvious since z_o and d are really just integration constants. The point is, of course, that u^* and the scaling lengths, z_o and d, are interlinked. Assuming u is given at 10 m in Eq. (7), the following expression is obtained:

$$z_o/(10\text{ m} - d) = \exp(-0.4u_{10m}/u^*) \qquad (12)$$

where heights are in meters and von Karman's constant has been assumed to equal 0.4. As stated in Section 2.4, z_o and d are just another

way of writing u^*/u. The friction velocity, u^*, is the more physically relevant variable and engineers are far more used to $\frac{1}{2}(u^*/u_{ref})^2$, which is a nondimensional shear stress, or local drag coefficient or skin friction coefficient, and these are traditionally tabulated in terms of the "surface roughness." Thus z_o and d are convenient but are not physically relevant or transparent variables. However there is a clear link with the engineering concepts of shear stress or drag coefficient.

As seen in Figure 5, agricultural meteorologists have found that the displacement length, d, is important for crops (e.g., corn and wheat) and for forests, where the roughness obstacles are closely spaced (e.g., de Bruin and Moore 1985; Garratt ,1977; Jackson, 1981; Raupach et al., 1980). These researchers found that d had to be included in the analysis in order to explain wind profile observations at heights less than about 2 H_r. Typically it is found that d is about 0.5 or 0.7 H_r for crops and forests. The displacement length may also be important for many urban areas where buildings are located adjacent to each other with narrow streets.

The values of z_o and d that would result from several alternate arrays of cylindrical obstacles were studied in a wind tunnel by Raupach et al. (1980). The observed normalized wind profiles, u/u^*, are plotted versus $\ln(z - d)$ in Figure 6, where the letters B through F represent different experimental arrays with progressively denser packing of the obstacles. The displacement length, d, is found to equal 0.17 H_r, 0.33 H_r, 0.5 H_r, 0.67 H_r, and 0.83 H_r for cases B through F, respectively. The point of the figure is that the lines are straight at heights above z_w, which represents the lower level of applicability of Eq. (2b). Below z_w is the "roughness sublayer" where the flow is influenced by the obstacle wakes and where the wind profile "flattens out." The shaded areas indicate uncertainty concerning whether the measurement point is behind an obstacle or between two obstacles. However, as emphasized in Section 3.4, the straight line can be extrapolated downward to H_r and below with errors of less than a factor of two.

3.3.2. Methods for Estimating z_o and d from Wind Observations

The application of the logarithmic wind speed Eq. (2b) is discussed for the case of straightforward boundary layers. The various methods of fitting a straight line to the wind speed observations are briefly reviewed

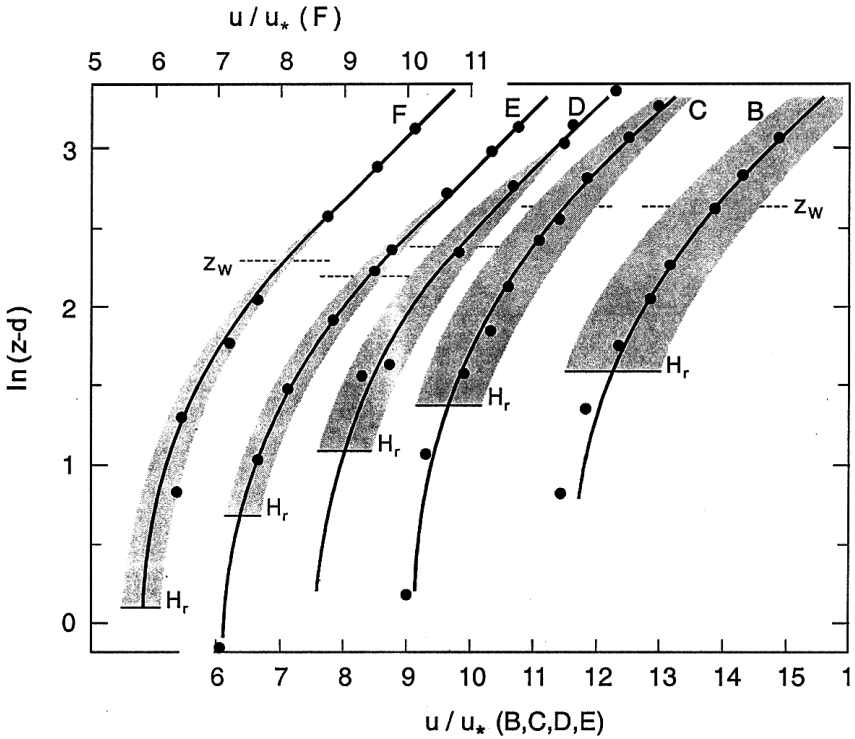

FIGURE 6. Average surface-layer normalized wind speed, u/u^*, profiles observed in a wind tunnel and predicted by Raupach et al. (1980, with kind permission from Kluwer) using a theory that accounts for the effects of the obstacle wakes at small heights. The axes are staggered for clarity. The points represent the observations and the lines represent the model predictions. The shaded areas represent uncertainties due to horizontal inhomogeneities in the obstacle wakes. The obstacle heights, H_r, and the estimated tops of the roughness sublayer, z_w, are marked. The categories B through F represent progressively denser packing of obstacles.

and examples presented of field observations of wind flows over a variety of urban and industrial surfaces.

As mentioned earlier, a problem occurs when trying to "best-fit" a straight line through wind profile observations because there are two free parameters (z_o and d). Researchers such as Stull (1997) and Garratt (1992) point out that there is much leeway and freedom of interpretation in this activity, especially if the data are limited (e.g., only two measurement levels on a tower) and if there are instrument uncertainties, internal boundary layers, and other problems.

There are about ten or more alternate methods proposed by different researchers for estimating z_o and d based on observations of winds

and temperatures at two or more levels on a meteorological tower. Many of these methods are reviewed by Petersen (1997), Macdonald et al. (1998), and Grimmond et al. (1998). The Grimmond et al. (1998) paper includes many examples of applications to urban and industrial areas, and will be used as a basis for most of our discussions. For simplicity, we assume here that the atmosphere is nearly neutral. Non-neutral boundary layers over rough urban surfaces are described by Hanna and Chang (1992).

The z_o and d estimation methods are usually computerized so that many data can be efficiently analyzed. In most methods, the goal is to select values of z_o and d that produce the minimum mean-square-error when comparing observed wind speeds with the "predicted" wind speeds given by the solution to Eq. (2b). Of course it is also possible for an experienced boundary layer meteorologist to look at the plotted profiles and adjust d values until the profiles appear to follow a straight line.

Whether the z_o and d estimates are made by computer or by eye, there is a need to decide what to do about outliers at elevations above about 2 H_r where a straight line is expected. For example, if there are four levels (z = 5 m, 10 m, 15 m, and 20 m) of wind observations and the observation at the 15 m level is always about 30% lower than expected after plotting the data as ln z versus u, the analyst may discard the data from that level. It is also necessary to decide whether the supposed outliers may in fact be valid points in equilibrium with another roughness surface some distance upwind (see Figure 2, which illustrates the concept of internal boundary layers). In the latter case, there may be a kink or bend in the plotted wind profile, with the lower points following a straight line representing the roughness length close to the meteorological tower and the upper points following another straight line representing the roughness length farther away. In addition, for measurement heights less than about 2 H_r, there is a need to decide how low to go before it can be assumed that the measurement is in the roughness sublayer (see Figures 3, 5, and 6).

As an alternative to the wind profile method of estimating z_o and d, some investigators use observations of the standard deviation of the along-wind horizontal component of the turbulent velocity, σ_u. It is well demonstrated that, for hourly average wind speed observations during neutral conditions, σ_u equals about 2.4 u^*, as suggested by Stull (1997) for generalized atmospheric boundary layers and as verified by

Roth (2000) for urban areas. Then, given an observation of σ_u and of wind speed, u, at a height z, it can be assumed that $u^* = \sigma_u/2.4$ and Eq. (2b) can used to estimate z_o and d. Of course, we again have the problem that several combinations of z_o and d will give the same σ_u and u^*. Therefore it is necessary to use data from many hours and days of observations to optimize the values of z_o and d.

Much research has been carried out concerning the ground surface area that is likely to have influenced a wind measurement or a σ_u observation at a given elevation, z, for a given wind direction and stability. This is because it is not the ground surface directly below the instrument that influences the boundary layer observations at the instrument height. Schmid (1994) presents a formula that suggests that, for neutral stability, the wind at elevation z is influenced by the ground surface in a plume-shaped upwind sector with maximum influence about 10 to 100 z upwind of the instrument. This concept will be described in more detail in Section 3.3.3.

The reader may be getting the idea from these discussions that there are uncertainties in the estimation of z_o and d from wind or σ_u observations at several levels on a meteorological tower in the field. This is indeed the case, which is why there is often a preference for the more robust methods based on the size and geometric shape of the obstacles, as described in Section 3.3.4. These geometric methods are known as morphological methods.

More than 50 studies that included observations of vertical wind profiles on tall towers over cities and neighboring commercial and industrial sites were studied by Grimmond et al. (1998). The objective was to use the data from these many sites in order to develop general relationships for estimation of z_o. They applied several criteria, such as uniformity of the site, interference from large upwind obstacles, elevation of the instruments above the obstacles, and instrument characteristics, in order to narrow the field down to data sets from Chicago, Los Angeles, Miami, and Vancouver. Table 2 lists the data sets from these four cities selected for analysis and includes information such as the heights of the wind sensors, the numbers of data points, and the averaging times. Note that the heights of the wind sensors range from 22 m to 70 m, which in all cases are at least two times higher than H_r. Table 3 contains the results of analysis of the observations from the four cities, including estimates of z_o and d . H_r is given in the table and ranges from 6.9 to 17.9 m. Obstacle morphology (i.e., geometry) parameters, λ_f and

TABLE 2
Location of Study Sites, Sensor Heights (z_s), and Ratio of Sensor Height to Roughness Obstacle Height (H_r)[a]

	Chicago, IL (41° 57' N, 87° 48' W)					Arcadia, Los Angeles, CA (34° 08' N, 118° 3' W)		Miami, FL (25° 44' N, 80° 22' W)	Vancouver, B.C. (49° 15' N, 123°04' W)
Code	C92w	C92w	C92w	C92w	C95u	A94w	A94	Mi95	Vs89
z_s (m)	24.6–69.5	24.6	43.1	69.5	27.0	32.8	32.8	40.8	22.5
$z_{s\,max}/z_{s\,min}$	2.8	na	na	na	na	na	na	na	na
z_s/H_r	3.1–8.7	3.1	5.4	8.7	3.1	2.8	3.2	5.9	3.8
Directions included (°)	150–210 270–90	0-90 150–360	0–210 270–360	0–90 150–360	0–20 75–360	0–150 (L)[1] 165–360 (L) 0–150 (I)[2] 220–360 (I)	0–40 70–110 130–360	60–210	135–304
N neutral[3]			2544		44	1950	3	63	2
N unstable[4]	na	na	na	na	v[5]	na	v	v	35
Averaging period (min)	15	15	15	15	30	15	30	30	60

[a]*Source*: Grimmond et al. (1998, with permission of Kluwer). Wind directions included are those without instrument or tower interference.
[1](L) Acceptable wind conditions for long term observations.
[2](I) Acceptable wind conditions for intensive observations.
[3]N neutral: Number of data points
[4]N unstable: Number of data points used in Tv method.
[5]v number of hours varied depending on criteria evaluated (no results reported here).

λ_p, are also given, and will be discussed further in Section 3.3.4. For some sites, different values are given by season and by wind direction sector. Usually the wind direction sectors are about 30 degrees or larger. It is interesting that nearly all z_o estimates are in the range from 0.2 m to 2.0 m and nearly all d estimates are in the range from 3 m to 5 m. Therefore, based on the averages of the results in Table 3, if there is no other information available, a good estimate of z_o in an urban area would be about 1 m.

Similarly, a good estimate of d would be about 4 m. These values correspond to a ratio z_o/H_r of about 0.1 and a ratio d/H_r of about 0.4, in agreement with rough estimates described in textbooks and handbooks.

Because the rate of dispersion of a pollutant cloud is proportional to the turbulent velocity components σ_u, σ_v, σ_w, there has been much interest in observations of these turbulent velocity components over urban, suburban, commercial, and industrial surfaces. For example, Figure 7 shows the results of an extensive measurement program in the St. Louis area, as reported by Clarke et al. (1978). The diurnal variations in observed lateral turbulence, σ_v, and vertical turbulence, σ_w, are plotted separately for residential, commercial, and rural surfaces. It is seen that, during the night, the turbulence over the residential and commercial surfaces is about two times the magnitude of that over the rural surface. During the day, the difference is less, about 20 or 30%. These diurnal differences are expected, because at night the roughness obstacles not only generate more turbulence but also force the atmosphere to be less stable. In addition, at night there is heat added to the atmosphere by man's activities.

A comprehensive analysis of turbulence data from eight urban field studies is presented by Roth (2000). He used only those data that satisfied stringent criteria similar to those used by Grimmond et al. (1998); for example, the measurement height had to be above about 2 H_r so that the data were minimally influenced by nearby obstacles. Also, it was desirable that the stability be nearly neutral. The results are listed in Table 4, which gives the city name, the ratio z_s/H_r, and the observed ratios of the turbulent velocity components to u^*. The most interesting result is that the average observed urban turbulent velocity ratios are consistent with the ratios reported in fundamental references for general types of rural surfaces, including flat grassland. This means that the boundary layer over surfaces with large obstacles, such as urban areas

TABLE 3. Summary of z_o and d Values for Each Study Site (See Table 2)[a]

Site	Land cover	Density Classes	Direc tions	Obs. Level (m)	λ_f	λ_p	H_r (m)	z_0 (m) Summer Mean	Summer s.d	Summer Median	Fall Mean	Winter Mean	Spring Mean	Number of observations Summer	Fall	Winter	Spring
A94w	R	Med	190-320	32.8	0.31	0.52	11.7	1.02	1.13	0.63	0.94	0.89					
A94	R	Med	190-320	32.8	0.31	0.52	10.3	0.72		1.02							
C92w	R	Med	110-180	43.1	0.27	0.44	8.0	0.57	0.73	0.38	0.66	0.47	0.61				
C92w	R	Med	150-180	69.5	0.26	0.45	7.9	0.45	0.75	0.21	0.52	0.37	0.44				
C95u	R	Med	200-360	27.0	0.33	0.44	8.0	1.32	0.45	1.32							
Mi95	R	Low	60-195	40.8	0.18	0.41	6.9	0.46	0.60	0.30							
Vs89	R	Low	281	22.5	0.19	0.42	8.7	0.60		0.60							
C92w	CR	Med	180-250	24.6	0.27	0.47	7.8	0.50	0.33	0.43	0.48	0.45					
C92w	CR	Low/Med	180-210, 270-60	43.1	0.24	0.45	7.9	0.79	0.97	0.59	0.67	0.51	0.62	507	171	1195	174
C92w	CR	Low/Med	180-60	69.5	0.25	0.41	8.7	0.81	0.77	0.50	0.72	0.44	0.67				
C92w	C	Low	250-60	24.6	0.20	0.50	7.4	0.56	0.55	0.44	0.50	0.38	0.47				
C92w	I	Low	60-110	43.1	0.16	0.41	8.6	0.61	0.86	0.30		0.40	0.77				
C92w	I	Low	60-110	69.5	0.20	0.43	8.7	1.09	1.34	0.62							
A94w	P	High	15-75	32.8	0.27	0.52	17.9				1.46	2.23					
C95u	G	Low	0-20	27.0	0.18	0.45	8.7	2.04		2.0							
C92w	R	Med	150-180	24.6-69.5	0.26	0.45	7.9	4.62	1.48	4.45	5.34	4.48	4.33	124	27	108	39
Vs89	R	Low	135-304	22.5	0.18	0.36	8.5	4.5									
C92w	CR	Low	180-210, 270-60	24.6-69.5	0.23	0.46	7.9	3.73	1.55	3.05	3.88	3.77	3.43	403	137	966	137
C92w	I	Low	60-90	24.6-69.5	0.17	0.41	8.6	3.05	1.35	2.46				39			

[a]Organized by land cover (R, Residential; CR, Commercial with Residential; C, Commercial; I, Institutional; P, Urban Park with Trees; G, Urban Park with Few Trees). "Density Classes" refer to the building densities. "Obs. Level" refers to the height of the wind instrument. Surface attributes are for the summer measurement periods except for A94wp, where winter values are reported. (From Grimmond et al., 1998, with permission of Kluwer).

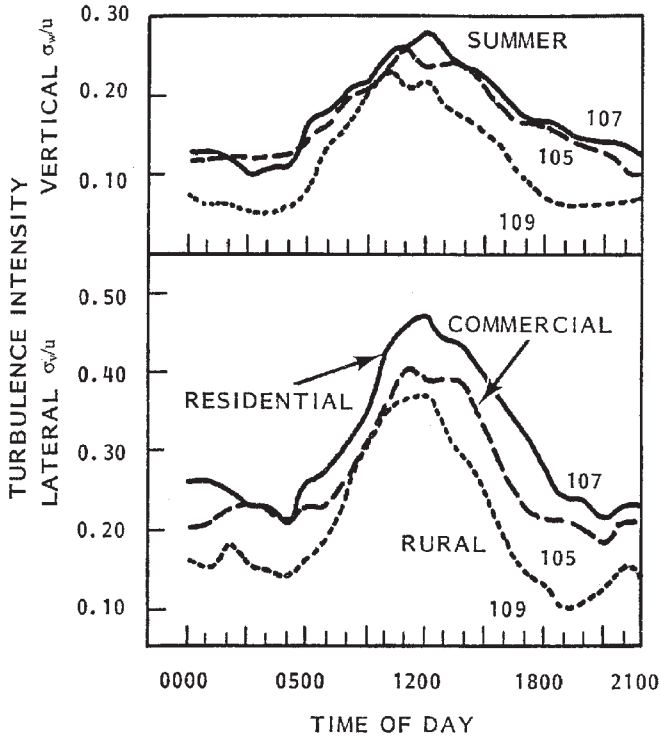

FIGURE 7. Diurnal variation of observed hourly averaged vertical (upper) and lateral (lower) turbulence intensities (σ_w/u and σ_v/u, respectively) at three sites during the summer in St. Louis at a height of 30 m. The three sites are: 105, commercial; 107, residential; and 109, rural. (From Clarke et al., 1978, with permission of the editor, S.-E. Gryning.)

and commercial or industrial areas, satisfies general similarity relations thought to be valid for the atmospheric boundary layer:

$$\sigma_u/u^* = 2.4 \qquad \sigma_v/u^* = 1.9 \qquad \sigma_w/u^* = 1.25 \tag{13}$$

The evidence therefore justifies the use of standard Monin–Obukhov similarity relations over urban and industrial sites. At heights less than H_r, there may be departures from these general similarity relations due to the proximity to individual roughness obstacles.

For given free-stream or geostrophic wind speed at the top of the boundary layer, u^* is a function of atmospheric stability as well as z_o and d. Generally, the greater the stability at night, the smaller u^* will be. The greater the instability during the day, the larger u^* will be. This dependence is known (e.g., Hanna et al., 1982; Stull 1997) and the calculations described above can be similarly performed for nonneutral

TABLE 4

Summary of Observed Ratios of Turbulent Velocity Components to u^* for Neutral Stability from Selected Urban Field Studies and Reference Results[a]

City	z_s/H_r	σ_u/u^*	σ_v/u^*	σ_w/u^*
Nantes	2.05	2.15	1.63	1.04
	3.05	2.21	1.69	
	4.05	2.23	1.67	1.14
	5.05	2.28	1.72	
	5.55	2.30	1.72	
	6.05	2.28	1.70	1.2
St. Louis	2.79	2.19	1.72	1.28
	3.20	2.39	1.78	1.17
	3.20	2.39	1.74	1.20
	5.64	2.41	1.78	1.29
	5.64	2.36	1.81	1.32
Uppsala	2.08	2.51	2.10	1.45
	6.25	2.80	2.40	1.35
Worcester	2.08	2.23	1.77	1.06
	2.13	2.43	2.20	1.19
	2.42	2.76	2.01	1.19
	2.42	2.91	2.32	1.17
	2.48	2.73	2.47	1.15
	2.50	3.08	2.30	1.28
Zurich	0.71		2.21	2.45
	0.91		1.91	1.39
	1.35		2.01	1.19
	1.65		1.40	0.95
	1.50	2.35		
Vancouver	2.62	2.20	1.70	1.20
Sapporo	0.77	2.13	2.04	1.28
	1.47	2.33	1.83	1.17
	2.57	2.15	2.08	1.27
Basel	1.50	2.48	1.96	1.37
	2.08	2.24	1.71	1.27
	3.17	2.27	1.78	1.35
Urban averages	$z_s/H_r > 0.7$	2.40±0.25	1.91±0.26	1.27±0.26
	$z_s/H_r > 2.5$	2.32±0.16	1.81±0.20	1.25±0.07
	$z_s/H_r \leq 2.5$	2.49±0.30	1.99±0.28	1.29±0.34
	Rural	2.50	1.90	1.25
	references	2.39±0.03	1.92±0.05	1.25±0.03

[a]Sensor heights are denoted by z_s and obstacle heights are H_r. The table is adapted from Roth (2000, with permission of the Royal Meteorological Society).

conditions. However, our emphasis in the current book is on neutral conditions because of the following three key points:

1. This book is primarily concerned with estimation of u^* based on observations of u near the ground.
2. The boundary layer is nearly neutral as the ground surface is approached.
3. Mechanical turbulence is relatively strong over urban and industrial sites.

3.3.3. Size of Surface Area That Influences Flow at a Given Height

Industrial and urban sites are characterized by different types of terrain in different directions and at different distances from potential hazardous gas source positions. For example, looking in one direction from the source position, the closest 200 m may be covered by structures, the next 200 m may be covered by a flat parking lot, and the next 200 m may be covered by a recreational field. Because many industries and urban areas are located on rivers and bays, water may comprise a large fraction of the area for which the surface roughness length must be estimated. Therefore different surface roughness lengths may need to be specified for the different wind sectors and different downwind source-receptor combinations.

There is always a concern about how large a spatial domain is needed to generate an equilibrium boundary layer. A 10-m-wide patch of flat parking lot does not impose its roughness characteristics on the entire area. Similarly, two tall buildings do not cause an equilibrium boundary layer to form. Usually a spatial domain of 100 m or more, and a total of at least 20 or 30 roughness obstacles, are needed to establish a roughness length and wind profile up to a height of about 10 m or more. In the worked example in Case 1 in Section 5.1, it will be shown that a small industrial processing plant, with width 24 m and with H_r of 2.9 m, is not sufficiently large to generate an equilibrium boundary layer of depth greater than H_r. Because of the need to have an equilibrium boundary layer, the roughness length, z_o, the displacement length, d, and the friction velocity, u^*, represent averages over some spatial extent. This question has been investigated by theoretical analyses and by experimental programs for several years, with most of the recent interest generated by the need for more precise estimates of surface fluxes for use in climate-change models.

The effective roughness length over terrain which consists of well-defined repeating patches of two different roughness surfaces was studied by Goode and Belcher (1999). They define the "blending height" as the top of the highest extent of the internal boundary layers from individual obstacles, above which the flow is "fully adjusted" to the combined roughnesses. In one of their numerical modeling tests, where the roughness patches alternated every 50 m with values of z_o = 0.004 m (typical of mowed grass) and z_o = 0.4 m (typical of small trees, brush, or a group of four meter high industrial or residential buildings), it was found that wind speed perturbations of as much as 20% occur at heights of 3 m. Slower wind speeds were found over the rough surface, as expected. At heights of 10 m or above, the wind speed perturbation was calculated to be less than 1%, implying that the blending height or the top of the internal boundary layer was at a height of about 10 m for this combination of roughness lengths and other conditions. The authors list a few alternate averaging formulas for heterogeneous ground surfaces, such as taking the geometric mean of the z_o values for the various patches. With this method, further weighting may be applied using the x distance covered by each roughness patch. The goal is to determine a representative average z_o that produces the observed average u^* value (i.e., the observed average surface stress) at a height above the blending height. This general approach is followed in our recommendation given later in Section 3.3.6, and will be used in worked examples 5, 6, and 7 (see Sections 5.5, 5.6, and 5.7).

Another view of the question is the "source area" or "source footprint" concept studied by Schmid (1994) and by Horst and Weil (1992, 1994). These researchers are interested in the location of the ground surface area that most strongly influences the observed wind speed, turbulence, and/or momentum flux at a height, z_m, on a meteorological tower. As mentioned earlier, the measurement is most influenced by the characteristics of the ground at some distance upwind of the instrument. The source area or footprint may be determined by considering that momentum is dispersed in the boundary layer in a manner very similar to the way a pollutant material is dispersed. Therefore if a source of pollutant exists at a certain point on the ground, then, at a distance, x_m, downwind, the mass-mean elevation of the pollutant will be at a height, z_m. It follows that an instrument at that height, z_m, on a tower will observe pollutant that originated at a distance, x_m, upwind of the tower. This concept is illustrated in Figure 8, which shows that the

observation at height z_m is influenced by an area centered on the distance, x_m, but having lesser weights at distances beyond and closer than x_m, and at either side of x_m. The weighting factor f describes the relative influence, at a given location, of the ground area on the observation at the sensor and is derived from momentum transport theory. On the figure, the source area, Ω_P, is defined as the area where f exceeds f_P. The distance, x_m, is found to be lesser for unstable daytime conditions and greater for stable nighttime conditions, and averages about 10 to 100 z_m for neutral conditions. For example, if an anemometer is located at a height of 20 m on a meteorological tower within an industrial plant, it will be responding to surface conditions centered at a distance of about 200 to 2000 m upwind of the tower. The Schmid method has been used by Grimmond et al. (1998) to estimate the land-use or surface roughness type that most influences the wind measurements on towers in urban areas, and the results were shown in Tables 2 and 3.

For the purposes of this book, we are more interested in the roughness of the areas downwind of the source point, rather than upwind of

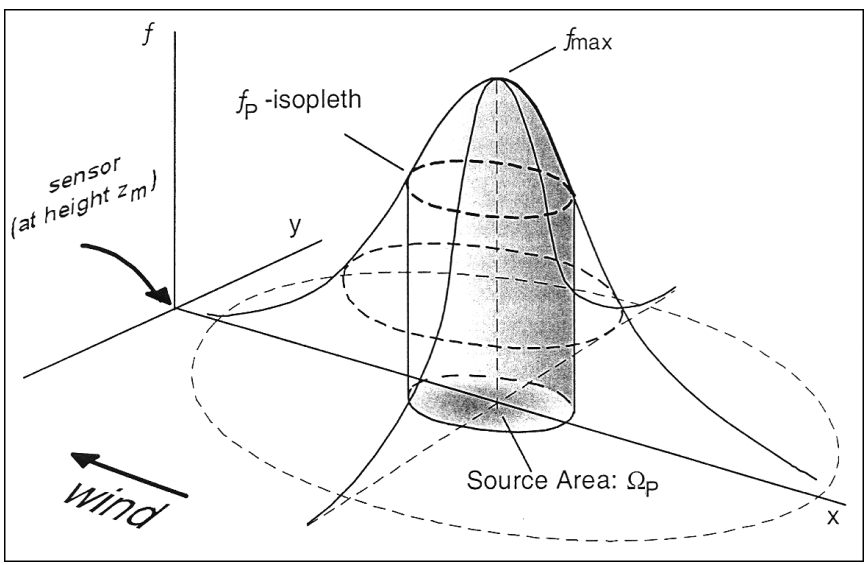

FIGURE 8. Schematic illustration of the surface source area that affects the wind measurements at the sensor at height z_m at the left side of the figure. The source weight function, f, describes the relative influence of the surface roughness at a specific location on the wind measurements at the sensor height. x is the along-wind distance and y is the crosswind distance. The surface roughness obstacles near the point where f_{max} occurs have the largest influence on the wind measurements at the sensor. The source area, Ω_P, defines the area where f exceeds f_P. From Schmid (1994, with kind permission from Kluwer).

the source. The hazardous cloud trajectory will naturally be along the downwind direction. This perception of the area of influence is 180 degrees opposite to the concept discussed by Schmid (1994) and shown in Figure 8, where the interest is in the ground surface area that most influences the wind observation at a given location. Nevertheless, the same figure would apply to the transport and dispersion analysis, except with the gas source height at z_s and the coordinate system turned in the downwind direction.

The methods described above are of most use to persons desiring very precise observations of surface fluxes and other boundary layer parameters. In the current method, we are interested in more pragmatic methods, such as simple geometric weighting of the roughnesses over two or three zones within the region of interest (discussed later in Section 3.3.6).

3.3.4. Estimation of z_o and d Based on Knowledge of Surface Roughness Obstacles' Dimensions and Geometric Relations (the Morphological Method)

Section 3.3.2 presented several ways by which observations of wind speeds and turbulence could be used to calculate z_o and d, and listed some examples of the applications of these methods to data from several urban areas and industrial/commercial areas. Some problems with the approach based on wind speed observations were addressed, such as the effects of spatial variations of the characteristics of the underlying roughness obstacles, the effects of variations in observations at heights less than about 2 H_r, and the ambiguity in calculating the values of z_o and d from observed wind profiles. Nevertheless, many persons have used observations from meteorological towers to calculate z_o and d for surface roughness obstacles such as vegetative canopies and a variety of types of urban and industrial surfaces (e.g., see the results from Grimmond et al., 1998, in Tables 2 and 3).

An alternate and more robust approach to the estimation of z_o and d is based on relations that have been developed between these parameters and the geometrical characteristics of the roughness obstacles. This alternate approach, also called the morphological method, briefly discussed in Section 2.2, does not require an on-site meteorological tower with the need for high-quality instruments and careful placement of the instruments and interpretation of the data. The current section summa-

rizes these geometric methods, gives examples of their use, and suggests simplified formulas.

The reference with the most comprehensive discussion of the morphological method is the paper by Grimmond and Oke (1999). They review and test many alternate methods, including the method used in the Petersen (1997) ROUGH computer program.

Many researchers use the morphological or geometric approach to simplify complex structures for analysis and for calculation of z_o and d. There are a great many references on this topic, covering analysis of data from field and fluid modeling experiments (e.g., Brown 2000; Cionco and Ellefsen, 1998; Counihan, 1971; Grimmond and Oke, 1999; Hanna and Chang, 1992; Kutzbach, 1961; Lettau, 1969; Macdonald et al. 1997, 1998; Marshall, 1971; Petersen, 1997; Petersen and Parce, 1994; Raupach, 1992; Raupach et al., 1980; Wooding et al., 1973). Geometric measures are used such as obstacle height, H_r, the ratio of obstacle plan area to ground area, λ_p, and the ratio of obstacle frontal area (as seen by the wind) to the ground area, λ_f (Grimmond and Oke, 1999). Figure 9, from Grimmond and Oke (1999), contains a schematic diagram of a uniform set of rectangular block-shaped roughness elements and illustrates the various geometric parameters, as defined below:

H_r = height of obstacles
L = along-wind length of obstacle
W = crosswind width of obstacle
S_x = along-wind separation between obstacles
S_y = crosswind separation between obstacles
A_p = horizontal or plan area of obstacle
A_f = vertical cross-section or frontal area of obstacle, facing the wind.
A_T = total lot area of each obstacle
$\lambda_p = A_p/A_T$ = ratio of obstacle plan area to lot area
$\lambda_f = A_f/A_T$ = ratio of obstacle frontal area to lot area

Of course, in a real urban area or industrial site, the obstacles are not all of uniform size and shape, and the above geometric parameters would be defined to represent averages over the area of interest. Furthermore, at a real site with an assortment of obstacle sizes and shapes, an additional parameter, σ_{H_r}, can be defined as the standard deviation of the obstacle heights. It is found that σ_{H_r} is approximately equal to

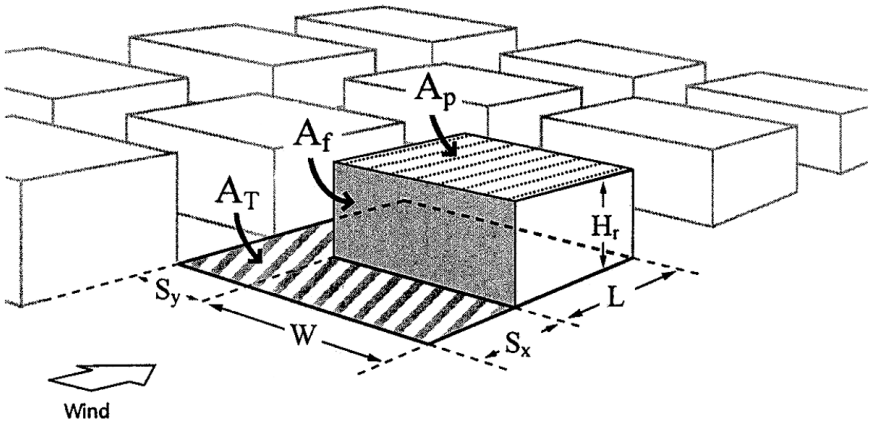

FIGURE 9. Definitions of surface dimensions used in morphometric analysis. The surface roughness obstacle portrayed has the characteristic mean dimensions, spacing, and total lot area (A_T) of the urban or industrial array. All parameters are defined as *averages* over the total domain of the obstacle array. Although drawn as building-like, the roughness obstacle should be considered to be generic, representing all obstacles relevant to the airflow. Similarly, the concept is not limited to a grid array. It could include scattered trees, differently shaped buildings or industrial structures, and winding streets. From Grimmond and Oke (1999), with kind permission of the American Meteorological Society.

about 0.5 to 1.0 times the average obstacle height, H_r, for a range of typical urban areas (Ratti et al., 2001). The averaged values for the above parameters can be estimated by eye by an experienced analyst, can be calculated from simple empirical relations, or can be estimated numerically using software such as the Petersen and Parce (1994) ROUGH program, which uses inputs from detailed plot plans and architectural drawings. Acquiring the data for input to the ROUGH program can be very time-consuming, since a typical urban or industrial site consists of hundreds or even thousands of individual obstacles.

The porosity is another morphological parameter that is sometimes added to the above list. This parameter accounts for the fact that the wind can blow through some types of obstacles such as pipe racks or trees. The parameter is used by the ROUGH program and also enters a few models for flow in the boundary layer over and through obstacle arrays.

The simplest rule of thumb, $z_o = 0.1\ H_r$, mentioned in Pasquill and Smith (1983) and Hanna et al. (1982), averages over the influence of factors such as obstacle shape and spacing.

For typical industrial plants such as large oil refineries, Petersen (1997) suggests that the following relation is valid:

$$z_o = D \lambda_f H_r \tag{14}$$

Lettau (1969) first suggested this relation with a dimensionless constant, D, of 0.5. Note that this relation reduces to the 0.1 H_r relation when λ_f equals 0.2, which is typical of many urban areas and industrial plants. For example, $\lambda_f = 0.25$ for an array of cubes of dimension H_r which are separated by H_r. Equation (14) ignores the ratio of the plan area of the obstacles to the ground area, λ_p, because it is assumed that the drag force of an individual obstacle is primarily determined by its frontal area, A_f. The linear behavior of z_o with λ_f is found to be valid for widely spaced obstacles, with $\lambda_f < 0.2$, which was satisfied in Kutzbach's (1961) and Lettau's (1969) experiments with bushel baskets and Christmas trees. The parameter λ_f is less than about 0.2 at most urban and industrial sites, which tend to have significant separations between obstacles to account for roads, parking lots, loading areas, and other open areas between structures. It is important that the linear equation (14) not be used when $\lambda_f > 0.2$, since it would give large overestimates of z_o.

Some researchers point out that Lettau's (1969) bushel baskets, with smooth rounded edges, would have had drag characteristics that were different from those for buildings or other similar obstacles with sharp corners. It may be necessary to represent the drag coefficient by means of a measure of the sharpness of the edges of the obstacles, because obstacles with sharp edges (e.g., the cubes or rectangles used in many fluid modeling experiments and present at many real industrial and urban sites) can have a drag coefficient and roughness length about two times higher than obstacles with rounded edges. Therefore a value of 0.5 for the dimensionless constant, D, in Eq. (14) may be valid for obstacles with rounded shapes such as oil tanks, but perhaps a value of about 1.0 for D would be more appropriate for objects such as buildings with sharp corners, as seen from the urban observations in Table 3.

The PERF 93-16 dispersion modeling project (Hanna and Steinberg, 2001) provides an example of a situation where the effects of sharp edges on the obstacles cannot be ignored. Typical wind profiles observed over three types of roughness obstacles during the field experiment were plotted in Figure 3. The PERF study used flat rectangular plywood obstacles with sawed edges, for which $\lambda_f = 0.03$ and the Lettau relation [Eq. (14)] would predict a z_o/H_r ratio of only about 0.015,

whereas the actual observed ratio was about 0.07. These flat plywood obstacles (sometimes called "billboards") would represent the extreme in sharp edges, and clearly lead to an implied drag coefficient four or five times larger than that for the bushel baskets.

Wind tunnel and field observations of flow over uniform-sized cubical obstacles were used by Macdonald et al. (1998) to derive a more general relation than that given in Eq. (14). The proposed formulas are intended to be valid over the complete range of λ_p and λ_f, including cases where the obstacles are more densely spaced. For obstacles of rectangular shape, Macdonald et al. (1998) suggest the following relations for displacement length, d, and roughness length, z_o:

$$d/H_r = 1 + K^{-\lambda p}\,(\lambda_p - 1) \tag{15}$$

$$\frac{z_o}{H_r} = \left[1 - \left(\frac{d}{H_r}\right)\right] \exp\left[-\left(0.5\beta \frac{C_D}{\kappa^2}\right)\left(1 - \frac{d}{H_r}\lambda_f\right)^{-1/2}\right] \tag{16}$$

where K is a "constant" that depends on the obstacle geometry and is found to equal about 4 for cubes, C_D is the drag coefficient (equal to about 1.2 for cubes), $\kappa = 0.4$ is the von Karman constant, and β is assumed to equal 1.0 for staggered obstacles and 0.55 for square arrays. Note that K and β have been "tuned" by Macdonald et al. (1998) by fitting curves through their data. Even though data from cubes were used to fit these curves, physical rationale was used by Macdonald et al. (1998) to generalize the relations for rectangular shapes and variable λ_f and λ_p.

Equations (15) and (16) conform to fundamental physical understanding but are also intended to fit Macdonald et al.'s (1998) observations plotted in Figure 10. For example, the differences between the z_o data in the figure for staggered and square arrays is explained by variations in the β factor. In the plot on the left side of the figure, z_o/H_r is seen to increase with λ at first [similar to the Lettau/Petersen linear relation in Eq. (14)], but then reaches a maximum of about 0.15 at λ equal to about 0.2, and then steadily decreases with further increases of obstacle coverage, λ. Note that λ is used in these figures and equations because $\lambda_p = \lambda_f = \lambda$ for the cubes used in these experiments. In the plot on the right side of Figure 10, d/H_r is seen to steadily increase from 0.0 to 1.0 as λ increases from 0.0 to 1.0.

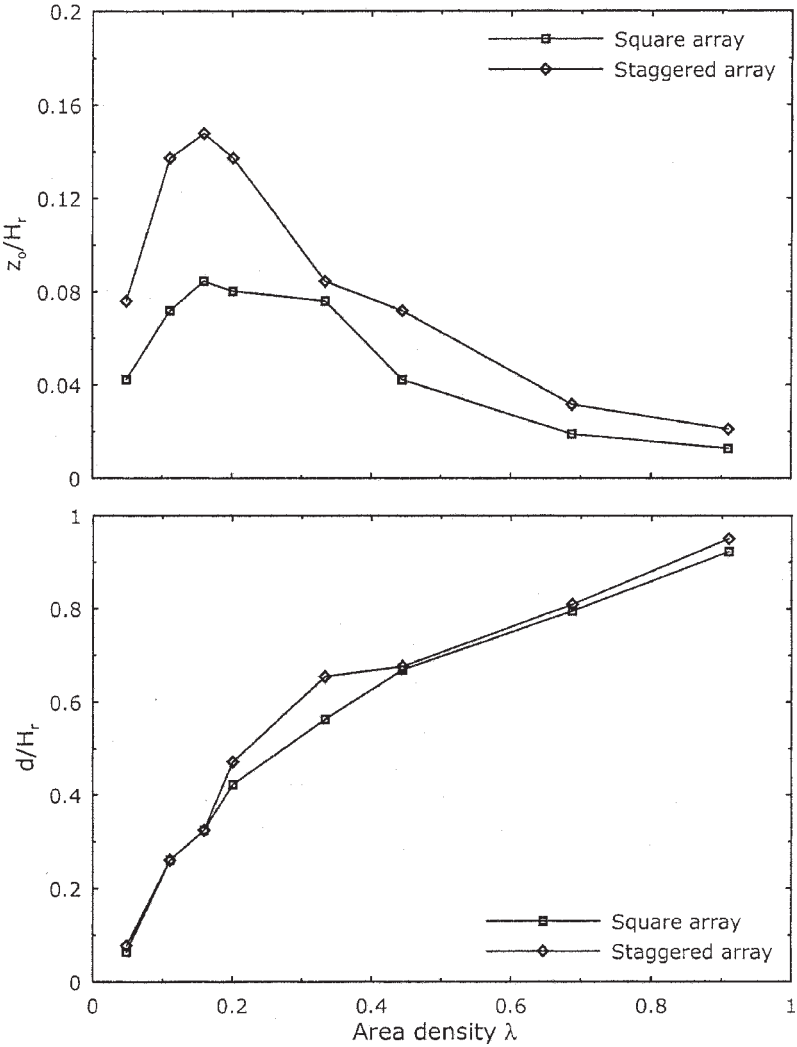

FIGURE 10. Observed variation of z_o/H_r and d/H_r with relative area density (λ) for wind-tunnel arrays of uniform-sized cubical obstacles in square and staggered geometries (data from Hall et al. 1998 and figure from Macdonald et al. 1998, with kind permission of Elsevier).

In this book, we recommend Eqs. (15) and (16) only as an alternate approach, since the equations have so many tuned parameters and since z_o approaches 0.0 at large λ. In the next few pages we recommend a more straightforward set of equations that have the desired feature that z_o remains at about 0.15 even as λ approaches 1.0.

Physical intuition supports the observation that, for uniform cubes with flat tops, there has to be a maximum in z_o/H_r at some intermediate value of obstacle coverage or area density λ. This is seen in the data in Figure 10. As λ increases above about 0.5, the flow slips into the "skimming flow regime" shown in Figure 4, where the cubes are so close together that the flow does not mix as much behind the individual obstacle wakes and therefore the drag or skin friction coefficient and also the z_o are less. Eventually, as the space between the cubes vanishes, a new flat surface is found at a height H_r above the original ground surface. Of course, this ideal flat situation would never occur for real urban and industrial areas, which consist of obstacles with variable heights and shapes, for which σ_{Hr} equals about 0.5 H_r (Ratti et al., 2001). For such real obstacles, the ratio z_o/H_r would be expected to remain at its highest value of about 0.15 as for all λ greater than about 0.2.

Figure 11, from the paper by Grimmond and Oke (1999), has a format similar to Figure 10 but presents a more general conceptual representation of the relations between z_o/H_r and d/H_r and λ_p and λ_f. The small diagrams in the upper left corner of Figure 11 illustrate the three flow regimes (isolated for $\lambda_p < 0.15$, wake for $0.15 < \lambda_p < 0.35$, and skimming for $0.35 < \lambda_p$) shown earlier in Figure 4. Horizontal dotted lines indicate the "average" values of $f_o = z_o/H_r = 0.1$ and $f_d = d/H_r = 0.7$ suggested for urban areas. The shaded areas on the figures indicate the expected ranges of normal variability to be found from one obstacle array or urban or industrial region to another. These shaded areas have been suggested by Grimmond and Oke (1999) on the basis of their experience in this area of research. It is anticipated that, for any theoretical formula, the predicted curves would fall roughly within these shaded areas.

For comparison with the conceptual representation in Figure 11, many sets of observations from wind tunnel or water channel experiments (labeled "model") and field experiments (labeled "field") have been plotted by Grimmond and Oke (1999) in a similar format in Figure 12. The so-called "observations" of z_o and d are based on analysis of vertical profiles of wind or water speed, using methods described in Section 3.3.2. The observed points in Figure 12 are quite scattered, showing that the data points roughly follow the shaded areas in Figure 11, whose bounds are marked by dotted lines in Figure 12. About 80% of the data points are within the areas enclosed by the dotted lines. It is

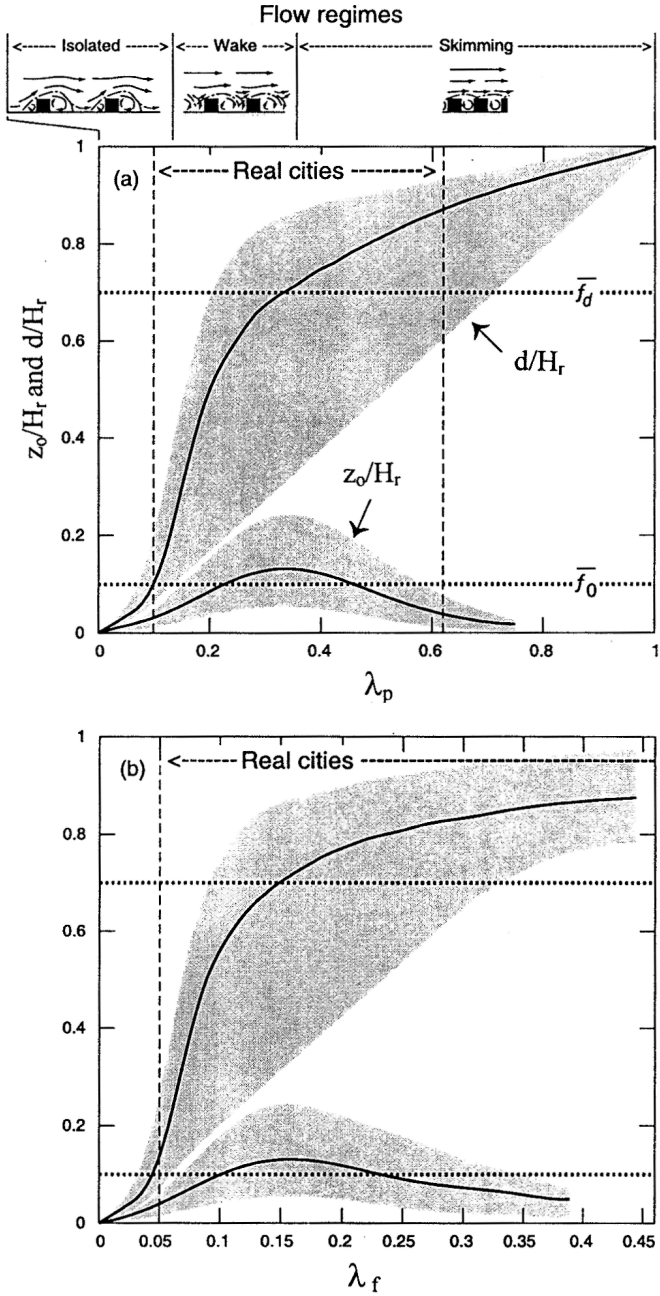

FIGURE 11. Conceptual representation of the relation between z_o/H_r and d/H_r and the packing density of roughness obstacles (a) using λ_p (based on plan area) and (b) using λ_f (based on frontal area) to describe relative area density (see Figure 10 and the text for further definitions). Shaded areas are the reasonable zones or envelopes referred to in the text. Mean values of observed $f_o = z_o/H_r$ and $f_d = d/H_r$ are from Garratt (1992). Flow regimes are drawn along the top. From Grimmond and Oke (1999), with kind permission of the American Meteorological Society.

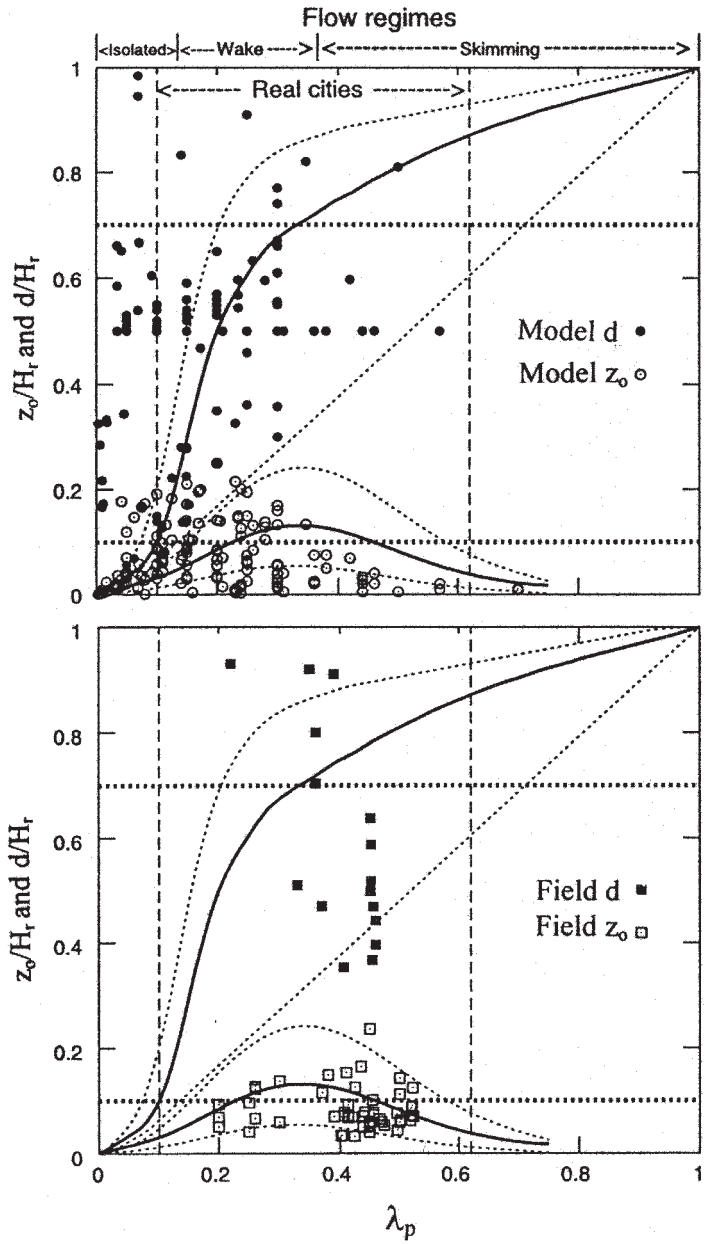

FIGURE 12 (facing pages). All available data used by Grimmond and Oke (1999, with kind permission of the American Meteorological Society) from scale model (mostly wind tunnel) and field (full scale) studies of z_o and d that fulfill the measurement criteria. Panels are organized with scale model results in the top two panels and field results in the bottom two. The two panels on the left use λ_P (based on plan area) to describe the surface form

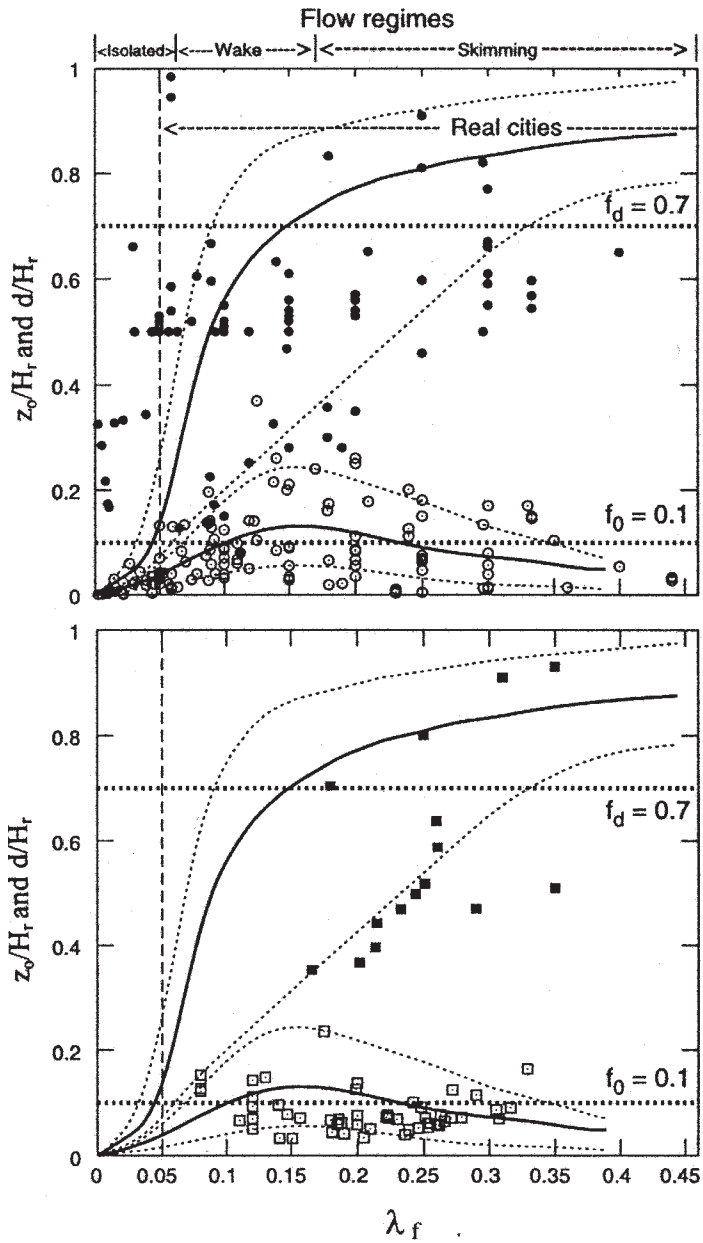

and the two on the right use λ_f (based on frontal area). Envelopes contained by the curved dashed lines represent reasonable limits. The vertical lines show the range of real-city roughness densities and the horizontal lines represent the averages $f_o = z_o/H_r = 0.1$ and $f_d = d/H_r = 0.7$.

interesting that there are no field (i.e., real urban) observations of z_o/H_r less than about 0.03, but many fluid model observations below $z_o/H_r = 0.03$. Also, the observed z_o/H_r values for the field or real urban sites do not suggest a decrease of z_o/H_r at large values of λ_p or λ_f. As suggested earlier, because of the variation in obstacle height in real urban areas, the observed z_o/H_r remains at about 0.10 to 0.15 at large λ_f.

Most equations for z_o and d [e.g., see Eqs. (15) and (16)] have been developed from fluid model data taken over uniform obstacles. The fluid model data are plotted in the panels at the top of Figure 12, and are seen to show much smaller values of z_o than the "field" observations at large λ_f. At real field sites, the effective z_o scales more with the upper range of obstacle heights (e.g., the 90th percentile) rather than the median. After all, the larger obstacles exert the most drag.

The data plotted in Figure 12 have been used by Grimmond and Oke (1999) to test several formulas for calculating z_o/H_r and d/H_r as a function of λ_p and/or λ_f. As expected from the scatter of the data on the figure, no single formula was found to magically produce excellent agreement with the field observations. All formulas showed a large amount of scatter and had points that fell outside of the "reasonable limits" defined by the authors. It is interesting that the "rule-of-thumb" model, which assumes that $z_o/H_r = 0.1$ and $d/H_r = 0.7$, performs fairly well.

In view of the scatter shown in Figure 12, we suggest some simple formulas that provide good fits to the "most reasonable" lines drawn near the middle of the shaded areas on Figure 11 and 12. Preference is given to fitting the field data rather than the laboratory (fluid model) data. We add the condition that z_o/H_r should remain at 0.15 at large λ_f, which has been shown to be valid at real urban and industrial sites. We believe that λ_f (normalized frontal area) is a better indicator than λ_p of z_o and d, since the obstacle drag is related more to the frontal area than the top area. The following formulas provide good fits to the urban observations plotted on the right side of Figure 12, accounting for the modification at large λ_f:

$$z_o/H_r = \lambda_f \qquad \text{for } \lambda_f < 0.15 \text{ (isolated and early wake regimes)} \qquad (17a)$$

$$z_o/H_r = 0.15 \qquad \text{for } \lambda_f > 0.15 \text{ (late wake)} \qquad (17b)$$

$$d/H_r = 3\lambda_f \quad \text{for } \lambda_f < 0.05 \text{ (isolated regime)} \tag{18a}$$

$$d/H_r = 0.15 + 5.5(\lambda_f - 0.05) \quad \text{for } 0.05 < \lambda_f < 0.15 \text{ (early wake regime)} \tag{18b}$$

$$d/H_r = 0.7 + 0.35(\lambda_f - 0.15) \quad \text{for } 0.15 < \lambda_f < 1.0 \text{ (late wake)} \tag{18c}$$

The restriction $\lambda_f < 1$ is given in Eq. (18c) because it is possible for λ_f to exceed 1.0 for closely packed obstacles whose height is much greater than their width. Equations (17) and (18) are expected to be useful for a wide range of surface roughness obstacles at urban and industrial sites. Methods of estimating z_o and d in regions where the roughness varies with wind direction and with distance are discussed in Section 3.3.6.

Equations (17) and (18) are valid when the average height of the roughness obstacles, H_r, is much less than the surface boundary layer depth of about 50 to 100 m. It is suggested that an upper limit to H_r should be 20 m and an upper limit to z_o is therefore about 3 m. Consequently these methods should not be used for skyscrapers in a large city center or for the Rocky Mountains.

3.3.5. Overview of Land Use Category Methods for Estimating z_o and d

Because of the lack of on-site research-grade wind profile observations needed to apply the wind profile methods in Section 3.3.2, and because of the difficulties involved in processing geometrical data from multiple individual roughness obstacles needed to apply some of the morphological methods in Section 3.3.4, these methods have not been widely used in the past for estimating roughness length for air-quality modeling applications. Instead, land-use methods are used in most applied dispersion models, such as the EPA's AERMOD model (Cimorelli et al., 1998). These methods are based on the tables or figures of z_o versus descriptive land-use types found in most basic textbooks (e.g., Stull, 1997). An example of this type of figure is given in Table 5a, from Stull (1997). The problem for those interested in industrial sites is that the land-use categories in Table 5a are very broadly defined, having to cover all land uses, ranging from ice-flats and deserts to water surfaces to crops and forests. For example, Table 5a contains no category for industrial sites. The table does contain four separate categories for "towns and cities," with z_o ranging from 0.3 m for "outskirts of towns"

TABLE 5a
Roughness Lengths, z_o, for Typical Terrain and Land Use Types[a]

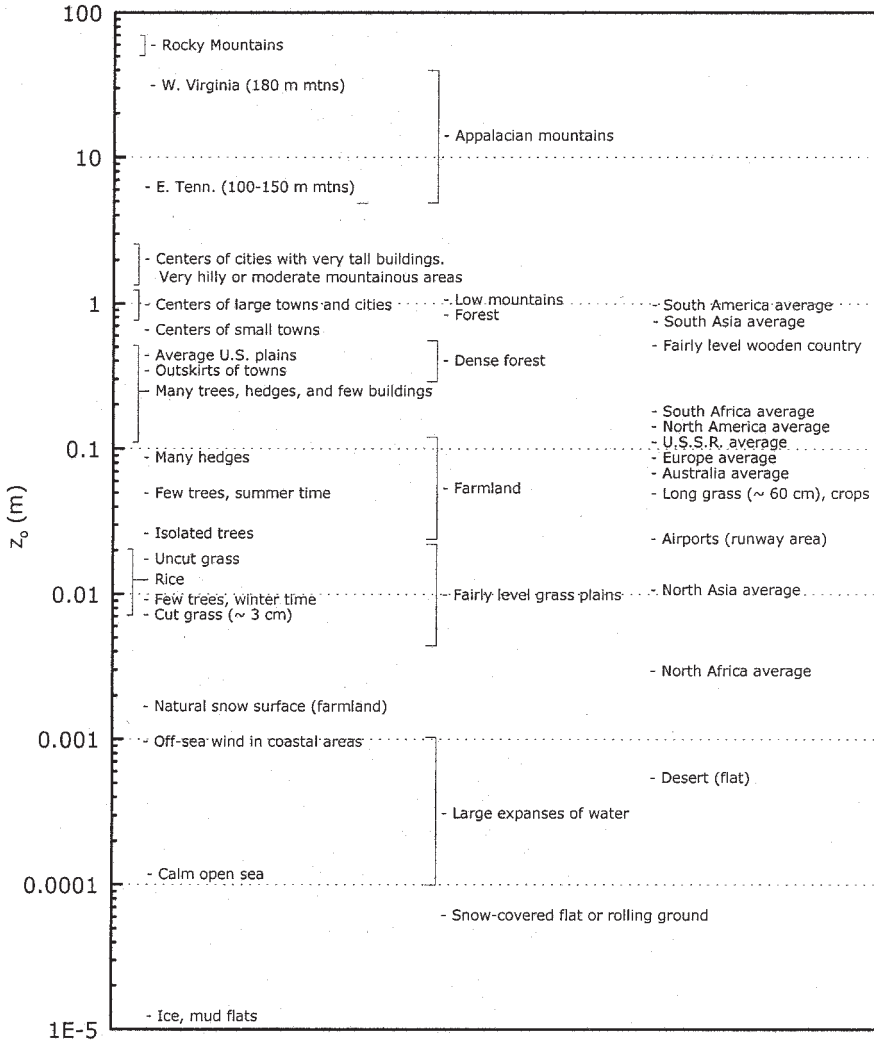

[a]From Stull (1997), with kind permission from Kluwer.

to 2 m for "centers of cities with very tall buildings." Roughness lengths of about 6 m to 60 m are suggested in the table for the "mountains" category. We believe that this category should be disregarded for our purposes since the heights of the mountains are much greater than the 50 m to 100 m depth of the surface boundary layer in which the logarithmic wind profile Eq. (2b) is valid.

A more detailed description of the relation of z_o to urban/industrial land use has been proposed by Davenport et al. (2000). A portion of their table is given in Table 5b, where surface roughness lengths, z_o, are listed for five categories of buildings and industrial obstacles. The z_o values range between about 0.1 and 2 m, in agreement with Stull's (1997) z_o suggestions for "towns and cities" in Table 5a.

As discussed in Chapter 2, Auer's (1978) methods, based on land use categories within a radius of 3 km of the source and approximate descriptions of building geometries, are used in the EPA Guidelines and form the basis for the decision in the ISC3 model whether the rural or urban dispersion curves should be used. The method is not used to assign specific z_o values in ISC3, but only to make the decision of urban vs. rural. Based on this decision, either the rural or urban dispersion

TABLE 5b
Updated Surface Roughness Lengths, z_o, for Five Urban and Industrial Categories[a]

Category	Surface Roughness Length, z_o	Urban/Industrial Site Description
Roughly Open	0.1 m	Moderately open country with occasional obstacles (e.g., isolated low buildings) at relative separations of at least 20 obstacle heights.
Rough	0.25 m	Scattered buildings and/or industrial obstacles at relative separations of 8 to 12 obstacle heights. Analysis may need displacement length, *d*.
Very Rough	0.5 m	Area moderately covered by low buildings and/or industrial tanks at relative separations of 3 to 7 obstacle heights. Analysis requires displacement length, *d*.
Skimming	1.0 m	Densely built-up area without much obstacle height variation. Analysis requires displacement length, *d*.
"Chaotic"	2.0 m	City centers with mixture of low-rise and high-rise buildings. Analysis by wind tunnel advised.

[a]This table is an abridged version of a table in Davenport et al. (2000).

curves are selected in Table 1. This method has led to assignment of the "rural" category in some scenarios where there is a large (1 or 2 km radius) industrial plant surrounded by grassland, desert, or water. A discrepancy may occur, since the trajectory of a pollutant cloud may be entirely over the industrial plant, even though a "rural" class has been assigned to the area.

None of the land use methods shown in Tables 5a and 5b or used in the EPA's ISC3 model include suggestions for the displacement length, d. The emphasis is on z_o, since that is the parameter asked for in most meteorological or transport and dispersion models. z_o affects the wind profile in the boundary layer over its full depth, whereas d affects the wind profile only at low heights less than 2 or 3 H_r.

An alternate land-use classification system for urban and industrial areas was suggested by Theurer (1999). His proposed nine land-use types include several configurations of residential, industrial, and commercial buildings. There are also two categories of parkland—grass with few trees, and forests. Key scaling lengths have been estimated for each class. For example, it is suggested that H_r ranges from 8 m to 20 m in industrial and commercial areas. The ratio of street width (i.e., obstacle lateral spacing) to H_r, is also given, since it is of interest in calculating concentrations of air pollutants released from motor vehicles in urban streets. These parameters are of less interest in industrial sites, where the major interest is in calculating concentrations at the site boundaries.

Yet another set of 12 urban land-use types has been proposed by Grimmond and Oke (1999). One category applies to "industrial" areas but a photograph of a typical site shows an area of large low and wide commercial buildings. Table 6 contains examples of scaling parameters for some of these land-use classes, grouped by λ_p. It is seen that z_o/H_r ranges from about 0.06 to 0.20, and d/H_r ranges from about 0.35 to 0.85. These numbers are consistent with those found in other studies.

3.3.6. Estimation of z_o for Surface Conditions Varying in Space

Section 3.3.3 provided background references on flow over heterogeneous or nonuniform terrain that varies in space. The published analyses (e.g., Goode and Belcher 1999; Horst, 1999; Schmid 1994) are all directed toward detailed characterizations, primarily from the viewpoint of determining the representative surface roughness length of the

upwind area that is influencing meteorological observations at a certain height on a certain tower. These analyses are generally too complicated for our purpose. A rough rule of thumb is that a meteorological instrument at a height, z_m, is most influenced by the ground surface at a distance of about 10 z_m in an upwind direction.

Very few transport and dispersion models allow inputs of space-varying z_o, and there are several problems in the cloud-matching methodologies at the boundaries between two roughness areas in those few models that purport to account for these variations. Instead, it may be more robust to simply estimate an average or representative z_o over the cloud's trajectory from source to receptor. Note that the receptor could be an instrument, a person, or a hypothetical location. This averaging procedure was followed in the PERF Kit Fox modeling by Hanna and Chang (2001). A problem in the use of this method is that, since the average z_o would depend on the wind direction and the distance to the receptor, there may be a different z_o for each source–receptor combination. This would not be so important if the study involves only a simple reconstruction of a past incident where a specific location was of interest (e.g., a school, a retirement home, or a plant fenceline). However, it would be more of a problem for planning studies where a large number of scenarios, distances, and directions would be included. The recommended way to simplify the method would be to assign average z_o values to 30 degree wind sectors and to source–receptor distance increments representing at least 20% of the distance from the source to the receptor.

Because the wind flow and the cloud dispersion rates are relatively insensitive to minor (say, factor of two) variations in z_o, it is sufficient to use a single averaged value of z_o for situations with minor variations of z_o associated with land use (e.g., forest to industrial site to suburb). The primary concern in this section is for scenarios where z_o varies by a few orders of magnitude (e.g., open desert to dense urban area to sea).

For the case of cloud trajectories over greatly varying surface types (say for factor of 2 or 3 or more differences in z_o), the recommended method for calculating a single representative z_o and d value is outlined below. The method for accounting for variations in downwind distance, x, is modified from guidance by Goode and Belcher (1999):

***Step 1*:** Use Eqs. (17) and (18) to calculate z_{oi} and d_i for the underlying surface in each individual distance range Δx_i between the source and receptor. To be considered in this calculation, a

TABLE 6
Typical Nondimensional Properties of Homogeneous Zones in Urban Areas, Ordered by Urban Density and Flow Regime[a]

Urban surface density—flow regime	λ_p[b]	H_r/W	d/H_r	z_o/H_r
Low density—Isolated flow				
Buildings and trees are small and widely spaced, e.g. modern single-family housing with large lots and wide roads; light industrial area or shopping mall with large paved or open space.	0.05–0.4	0.08–0.3	0.35–0.5	0.06–0.10
Medium density—Wake interference flow				
Two to four story buildings and mature trees, elements of various heights occupy more than 30% surface area and create semi-enclosed spaces (street canyons, courtyards), e.g. closely spaced, large and semidetached houses, blocks of flats in open surroundings. Mixed houses with shops, light industry, churches, and schools.	0.3–0.5	0.3–1	0.55 – 0.7	0.08–0.16[c]
High density—Skimming flow				
Buildings and trees closely packed and of similar height, narrow street canyons, e.g. old town centres, dense row and semi-detached housing, dense factory sites.	0.5–0.8	0.65–2	0.60–0.85	0.07–0.12
High-rise—Chaotic or mixed flow[d]				
Scattered or clustered tall towers of different heights jutting up from dense urban surroundings, e.g. modern city core, tall apartment, major institution.	>0.4	>1	0.50–0.70	0.10–0.20

[a] From Grimmond and Oke (1999), with kind permission of the American Meteorological Society).
[b] Plan areas of buildings only.
[c] Largest values likely to apply to mid-range of λ_p and H_r/W.
[d] Unique distribution of major elements makes it difficult to generalize, except to expect that roughness is enhanced by addition of tall elements.

roughness surface should extend laterally over an angle of at least 30 degrees. The roughness surface should also extend in the x direction over a distance of at least 20% of the total distance from source to receptor, x_t. However, for there to be an equilibrium boundary layer over a new roughness surface, it should cover a distance greater than the maximum of 20 m or 10 H_r. Differences in z_o from one sector or distance range to another should be accounted for only if the difference is more than a factor of two. Note that x_t is the sum of the Δx_i values.

Step 2: Calculate the effective z_o and d over the distance, x_t, and the 30 degree sector using the following formulas for the geometric mean:

$$\ln z_o = (1/x_t) \sum(\Delta x_i) \ln z_{oi} \tag{19a}$$

$$\ln d = (1/x_t) \sum(\Delta x_i) \ln d_i \tag{19b}$$

Note that the weighting factor, $(\Delta x_i)/x_t$, does not depend on nearness to the source or the receptor.

The numerical criteria, such as the requirements for at least a 30 degree angular coverage, a 0.2 x_t distance coverage, and a factor of two difference in z_o, are based on the opinions of the authors after extensive study of this problem. However, these criteria may be modified after more experience is gained in applications.

As an example of the use of this method, consider that there are two areas of roughness. The first area, at distances of 0 to 1000 m from the source, consists of an industrial site with z_o = 1 m and d = 5 m. Therefore z_{o1} = 1 m, d_1 = 5 m, and Δx_1 = 1000 m. The second area, at distances of 1000 m to 3000 m from the source, consists of a desert with a few small bushes with z_o = 0.01 m and d = 0.05 m. Therefore z_{o2} = 0.01 m, d_2 = 0.05 m, and Δx_2 = 2000 m. Furthermore, it is seen that $x_t = \Delta x_1 + \Delta x_2$ = 3000 m.

For these cases, according to Eq. (19a):

$$\ln z_o = (1/3000 \text{ m}) [(1000 \text{ m}) \ln(1.0) + (2000 \text{ m}) \ln(0.01)] = -3.07,$$

giving z_o = 0.046 m.

According to Eq. (19b):

$$\ln d = (1/3000 \text{ m}) [(1000 \text{ m}) \ln(5.0) + (2000 \text{ m}) \ln(0.05)] = -0.96$$

giving d = 0.23 m.

These estimates are about ½ of the geometric mean of the two numbers. Note that the geometric mean of z_{o1} and z_{o2} is $(z_{o1}z_{o2})^{½}$. For the example calculation above, the ½ factor enters because the smaller roughness covers a distance, Δx, twice the size of the larger roughness.

Other examples of the use of Eqs. (19a) and (19b) are given in worked examples 5, 6, and 7 in Section 5.

As mentioned above, z_o and d can be calculated for 30 degree wind direction sectors. For general analyses, these sectors should be at regular intervals of 0 to 30 degrees, 30 to 60 degrees (from north), and so on. The 30 degree criterion was picked because that is roughly the angle covered by a dispersing pollutant plume. However, for single cases with specific wind directions from a source toward a receptor position of interest, the 30 degree sector could be centered on the direction that would cause a plume or cloud to be advected parallel to the border between two greatly different roughness zones. For example, consider a case where one side of the plume would be over an urban area, with z_o = 1 m, and the other side of the plume would be over the water, with z_o = 0.0001 m. This difference should be accounted for so that the resulting z_o will vary smoothly with wind direction rather than having a discontinuity. Our recommendation is that, if the z_o differs by more than a factor of 2 or 3 between the two zones that occupy the 30 degree sector for a specific direction, then the geometric mean of the two z_o values should be estimated using Eq. (19c) below, with weighting by the sector, ΔWD_j, covered by each z_o.

$$\ln z_o = \frac{\sum \left(\Delta WD_j\right) z_{oj}}{30 \text{ degrees}} \tag{19c}$$

For example, for the case described above, where z_o = 1 m on one side (a 15 degree sector) of the plume, and z_o = 0.0001 m on the other side (the other 15 degree sector) of the plume, then

$$\ln z_o = \frac{(15 \text{ degrees}) \ln(1.0) + (15 \text{ degrees}) \ln(0.0001)}{30 \text{ degrees}} = -4.61$$

giving z_o = 0.01 m

Another example of the use of this method will be given in Section 5.7.

3.4. Flow Through an Obstacle Array

Within, and near to, an obstacle array the flow is directly affected by the obstacles themselves, causing flow around and over individual obstacles. The flow will commonly separate from the obstacles producing areas of recirculation and also low velocity wakes in the lee of the obstacles.

There is a substantial literature on the flow around buildings, particularly with a view to dispersion near to and around individual buildings (e.g., EPA, 1986; Hosker, 1984; Meroney, 1982; Robins et al., 1997). The literature on flow and dispersion around individual buildings near other buildings or immersed in an array of buildings is less substantial and is frequently site-specific. Some generic work is available, see Britter and Hunt (1978), Wilson and Chui (1987), and there have also been many more recent papers on flow and dispersion in street canyons, e.g., Pavageau et al. (1997).

However, here we are interested in flow and dispersion within, and near to, the obstacle array rather than the flow and dispersion near any individual obstacle.

When there is a wide spacing between obstacles, the flow around each obstacle will be isolated. For more closely spaced obstacles, the flows around each obstacle will interfere. Very dense packing of uniform-shaped obstacles, with constant H_r, causes the flow to skim over the tops of the obstacles with limited penetration of the flow into the obstacle array itself. These three regimes have been commonly labeled as: "isolated flow," "wake interference flow," and "skimming flow" (see Figure 4 for schematic diagrams illustrating the three regimes). The category limits for the three regimes are given by Grimmond and Oke (1999), based on the plan area ratio, λ_p, of 0–0.12 for isolated flow, 0.12–0.34 for wake interference flow, and 0.34–1.00 for skimming flow. However, MacDonald, Griffith, and Cheah (1996) use slightly different values, $\lambda_p < 0.09$, $0.09 < \lambda_p < 0.17$, and $\lambda_p > 0.17$, for the three regimes, respectively. Both of these references make use of the earlier analyses by Hussein and Lee (1980).

The isolated flow and the wake interference flow are fundamentally different from the skimming flow. In the first two, the flow within the obstacle array can be viewed as a flow driven through the obstacle array by the acquisition of momentum from the flow above the obstacle

array. This momentum is lost through the drag force of the obstacles on the flow through the obstacle array.

In the skimming flow there is limited direct penetration of the flow above the obstacle array down into the obstacle array and there may be negligible mean velocity deep within the obstacle array. The direct penetration of the flow above the obstacle array produces a drag force on the upper portions of the obstacles and there can be unsteady vortex structures extending deeper into the obstacle arrays but these are recirculating in nature rather than part of a flow through the obstacle array. As the spacing between the obstacles becomes small compared with the height of the obstacles the unsteady vortex structure penetrates only partially down into the obstacle array. Experiments show that, for $\lambda_p > 0.40$ and uniformly shaped obstacles, the flow below $z = H_r$ is effectively stagnant (Hall et al., 1998). Experiments during September and October 2000, in the downtown area of Salt Lake City also suggested that the flow near street level was effectively stagnant, even in the presence of moderate wind speeds at heights above the buildings (M. Brown, personal communication).

As mentioned earlier, this description of the skimming flow is commonly derived from idealized experimental studies using obstacles of constant height. This flow will be markedly altered when the obstacles are of significantly different heights, where taller obstacles will intersect the flow above the obstacle array and bring higher velocity fluid down into the obstacle array.

It was described in Section 3.3.4, how, for fixed external flow, the surface stress, and by implication, z_o, first increases with increased obstacle packing density, then reaches a maximum plateau and then declines toward the nonobstacle value. The decline toward the nonobstacle value is primarily observed in specialized experiments with uniform obstacles. The decline will be less evident or will be absent for real obstacle arrays with different obstacle heights. This is very apparent in Figure 12, from the review by Grimmond and Oke (1999), when comparing field studies with laboratory studies (though not all of the laboratory studies were of an idealized nature).

Although the velocity field will have significant spatial variability within, and near, the obstacle array a spatially averaged mean wind profile may be defined, as may turbulence intensities. This spatially averaged velocity field and the turbulence intensities will be appropriate in addressing dispersion within, and near, the obstacle array pro-

vided the dispersion is over a large enough area to encompass many obstacles.

The objective of this section is to provide a technique for determining the mean velocity and turbulence near to, and within, an obstacle array. The obstacle array may be, for example, an industrial facility or surrounding built-up urban areas.

The expected spatially averaged velocity profile is sketched in Figure 13. This is drawn for the isolated flow and wake interference

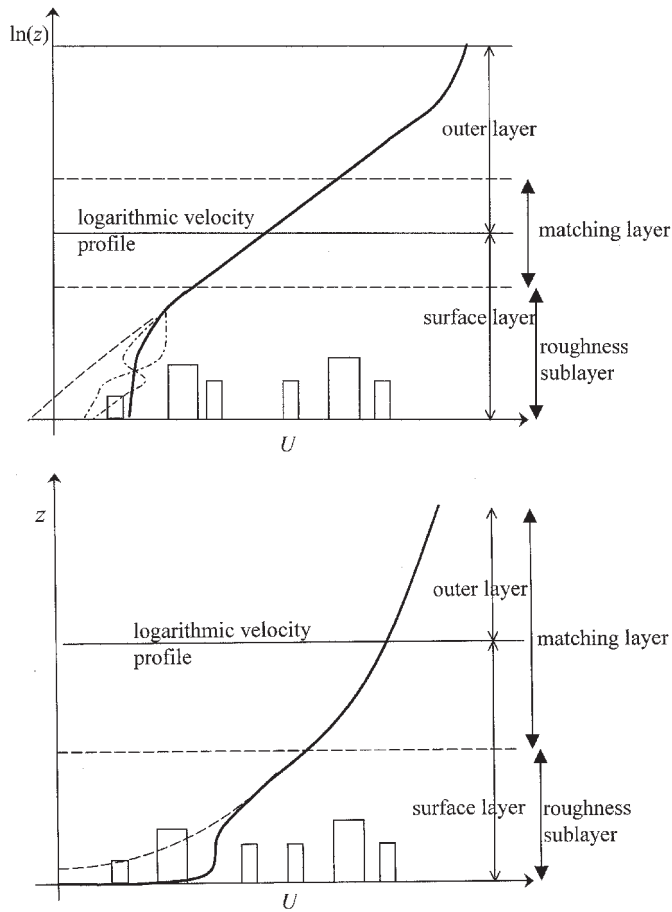

FIGURE 13. Schematic diagram of wind profile over roughness obstacles. The top panel plots u versus ln z and the bottom panel plots u versus z. The various layers are indicated. Note that $\partial u/\partial z$ depends upon u^*, mixing depth, Coriolis force, and z in the outer layer, and on u^*, z and z_0 in the surface layer (above the roughness sublayer). Within the matching layer $\partial u/\partial z$ depends only upon u^* and z and this leads to the logarithmic velocity profile (after Bottema, 1997).

flow. It is uncertain whether or not the skimming flow will have a similar velocity profile with the lower part of the profile reduced to zero velocity.

The region over which there is a deviation from the logarithmic velocity profile presented in Section 2.1 is commonly called a roughness sublayer. It is within this region that we seek predictive descriptions of the flow field.

It must be stressed that there are currently no available operational models in the public domain that address the flow and dispersion within an obstacle array such as a typical urban area, oil refinery, or industrial processing facility. Consequently the following arguments and analysis are novel and based on limited experimental evidence.

3.4.1. Extent of the Roughness Sublayer

The roughness sublayer is the region in which the flow depends explicitly on the presence of the obstacles, their sizes and their geometries. This layer extends from the ground surface up to about 1.5 or 2 H_r. Raupach et al. (1980) state that horizontal spatial inhomogeneities are nonnegligible in this layer, and point out that the effects of obstacle wake diffusion are important for $z < H_r + 1.5W$, where W is the obstacle breadth.

This and similar comments have commonly been interpreted as a restriction that the logarithmic velocity profile is valid down to $z \approx 2.5$ H_r and that this is the depth of the roughness sublayer. This restriction is of great importance when selecting meteorological observations at various heights in order to determine parameters such as z_o and d and is a wise restriction to employ when undertaking such calculations.

However, the 2.5 H_r criterion is likely to be unnecessarily restrictive when trying to determine a spatially averaged velocity profile within and near the obstacle array. For example, when the obstacles are sparsely spaced (i.e., are relatively far apart), we expect only a minor perturbation to the velocity profile away from the logarithmic law down to obstacle height levels and possibly lower. The logarithmic law holds down to virtually the top of the roughness elements, according to data reported by Raupach et al. (1980) quoting Thom (1971).

Of course, the real question is: how far down may we use the logarithmic law to an accuracy acceptable for operational dispersion calculations?

As shown in Figure 6 (page 57), Raupach et al. (1980) produced five spatially averaged velocity profiles with five different spacings of obstacles. These spacings correspond to λ_f's having values of 0.011, 0.023, 0.045, 0.091, and 0.18 for categories B through F, respectively, in Figure 6. At $z = 1.5\ H_r$, the errors produced by using the logarithmic law down to that height were underestimates of approximately 2%, 5%, 4%, 5%, and 7%. These would seem to be acceptable levels of error in the determination of the mean velocity above an obstacle array. For much larger values of λ_f we would expect the error eventually to decline.

Thus we have confidence in using the logarithmic velocity profile down to $z \approx 1.5\ H_r$ and even lower when the ratio of frontal area to plan area, λ_f, is small. For example, suppose that an error of 10% is acceptable. Then Raupach et al.'s (1980) results in Figure 6 show that, for $\lambda_f = 0.011$ (Category B), the logarithmic law is acceptable down to $z \approx 0.8\ H_r$.

Similar data covering a plan area ratio, λ_p, from 0.049 to 0.91 show that the logarithmic velocity profile is operationally satisfactory down to a value of $(z - d)/z_o$ of about 5 or even smaller, supporting the above conclusions (Hall et al., 1996).

3.4.2. Wind Velocity Fields within and Near Obstacle Arrays

The velocity field within the obstacle array (the industrial plant complex or the urban canopy) and in its immediate vicinity has been studied far less than the velocity field well above the obstacle array.

There have been studies in small regions within the obstacle array and in regions covering one or two specific obstacles. The most common occurrence of these are "street canyon" studies for urban air quality considerations and these have been both generic and also site-specific studies. Simple integral modeling techniques have been employed as well as more complex computational fluid dynamics (CFD) techniques. However these studies are of limited operational interest for the study of the varied velocity field arising within general obstacle arrays, as found in urban and industrial complexes. A simpler, and possibly more robust, approach is required.

There have been few laboratory or field studies looking at the velocity field within an experimental array. It is difficult to extract data from these studies that can be used for model development. Frequently the

data are peripheral to velocity data obtained well outside the obstacle array. Due to strong current interest in flow and dispersion in complex geometries, data are now becoming more prevalent.

There have been attempts at developing models for flow within the obstacle array and these range from "distributed porosity" models used as modules within a CFD calculation (see Brown, 2000) to semi-analytical models based on linearized perturbation models, Jerram et al. (1994). These however are not models that can be simply applied to real obstacle array scenarios. Here we look for simpler, more understandable techniques consistent with the approaches described elsewhere in this volume for the velocity field outside the obstacle array.

It can be argued that the velocity field within and close to an obstacle array will be very site specific and so seeking models for this velocity field is fraught with difficulty. However a spatially and temporally averaged velocity field does exist and it will be directly useful for the subsequent development of a dispersion model. Thus we do seek a model for the velocity field, encouraged by the pragmatic view that accuracy requirements for operational dispersion models for flows within the obstacle array need only to be consistent with operational dispersion models for flows above the obstacle array.

We also, initially, seek solutions to the flow field well within the array where the spatial variations near the edges of the array have declined. Thus our model assumes spatial horizontal homogeneity. Of course the intent will be to use such a model in situations with some spatial homogeneity. The question then becomes, what level of spatial inhomogeneity is acceptable, consistent with the accuracy requirement of the dispersion model?

In a similar vein the model is intended to be applied to areas over which spatial homogeneity is not an unreasonable assumption. Thus application to flow around one isolated building would be unreasonable.

3.4.2.1. VELOCITY PROFILE DESCRIPTION WITHIN THE OBSTACLE ARRAY

The typically observed velocity profile shown in Figure 13 depicts a substantial region of approximately uniform velocity within the obstacle array. A characteristic velocity, u_c, within the array is apparent and can be defined as the average velocity over the height of the array. It is recommended here that the velocity profile in Figure 13

should be approximated by a combination of the logarithmic velocity profile above and a uniform velocity below, both extended until they intersect.

Obviously, more sophisticated profile descriptions are possible which, if nothing else, can meld together to ensure no slope discontinuities. However, given the uncertainty of the flow field and the level of accuracy generally deemed acceptable for solutions to dispersion problems, it is thought here that the exact specification of the profile of the spatially averaged velocity field is not the greatest priority. A cloud of released material, as it diffuses, will eventually sample much of the velocity field.

For example, for the extensive unpublished data from Snyder (see 3.4.2.4), a comparatively uniform velocity profile was found at heights less than H_r. The velocity was observed to decrease by only 30% as height decreased from $z = H_r$ to $z = 0.2H_r$, implying a variation of only $\pm 15\%$ from an assumed uniform velocity.

More complex profiles have been used for the wind profile within arrays of obstacles, such as one that is linear from the ground to H_r or one that is exponential and of the form (Cionco, 1972)

$$u/u_{H_r} = \exp[-a(1 - z/H_r)] \tag{20}$$

with a an empirical constant called the attenuation coefficient. The exponential solution arises by application of a simple Prandtl mixing-length model to an array of obstacles of uniform cross-section. It is assumed that the velocity, u_{H_r}, is known or can easily be calculated in both the linear and the exponential wind profile formulas. This is often not the case and the velocity may be changing quite rapidly in the immediate vicinity of H_r (see Figure 5). The exponential profile in Eq. (20) has been found to provide a good fit to laboratory data in the range $0.05 < \lambda_f < 0.20$ (Macdonald, 2000). *H*owever, the exponential profile in Eq. (20) has the slight disadvantage that the ground velocity (at $z = 0.0$) is nonzero, and the solution as $\lambda_f \to 0$ is unrealistic.

A characteristic velocity associated with the exponential wind profile Eq. (20) may be obtained by averaging the velocity over the depth of the obstacles and is $(1 - e^{-a})/a$ times the velocity at $z = H_r$. The attenuation coefficient a has been linked by Macdonald (2000) with λ_f from his experiments:

$$a = 9.6\,\lambda_f$$

3.4.2.2. DEVELOPMENT OF A SIMPLE MODEL FOR THE CHARACTERISTIC VELOCITY, u_c, WITHIN THE OBSTACLE ARRAY

In this section we develop a simple model for the characteristic velocity, u_c, within the obstacle array in terms of accessible parameters.

Techniques for estimating z_o and d were reviewed and recommended in Section 3.3. The surface shear stress, τ_o, is simply calculated from Eq. (2b) for any given wind speed (provided at some reference height which is well above the obstacle array) by determining u^* and then using $\tau_o = \rho u^{*2}$. Thus, λ_p, λ_f, H_r, z_o, d, and u^* are accessible parameters.

The surface shear stress, τ_o, arises from shear stresses on the underlying surface and elsewhere and pressure asymmetry across each obstacle due to flow separation. When the obstacles are very widely spaced the former may be important, but, typically, the latter is dominant.

Considering only the source of the surface shear stress due to the pressure asymmetry across each obstacle, we note that this stress arises due to the forces applied to all of the obstacles/per unit plan area, and is produced by the velocity field within the obstacle array. We characterize the mean velocity field in the array by u_c. The variable u_c is the characteristic velocity and if necessary or convenient a velocity profile can be introduced later based on this characteristic velocity. But there is no need to introduce this complication at this stage of model development.

The surface shear stress is given by

$$\tau_o = \rho u^{*2} = I \sum F_d A_p \tag{21}$$

where F_d is the drag force on each obstacle in isolation, and $\sum F_d$ is the sum of all these drag forces. The coefficient I allows for interference of the flow due to the obstacles not being in isolation.

The drag force on an obstacle in isolation is conventionally written in terms of a drag coefficient C_d and its individual frontal area A_{fi} by

$$F_d = \tfrac{1}{2} \rho u_c^2 C_d A_{fi} \tag{22}$$

We rewrite the right side of Eq. (21) and sum over all F_d so that

$$\tau_o = \rho u^{*2} = \tfrac{1}{2} \rho u_c^2 I \left(C_D \frac{A_f}{A_p} \right) \tag{23}$$

where A_f is the total frontal area of the obstacles and C_D is an "average" of the drag coefficients taken for the obstacles in isolation such that $C_D A_f = \sum C_D A_{fi}$ and $A_f = \sum A_{fi}$.

Thus

$$\tau_o = \rho u^{*2} = \tfrac{1}{2}\rho u_c^2 \lambda_f I C_D \tag{24}$$

So, for example, when the obstacles are widely spaced there is no flow interference and $I = 1$ such that

$$\tau_o = \rho u^{*2} = \tfrac{1}{2}\rho u_c^2 \lambda_f C_D \tag{25}$$

But, more generally, we have a predictive equation for u_c, the characteristic velocity, within the obstacle array, given by

$$\frac{u_c}{u^*} = \left(\frac{I C_D}{2}\right)^{-1/2} \lambda_f^{-1/2} \tag{26}$$

and λ_f is easily calculated and has probably been used already in determining z_o and d using the method outlined in Section 3.3.

When the obstacles are widely spaced and not interfering (i.e., small λ_f)

$$\frac{u_c}{u^*} = \left(\frac{C_D}{2}\right)^{-1/2} \lambda_f^{-1/2} \tag{27}$$

The determination of IC_D for the more general case when the obstacles interfere is not straightforward and this might be thought to limit the usefulness of this approach.

However, the model of Lettau (1969) based on his experimental results [see Eq. (14)] can be interpreted as

$$\frac{z_o}{H_r} = \lambda_f I C_D \tag{28}$$

if it is assumed that λ_f is less than about 0.2. If all the obstacles are identical, then $IC_D = C_D$.

It is suggested by Bentham and Britter (2001) that $\lambda_f IC_D$ in Eq. (26) can, in general, be replaced by z_o/H_r, and therefore u_c/u^* can be written as:

$$\frac{u_c}{u^*} = \left(\frac{z_o}{2H_r}\right)^{-1/2} \tag{29}$$

This formula is recommended for determining u_c in terms of the accessible parameters H_r, z_o, and u^*. The $z_o/H_r \propto \lambda_f$ relation is valid only

for $\lambda_f \leq 0.15$, as seen in Eq. (17a). At larger λ_f, Eq. (27) should be used with C_D equal to about 1.0.

In the limit of very sparse obstacle spacing (i.e., relatively large spacing between obstacles), the surface shear stress will have a contribution from the shear stress on the underlying surface rather than only from the obstacles. For a given wind speed at a reference height there will be a known surface shear stress on the underlying surface $\rho u_o{}^{*2}$, provided a z_o can be estimated for the underlying surface (i.e., the surface with the obstacle array removed). This should not be a difficult estimate to make. Thus $u_o{}^*$ is known.

Including the surface stress on the underlying surface not covered by obstacles [i.e., the area $(1 - \lambda_p)A_p$], produces the result that

$$\frac{u_c}{u^*} = \left(\frac{\lambda_f}{2}\right)^{-1/2} \left(1 - \left(1 - \lambda_p\right)\frac{u_o^{*2}}{u^{*2}}\right)^{1/2} \tag{30}$$

The treatment for very closely spaced obstacles has not been developed here, since this is a scenario where a somewhat different approach may be necessary. The skimming flow will not be represented by a u_c covering much of the region within and near the obstacle array, but will instead be a higher velocity extending only a small distance (comparable to the gap between the obstacles) into the obstacle array. A better model for very closely spaced obstacles, as in the downtown area of a large city, may be to acknowledge an essentially zero mean velocity at heights less than those about 0.5 H_r within the obstacle array. In this case, the momentum transport from above the canopy to within the canopy would be due to the direct exchange of high velocity fluid from above with zero (mean) velocity fluid within the canopy. This flow is exemplified by the flow over an enclosed cavity.

Heterogeneous obstacle heights, typical of real urban or industrial areas, will further complicate the picture for the case of closely spaced obstacles. Obstacles extending above the average height of the obstacles are quite effective at intercepting high wind speeds and bringing them down toward the ground. In this case, the heterogeneity of the obstacle heights becomes a dominant feature and will need direct consideration. For the $\lambda_p = 0.16$ case, z_o/H_r is observed to double as σ_H/H_r changes from 0% to 50%, while for the $\lambda_p = 0.44$ case, z_o/H_r is observed to increase by a factor of 6 for the same variation of σ_H/H_r (Macdonald et al., 1999). Here, σ_H is the standard deviation of the roughness height around H_r.

As mentioned at the end of Section 3.4.2.1, an alternative technique to determine a characteristic velocity, u_c, within the array is to integrate the exponential profile [Eq. (20)] from $z = 0$ to $z = H_r$ to deduce that

$$u_c / u_{H_r} = (1 - e^{-a})/a$$

However, this does still leave the difficulty of how best to determine the velocity at the top of the obstacle array u_{H_r}.

3.4.2.3. MODEL RECOMMENDATION

The approach adopted here is to determine the characteristic velocity in the obstacle array u_c. The recommendation is to use the logarithmic velocity profile down until the velocity equals u_c and then use u_c at lower heights within the array. This is a very simple and direct modeling approach. It would seem to be more appropriate when the point of intersection of the constant velocity u_c and the logarithmic velocity profile was comparable with or larger than the height of the roughness elements. When the point of intersection was well below the height of the roughness elements (possibly for small λ_p or λ_f, less than 0.01, say) some reconsideration may be required to take into account the drag force on the obstacles due to the logarithmic profile extending well into the roughness array. The impacts of these alternate assumptions on applied model results are not well known and should be studied by sensitivity analyses with alternate technical algorithms.

3.4.3. Model Comparison with Experimental Data

Several available data sets were used to assess the accuracy of the model for the wind speed profile above and within obstacle arrays

Figure 6 (see page 57) contains five observed velocity profiles reported by Raupach et al. (1980). These observed profiles extend down to the height of the roughness elements and, in a few cases, below that height. In addition the authors provide results of a wake diffusion model that allows some extrapolation of the data to within the array of cylindrical obstacles. Each velocity profile in Figure 6 is the average from several spatial positions within the array. A characteristic velocity within the obstacle array has been estimated by taking either the lowest data point or the extrapolated velocity profile.

A total of 252 separate measurements of the mean and turbulent velocity field within an obstacle array were made by Snyder (unpublished) in a wind tunnel. The time- and space-averaged velocities obtained with a pulsed-wire anemometer within the array have been determined from the unpublished data.

Wind tunnel data were reported by Peterson and Ratcliff (1989), where the ratio of the characteristic velocity u_c to u^* has been estimated from the velocity profiles for a tank farm geometry. Many other individual profiles near refinery units produced very good agreement between u_c/u^* and $(z_o/2H_r)^{-1/2}$ but these were often in the lee of obstacles and the agreement may have been fortuitous.

Wind profile observations in a wind tunnel in arrays of bill-board shaped obstacles were described by Havens, Walker, and Spicer (2001). The ratio of the characteristic velocity u_c to u^* and the ratio of z_o/H_r have been estimated from the velocity profiles in the manuscript.

Cubes in square and staggered arrays were studied by Macdonald et al. (2000) with $\lambda_f = 0.0625$, 0.16, and 0.44. For each array, the mean wind profiles are calculated as the average of five velocity profiles (e.g., one profile was behind an obstacle, one profile was in the gap between obstacles, etc.). Some uncertainty is found in their determination of u^*, which was based on their recommendation to use results from direct measurement of u^* from turbulence observations. These u^* values have been adopted here.

Analyses of the data from these five sources are given in Table 7 and plotted in Figure 14. Provided $\lambda_f \leq 0.2$, the predictions of u_c/u^* given by $(z_o/2H_r)^{-1/2}$ appear to be operationally acceptable. The argument in Bentham and Britter (2001) that z_o/H_r should be equated with $IC_D\lambda_f$ was based on possible interference of the flow around each obstacle. However, it might be argued that the magnitude of u_c has already accounted for any interference of the flow fields, since, on average, the obstacles experience a velocity u_c. If this is the case, the model could revert to using λ_f always rather than z_o/H_r. This is particularly evident in the results from Macdonald et al. (2000) with $\lambda_f = 0.44$.

It is recommended here that u_c/u^* should be determined using z_o/H_r via Eq. (29) for $\lambda_f \leq 0.2$ if z_o/H_r is available from a predictive model. If this is not available, λ_f should be used directly instead of z_o/H_r, but this is less preferred. For $\lambda_f > 0.2$, λ_f should be used directly instead of z_o/H_r, and the model should be treated with caution for $\lambda_f \geq 0.4$.

TABLE 7
Observations of λ_f and u_c/u^* and Calculations of $(z_o/2H_r)^{-1/2}$ from Five Laboratory Experiments

Source	Case	λ_f	u_c/u^*	$(z_o/2H_r)^{-1/2}$	$(\lambda_f/2)^{-1/2}$
Raupach et al. (1980)	B (see Figure 6)	0.011	11.4	14.9	13.5
	C (see Figure 6)	0.023	9.0	9.1	9.3
	D (see Figure 6)	0.045	7.6	7.5	6.7
	E (see Figure 6)	0.091	6.1	5.9	4.7
	F (see Figure 6)	0.179	5.7	5.5	3.3
Snyder (unpublished)		0.021	4.8	4.5	9.8
Petersen and Ratcliff (1989)	x = 1.35m	n.a.	5.7	5.0	NA
Tank Farms	x = 2.7m (3 cm z_o)	n.a.	7.7	9.8	NA
	x = 2.7m (50 cm z_o)	n.a.	5.6	7.4	NA
Havens et al. (2001)	Mean of 7 repeat measurements	0.016	8.8	10.5	11.2
	Mean of 4 repeat measurements	0.028	8.3	8.9	8.5
Macdonald et al. (2000)	Square array	0.0625	6.4	4.6	5.7
	Staggered array	0.0625	5.3	4.3	5.7
	Square array	0.16	3.3	4.5	3.5
	Staggered array	0.16	3.8	3.7	3.5
	Square array	0.44	1.4	6.9	2.1
	Staggered array	0.44	0.7	6.0	2.1

3.4.4. The Turbulence Field within the Obstacle Array

There is only limited information about turbulence within, and near to, obstacle arrays.

A recent review of atmospheric turbulence over cities is provided by Roth (2000), and Table 4 contained a summary of the data he analyzed. The data above the obstacle array are consistent with the hypothesis that the turbulence components nondimensionalized with u^* are independent of height, that is $\sigma_u/u^* \approx 2.4$, $\sigma_v/u^* \approx 1.9$, and $\sigma_w/u^* \approx 1.3$.

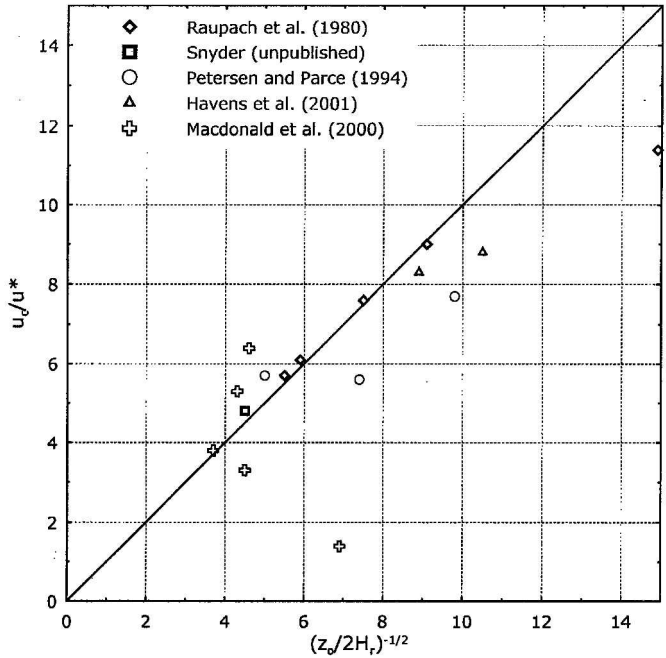

FIGURE 14. Comparison between observations of u_c/u^* and predictions given by $u_c/u^* = (z_o/2H_r)^{-1/2}$, for the same data as listed in Table 7.

Turbulence observations which extended down to about $z/H_r \approx 0.7$ were reported by Rotach (1995) from a field experiment in Zurich. The geometrical scenario was more typical of a densely packed urban area than a widely spaced obstacle array. Data for nearly neutral conditions at the lowest measurement height give $\sigma_u/u^* = 1.22$, $\sigma_v/u^* = 1.13$, and $\sigma_w/u^* = 1.25$. The typical observed variability in these ratios was about 25 to 50%. The reduction in the horizontal components, σ_u/u^* and σ_v/u^*, may be due to the confinement in the street canyons.

The unpublished data from Snyder for $\lambda_f = 0.027$ quoted in section 3.4.2.3 also provided comprehensive turbulence data (all three components) throughout the obstacle array. The turbulence levels were surprisingly constant throughout the array, particularly in the vertical direction. The spatially averaged turbulence levels were scaled with u^* to produce $\sigma_u/u^* \approx 1.6$, $\sigma_v/u^* \approx 1.46$, and $\sigma_w/u^* \approx 1.07$.

A larger value of $\lambda_f = 0.16$ was used in the water flume experiments by Macdonald et al. (2000) using cubes and billboard shapes. Typically five vertical profiles were combined to form averages. The turbulence

levels within the array were *less* than those outside the array. For cubes in a square array $\sigma_u/u^* \approx 1.8$, $\sigma_v/u^* \approx 1.3$, and $\sigma_w/u^* \approx 1.1$ and for staggered arrays $\sigma_u/u^* \approx 1.4$, $\sigma_v/u^* \approx 1.3$, and $\sigma_w/u^* \approx 0.9$. For billboards $\sigma_u/u^* = 1.9$ and 1.4 for the two array types. Averaging both array types and obstacle types gives $\sigma_u/u^* \approx 1.6$, $\sigma_v/u^* \approx 1.3$, and $\sigma_w/u^* \approx 1.0$. Less extensive experiments for more widely spaced obstacles with $\lambda_f = 0.0625$ showed similar results with $\sigma_u/u^* = 1.9$ for cubes in a square array and $\sigma_u/u^* = 1.6$ for cubes in a staggered array.

Broadly speaking, all these results suggest that for $\lambda_f = 0.027$, 0.0625 and 0.16 the turbulence levels may be assumed to be approximately uniform throughout the array, and may be assumed to scale on u^*, and to be less than outside the array. Typical values found are $\sigma_u/u^* \approx 1.6$, $\sigma_v/u^* \approx 1.4$, and $\sigma_w/u^* \approx 1.1$, which can be compared with values of 2.4, 1.9 and 1.3 outside the array. The biggest effect of the obstacles appears to be the removal of the influence of large horizontal eddies, which cannot exist in the relatively narrow confines between the obstacles. The vertical component is not affected as much, since those eddies are relatively small to begin with and since vertical motions are not inhibited in the upward direction. Of course these turbulence levels represent averages of many point measurements and they will contribute to the dilution of any pollutant release. There will be an additional contribution to the dilution of a release arising from the spatial variation of the mean velocity in the horizontal plane due to obstacles. This will enhance the diluting effect of the turbulence and likely lead to "effective" turbulence levels within the obstacle array similar to those outside the array.

It may also be appropriate in modeling activities to consider an isotropic (i.e., constant in all directions) velocity fluctuation within the array. Averaging the three components of energy would produce a velocity fluctuation of 1.4 u^* within the obstacle array. This result is consistent with the limited field data from Rotach (1995) for a situation with much larger λ_f.

The experimental results are generally supportive of models which would assume uniform turbulence levels throughout the array. A model for the spatially averaged velocity profile developed by Raupach et al. (1980) assumed a constant turbulent velocity and turbulent viscosity within the roughness sublayer. Briggs (2000, private communication) suggests that both the turbulent viscosity and the dissipation rate

of turbulent kinetic energy are likely to be more uniform within the obstacle array than their variation above the obstacle array.

3.4.5. Extensions to Other Effects within the Obstacle Array

3.4.5.1. THE EFFECT OF ATMOSPHERIC STABILITY

There is little experimental evidence to assist understanding of the effect of atmospheric stability on the previous conclusions. This is partly because nearly all the well-controlled laboratory experiments are for neutral stability and partly because the specification of atmospheric stability for very rough surfaces such as cities is unclear. Nevertheless we expect that the enhanced turbulence arising due to the rough surface will tend to reduce the effect of nonneutral atmospheric stabilities, particularly when dealing with the flow within and near the roughness elements themselves. Thus we expect our previous arguments to remain valid for nonneutral atmospheric stabilities.

Possibly of more concern will be the effect of thermal sources within the obstacle array due to, for example, thermal sources from energy stored in building structures from solar radiation or from direct generation within a building or industrial plant. These sources may be seen to reduce the likelihood of stable atmospheric conditions. They may also provide a source of turbulent kinetic energy within the obstacle array in addition to mechanically produced turbulence. These thermal sources may be mimicked through the use of an effective convection velocity w^* in place of the friction velocity u^*.

A convection velocity may be estimated as

$$w^* = \left(\frac{g H_s H_r}{\rho c_p T} \right)^{1/3}$$

where g is the acceleration due to gravity, ρ, c_p, and T are the density, specific heat, and temperature of the air and H_s is the heat generation or release rate divided by the site area. H_r is still the average obstacle height. Such a convection velocity is commonly used when studying the convective mixed layer. Its application to turbulence generation due to heat release within an urban area or industrial complex is speculative but likely to be appropriate. Its operational application would be to specify that whenever u^* fell below w^* then w^* should replace u^*.

3.4.5.2. THE TRANSITION REGION BETWEEN THE UPSTREAM VELOCITY FIELD AND THE FULLY DEVELOPED VELOCITY FIELD WITHIN AND NEAR THE OBSTACLE ARRAY

When the upstream atmospheric flow encounters an urban area or industrial complex, or other changes in the surface conditions, there will be a transition distance where the upstream flow changes to the fully developed velocity field downwind that has been the subject of this section.

For the flow above the roughness elements, this change is interpreted as the growth of an internal boundary layer, as in Figure 2. At lower levels, near the roughness elements there are large alterations to the flow field at the upwind edge of the roughness change which then relax back to a nearly unchanging, fully developed velocity field downwind. This relaxation requires a distance of about five to ten obstacle heights (Britter, 1982).

For the mean velocity field, Jerram et al. (1994), using laboratory and field data with cubes, show that a distance corresponding to about five obstacle heights was necessary to approach a fully developed flow. Macdonald et al. (2000), also using cubes and with $\lambda_f = 0.16$, found that the velocity field near to the roughness elements showed little further development beyond the first or second row of obstacles, a distance into the array of only 2–4 obstacle heights.

It appeared that the flow within the obstacle array adjusted more rapidly than the flow well above the array. On the basis of these limited experiments, it appears that the fully developed velocity field will have been attained within a distance of five obstacle heights into the array.

Real industrial sites and urban areas will have far more complex changes in surface geometry, and transition regions between different roughness regimes will be less easy to define. Nevertheless if H_r can be estimated for the site, it is expected that the velocity field within the complex geometry will take a distance less than 5 H_r to reach some fully developed state.

In the transition region at the upwind edges of an urban or industrial site, the mean velocities and turbulence levels will be larger than in the fully developed boundary layer over the site. Thus, assuming zero transition distance could lead to concentration overestimates in a dispersion calculation, although the magnitudes of these overestimates are difficult to specify. To be conservative, it is recommended here that the transition distance be ignored in dispersion calculations.

3.4.6. Summary of Recommendations for Wind Speed and Turbulence within Obstacle Arrays

The essential points arising from Section 3.4 are as follows:

1. The average wind velocity, u_c, below the obstacle height can be estimated in terms of u^*, z_o, and H_r using Eq. (29).
2. The average turbulent speed below the obstacle height is proportional to u^* with the coefficients of 1.6, 1.4, and 1.1 for the longitudinal, lateral, and vertical velocity fluctuations, respectively.
3. In terms of the dispersing ability of the flow, an effect due to the spatial variation of the mean velocities will produce "effective" levels of turbulence that may be assumed to be similar to the levels of turbulence above the obstacles. That is, they will scale on u^* with coefficients of 2.4, 1.9, and 1.3, respectively.

3.5. Summary of Recommended Methods for Estimating z_o, d, and Flow Characteristics Such as Wind Profiles, Friction Velocity (u^*), and Turbulence Velocities in Urban and Industrial Areas

Sections 3.3 and 3.4 reviewed the literature and described specific formulas recommended for estimating flow characteristics in the presence of surface obstacles typical of urban and industrial sites. In this section we bring these recommendations together in a structured format which may be operationally useful to the reader.

For many readers the principal use of this section is the provision of specific guidance in determining the parameter z_o to enter into available operational transport and dispersion models. Somewhat more sophisticated, though possibly not commercially available, transport and dispersion models would likely require the parameters d and u^* as inputs and guidance is provided here for their selection also. Additionally, we provide recommendations for the mean wind velocity profile, and turbulent velocities above and within the array of surface roughness obstacles.

The recommendations for flow within the array of obstacles are novel and are based on limited experimental information and analysis. This book focuses on the combined effects of many obstacles on the averaged flow and does not emphasize the specific flow details around individual obstacles. Such details are discussed in basic references (e.g.,

Hosker, 1984), which emphasize phenomena such as the size and flow structure of recirculating zones behind buildings

A computer program, ROUGH, that calculates the averaged geometric parameters H_r, λ_f, and λ_p characterizing an array of roughness obstacles in an industrial facility or an urban area is described in Section 3.5.5. Alternate simplified methods are also suggested.

Finally, we address the problems of specifying the mean velocity and the atmospheric stability category to be used as inputs to the dispersion model.

3.5.1. Definition of Region of Interest (from Source to Receptor)

A pollutant cloud travels over a distance, x_t, from the source to a given receptor position. Note that a receptor could be a monitoring instrument, or a potentially sensitive location such as a school, or any hypothetical location where an estimate of the pollutant concentration is desired. The cloud passes over a surface characterized by one or more roughness obstacle types. If the roughness obstacle types are different, it may be necessary to account for the changes in underlying roughness over the cloud's trajectory. If the roughness obstacle types are generally similar (i.e., vary by less than a factor of two) over the cloud's trajectory, then a single averaged roughness length can be assumed. The "factor of two" criterion is suggested because it is known that maximum C/Q is roughly proportional to $z_o^{-0.2}$, implying that a factor of two change in z_o will cause a 15% change in maximum C/Q. Even if the obstacle types and roughness lengths vary greatly with distance, it is not necessary to account for areas of roughness obstacles that occupy so small a space that they have hardly any effect on the flow and dispersion properties. By "small" we mean a distance of less than the maximum of 10 H_r, 20 m, and about 20% x_t in an along-wind direction and/or an angular coverage of less than about 30 degrees. These criteria are based on discussions in previous sections and are suggested as preliminary guidance, which is expected to be refined as further data and theories are developed. It follows that the effective roughness length over the cloud's trajectory will depend on the distance and the wind angle, as well as the season of the year if vegetation is present. As an additional criterion, as discussed in Section 3.4.5, a group of roughness obstacles is to be considered only if there are about 20 or more obstacles in the group.

It is implied from the 30-degree angle criterion that the calculations of effective z_o should not be broken down into less than 30-degree sectors. Furthermore, as stated above, differences in z_o of less than a factor of two are insignificant and would justify combining of wind sectors.

The recommended method for calculating a single representative z_o and d value is outlined below, based on discussions in Section 3.3 and Eqs. (19a), (19b), and (19c), where example calculations were given. The recommendation in Section 3.3 is repeated below.

Step 1: Use Eqs. (17) and (18) to calculate z_{oi} and d_i for each individual distance range Δx_i between the source and receptor. The total number of distance increments is n. To be considered in this calculation, a roughness surface should extend laterally over an angle of at least 30 degrees, since this is approximately the angle covered by a pollutant plume. The roughness surface should also extend in the x direction over a distance of at least 20% of the total distance from source to receptor, x_t. This distance should also exceed the maximum of 20 m or 10 H_r, in order to assure that an equilibrium boundary layer has been generated by a new roughness surface. Note that x_t is the sum of the Δx_i values and is the total distance from the source to the receptor.

Step 2: Calculate the effective z_o and d over the distance, x_t, and the 30-degree sector using the following formulas for the geometric mean:

$$\ln z_o = (1/x_t) \sum(\Delta x_i) \ln z_{oi} \qquad [19a]$$

$$\ln d = (1/x_t) \sum(\Delta x_i) \ln d_i \qquad [19b]$$

This method weights all roughness surfaces equally, with no dependence on nearness to the source or the receptor. This method also gives no weight to roughness upwind of the source.

Variations in z_o and d can be accounted for in 30-degree sectors around the compass. For specific directions of special interest, where there is a major z_o variation within the 30-degree sector centered on that direction, a smooth interpolation of z_o is assured by use of the formula:

$$\ln z_o = \frac{\sum \left(\Delta WD_j \right) z_{oj}}{30 \text{ degrees}} \qquad [19c]$$

where z_{oj} is the roughness appropriate for the sector ΔWD_j. Section 5.7 gives a worked example showing the use of Eqs. (19a) and (19c).

3.5.2. Determination of z_o and d

Recommended formulas for z_o and d are given for a hierarchy of complexity in the paragraphs below. Similarly, the techniques increase in objectivity and, probably, in accuracy. In addition, the dependence on arbitrary user decisions decreases as the complexity increases.

It is important to recognize that, for all techniques described below, an equilibrium boundary later develops only after the air has flowed over many individual obstacles. This could be interpreted as flow over any "rows" of obstacles—on the order of five to ten or more rows. Although there is no firm rule, it can be recommended that, for fairly regular spacing of obstacles, a z_o and d approach is useful only if there are at least five rows of obstacles (or at least 20 or 30 total obstacles), as discussed in Section 3.4.5. Earlier, we recommended that the criterion max (2 m, 10 H_r) be used for establishment of an equilibrium boundary layer.

3.5.2.1. METHODS OF ESTIMATING z_o AND d BASED ON EXPERIENCE

Experience Method (1): Detailed studies of urban areas and industrial sites and more complex calculations at specific sites suggest that z_o will be within 0.2 and 3.0 m with a reasonable estimate being 1 m (e.g., see Tables 3, 5a, and 5b). The displacement length, d, can be assumed to be about 5 m for first-cut scoping studies.

Experience Method (2): More discrimination can be provided in a second approach by comparing a specific site with the characteristics of standard sites, for which measured or calculated values of z_o had been obtained. For example, consider a range of types or urban and industrial sites, such as those discussed in Table 5b. Three categories of industrial sites can be considered, based on discussions by Petersen and Parce (1994), Grimmond and Oke (1999), and Davenport et al. (2000):

Category 1 ("Rough" category in Table 5b)—There are scattered buildings and/or industrial obstacles at relative separations of 8 to 12 obstacle heights. This category corresponds to a moderate-sized fairly open residential area or industrial site with H_r = 5 m and λ_f and λ_p = 0.01 to 0.05. In this case z_o is about 0.25 m and d can be assumed to be about 2 m.

Category 2 ("Very Rough" category in Table 5b)—There is moderate-sized typical congestion, covered by low buildings and/or industrial tanks at relative separations of 3 to 7 obstacles heights, with H_r = 5 to 10 m and λ_f = 0.1 to 0.3. In this case z_o is about 0.5 to 1.0 m and d is about 5 m. This category would apply to most urban and industrial sites.

Category 3 ("Chaotic" categories in Table 5b)—This is a large and compact (many close obstacles) urban or industrial site, possibly surrounded by other industrial sites or urban areas with H_r = 10 to 20 m and λ_f = 0.4 or 0.5. In this case z_o is about 1.0 to 2.0 m and d is about 5 to 10 m.

These recommendations for z_o and d are primarily based on the authors' review of many documents in preparing this handbook and are consistent with our recommended equations (17) and (18).

3.5.2.2. METHODS OF ESTIMATING z_o AND d BASED ON THE SIMPLEST GEOMETRIC DESCRIPTION OF THE SITE

If we accept an uncertainty of a factor of two in z_o, the recent review by Grimmond and Oke (1999) suggests that for λ_f between 0.1 and 0.4, or for λ_p between 0.2 and 0.6, we might simply assume the rule of thumb:

$$z_o/H_r = 0.1 \tag{33}$$

Similarly,

$$d/H_r = 0.5 \tag{34}$$

For a typical urban or industrial site, the λ_f and λ_p parameters are nearly always between about 0.1 and 0.3. Since the average building or obstacle height, H_r, is about 10 m, it follows that the following single estimates of z_o and d are appropriate for individual sites.

$$z_o = 0.1 * 10 \text{ m} = 1 \text{ m} \tag{35}$$

and

$$d = 0.5 * 10 \text{ m} = 5 \text{ m} \tag{36}$$

These estimates are consistent with the estimates for the typical "Category 2" site in the previous section.

The data in the references demonstrate that these simple constants are likely to be within a factor of two of the local "observed" values at individual field sites.

It is important to mention the upper limit to H_r in these geometric methods. Because the z_o concept is valid only in the surface boundary layer, which is about 50 to 100 m deep, the obstacle heights, H_r, should not exceed about 25 to 50 m. This means that the geometric methods should not be used when H_r is greater than about 20 m and therefore formulas such as $z_o = 0.1\ H_r$ are not valid in the centers of large cities with tall skyscrapers.

At smaller and larger values of the λ parameter, the larger values being appropriate for more densely packed obstacles typical of urban centers, a more detailed analysis may be required.

It must be noted that the determination of the "roughness element height" or the "average building height," H_r, will produce the greatest uncertainty in application. Earlier, it was stated that the standard deviation in obstacle heights, σ_{H_r}, is approximately equal to 0.5 or 1.0 H_r for several urban areas. The standard deviation σ_{H_r} would be relatively large at industrial plants, too, where stacks and other tall structures are often present. Objective ways to determine the average H_r will be described in Section 3.5.5. In general, it is necessary first to prescribe an area for analysis; then information on obstacle geometry is used to estimate the required parameters. However, despite this appearance of complexity, it is interesting to note that the estimates of H_r made by Grimmond et al. (1998) for a wide variety of urban surfaces and listed in Table 3 usually come out to be about 5 to 15 m.

Because the parameter z_o and d are scaling lengths that characterize the drag effects of the surface roughness obstacles, we assume that they are not dependent on atmospheric stability.

3.5.2.3. METHODS OF ESTIMATING z_o AND d BASED ON H_r, λ_f, AND λ_p

At small values of the λ_f parameter (i.e., less than about 0.1) the approach of Lettau (1969) appears to be satisfactory. However, we recommend a leading coefficient of 1.0 rather than 0.5 in his formula, to account for the fact that the obstacles in real urban and industrial sites have sharper edges and corners than those used by Lettau. The resulting simple formula is given below:

$$z_o/H_r = 1.0\ \lambda_f \qquad \text{(for small } \lambda_f\text{, less than about 0.1)} \qquad (37)$$

The Grimmond and Oke (1999) review would also suggest a correlation with λ_p:

$$z_o/H_r = 0.5\ \lambda_p \qquad \text{(for small } \lambda_p\text{, less than about 0.2)} \qquad (38)$$

The work of Grimmond and Oke (1999) suggests that, for small λ_f, a simple correlation for the displacement height d would be:

$$d/H_r = 3.0\,\lambda_f \text{ or } 1.5\,\lambda_p \qquad \text{(for small } \lambda_f \text{ or } \lambda_p\text{)} \tag{39}$$

For the general situation where the roughness obstacles could have any types of spacing, and a more accurate estimate of z_o and d is desired, it may be appropriate to account for the nonlinear dependency of z_o/H_r and d/H_r on λ_f and λ_p. A set of simple analytical equations has been suggested in Section 3.3.4 that provides a fit to the observed urban data reported by Grimmond and Oke (1999) and plotted in Figure 12. These formulas account for the fact that, in a real industrial plant or urban area, the ratio z_o/H_r does not approach zero as obstacles become very close together, since real obstacles (e.g., buildings and tanks) are not cubes with uniform heights and shapes, but have a relatively large effective roughness even when packed closely. Therefore we assume a value of $z_o/H_r = 0.15$ at the limit of close obstacle packing. The formulas are based on λ_f (normalized frontal area), since we believe that parameter is the best indicator of z_o and d, because the obstacle drag is related more to the frontal area than the top area. However, since λ_f can exceed 1.0, for closely packed obstacles that are much taller than they are wide, we restrict λ_f to be less than 1.0 in these formulas.

For the entire range of obstacle densities (λ_f), the following formulas account for the limit at large λ_f and provide reasonable fits to the data at smaller λ_f:

$$z_o/H_r = \lambda_f \qquad \text{for } \lambda_f < 0.15 \text{ (isolated and early wake regimes)} \tag{40a}$$

$$z_o/H_r = 0.15 \qquad \text{for } \lambda_f \geq 0.15 \text{ (interacting wakes)} \tag{40b}$$

$$d/H_r = 3\lambda_f \qquad \text{for } \lambda_f < 0.05 \text{ (isolated regime)} \tag{41a}$$

$$d/H_r = 0.15 + 5.5(\lambda_f - 0.05) \quad \text{for } 0.15 > \lambda_f \geq 0.05 \text{ (wake regime)} \tag{41b}$$

$$d/H_r = 0.7 + 0.35(\lambda_f - 0.15) \quad \text{for } 1.0 \geq \lambda_f \geq 0.15 \text{ (interacting wakes)} \tag{41c}$$

(If $\lambda_f > 1.0$, then set $\lambda_f = 1.0$.)

Note that Eqs. (40a) through (41c) are repeats of Eqs. (17a) through (18c), respectively.

The descriptive terms (e.g., isolated regime) are taken from the schematic diagram in Figure 4, with the correction that we do not consider the skimming flow regime to be appropriate for real urban or industrial sites.

These piecewise linear formulas provide good fits to the observed behavior of z_o/H_r, which first increases as λ_f increases, and reaches a maximum of 0.15 at $\lambda_f = 0.15$. We assume that z_o/H_r remains nearly constant as λ_f becomes large, since the real-world obstacles have a range of heights such that $\sigma_{H_r}/H_r = 0.5$ to 1.0. Similarly, d/H_r increases slowly at first, then more rapidly, and finally gradually approaches 1.0 as λ_f approaches 1.0.

3.5.3. General Simple Formulas for u, u(z), and Turbulent Velocities*

Given the estimates of z_o/H_r and d/H_r from the alternate methods in Section 3.5.2, the friction velocity can be estimated from a wind speed observation or estimate, u, at some height, z, which is above H_r:

$$u^* = \frac{0.4u(z)}{\ln[(z-d)/z_o]} \tag{42}$$

In the case of nonneutral stability, terms involving z/L must be added to Eq. (42), where the detailed formulas are given in basic references such as Stull (1997).

Within the urban or industrial site, the wind speed, u_c, below the obstacle heights, H_r, is given by:

$$u_c/u^* = (z_o/2H_r)^{-1/2} \tag{43}$$

The log-linear wind profile is assumed to apply down to a height, z_{int} , such that $u(z_{int}) = u_c$:

$$u(z) = (u^*/0.4)\ln[(z-d)/z_o] \tag{44}$$

For obstacles with large spacings (i.e, λ_f approaching zero), z_{int} can become much less than H_r and iteration is required to estimate u_c.

The turbulent velocities in the urban or industrial region are given by the following relations at all heights, above and below H_r:

$$\sigma_u/u^* = 2.4\sigma_v/u^* = 1.9\sigma_w/u^* = 1.3 \tag{45}$$

3.5.4. Selection of an Appropriate Mean Wind Speed and Stability

Transport and dispersion models can be typically run in two modes:

1. The hypothetical or "what-if" mode, where the user picks an appropriate set of input conditions which may represent average or worst-case conditions.
2. Real-time or retrospective mode, where the user is using observations to simulate a specific set of conditions.

In the first mode, the worst-case wind speed may be arbitrarily chosen to be a value such as 1 m/s, and the worst-case L may be chosen to be a stable value such as 10 m. But in the second mode, where observations must be used, the problem usually arises that the available observations are not from the best location. For example, the wind speed may be observed at an airport 5 km away, and there is rarely an on-site observation of the turbulent heat flux and momentum flux, used for determining the stability parameter, L.

A simple method is given here for extrapolating the wind speed from a height of, say 10 m, at a nearby airport or other flat site, to a height of 10 m in the industrial area. We assume that the wind speed over both sites is the same at a height such as 30 m and that stabilities are neutral. The 30 m assumption could be based on the fact that the internal boundary layer from a new roughness surface such as an industrial site of width 300 m would rise to that elevation as the air passes over the site. Then, given an estimate of the surface roughness length, z_{o1}, at the airport or other flat site and the surface roughness length, z_{o2}, at the industrial site, we use Eq. (2a) to calculate the airport wind speed at 30 m:

$$u_1(30\text{ m}) = u_1(10\text{ m})\ \ln(30\text{ m}/z_{o1})/\ln(10\text{ m}/z_{o1})$$

Wind speed at $z = 30$ m over airport.

Given $u_1(30\text{ m})$, the wind speed at 10 m over the industrial site is then given by:

$$u_2(10\text{m}) = u_1(30\text{ m})\ \ln(10\text{ m}/z_{o2})/\ln(30\text{ m}/z_{o2})$$

Wind speed at $z = 10$ m over site.

As mentioned earlier, at any given time, the stability over an urban or industrial site is closer to neutral than the stability over the airport or other nearby flat site. This is because the increase in z_o over the rough site causes increases in u^*. And since u^* is cubed in stability parameters

such as L, a factor of 2 increase in u^* results in a factor of 8 increase in L. In the Kit Fox experiments (Hanna and Steinberg, 2001) during evening conditions, L over the rough surface was 100 times larger (i.e., closer to neutrality) than that over the flat desert surface.

Models such as the EPA's ISC3 model handle stability in urban areas by not allowing the extremely stable Pasquill class F to occur at all and by forcing other stability classes toward neutrality (class D) (see Table 1). The EPA's new AERMOD model (Cimorelli et al., 1998) assumes that the stability class over urban areas is never stable, due to the mechanical turbulence and to the heat from an urban area, and then calculates u^* from a surface energy balance. Hanna and Chang (1992) suggest that, over urban areas, during stable conditions, L never be allowed to drop below $3H_r$, since it is argued that the size of the roughness obstacles determine the typical turbulent eddy sizes.

For the purposes of this book, a more simplified approach is desired. Given that hazardous models such as HEGADAS are looking for input of z_o, u^*, and L, we suggest a few simple approximations for typical neutral, unstable, and stable values of L. The nearly neutral L should be input as infinity, as is customary. The unstable L over urban or industrial areas should be assumed to be –100 m and the stable L should be assumed to be 100 m. The more complex alternative is to use a boundary layer meteorology preprocessor code such as SIGPRO (Hanna and Chang, 1992) or the preprocessor code for AERMOD (Cimorelli et al, 1998).

3.5.5. *Estimates of Urban and Industrial Geometric Parameters H_r, λ_f, and λ_p Using the ROUGH Code*

Previous sections contained simplified methods for estimating the geometric parameters H_r, λ_f, and λ_p. If the user has sufficient data concerning the sizes and locations of the hundreds or thousands of buildings, tanks, and other roughness obstacles, he can use the ROUGH software, described by Petersen and Parce (1994), to more precisely calculate these geometric parameters. The primary objective of the ROUGH code is to calculate H_r, λ_f, and λ_p, and most of the lines of the code deal with this issue. ROUGH also contains, as a secondary objective, some equations that may be used to calculate z_o from these parameters. The recommended z_o approach follows Lettau's (1969) formula [see Eq. (14) in this book, page 71]. The ROUGH software does not explicitly calculate

the displacement length, d, although the software contains some internal algorithms that calculate d as part of an interim step in the calculation of z_o.

If there is an interest in making precise calculations of the geometric parameters, the reader should obtain a copy of the ROUGH technical documentation and users guide (the report number and address are given in the list of references under Petersen and Parce, 1994).

The following inputs are required for ROUGH for each roughness obstacle:

1. x and y location of obstacle center
2. Height, length, and width of obstacle
3. Orientation of obstacle as defined by angle from north through obstacle center
4. Vertical solidity (VS) or lack of porosity of frontal area, A_f. Frontal area is calculated as $A_f = VS\, H_r\, W$. $VS = 1.0$ for a solid obstacle and $VS = 0.5$ for a pipe rack.
5. Horizontal solidity (HS) or lack of porosity of top or plan area, A_p. Plan area is calculated as $A_p = HSLW$. $HS = 1.0$ for a solid obstacle and $HS = 0.5$ for a pipe rack.
6. Shape (rectangular, vertical cylinder, or sphere)
7. Stacked or not? Used to calculate plan area, A_p, which is assumed to be valid for the larger element in the stack. This parameter is of use for buildings where the bottom section covers a larger area than the top section.

Once all the obstacle data are entered as inputs to ROUGH, the user can select a sub-area for calculation of the parameters. It is recommend that the area to be selected for calculating H_r and the λ parameters be primarily in the downwind sector of width at least 20 degrees, since the transport and dispersion processes will be occurring in a downwind direction.

Sections 5.1, 5.2, and 5.3 contain some worked examples of the application of the ROUGH code to calculate H_r and λ_f for some typical industrial and urban sites.

After all the effort is expended to collect input data for the ROUGH code, there is no evidence that the resulting estimates of H_r and λ_f are more accurate than the estimates made with one of the simpler methods described earlier. Nevertheless, the ROUGH code is useful in combination with detailed databases of major urban and industrial areas

currently being developed based on architectural drawings, aerial photographs, and other sources. This detailed building data is also useful for estimating flow and dispersion around specific buildings.

We do not recommend the z_o formulas given in the ROUGH software, since the primary formula is the Lettau (1969) formula, and we noted earlier in this section that the formula uses too small a drag coefficient for buildings and therefore underestimates z_o by about a factor of two. Instead, we recommend the simple formulas for z_o given in equations (40) and (41) in Section 3.5.2.3. These formulas make use of H_r and λ_p.

Independent of the ROUGH code, Eqs. (19a) through (19c) provide weighting formulas to be used in case the z_o and d varied substantially over the path from a source to a receptor or over a wind sector (see Section 3.5.1 for a summary recommendation). This formula should be used, for example, if the plume would travel over 200 m of industrial plant obstacles, then travel over 400 m of river surface before reaching a receptor on the shore of the river.

3.5.6. *Range of Uncertainty in Estimates of z_o, d, u*, u(z), and Turbulent Velocities*

The formulas suggested in this book are most valid for the ranges of experimental conditions used in their derivation and evaluation. The corollary of this statement is that the formulas are least valid for conditions outside these ranges, and therefore the resulting models will be least accurate in these conditions. Fortunately, the meteorological variables such as wind speed and turbulence are not very sensitive to factor of two uncertainties in z_o or d. This is because z_o and d enter the formulas as $\ln[(z - d)/z_o]$ and the natural logarithm of a variable changes by only a factor of 2.3 for each order of magnitude change in the variable (i.e., $\ln 10 = 2.3$).

The field data collected by Grimmond and Oke (1999) and shown in Figure 12 illustrate that there is much uncertainty or scatter (about a factor of two or three) about the best-fit lines for z_o and d. Furthermore, it is important to note that Grimmond and Oke (1999) screened many potential urban and industrial data sets and eliminated many data sets because of problems such as poor siting and instrument errors. Therefore, the factor of two or three scatter exists for the "cream of the crop" data sets, characterized by fairly uniform roughness obstacle arrays and

well-sited meteorological towers and instruments. For obstacle arrays characterized by much heterogeneity, uncertainties much greater than a factor of two can be expected.

Note that all the formulas for z_o and d use the average obstacle height, H_r, as a scaling or normalizing parameter. But H_r itself is subject to uncertainty, which may account for much of the scatter in Figure 12. Even for a "homogeneous" urban or industrial site, σ_{H_r} is about 0.5 or 1.0 H_r. This book recommends that H_r be calculated for a downwind sector in the urban or industrial complex. The average obstacle height, H_r, depends on the area chosen to take the average and also may depend on the direction the wind is blowing from the source position. The principle was also used in Eqs. (19), which can be applied to regions with variable z_o over a range of surface types. For example, one portion of an oil refinery complex may consist of tanks with height 15 m and another portion may consist of a group of porous pipe racks with height 8 m. Fortunately, as stated above, u^* and other boundary layer parameters are relatively insensitive to factor of two uncertainties in z_o and d.

4

Integration of Roughness into Dispersion Models

4.1. Objectives and Fundamental Physical Concepts

The objective of this chapter is to describe how structures or obstacles (such as buildings and storage tanks) at an industrial site or an urban site affect transport and dispersion and show how these effects can be parametrized in consequence models, using the principles presented in Chapters 1 through 3.

It is generally true that the maximum normalized near-ground-level concentration, C/Q, on the centerline of the pollutant cloud depends on the speed (called the effective transport or advective speed u_e) at which the cloud is moving, and on the turbulent dispersion coefficients, σ_x, σ_y, and σ_z. Of course, this statement is true for clouds released below or above the average roughness obstacle height, H_r. It has been shown in Chapters 2 and 3 that the effective advective speed, u_e, and the turbulent dispersion coefficients, σ_x, σ_y, and σ_z, are all proportional to the friction velocity, u^*, and u^* itself will, in general, increase as the surface roughness increases.

Figure 15 provides a schematic view of the various regimes discussed in previous chapters and emphasized in this chapter. In both parts of the figure, a similar urban/industrial grouping of surface

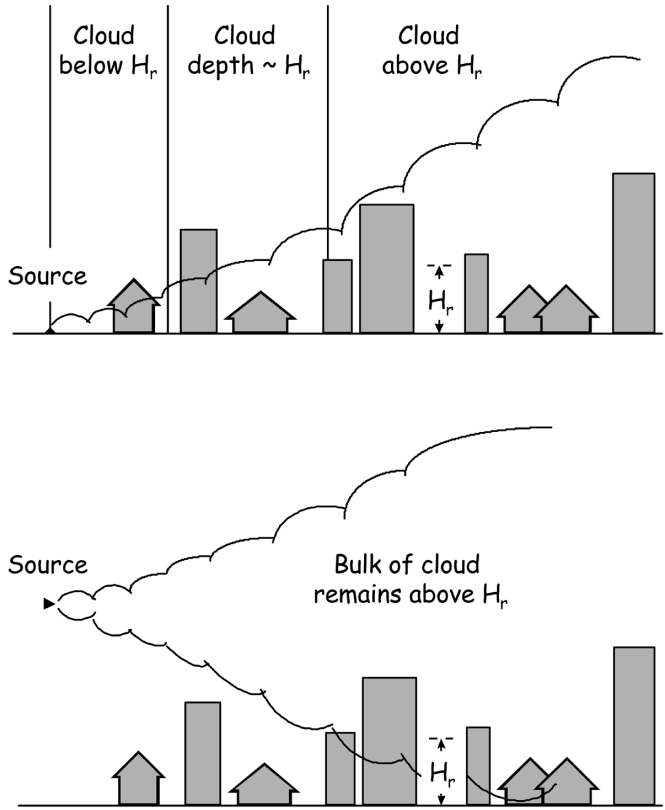

FIGURE 15. Schematic diagram of cloud released at the ground (top) and at a height well above H_r (bottom) illustrating the three regimes discussed in the text.

roughness obstacles is shown with average obstacle height H_r. The top part of the figure illustrates the vertical cloud growth for a near-ground release, where the cloud is initially confined below H_r, then passes through a transition regime with the cloud depth approximately equal to H_r, and finally reaches a regime where the bulk of the mass of the cloud is above H_r. These three regimes are discussed in more detail in later sections. The bottom part of the figure illustrates the vertical cloud growth for a release well above H_r, where the bulk of the mass of the cloud remains above H_r even after the cloud base has dispersed down to the ground. Note that the range of heights defined by 0.5 H_r to 2 H_r is commonly called the urban roughness sublayer.

Figure 16 is included in order to show how the cloud advective speed, u_e, will increase as the cloud grows vertically as it moves down-

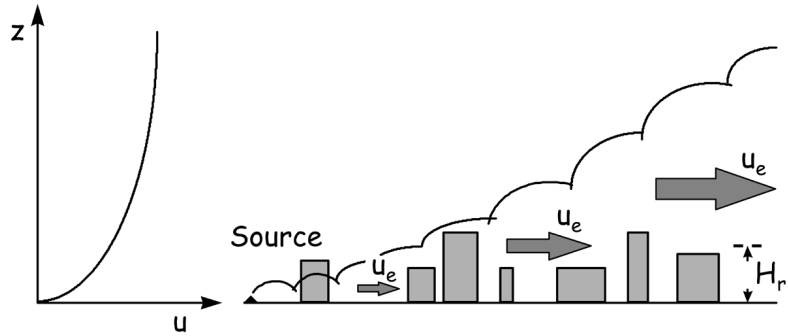

FIGURE 16. Schematic diagram of cloud released at the ground illustrating how the cloud advective speed, u_e, increases with downwind distance. The u_e vectors are plotted at the mass-median height of the cloud. The length of the vector represents the wind speed, and the wind speed profile is plotted on the left.

wind, for clouds released near the ground. The corresponding boundary-layer wind profile is drawn on the left side of the figure. Each u_e vector is drawn at the mass-weighted mean height of the cloud, which is defined in Eq. (1) and which is generally assumed to equal about 0.5 to 1.0 σ_z for a cloud on the ground.

Section 2.3.2 illustrated the dependence of plume centerline normalized concentration, C/Q, on z_o and on u^* for a simple Gaussian plume model. To illustrate the importance of u^*, consider the simple Monin–Obukhov similarity model for near-ground-level releases. Assume a straightforward scenario where a continuous plume is released at rate Q from the ground during nearly neutral conditions over a uniform surface such that the cloud depth exceeds H_r. In this case, the friction velocity u^*, and the downwind distance, x, are found to completely determine the solution for the plume centerline normalized concentration, C/Q, and for the crosswind-integrated normalized concentration, C_y/Q (Hanna et al. 1990, Britter et al. 2000). C_y is defined as $\int C\,dy$, where the integration takes place along a horizontal line perpendicular to the plume centerline axis. The following equations express these simple relationships and have been validated by Hanna et al. (1990) using data from the Prairie Grass dispersion experiment.

$$C/Q = 3.0/(u^*x^2) \tag{46}$$

$$C_y/Q = 1.6/(u^*x) \tag{47}$$

The Prairie Grass experiments involved neutrally buoyant plumes (i.e., passive dispersion). Equations (46) and (47) have been shown to

be valid for nearly neutral conditions (i.e., very large L) over distances, x, ranging from 50 to 800 m at the Prairie Grass site. For nonneutral ambient boundary layers, a simple power law function of x/L is added to the equations. These equations show that C/Q and C_y/Q are inversely proportional to the friction velocity, u^*, thus implying that C/Q and C_y/Q will decrease as roughness increases, since u^* is increased by an increase in roughness.

For negatively buoyant (i.e., dense gas) releases at ground level, Briggs et al. (2001) studied three parallel experiments in different wind tunnels and found (somewhat surprisingly) that all the effects of surface roughness on vertical dispersion were through the variation of u^* with z_o. The form of their equation is similar to Eq. (47), with a correction for plume density. These experiments involved cloud depths evolving from less than H_r through much greater than H_r, similar to the scenario depicted in the top part of Figure 15.

If a cloud is released at a height much greater than H_r, as shown in the bottom part of Figure 15, the ground-level concentration can be estimated by the simple Gaussian plume model [Eq. (9)], with u_e constant (at the height of release). As before, u_e and the turbulent dispersion coefficients are all proportional to u^*. For such releases, the near-field maximum concentrations at ground level are likely to increase as the roughness increases due to the enhanced vertical dispersion, which more quickly disperses the base of the plume to the ground. It is also possible in many situations for concentrations at ground level to increase near roughness obstacles such as buildings and storage tanks if the elevated plume is caught in the wake behind individual obstacles and mixed down to the ground. At larger distances downwind, as seen on the right side of the bottom part of Figure 15, the cloud is well-mixed all the way down to the ground surface (i.e., σ_z exceeds the source release height), and the effect of increases in surface roughness will be to decrease the ground-level concentrations, in the same way as for near-surface releases.

If a cloud is released at a height much lower than H_r and the cloud depth is smaller than H_r, as shown on the left side of the top part of Figure 15, the concentration prediction equations are slightly different from Eqs. (46) and (47) but the wind speed and the dispersion coefficients are still proportional to u^*. In most of these cases where the cloud is below H_r, concentrations will decrease as the roughness increases. However, in some situations involving ground-level releases of contin-

uous plumes or clouds in more densely packed obstacle arrays, when the cloud height is lower than H_r, ground-level concentrations may not decrease as roughness obstacle heights increase. Because the wind speed acts to dilute a continuous plume or cloud, if the wind speed is markedly decreased down within the obstacles, the reduction in dilution may sometimes dominate over the increase in turbulent velocities and may cause C/Q to increase. This situation is most likely to happen for dense obstacle packing (i.e., large λ_f and λ_p).

It is important to have the solutions exhibit a smooth transition in the urban roughness sublayer between the "above H_r" case and the "below H_r" case (i.e., for the two cases shown in Figure 15). Also, the transition should be smooth for the "below H_r" case as the cloud is carried downwind and passes through the three regimes shown in the top part of Figure 15. Otherwise there could be large differences in model calculations of C/Q over very short increments of distances. It will be seen that, since our methodology depends so strongly on u^*, the transition is smooth.

The Gaussian model [e.g., Eq. (9)] is used as the basis for our discussions in subsequent sections. It is assumed that the Gaussian model applies both above and below H_r, and that all we have to do is specify the cloud speed u (or more accurately, u_e) and the three dispersion coefficients (σ_x, σ_y and σ_z), which are all functions of u^* and therefore are functions of z_o and d.

The following sections describe the recommended approaches. They are divided into categories according to whether the cloud extends above H_r, is below H_r, or is approximately equal to H_r.

4.2. Dispersion Models for Clouds Extending Above H_r

4.2.1. Introduction to General Characteristics of Models

If the cloud depth and/or the cloud release height greatly exceed H_r, the problem simplifies to the standard atmospheric transport and dispersion problem studied by researchers and model developers for decades. This is the situation depicted on the right side of the top panel and depicted in the entire bottom panel of Figure 15. Dozens of models exist and are used for a wide variety of purposes, including regulatory applications and hazard assessments (e.g., DeVaull et al., 1995; Hanna et al., 1996).

Whether the model is a Gaussian plume or puff model, a similarity model [see Eqs. (46) and (47)], a Lagrangian particle dispersion model, an Eulerian grid model, or any other model dependent on knowledge of the atmospheric boundary layer, Monin–Obukhov scaling applies and the model parameters can be expressed in terms of u^* and L, or w^* and z_i in convective conditions. All models require an estimate of the cloud advection speed, u_e, and a measure of the rate of dispersion. Therefore, the concepts discussed in this book are applicable to any of these types of models. As was well established in Chapters 1 through 3, estimation of z_o and d are crucial to estimation of u^*.

If the cloud is denser than air or is more buoyant than air, the transport and dispersion will also depend on the difference between the cloud density and the air density. For example, a dense cloud will tend to have a smaller vertical size and a larger lateral size than a neutrally buoyant cloud. A positively buoyant cloud, such as a hot plume from a combustion process, may be dominated by its internal buoyancy rather than ambient turbulence in its initial stages and may rise above the height at which it was initially released.

4.2.2. Summary of Dispersion Experiments over Rough Surfaces

As discussed in Section 2.4, full-scale urban tracer experiments, such as the St. Louis tracer study (McElroy and Pooler, 1968), confirm our expectations that, for a given stability class, the dispersion coefficients for urban conditions are consistently larger than the dispersion coefficients for rural conditions. On a smaller scale, but still in the field, the Kit Fox field experiments demonstrate a very clear trend, where the maximum normalized concentration, C/Q, on the plume centerline decreases as the surface roughness increases. The observed maximum C/Q values at the Kit Fox site are proportional to $z_o^{-1/2}$; i.e., the maximum C/Q decreases by about a factor of about three with each order of magnitude increase in z_o.

Some laboratory studies have been made of flow and dispersion over arrays of roughness elements where the plume size exceeds H_r and therefore the elements can be parametrized through z_o. These studies confirm that the concentration would decrease as the roughness increases, for all other conditions the same (see Roberts et al., 1994). Other laboratory data confirm that it is appropriate to parametrize the effects of an industrial area on dispersion by means of a surface roughness length, z_o (see Britter et al., 1991).

Most of the small-scale field studies and laboratory studies have made use of obstacles with uniform shapes and sizes. Consequently, these results should be extrapolated with caution to real urban and industrial areas, which consist of a mixture of obstacle shapes and sizes.

4.2.3. Gaussian Plume and Puff Model

The Gaussian plume and puff model is used here to illustrate the fundamental physical relations. Note that in these discussions, the term cloud is synonymous with plume or puff. For a continuous nonbuoyant plume with emission rate, Q (g/s), released at height h_e (m) above ground, the near-ground-level concentration, C (g/m^3), predicted by the *Gaussian plume formula* is:

$$C = \left(\frac{Q}{u\pi\sigma_y\sigma_z}\right)\exp\left(-\frac{(y-y_o)^2}{2\sigma_y^2}\right)\exp\left(-\frac{h_e^2}{2\sigma_z^2}\right) \tag{9}$$

where the lateral position of the cloud centerline is y_o. In the case of an instantaneous release of mass Q_t at height h_e, the near-ground level concentration predicted by the *Gaussian puff formula* is:

$$C = \left(\frac{Q_t}{2^{1/2}\pi^{3/2}\sigma_x\sigma_y\sigma_z}\right)\exp\left(-\frac{(x-x_o)^2}{2\sigma_x^2}\right)\exp\left(-\frac{(y-y_o)^2}{2\sigma_y^2}\right)\exp\left(-\frac{h_e^2}{2\sigma_z^2}\right) \tag{48}$$

where x_o is the along-wind position of the center of the cloud. The wind speed, u, in Eq. (9) is more precisely the local cloud advective velocity, u_e, at the downwind position of interest. The distance, x_o, in Eq. (48) is more precisely the integral with time of u_e over the entire cloud trajectory [$x_o = \int u_e(t)\, dt = u_{avg}\, t$], where u_{avg} is the average cloud speed over the time of travel, t.

The horizontal dispersion coefficients, σ_x and σ_y, are proportional to u^*t for travel times up to about fifteen minutes or more. The vertical dispersion coefficient, σ_z, is proportional to u^*t for times up to about 1000 s during sunny light-wind days but only for times up to about 10 to 100 s for stable nighttime boundary layers (Hanna et al., 1996). At larger travel times, it may be necessary to account for a vertical integral scale for turbulence, T_{lz}, as discussed below.

In most practical applications, the concentrations are predicted and assessed at certain downwind distances, x, rather than at travel times, t. Therefore, expressions such as $\sigma_y = 2u^*t$ must be converted to $\sigma_y = 2u^*x/u_{avg}$, since the variables x and t are related through $t = x/u_{avg}$. For nonbuoyant (passive) plumes at heights much greater than H_r, the local effective cloud speed, u_e, is nearly constant with x and t and is easy to determine (see the bottom panel of Figure 15). However, as mentioned earlier, for near-ground-level releases, the local u_e will vary with transport time, since the cloud will steadily disperse upward and will therefore accelerate (see Figure 16). For the Kit Fox field experiments, u_e was observed to increase by a factor of four or five as x increased from 25 to 225 m (Hanna and Chang, 2001). As a general procedure, most hazardous gas models (e.g., HEGADAS) assume that u_e equals the speed at a height of about 0.5 to 1.0 σ_z for near-ground-level releases.

Instantaneous releases (puffs) are likely to be more affected than continuous releases (plumes) by variations in surface roughness. This is because puffs have an additional dimension, as described by the along-wind dispersion coefficient, σ_x, which is also influenced by u^* and by surface roughness. The effect of roughness on maximum ground-level concentrations due to instantaneous puff releases (Q_t in units of mass) near the ground can be approximated from the Gaussian puff Eq. (48) by making several assumptions:

$$C/Q_t = (2^{1/2}\pi^{3/2}\sigma_x\sigma_y\sigma_z)^{-1} = (u_{avg}/u^*)^3(2^{1/2}\pi^{3/2}5.2x^3)^{-1} \qquad (49)$$

where it is assumed, as before, that $\sigma_x = 2u^*t = 2u^*x/u_{avg}$; $\sigma_y = 1.9u^*t = 1.9u^*x/u_e$; $\sigma_z = 1.25u^*t = 1.25u^*x/u_{avg}$; and u_{avg} is the average puff advective speed over its total time of travel. Eq. (49) is valid for the maximum concentration at the center of the puff (i.e., $y = y_o$ and $x = x_o$) for a near-ground-level release (i.e., with $h_e = 0.0$), which causes the three "exp" terms in Eq. (48) to equal 1.0. Equation (49), which is valid for relatively short travel times (about 100 s or less), may be used to demonstrate two effects. First, it is clear that C/Q_t will decrease as z_o increases, since u^* (in the denominator) will increase with z_o, and u_{avg} (in the numerator) will decrease with z_o, for the same free stream or geostrophic wind speeds at the top of the boundary layer. Second, for a given puff release during nearly neutral stability and for a given z_o and x, C/Q_t will not vary with wind speed, since the ratio u_{avg}/u^* will be constant. This latter effect has been seen in the Kit Fox [Enhanced Roughness Pattern (ERP) and Uniform Roughness Array (URA)] and

EPA field trials at the Nevada Test Site, where little trend was seen in C/Q_t with u for the puff releases for all three roughness types and for four downwind distances.

As stated above, the turbulent dispersion coefficients, σ_x, σ_y, and σ_z are proportional to u^*t or u^*x/u_{avg} in the near-field. At larger distances, σ_x, σ_y, and σ_z are observed to be less than linear in t or x. This means that the travel time has exceeded the Lagrangian integral time scale, T_I, for the direction of concern. This behavior is seen in the equations in Table 1, which presents the Briggs formulas for σ_y and σ_z for rural and urban conditions, which are used in many regulatory dispersion models. The along-wind dispersion coefficient, σ_x, can be thought to be proportional to σ_y. Most of the equations in Table 1 involve an initial term which is linear in x and can thought to be proportional to u^*, and a second term of the form $(1 + ax)^b$, which can be related to the term $(1 + t/2T_I)^{-1/2}$ in the statistical theory of dispersion (Hanna et al., 1996). From Table 1 and from the above mathematical expressions, it follows that T_{Ix} and T_{Iy} for the x and y (horizontal) components are about 1000 s or about 15 minutes.

The vertical Lagrangian integral time scale, T_{Iz}, inferred from Table 1 varies with stability, being very large (effectively infinity) for unstable daytime conditions, and relatively small (a few tens of seconds) for stable conditions. For nearly neutral conditions and $u = 5$ m/s, it can be assumed that T_{Iz} equals about 60 s for rural terrain and about 300 s for urban terrain. The effect of stability on dispersion is much more pronounced in the vertical than in the horizontal directions. For stable conditions over rural terrain, the second term in Table 1 has a power of about –1 and the effective T_{Iz} equals about 600 s for rural conditions. For stable conditions over urban terrain, the second term in Table 1 has a power of $-1/2$ and T_{Iz} equals about 60 s.

The above T_I values inferred from Table 1 can be combined and simplified for general use in urban and industrial areas as follows:

$$\sigma_y = \sigma_v t\,(1 + t/2T_{Iy})^{-1/2} \tag{50}$$

$$\sigma_x = \sigma_u t\,(1 + t/2T_{Ix})^{-1/2} \tag{51}$$

$$\sigma_z = \sigma_w t\,(1 + t/2T_{Iz})^{-1/2} \tag{52}$$

where

$$T_{Iy} = T_{Ix} = 1000 \text{ s} \tag{53}$$

$$T_{Iz} = \infty \quad \text{unstable} \tag{54}$$

$$T_{Iz} = 300 \text{ s neutral} \quad \text{and} \quad T_{Iz} = 60 \text{ s stable} \tag{55}$$

The above values of the integral time scales of turbulence should be used for estimating dispersion at heights above H_r in urban and industrial areas. Section 4.3 suggests formulas for T_I for pollutant clouds located at heights below H_r.

The friction velocity, u^*, is a key variable that can be estimated from an observation of wind speed and from knowledge of z_o and d, which depend on the average obstacle height, H_r, and on obstacle shapes and spacings. Section 3.5 suggests a hierarchy of straightforward methods for estimating z_o, d, and u^*. If we accept an uncertainty of a factor of two in z_o then, for most scenarios typical of urban and industrial areas, the rules of thumb: $z_o/H_r = 0.1$ and $d/H_r = 0.5$, can be assumed. Since the average building or obstacle height, H_r, is 10 m, it follows that $z_o = 0.1*10$ m = 1 m and $d = 0.5*10$ m = 5 m. More precise estimates of z_o and d as a function of λ_f can be made using Eqs. (17) and (18).

As shown by the above equations, for clouds much deeper than H_r (seen on the right hand side of the top panel in Figure 15), there can be a wide range of obstacle densities (say λ_f greater than about 0.1) for which the maximum cloud concentrations will not be sensitive to the obstacle density. But, as implied earlier, a further influence on lateral dispersion will be the setting of a spatial turbulence scale by the size, geometry and specific spatial arrangement of the obstacles. This might be interpreted as a "flow-channeling" (Roberts et al., 1994). Flow channeling, however, may be more an artifact of idealized experiments than would be expected in a real urban or industrial scenario.

4.3. Dispersion Models for Clouds below H_r

In this section we consider the dispersion of material when the plume is located below H_r within the urban area or industrial plant, here called the obstacle array. This situation is depicted by the regime on the left side of the top part of Figure 15. In this case the bulk of the plume is within or below the urban roughness sublayer.

Consistent with the approach in Section 3.4 and this book in general, the approach is not to consider individual buildings or structures but to model them using parameters such as λ_p, λ_f, z_o, or d.

There is evidence from experiments in the laboratory and the field (e.g., Davidson et al., 1995; Macdonald et al., 1997, 1998) that the structure of a conventional Gaussian plume or puff model [see Eqs. (9) and (48)] is appropriate for the problem. Clearly the increased turbulence within the obstacle array will cause the dispersion coefficients, σ_y and σ_z, to increase, thus tending to decrease the maximum normalized concentration, C/Q. It is expected that, for loosely packed obstacles where there is less of a decrease in u, the maximum normalized concentration, C/Q, may decrease as the roughness increases. But for some configurations of densely packed obstacles, where there is more of a decrease in u at levels below $H_r/2$, the maximum normalized concentration, C/Q, may not decrease and may possibly increase under certain scenarios.

There have been some small-scale field experiments with plumes whose mass is mostly below H_r. For example, Macdonald et al. (1997) used movable cubes in a flat grassy field. A point source plume was released at a height of 0.5 H_r from a position about 2 H_r upwind of the edge of the array. The results showed little effect of the obstacles on the maximum normalized near-ground-level concentration at a given downwind position within the obstacle arrays. For increased obstacle density, the plume dispersion increased, thus tending to decrease the concentration, but at the same time, the wind speed decreased, tending to increase the concentration. The two effects roughly canceled out for this specific scenario. Davidson et al. (1995) carried out a similar small-scale field experiment and used a similar source position. A similar conclusion was reached that the maximum normalized concentration, C/Q, at a given downwind position was not so much different than that in the absence of the obstacles.

Several wind tunnel studies have concerned plumes released at heights less than H_r in obstacle arrays. Hall et al. (1998) and Davidson et al. (1996) carried out wind tunnel experiments of plume dispersion in regularly spaced obstacle arrays, closely matching the geometry of the small scale field experiments by these same groups that were discussed above (Macdonald et al., 1997, and Davidson et al., 1995, respectively). Davidson et al. (1996) concluded that the obstacle arrays had little effect on the ground-level concentration, but this was for plume released from a point 2 H_r upwind of the array. Hall et al. (1998) found reduction in the maximum ground-level concentrations for small λ_f , but as λ_f was increased the concentration became constant and even began to increase for large λ_f.

When a conventional Gaussian plume or puff dispersion model is used [e.g., Eq. (9) or (48)], it is necessary to specify the plume advection velocity, u_e, the puff average cloud speed, u_{avg}, over the trajectory, the plume location, and the plume size, characterized by σ_y, σ_z (and σ_x for short duration or transient releases). This section considers these variables and how they may be specified in terms of accessible parameters.

4.3.1. The Cloud Velocity, u_e or u_{avg}, below H_r

In simple Gaussian plume and puff models the cloud's local advection velocity, u_e, and averaged velocity over the cloud trajectory, u_{avg}, are commonly taken to be a constant equal to the wind speed at a fixed height. In slightly more complex models, u_e and u_{avg} are allowed to vary as the plume depth increases and the top of the plume extends to heights with larger wind speeds (see Figure 16). u_e and u_{avg} can be assumed to be the wind speed at the height of the cloud centerline for an elevated release, or u_e can be assumed to be the wind speed at a height of about 0.5 to 1.0 σ_z for a near-ground release.

The in-canopy velocity u_c that was discussed in detail in Section 3.4 is a reasonable choice for local u_e and u_{avg} for releases below H_r, at least until the plume extends well above the roughness height H_r. Note that u_c was also referred to as the characteristic velocity within the obstacle array. Macdonald et al. (2000) have deduced (as opposed to measured) a local plume advection velocity, u_e, through an array of cubical obstacles, for various λ_f ($= \lambda_p$) as a function of x/H_r. At a fixed downwind position, u_e decreases significantly as λ_f is increased, a variation generally consistent with the arguments in Section 3.4. u_e increases on average with x/H_r. However, if data are considered for which much of the plume is below H_r, the average advection velocities are roughly equal to u_c.

Only a few Gaussian-based models account for the difference between u_e and u_{avg} and their variations with travel time or distance. Such models must use the local mass-weighted mean height of the cloud and then the wind speed at that height to obtain u_e. These models then must calculate u_{avg} from its definition, $u_{avg} = x/t = (\int u_e \, dt)/t$.

4.3.2. The Vertical Plume Dimension σ_z Below H_r

The turbulence and flow generated by the obstacles below H_r will act to increase the plume dimensions compared to the corresponding dimen-

sions in rural areas, since the turbulent velocities are larger over the rougher surface. The plume growth can be interpreted in either time or distance, since $x = u_{avg}t$. Furthermore, for the same turbulent velocities, reducing the wind speed (i.e., u_{avg}) will act to increase the growth of the vertical plume dimension, σ_z, with respect to x.

For vertical cloud growth above H_r in an urban or industrial area, the urban curve for neutral conditions (class D) in Table 1 suggests that $d\sigma_z/dx = 0.14$. Experiments on the growth of the cloud dimensions at heights below H_r are few.

The Kit Fox field experiments (Hanna and Chang, 2001), clearly demonstrate the increase in the growth rate in the vertical dimension caused by the obstacles in the array. The cloud (plume and puff) depth in the array has a growth rate, $d\sigma_z/dx$, larger than 0.16 for $\lambda_f = 0.12$. This growth rate is similar to the value, 0.14, mentioned in the preceding paragraph for clouds larger than H_r.

In a laboratory experiment using two-dimensional bluff obstacles (infinitely high obstacles), Melia and Britter (1990) and Melia (1991) observed a linear growth rate of σ_z for (an equivalent) $\lambda_f = 0.037$ and 0.056. It is found that $d\sigma_z/dx = 0.10$, which is slightly less than that found for the Kit Fox experiments.

Extensive experiments by Macdonald et al. (1998) on dispersion through obstacle arrays also showed enhanced vertical growth rates for σ_z due to the obstacles. For $\lambda_f = 0.16$, $\sigma_z/H_r = 1.3$ at $x/H_r = 10$, and this might suggest a growth rate of 0.13. Similar calculations at $x/H_r = 5$ imply a growth rate of 0.15. However the growth of the vertical dimension was considerably larger close to the source, declining at larger x/H_r. The implication is a rapid growth rate within the first few rows of obstacles with the plume being mixed up to H_r. Somewhat surprisingly, much the same conclusions can be made for λ_f in the range between 0.05 and 0.91, and all growth rates were larger than the growth rates for the no-obstacle case ($\lambda_f = 0$).

There is slight confusion with some of these data sets concerning the position of the source in many of the experiments, and this is important in interpretation of the results. If the source is slightly upstream of the array, the plume is strongly influenced by the deceleration of the atmospheric flow as it approaches the array and the consequent increase of plume dimensions with no dilution. This is a purely kinematic effect. This was the arrangement for the experiments by Davidson et al. (1995)

and Macdonald et al. (1997), where the release point was 2 H_r upwind of the array.

The data from all the work summarized above suggest that the growth rate, $d\sigma_z/dx$, of the vertical dimension of the plume is typically between 0.10 and 0.15 for a very wide range of λ_f (0.037 – 0.91) and heights below H_r.

To introduce some theoretical backing, the data from Melia (1991) have been analyzed further. Both the vertical concentration profile and its along-stream development through the array are consistent with the theoretical analysis of Calder (1952). His analysis was for a uniform velocity profile and a turbulent diffusivity proportional to the distance from the ground and to a constant representative turbulence velocity (a situation close to that being considered here). As a consequence the growth rate of the vertical plume dimension at heights below H_r is:

$$\frac{d\sigma_z}{dx} = A\frac{\sigma_w}{u_c} \qquad \text{for } z < H_r \tag{56}$$

where A is an experimentally determined constant that is calculated below.

Use can be made of the work in Section 3.4.3 where we estimate $\sigma_w/u^* = 1.1$ and the work in Sections 3.4.2.2 and 3.4.3 where it was found that

$$\left(\frac{u_c}{u^*}\right) = \left(\frac{z_o}{2H_r}\right)^{-1/2} = \left(\frac{\lambda_f}{2}\right)^{-1/2} \tag{57}$$

where Eq. (17a) is used to justify that $z_o/H_r = \lambda_f$, which is valid for $\lambda_f < 0.15$.

Combining Eq. (56) and the latter term of Eq. (57), and assuming $\sigma_w/u^* = 1.1$, the growth rate of the vertical plume dimension is given by

$$\frac{d\sigma_z}{dx} = 1.1A\left(\frac{\lambda_f}{2}\right)^{1/2} \qquad \text{for } z < H_r \tag{58}$$

Melia's (1991) observations can be used to show that $A = 0.60$, where the average λ_f was 0.0465.

Extending this argument to the Kit Fox field experiments, where $\lambda_f = 0.12$, leads to a growth rate of $d\sigma_z/dx = 0.16$. For a practically large λ_f of 0.15, say, the growth rate would be 0.18. That is, the verti-

cal plume dimension increases so that it equals the building or obstacle height, H_r, in a downwind distance of about 5 H_r.

It is recommended here that Eq. (58) be used with $A = 0.60$ and with λ_f set equal to 0.15 whenever λ_f exceeds 0.15, as suggested by Eq. (17b).

These arguments would be aided by further experimental comparisons. However, it is certainly the case that the growth rate of the vertical plume dimension may be assumed constant and it is not smaller than the growth rate for the cloud when $\sigma_z \gg H_r$. This may be a useful operational observation. Of course, for λ_f very small, the σ_z should not fall below a prediction based on no obstacles (e.g., the "rural" curves in Table 1, for which $d\sigma_z/dx = 0.06$ for neutral conditions (class D) at small x).

4.3.3. The Lateral Plume Dimension σ_y below H_r

The growth of the lateral plume dimension, σ_y, at heights below H_r is influenced by the turbulence levels generated within the array, the spatial scale of the turbulence within the array, and a 'topological diffusion' related to the physical presence of the obstacles. Several experiments show that σ_y is less strongly dependent upon the obstacle density than might be expected. Observations of dispersion within and above cube-shaped obstacles for which $\lambda_f = \lambda_p$ are presented by Macdonald et al. (2000). Close to the source, where the cloud is principally below H_r , σ_y is much the same for $0.11 < \lambda_f < 0.91$ with all these results being significantly larger than for $\lambda_f = 0.0$ (i.e., a flat surface). In addition, the growth of σ_y with x is more parabolic than linear. The data can be fitted with the curve

$$\frac{\sigma_y}{H_r} = 0.50\left(\frac{x}{H_r}\right)^{1/2} \qquad \text{for } z < H_r \tag{59}$$

to acceptable accuracy.

Lateral dispersion within an obstacle array can be usefully analysed with a turbulent diffusion model with the turbulent diffusivity scaled on the turbulence levels and a Lagrangian integral time scale, T_I, which is approximated by the obstacle size, or the obstacle spacing, divided by the characteristic velocity, u_c. In the case where the obstacle dimension is H_r, then $T_I = H_r/u_c$, and the Taylor equations (50) or (51) may be used to estimate σ_y.

At large time, t, and recognizing that $t = -x/u_c$, Eq. (50) has the solution:

$$\sigma_y^2 = 2\sigma_v^2 \frac{H_r}{u_c} \cdot \frac{x}{u_c} \qquad \text{for } z < H_r \tag{60}$$

Or, taking the square root of Eq. (60) and dividing by H_r, we obtain

$$\frac{\sigma_y}{H_r} = \sqrt{2}\frac{\sigma_v}{u_c}\left(\frac{x}{H_r}\right)^{1/2} \qquad \text{for } z < H_r \tag{61}$$

This approach would be a good model of the experimental data at heights below H_r provided there were some justification for assuming $\sigma_v/u_c = 0.35$, which is required in order to give agreement with Eq. (59). The analysis in Section 3.4 indicates that typically $\sigma_v/u^* = 1.4$ for $z < H_r$. This is achieved when $u^*/u_c = 0.25$ and this is predicted to occur when $z_o/2H_r = 0.125$ or $\lambda_f = 0.25$. Thus, if $\sigma_v/u^* = 1.4$ and $u^*/u_c = 0.25$, then $\sigma_v/u_c = 0.35$ and the data agree with the model.

What is difficult to understand is why the laboratory data show relatively small variations in σ_y over a wide range of λ_f. This result could be explained by the square root dependence of σ_y on the variables in Eqs. (59) through (61). Thus a factor of five variation in λ_f only leads to about a factor of two variation in σ_y. The variation is reduced even further when one considers that, as λ_f is increased, the integral spatial scale will reduce from H_r to a scale based on the face-to-face spacing, S_y, between the obstacles. Thus, expressing Eq. (60) in the form

$$\sigma_y^2 = 2\frac{\sigma_v^2}{u_c^2} H_r \cdot x \qquad \text{for } z < H_r \tag{62}$$

we see that an increase in λ_f will increase $(\sigma_v/u_c)^2$, but H_r must be replaced with a smaller length S_y. These two effects are in opposition thus further reducing the dependence of σ_y on λ_f.

Macdonald et al. (1998) found that changing the aspect ratio of the obstacles has a significant effect on the lateral growth rate in his experiments with simple obstacle shapes. For example, wide flat buildings are found to be effective in increasing the lateral plume dimension. This might be mimicked by replacing the integral time scale H_r/u_c with W/u_c where W/H_r is a typical building width to height ratio.

Consequently Eq. (61) can be written as

$$\frac{\sigma_y}{H_r} = \sqrt{2}\frac{\sigma_v}{u_c}\left(\frac{x}{H_r}\right)^{1/2}\left(\frac{W}{H_r}\right)^{1/2} \qquad \text{for } z < H_r \tag{63}$$

and using the experiments with cubes to calibrate the model produces the result

$$\frac{\sigma_y}{H_r} = 0.50\left(\frac{x}{H_r}\right)^{1/2}\left(\frac{W}{H_r}\right)^{1/2} \qquad \text{for } z < H_r \tag{64}$$

This variation with W/H_r is well reflected in the experimental results of Macdonald et al. (1998). The ratio W/H_r is approximately equal to the ratio λ_p/λ_f. Real buildings are found to have W/H_r greater than 1.0.

To reintroduce the effect of λ_f on the lateral growth rate it is recommended that

$$\frac{\sigma_y}{H_r} = \sqrt{2}(1.4)\left(\frac{\lambda_f}{2}\right)^{1/2}\left(\frac{x}{H_r}\right)^{1/2}\left(\frac{W}{H_r}\right)^{1/2} \qquad \text{for } z < H_r \tag{65}$$

for $0 \le \lambda_f \le 0.125$ and assuming $\lambda_f = 0.125$ for $\lambda_f > 0.125$. For λ_f very small, σ_y should not be allowed to fall below the estimate in Table 1 for dispersion with no obstacles (i.e., rural conditions). For example, for neutral (class D) conditions, the formula for rural conditions in Table 1 suggests $\sigma_y/H_r = 0.08\, x/H_r$.

Hall et al. (1998) found that the plumes could suffer a significant lateral displacement when passing through *regular* (e.g., square or staggered) arrays of obstacles and it has been argued that this may lead to enhanced σ_y as the wind velocity direction varies. This may be so; however, the observation is probably of little relevance for real sites with much more random geometry.

4.3.4. The Along-Wind Puff Dimension σ_x below H_r

For transient or puff releases the released material will spread longitudinally as well as vertically and laterally, causing increased dilution [see Eq. (48)]. Thus, the along-wind dimension of the puff, σ_x, is required. The along-wind dimension is increased by turbulence, and is increased by shear dispersion due to the puff sampling regions of differ-

ent mean velocities at different heights. For flow through an industrial plant or urban area, material will enter recirculating cavities and leak out from these gradually. This puff delaying mechanism will appear as an increase in σ_x. Again, little data are available but at heights above H_r over rough surfaces, Hanna and Franzese (2000) suggest that $\sigma_x = A' u^* t$, where t is the time of cloud travel, u^* is the friction velocity, and A' is expected to range between 2 and 4. Extending the same result to below H_r gives

$$\sigma_x = (A')\frac{u^*}{u_{avg}} x \qquad \text{for } z < H_r \tag{66}$$

or

$$\frac{d\sigma_x}{dx} = (A')\left(\frac{\lambda_f}{2}\right)^{1/2} \tag{67}$$

Equation (67) is derived from Eq. (66) by using Eq. (57) and assuming $u_{avg} = u_c$.

Until further information is available, this formula is recommended with $A' = 3$. There is no guidance as to whether this correlation is applicable for only a limited range of obstacle densities. Consistency with the correlations for the vertical and horizontal dispersion coefficients and conservatism suggest that for cases where λ_f is greater than 0.15, λ_f should be restricted to a maximum value of 0.15 in Eq. (67).

4.3.5. The Effect of u_c, σ_x, σ_y and σ_z on the Concentration at Heights below H_r

As seen in Eqs. (9) and (48), the maximum normalized pollutant concentration in a continuous plume is inversely proportional to $(u_e\sigma_y\sigma_z)$, and in a puff is inversely proportional to $(\sigma_x\sigma_y\sigma_z)$. The analyses in the previous subsections speculate on how the obstacle array will affect the effective advection velocity, u_e, and the plume or puff dimensions at heights below H_r.

It was argued that the velocity and the dimensions at $z < H_r$ would be given by

$$\left.\begin{aligned} u_c &= u^*(\lambda_f/2)^{-1/2} \\ \sigma_z &\propto (\lambda_f/2)^{1/2} \\ \sigma_y &\propto (\lambda_f/2)^{1/2} \end{aligned}\right\} \qquad \text{for } x < H_r \tag{68}$$

and the maximum normalized concentration for a continuous plume at a given x would therefore be inversely proportional to $u^*(\lambda_f/2)^{1/2}$, according to Eq. (58) and (65). For a puff at heights less than H_r, where σ_x, σ_y, and σ_z are each proportional to $(\lambda_f/2)^{1/2}$, it follows that the maximum normalized puff concentration would be inversely proportional to $(\lambda_f/2)^{3/2}$ at a given x, based on these experiments.

We know that, for sparsely spaced obstacles, u^* will increase with increasing λ_f. Thus, for sparsely spaced obstacles, the maximum normalized concentration for a continuous plume must decrease with increasing λ_f. That is, the more roughness obstacles, the greater the dilution and the lower the plume concentration, as we might intuitively expect.

However, the available laboratory experiments showed that σ_y and σ_z increase with λ_f initially but then remain approximately constant at large λ_f. Thus, for closely spaced obstacles (large λ_f), σ_y and σ_z are constant and the continuous plume concentration will be inversely proportional to $u_c = u^* (\lambda_f/2)^{-1/2}$. For large λ_f, u^* is constant, or even decreases with λ_f in idealized laboratory experiments with obstacles of constant H_r. For closely spaced obstacles, the maximum normalized concentration for a continuous plume at heights near the ground must increase with increasing λ_f, since the wind speed is very small and the lateral plume spread is constrained . That is, the more roughness obstacles, the weaker the dilution and the greater the maximum normalized plume concentration. This counterintuitive result arises because, while the obstacles reduce the wind velocity in the array, they also interact in a way that the continuous plume sizes are not greatly affected.

This variation was evident in the data described by Hall et al. (1998), since the observed maximum normalized concentrations, C/Q, in a continuous plume were generally reduced by obstacle arrays of cubes compared with the case with no obstacles. The trend was for a marked reduction in maximum normalized concentrations for λ_f up to $\lambda_f = 0.11$, little further variation up to $\lambda_f = 0.44$, and with a rise in C/Q back toward the no-obstacle case at even larger λ_f. The rise in concentration at large λ_f would be expected primarily for uniformly shaped laboratory cubes, and may not be seen for real-world scenarios.

For puff releases at $z < H_r$, the maximum normalized concentration, C/Q_t, is inversely proportional to $(\lambda_f/2)^{3/2}$. C/Q_t decreases monotonically with increasing λ_f, though possibly more weakly at larger λ_f when the dependence of the dispersion coefficients on $(\lambda_f/2)^{1/2}$ is not maintained. Additionally, the dose (i.e., the time-integrated con-

centration) will not decrease as rapidly due to the lower effective advection speed and correspondingly longer time for the cloud to dilute before it reaches a given distance, x.

4.3.6. Extension to Positively and Negatively Buoyant Releases below H_r

The reduced mean effective velocity, u_e, within the industrial complex or urban area will assist in the buoyant rise of the pollutant cloud. The enhanced turbulence will aid dilution of the release but also act to reduce buoyant rise. Conventional jet/plume models (Hanna et al., 1982) could easily be modified to take into account the changes in the mean velocity and the turbulence levels in their entrainment parametrizations. This approach, however, will not model the interaction of a buoyant release with any particular building.

A negatively buoyant (dense gas) release will also be influenced by the mean effective velocity, u_e, and enhanced turbulence within the industrial complex. The reduced u_e will lead to a larger cloud in the y and z directions at a given x. The enhanced turbulence levels should act to increase the dilution of the release. These effects could be incorporated directly into conventional dense gas models, but with some uncertainty how best to introduce the turbulence levels. Until further clarifying information is available, a reasonable choice would be to incorporate the turbulence by using the friction velocity u^* as the input to the model.

For large closely spaced obstacles of uniform height, where the flow is of the "skimming" type, some caution would be required in using the results. Additionally, the obstacles themselves can inhibit the gravitational spreading seen with dense-gas releases. Any model being used for such problems should be checked to see whether some account is taken for the effect of obstacles on the gravitational spreading.

4.4. Transition Methods for Clouds of Height Close to H_r within the Urban Roughness Sublayer

Sections 4.2 and 4.3 addressed the regimes on the right and left ends of the top part of Figure 15; namely, situations where the cloud depth exceeds H_r and situations where the cloud depth is less than H_r, respectively. The methods in Section 4.2 are also valid for the scenario drawn

in the bottom part of Figure 15; namely, point source releases at heights above H_r. The current section outlines methods which can assure that the solution for the ground level concentration is smoothly varying as the cloud depth increases through H_r in the middle section of the top part of Figure 15, and as the source release height, h_e, in the bottom part of Figure 15 varies in the range from about 0.5 H_r to 2 H_r. This is the range of heights called the urban roughness sublayer.

It has been shown above that, for clouds above and below H_r, the maximum near-ground-level normalized concentration, C/Q, in an urban or industrial area can be approximated given knowledge of the wind speed, u, at some height, z, above the surface roughness obstacle height, H_r, and a measure of the obstacle density parameter, λ_f. During nearly neutral stabilities, these parameters allow the surface roughness length, z_o, the displacement length, d, the friction velocity, u^*, and the entire wind profile above and below H_r to be prescribed. The turbulent velocity components, σ_v, σ_u, and σ_w, can then be estimated from u^*, as well as the dispersion coefficients, σ_y, σ_x, and σ_z, which also require estimates of the integral time scales T_I.

Smooth transitions in the solutions from one regime to the other are assisted in our methodology by the fact that both regimes make use of the same (Gaussian) dispersion model, the same roughness parameters H_r, z_o, d, and λ_f , the same u^*, and the same vertical wind profile formula. Transitions in the integral time scales, T_I, are discussed below.

Given the estimates of z_o/H_r and d/H_r from Eqs. (17) and (18), the friction velocity, u^*, can be estimated from Eq. (2b), given a wind speed observation or estimate, u, at some height, z, which is above H_r. The characteristic wind speed, u_c, below the obstacle heights is given by:

$$u_c/u^* = (\lambda_f/2)^{-1/2} \qquad z < z_{int} \tag{29}$$

which equals $(z_o/2\,H_r)^{-1/2}$ for $\lambda_f < 0.15$. The log-linear wind profile [Eq. (2b)] is assumed to apply down to a height, z_{int} , such that $u(z_{int}) = u_c$. The height z_{int} is calculated by setting Eqs. (2b) and (29) equal to each other and solving for z_{int}, where the two u solutions are equal. For obstacles with large spacings (i.e, λ_f approaching zero), z_{int} can become much less than H_r and iteration may be required to estimate u_c.

Because of the variability of the obstacle heights at real sites, the determination of the "roughness element height" or the "average building height," H_r, will produce the greatest uncertainty in application. Also for some situations with densely packed buildings with a few

imbedded very tall buildings, the surface drag and surface roughness length may be determined by the upper ranges of the distribution of obstacle heights rather than the mean H_r.

As the source height and the cloud height vary across the urban roughness sublayer, the turbulent velocities are assumed to be given by the following relations at all heights above H_r: $\sigma_u/u^* = 2.4$, $\sigma_v/u^* = 1.9$, and $\sigma_w/u^* = 1.25$. These basic constants are discussed in most boundary layer textbooks such as Stull (1997) and have been verified at heights near to and slightly below H_r by Rotach (1999) and Roth (2000). The authors often report a peak in turbulence at or just above H_r, but this peak is usually only 20 or 30% greater than the values at heights of about 2 H_r, and the differences are ignored in the simple model presented here. Furthermore, limited data discussed in the previous section suggest that the turbulent velocities may be slightly less at heights less than H_r. It is expected that current research is likely to improve these estimates of turbulent velocities below H_r.

The turbulent integral time scales, T_I, for the situations with cloud depth exceeding H_r were discussed in Section 4.2 and some simple estimates were suggested in Eqs. (50) through (56). For the lateral component [see Eq. (50)], the following equation illustrates how T_{Iy} is used:

$$\sigma_y = \frac{\sigma_v t}{\left(1 + t/2T_{Iy}\right)^{1/2}} = \frac{2u^* \left(x/u_{avg}\right)}{\left(1 + x/2u_{avg}T_{Iy}\right)^{1/2}} \tag{69}$$

Note that the relation $\sigma_v = 1.9\ u^*$ is rounded to $2u^*$. The solution is linear in t for $t < T_{Iy}$ and approaches a $t^{1/2}$ relation for $t > T_{Iy}$. Eq. (53) suggests that T_{Iy} (and T_{Ix}) equals 1000 s (or about 15 minutes), implying that σ_y will be linear in t or x for travel times less than about 15 minutes or travel distances less than about 5 km (assuming an average cloud advective speed, u_{avg}, of about 5 m/s).

For the vertical component, the integral time scale, T_{Iz}, for clouds dispersing above H_r is very large for daytime unstable conditions, is 300 s for nearly neutral conditions, and is 60 s for nighttime stable conditions [Eqs. (54) through (56)].

For clouds below H_r, it has been suggested by Hall et al. (1997) that $T_{Ix} = T_{Iy} = T_{Iz}$ and are proportional to about H_r/u_c or S_y/u_c, where S_y is the crosswind obstacle spacing. It is argued that the horizontal eddy sizes below H_r can be no larger than the spaces between the obstacles.

For typical spacings and advective speeds in industrial and urban sites, these time scales range from a few seconds to a few minutes.

For the transition regime in the urban roughness sublayer, where cloud depth is approximately equal to H_r, or where the point source release is close to H_r, the following methods are recommended:

Case 1, where the cloud is released near the ground and grows so that its depth exceeds H_r. Use the "below H_r" σ_x, σ_y, and σ_z prediction methods until max (σ_z, h_e) exceeds H_r. Then use the "above H_r" σ_x, σ_y, and σ_z prediction methods but implementing a virtual source procedure once max (σ_z, h_e) exceeds H_r. A different virtual source is used for each of the three components (i.e., x, y, and z). Hanna et al. (1996) discuss the virtual source methodology, which is straightforward and is illustrated in Figure 17. Considering the lateral component, σ_y, the vertical source method begins with the σ_y (x) estimated by the "below H_r" formulas at the transition distance, and then calculates the upwind virtual distance

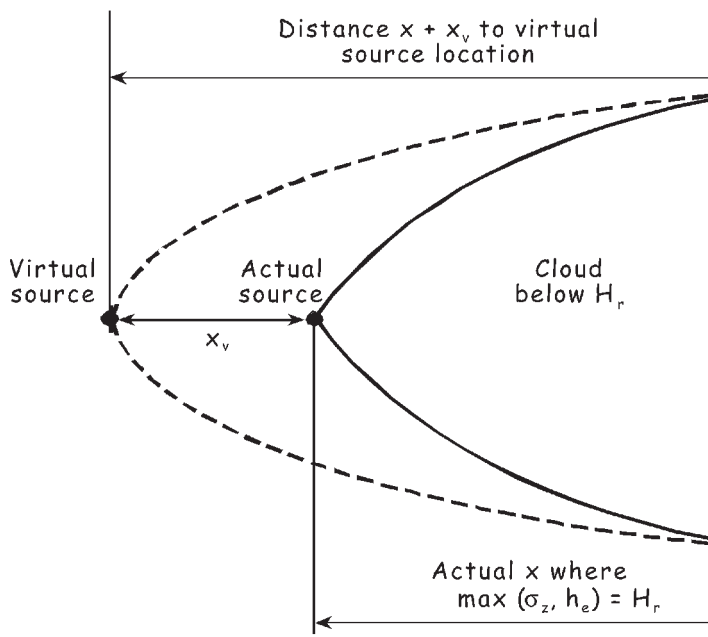

FIGURE 17. Schematic diagram of virtual source concept. It assumed that σ_y (x) for the dispersion model for the cloud at heights below H_r can be set equal to $\sigma_y(x + x_v)$ for the dispersion model for the cloud above H_r. The cloud is released near ground level at the actual source location. Once the cloud disperses above H_r, the subsequent σ_y values are calculated as if the source were at the virtual source location, which is a distance x_v behind the actual source.

from the actual source, x_v, required so that $\sigma_y\,(x + x_v)$ from the "above H_r" formula equals $\sigma_y\,(x)$ from the "below H_r" formula.

Case 2, where the cloud is released from a point or with very small initial dimensions at an elevation close to H_r. Calculate max (σ_z, h_e). If max (σ_z, h_e) is greater than H_r, use the "above H_r" σ_x, σ_y, and σ_z prediction methods. If max (σ_z, h_e) is less than H_r, use the "below H_r" σ_x, σ_y, and σ_z prediction methods, with a transition to the "above H_r" values employing the virtual source method as discussed above.

These two approaches are appropriate for calculating ground level concentrations. It is important to point out that there have not been many measurements of turbulence and dispersion in real urban and industrial sites and there may be a need to revise the method as additional data become available.

4.5. Summary and Recommendations

In this section we summarize some of the more important results of this chapter and offer recommendations.

4.5.1. Dispersion Models for Clouds Extending above H_r

1. Many operational models exist for this scenario. These models often require as input flow parameters such as z_o, d, and u^* and methods for determining these parameters have been provided in Chapter 3.
2. The above statement holds for passive, heavy, and light gas releases.
3. For passive releases (both puffs and plumes) at any height we have provided the Gaussian model solutions for concentration in Eqs. (9) and (48) in terms of the dispersion coefficients. We have also provided correlations for the dispersion coefficients in terms of u^* and (in the far-field) the integral time scale T_I [see Eqs. (50) through (56)].

4.5.2. Dispersion Models for Clouds Released above or Near H_r

1. No distinction is made between this scenario and that addressed in 4.5.1. The implication of this choice is that the flow in which

the release is dispersing is that determined by the underlying roughness. This will be a less valid assumption for releases well above H_r and when the release is close to the upwind edge of the roughness but this would be an unlikely situation.

3. The above statement holds for passive (neutral) and buoyant gas releases. It is likely to hold for heavy gas releases until the cloud trajectory descends well inside the roughness obstacles.

4.5.3. Dispersion Models for Clouds below H_r

1. Currently there are only a few preliminary operational models for this scenario and they have been subjected to limited testing with field observations. The analysis and arguments for this scenario are novel.
2. There is evidence that a Gaussian model is appropriate for this case. This requires specification of an advection velocity and correlations for the dispersion coefficients.
3. The correlation for the advection velocity is given by Eq. (29) and those for the vertical, lateral and longitudinal dispersion coefficients by Eqs. (58), (65), and (67), respectively.
4. The correlations show that, on the centerline of a continuous plume, at a fixed downwind distance, the maximum normalized concentrations initially decrease with increasing roughness but eventually become constant and then may increase slightly for very large roughness. For puffs the correlations predict a monotonic decrease in concentration with increasing roughness.
5. All the above is applicable for passive and light gas releases. For heavy gas releases a modification would be required to existing operational models to account for changes to the velocity profile within the roughness obstacles.
6. Recommendations are provided in Section 4.4 to accommodate the transition in the urban roughness sublayer for clouds growing from heights below H_r to heights above H_r.

4.5.4. Dispersion Models for Scenarios where the Upwind and Downwind Roughness Is Different

The approach that has been adopted here has been to only include the effects of roughness downwind of the source. Thus, the roughness to be

considered is a weighted average of the roughness between source and receptor [see Eq. (19a)]. This approach may lead to concentration overprediction close to the source for the situation where the source is near the downwind edge of the urban or industrial site. In that situation, the extreme rough surface upwind of the source would not be accounted for.

4.5.5. Dispersion Models for Clouds Released Upwind of the Roughness and Traveling into and Through the Roughness

The approach that has been adopted here has, again, been to consider the roughness between the source and receptor, and by implication to use an advection velocity determined by this roughness. This is a very simplistic model of the complex flow as the atmospheric boundary layer impinges upon a finite area of increased roughness.

5

Worked Examples of Calculations of Surface Roughness Length for Seven Industrial and Urban Scenarios

In this chapter, seven examples of industrial and urban scenarios are given and the surface roughness length, z_o, is estimated using the methods recommended in Section 3.5. It is shown how basic geometric parameters such as H_r and λ_f are calculated as well, since they are needed in the more detailed equations used for the estimation of z_o.

The seven examples are intended to provide a representative cross-section of scenarios that may be encountered. They range from a small industrial complex to a large urban area, and include combinations of industrial plants surrounded by urban areas, by a water surface, and by a flat desert.

Although no dispersion calculations are made in these worked examples, it would be straightforward to apply the dispersion equations listed in Chapter 4. Also, the derived z_o values can be used as inputs to new dispersion models such as AERMOD.

The last section in this chapter provides a summary of the results for the seven scenarios.

5.1. Case 1: Small (18 m by 24 m) Industrial Plant

Case 1 is a small industrial processing facility consisting of a few buildings, tanks, and pipes. It shows the typical types of roughness obstacles encountered at an industrial facility and demonstrates the use of the ROUGH software for estimating the geometric parameters such as H_r and λ_f and λ_p. Several alternate equations for estimating z_o and d are compared, including a few simpler methods.

A three-dimensional view of the 18 individual elements in the 18 m by 24 m facility is shown in Figure 18, from the report by Petersen and Cochran (1998), who describe the use of the ROUGH software for estimating H_r, λ_f and λ_p (see Section 3.5.5, page 113, for more details). This is one of the test cases provided in the Peterson and Cochran (1998) report. The sizes and locations and orientations of the 18 elements are used as an input file for the ROUGH software. Additional information required for each element include the "solidity" and "shape factor" as defined in Section 3.5.5. The solidity is less than 1.0 for the pipe racks shown in Figure 18. The ROUGH software also requires input of the wind direction, since the cross-section facing the wind for each obstacle may vary as the wind direction varies.

The ROUGH code was used to estimate the following geometric parameters for wind directions of 0 degrees (from the north) and 90 degrees (from the east):

- Average height H_r
- Frontal area A_f and dimensionless scaling parameter $\lambda_f = A_f/A_t$
- Plan area A_p and dimensionless scaling parameter $\lambda_p = A_p/A_t$

These output parameters are listed in Table 8, which also includes calculations of the displacement height d from our recommended Eq. (18), and calculated z_o in four ways: using Eq. (14) from Lettau (1969); using our recommended Eq. (17); using 0.1 H_r, and using Eq. (16) from Macdonald et al. (1998)

In addition to the four z_o estimates listed in Table 8, we also could have estimated z_o from the hierarchy of simplified categories described in Section 3.5. However, because the average obstacle height, H_r, is only 2.9 m for the small industrial processing plant in Case 1, and the hierarchy of categories is based on typical urban or large industrial H_r of about 5 or 10 m or more, the simplified categories are not applicable to this case.

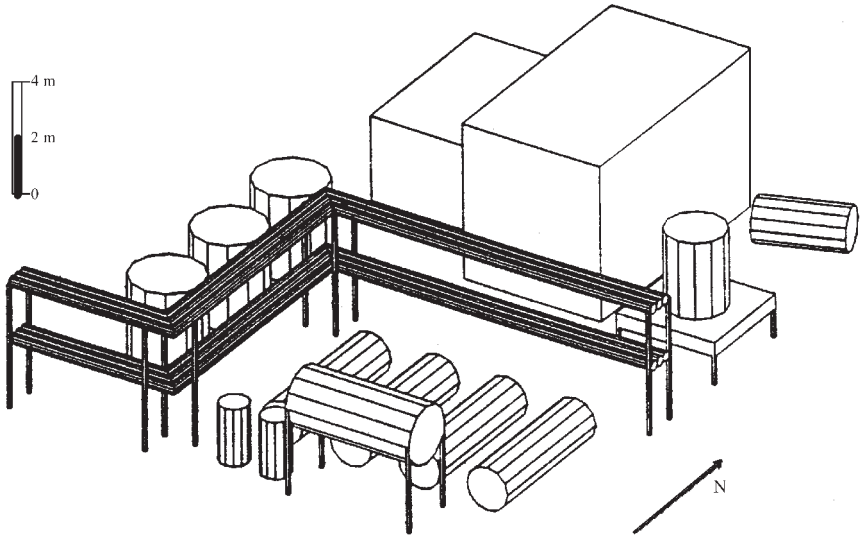

FIGURE 18. Three-dimensional view of small 18 m by 24 m industrial processing facility considered in Case 1 (from Petersen and Cochran, 1998).

Table 8 shows that, for the two wind directions, there are differences in λ_f of about 23%, which cause differences in the Lettau z_o estimate of about 23% and in the Macdonald z_o estimate of about 10%. These differences occur because the frontal area of the obstacles exposed to the wind direction is larger for a wind direction of 90 degrees than for a wind direction of 0 degrees. This relatively small difference in z_o would have little effect on the estimated u* or the maximum normalized concentration, C/Q, on the plume centerline. This result would be true for most industrial and urban areas, where the effects of individual obstacles tend to cancel each other, and the total group of obstacles usually presents a similar face to the wind from any direction. Of course there are some exceptions because buildings often have to be aligned along terrain features or roads.

The recommended z_o equation (17) yields $z_o = 0.15\ H_r$ for all λ_f greater than 0.15. Because $\lambda_f = 0.26$ for a wind direction of 0 degrees (from the north) and $\lambda_f = 0.33$ for a wind direction of 90 degrees (from the east), then $z_o = 0.15\ H_r = 0.44$ m for both wind directions for Case 1.

The results in Table 8 show z_o ranging from about 0.22 to 0.44 m for the average over the two wind directions. However, as mentioned in paragraph 2 of Section 3.3.3, the size of the area (18 m by 24 m) covered by obstacles in Case 1 is relatively small and would probably not gener-

TABLE 8. Summary Outputs of Geometric Parameters H_r, A_f, A_p, λ_f and λ_p from ROUGH Software for the Small Industrial Plant in Case 1, Plus Estimates of d for One Method and z_o for Four Alternate Methods. The steps in the calculations are shown in the footnotes.

Wind dir. (deg)	Lot width (m)	Lot length (m)	Total area A_t (m^2)	No. of elements	Average height H_r (m)	Frontal area A_f (m^2)	Plan area A_p (m^2)	Ratio $\lambda_f=A_f/A_t$	Ratio $\lambda_p=A_p/A_t$	Eq. (18) d (m)	Eq. (17) z_o (m)	Lettau z_o (m) from eq. (14)	$z_o=0.1H_r$ (m)	Macdonald z_o (m) from eq. (16)
0	18	24	432	18	2.9	112	171	0.26	0.4	2.14[a]	0.44[b]	0.38[c]	0.29	0.24[d]
90	24	18	432	18	2.9	143	171	0.33	0.4	2.21[a]	0.44[b]	0.48[c]	0.29	0.20[d]
Average over wind directions:				18	2.9	128	171	0.30	0.4	2.18	0.44	0.43	0.29	0.22

[a] $d = [0.7 + 0.35(\lambda_f - 0.15)]H_r$.
For 0 deg. wind direction, $d = [0.7 + 0.35(0.26 - 0.15)]\ 2.9\ m = 2.14\ m$.
For 90 deg. wind direction, $d = [0.7 + 0.35(0.33 - 0.15)]\ 2.9\ m = 2.21\ m$.

[b] $z_o = 0.15H_r$.
For 0 and 90 deg. wind direction, $z_o = 0.15*2.9\ m = 0.44\ m$.

[c] $z_o = 0.5\lambda_f H_r$.
For 0 deg. wind direction, $z_o = 0.5*0.26*2.9\ m = 0.38\ m$.
For 90 deg. wind direction, $z_o = 0.5*0.33*2.9\ m = 0.48\ m$.

[d] $z_o = (1 - d/H_r)\exp\{-[0.5(C_D/\kappa^2)(1 - d/H_r)\lambda_f]^{-0.5}\}H_r$, where d/H_r is given by formula (15), namely: $d/H_r = 1 + K^{\lambda_p}(\lambda_p - 1)$.
Recommended values for parameters: $C_D = 1.2$ and $K = 4$. $\kappa = 0.4$ is the von Karman constant.
For 0 deg. wind direction, $d/H_r = 1 + 4^{-0.4}(0.4 - 1) = 0.67$; $z_o = (1 - 0.67)\exp\{-[0.5(1.2/0.4^2)(1 - 0.67)0.26]^{-0.5}\}\ 2.9\ m = 0.24\ m$
For 90 deg. wind direction, $d/H_r = 1 + 4^{-0.4}(0.4 - 1) = 0.67$; $z_o = (1 - 0.67)\exp\{-[0.5(1.2/0.4^2)(1 - 0.67)0.33]^{-0.5}\}\ 2.9\ m = 0.20\ m$

ate an equilibrium boundary layer. Since the slope of the internal boundary layer is about 0.1 (see Section 3.3.3), the roughness site of width 24 m would affect the boundary layer only up to an elevation of about 2.4 m. This is barely equal to H_r. Consequently, the Case 1 obstacles do not cover a wide enough area to cause a significant change in the boundary layer and in the associated roughness length.

5.2. Case 2: A Group of Industrial Warehouses Covering a 250 m by 250 m Area

The "commercial" land-use category is one of those considered by Grimmond et al. (1998) in Table 3. This category is fairly common and consists of a number of large box and cylinder shaped structures of approximate height 5 to 15 m and approximate width 10 to 100 m or more. These could be warehouses, large tanks, or large commercial buildings such as lumber yards. Case 2 is a contrived (artificial) example of such a group of industrial warehouses and cylindrical structures, distributed over an area of 250 m by 250 m, with a repeating quilt-like obstacle plan as shown in Figure 19.

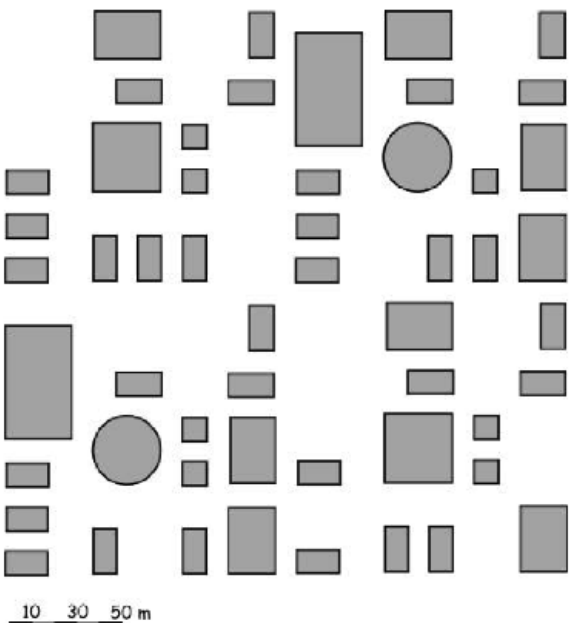

FIGURE 19. Plot plan of hypothetical group of industrial warehouses considered in Case 2.

The obstacles in Figure 19 have the following geometric characteristics:

7 elements	10 m × 10 m × 5 m (length × width × height)
32 elements	20 m × 10 m × 8 m
8 elements	30 m × 20 m × 10 m
2 elements	50 m × 30 m × 12 m
2 elements	30 m × 30 m × 12 m
2 cylindrical elements with diameter = 30 m and height = 12 m	

Case 2 has been treated in a similar way as Case 1. For example, the ROUGH software has been applied to estimate the geometrical parameters, H_r, A_p, A_f, λ_f and λ_p. One method has been used to estimate d and four alternate equations have been applied to estimate z_o. These are the same equations as used in Case 1. Two alternate wind directions are considered (0 degrees and 90 degrees). The results are given in Table 9.

For the average over the two wind directions, the estimate of d from our recommended Eq. (18) is 5.42 m. The four estimates of z_o range from 0.52 to 1.18 m in Table 9. There is very little variation with wind direction, since the array of obstacles looks so similar from any direction.

Other estimates of z_o can be made using the hierarchy of simplified categories described in Section 3.5. For example, under Section 3.5.2.1 (Methods Based on Experience), the simplest gross estimate is z_o = 1.0 m, while the estimate for a combined Category 1 and Category 2 would be in the range z_o = 0.5 to 1.0 m. It can be concluded that all available methods lead to the expectation that z_o is approximately in the range from 0.5 m to 1.0 m for Case 2.

Unlike Case 1, the size of the area occupied by roughness obstacles in Case 2 is large enough (250 m by 250 m) that the roughness surface will have significantly affected the boundary layer. With a width of 250 m, the Case 2 area will have influenced the boundary layer up to a depth of about 0.1 times 250 m, or 25 m (see Section 3.3.3, where the slope of the internal boundary layer is stated to be about 0.1). This height is three times the average height of the roughness obstacles, H_r.

The estimate of z_o equal to 1.0 m can be used as input to a dispersion model such as AERMOD or HEGADAS. If z_o were to vary by more than about a factor of two for the two wind directions in Table 9, then these different z_o values should be input for the two quadrants. Otherwise, use the same z_o for all wind directions.

TABLE 9. Summary of Geometrical Output Parameters from ROUGH for the Group of Industrial Warehouses in Case 2, Plus Estimates of d Using Eq. (18) and z_o for Four Alternate Methods, for Two Wind Directions. The steps in the calculations are shown in the footnotes.

Wind dir. (deg)	Lot width (m)	Lot length (m)	Total area A_t (m^2)	No. of elements	Average height H_r (m)	Frontal area A_f (m^2)	Plan area A_p (m^2)	Ratio $\lambda_f=A_f/A_t$	Ratio $\lambda_p=A_p/A_t$	Eq. (18) d (m)	Eq. (17) z_o (m)	Lettau z_o (m) from eq. (14)	z_o=0.1 H_r (m)	Macdonald z_o (m) from eq. (16)
0	250	250	62500	53	8.4	8490	18114	0.14	0.29	5.42[a]	1.18[b]	0.59[c]	0.84	0.51[d]
90	250	250	62500	53	8.4	8690	17714	0.14	0.28	5.42[a]	1.18[b]	0.59[c]	0.84	0.54[d]
Average over wind directions:				53	8.4	8590	17914	0.14	0.29	5.42	1.18	0.59	0.84	0.52

[a] $d = [0.15 + 5.5(\lambda_f - 0.05)]H_r$
For 0 and 90 deg. wind direction, $d = [0.15 + 5.5(0.14 - 0.05)]\ 8.4\ m = 5.42\ m$

[b] $z_o = \lambda_f H_r$
For 0 and 90 deg. wind direction, $z_o = 0.14*8.4\ m = 1.18\ m$

[c] $z_o = 0.5\lambda_f H_r$
For 0 and 90 deg. wind direction, $z_o = 0.5*0.14*8.4\ m = 0.59\ m$

[d] $z_o = (1 - d/H_r)\exp\{-[0.5(C_D/\kappa^2)(1 - d/H_r)\lambda_f]^{-0.5}\}H_r$, where d/H_r is given by formula (15), namely: $d/H_r = 1 + K^{-\lambda_p}(\lambda_p - 1)$.
Recommended values for parameters: $C_D = 1.2$ and $K = 4$. $\kappa = 0.4$ is the von Karman constant.
For 0 deg. wind direction, $d/H_r = 1 + 4^{-0.4}(0.29 - 1) = 0.54$; $z_o = (1 - 0.54)\exp\{-[0.5(1.2/0.4^2)(1 - 0.54)0.14]^{-0.5}\}\ 2.9\ m = 0.51\ m$
For 90 deg. wind direction, $d/H_r = 1 + 4^{-0.4}(0.28 - 1) = 0.53$; $z_o = (1 - 0.53)\exp\{-[0.5(1.2/0.4^2)(1 - 0.53)0.14]^{-0.5}\}\ 2.9\ m = 0.54\ m$

5.3. Case 3: Medium-Sized (400 m by 400 m) Refinery

Case 3 is a typical medium-sized refinery, representing a 400 m by 400 m portion of the so-called refinery number 3 studied by Petersen and Cochran (1998). Figure 20 is a photograph of a scale model of the refinery complex as simulated in their wind tunnel. This scale model, of width about 2 m, was constructed based on known locations and dimensions of buildings and tanks in an actual refinery.

Petersen and Parce (1994) and Petersen and Cochran (1998) have reported the results of wind tunnel studies of winds and turbulence over the refinery model in Figure 20. They analyzed the observed winds in order to make estimates of "observed" z_o and d. These observations can be compared with the predictions of the same equations and methods already tested above in the discussions of Cases 1 and 2.

The reader may notice the seemingly odd result in Table 10 that the number of individual elements in Case 3 varies between 364 and 367 depending on the wind direction. This is because some adjacent elements are combined by the ROUGH software for certain wind directions. An average roughness obstacle height H_r of 10 m is calculated by the software. Note that H_r is not weighted over the frontal or the plan areas of the elements, but is the pure arithmetic mean of all element

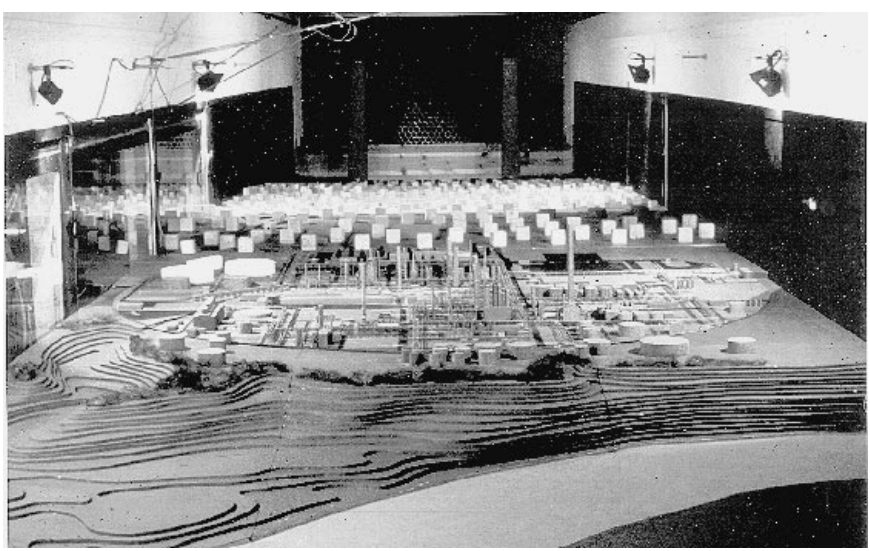

FIGURE 20. Photograph of a scale model of refinery 3 complex as used in the CPP wind tunnel. This refinery is the basis for Case 3. (Courtesy of CPP, Inc., Fort Collins, CO.)

TABLE 10. Summary Outputs of Geometric Parameters from ROUGH for Case 3 (Refinery), Plus Estimates of *d* from Eq. (18) and z_o from Four Alternate Methods. Four Wind Directions Are Considered. The steps in the calculations are shown in the footnotes.

Wind dir. (deg)	Lot width (m)	Lot length (m)	Total area A_t (m^2)	No. of elements	Average height H_r (m)	Frontal area A_f (m^2)	Plan area A_p (m^2)	Ratio $\lambda_f = A_f/A_t$	Ratio $\lambda_p = A_p/A_t$	Eq. (18) d (m)	Eq. (17) z_o (m)	Lettau z_o (m) from eq. (14)	$z_o = 0.1H_r$ (m)	Macdonald z_o (m) from eq. (16)
0	400	400	160000	364	10.1	18772	19723	0.12	0.12	5.4[a]	1.21[b]	0.61[c]	1.01	1.31[d]
45	"	"	"	367	9.8	24795	18493	0.15	0.12	6.86[a]	1.47[b]	0.74[c]	0.98	1.52[d]
90	"	"	"	364	10.1	18602	19723	0.12	0.12	5.4[a]	1.21[b]	0.61[c]	1.01	1.31[d]
135	"	"	"	367	9.8	24395	19411	0.15	0.12	6.86[a]	1.47[b]	0.74[c]	0.98	1.52[d]
Average over wind directions:				366	10.0	21641	19338	0.14	0.12	6.13	1.34	0.67	1.00	1.41

[a] $d = [0.15 + 5.5(\lambda_f - 0.05)]H_r$

For 0 and 90 deg. wind direction, $d = [0.15 + 5.5(0.12 - 0.05)]\ 10.1\ m = 5.4\ m$

For 45 and 135 deg. wind direction, $d = [0.15 + 5.5(0.15 - 0.05)]\ 9.8\ m = 6.86\ m$

[b] $z_o = \lambda_f H_r$

For 0 and 90 deg. wind direction, $z_o = 0.12*10.1\ m = 1.21\ m$

For 45 and 135 deg. wind direction, $z_o = 0.15*9.8\ m = 1.47\ m$

[c] $z_o = 0.5\lambda_f H_r$

For 0 and 90 deg. wind direction, $z_o = 0.5*0.12*10.1\ m = 0.61\ m$

For 45 and 135 deg. wind direction, $z_o = 0.5*0.15*9.8\ m = 0.74\ m$

[d] $z_o = (1 - d/H_r)\exp\{-[0.5(C_D/\kappa^2)(1 - d/H_r)\lambda_f]^{-0.5}\}H_r$, where d/H_r is given by formula (15), namely: $d/H_r = 1 + K^{-\lambda_p}(\lambda_p - 1)$.

Recommended values for parameters: $C_D = 1.2$ and $K = 4$. $\kappa = 0.4$ is the von Karman constant.

For 0 and 90 deg. wind direction, $d/H_r = 1 + 4^{-0.12}(0.12 - 1) = 0.26$; $z_o = (1 - 0.26)\exp\{-[0.5(1.2/0.4^2)(1 - 0.26)0.12]^{-0.5}\}\ 10.1\ m = 1.31\ m$

For 45 and 135 deg. wind direction, $d/H_r = 1 + 4^{-0.12}(0.12 - 1) = 0.26$; $z_o = (1 - 0.26)\exp\{-[0.5(1.2/0.4^2)(1 - 0.26)0.15]^{-0.5}\}\ 9.8\ m = 1.52\ m$

heights. Other geometrical parameters calculated by ROUGH are listed in Table 10, as well as estimates of d by Eq. (18) and z_o by four alternate equations. Calculations are made for four wind directions: 0, 45, 90, and 135 degrees from north. In Figure 20, 0 degrees would represent a wind blowing toward the array in the photograph.

It is seen that the frontal area, A_f, and hence the dimensionless parameter λ_f, is about 30% larger for wind directions of 45 or 135 degrees than for wind directions of 0 or 90 degrees. Consequently, the z_o estimated from our recommended Eq. (17) is about 30% higher for directions of 45 and 135 degrees. Averaged over all wind directions, the estimated d is 6.13 m and the estimated z_o ranges from 0.67 to 1.41 m.

Other estimates of z_o can be made using the simplified categories described in Section 3.5. For example, under Section 3.5.2.1 (Methods Based on Experience), the simplest gross estimate is z_o = 1.0 m, while the estimate for Category 1 or 2 would be z_o = 0.5 to 1.0 m. It can be concluded that all available methods lead to the expectation that z_o is in the range from about 0.5 m to 1.4 m for the medium-sized refinery in Case 3.

The estimated or modeled values of z_o and d in Table 10 and in the above paragraph can be compared with "observations" in the wind tunnel as reported by Petersen and Parce (1994) and Petersen (1997). These "observations" are based on measurements of the vertical variation of wind speed and turbulence, from which z_o is calculated using seven alternate methods (some of which are reviewed in Section 3.3.2). The displacement length, d, is parametrized by Petersen and Parce (1994) to equal $(H_r - z_o/A_L)$, where the dimensionless parameter A_L is either 0.26 or 0.36. With these methods, the "observations" range from 0.21 m to 1.28 m for z_o and from 5.2 m to 9.5 m for d. Three of the four modeled z_o values in Table 10 (for the average over all wind directions) are included in this range of "observations," although most are near the high end. The modeled d of 6.1 m is within the range of the "observations."

The size of the area occupied by roughness obstacles in Case 3 is large enough that the roughness surface will have significantly affected the boundary layer. Given the width of 400 m and making the standard assumption that the slope of the internal boundary layer is 0.1, the Case 3 area will have influenced the boundary layer up to a depth of about 40 m. This height is about four times the average height of the roughness obstacles. Farther downwind of the edge of the refinery, the

boundary layer will gradually revert back to an equilibrium with the new underlying surface. This will occur over a distance of 10 to 20 H_r.

5.4. Case 4: Typical Urban Area (Chicago)

Case 4 is a low to medium density urban area in Chicago. Because no data are available for individual obstacles, no ROUGH runs could be made to estimate the geometrical parameters. The geometrical (morphological) characteristics such as H_r, λ_f, and λ_p, and the "observed" z_o and d can be taken from Grimmond and Oke's (1999) data for Chicago, as described in Tables 2 and 3 in Section 3.3.4.

Table 11 contains morphological data reported by Grimmond and Oke (1999), their observations of d and z_o, and estimates of d from Eq. (18) and z_o from four alternate methods. Table 3 (row 9) presented the Chicago observations of d and z_o, along with similar data from other urban areas. The calculated d in Table 11 is 5.78 m, and the four values of calculated z_o range from 0.30 m to 1.19 m. Other estimates of z_o for Case 4 can be made using the simplified categories described in Section 3.5. For example, under Section 3.5.2.1 (Methods Based on Experience), the simplest gross estimate is z_o = 1.0 m, while the estimate for Category 1 or 2 would be z_o = 0.5 to 1.0 m. It can be concluded that the various methods lead to the expectation that z_o is within the range from about 0.3 m to 1.2 m for the Chicago urban area in Case 4. The "observed" z_o given by Grimmond and Oke (1999) is 0.65 m, which falls within the range of the modeled or estimated values.

The observed and predicted displacement lengths, d, can also be compared for Case 4. Our recommended Eq. (18) gives d = 5.78 m, and this estimate is entered in Table 10. Simple rules of thumb can also be applied, such as $d = 0.5$, H_r = 4.0 m or $d = 0.7$, H_r = 5.6 m. These various estimates of d range from 4.0 m to 5.78 m, slightly larger than the "observed" value of d = 3.7 m reported by Grimmond and Oke (1999).

No horizontal dimensions are given for the urban area in Case 4. However, the size of the area occupied by roughness obstacles in Chicago in Case 4 is large enough that the roughness surface will have significantly affected the boundary layer. With a width of more than 1000 m, the Case 4 area will have influenced the boundary layer up to a height of a hundred meters or more.

TABLE 11. Morphological Data and z_o Estimates for the Chicago Area (Case 4). The steps in the calculations are shown in the footnotes.

Observations (from Grimmond and Oke, 1999)						Estimates				
Average height H_r (m)	Ratio $\lambda_f=A_f/A_t$	Ratio $\lambda_p=A_p/A_t$	Observed d (m)	Observed z_o (m)		Eq. (18) d (m)	Eq. (17) z_o (m)	Lettau z_o (m) from eq. (14)	$z_o=0.1H_r$ (m)	Macdonald z_o (m) from eq. (16)
7.9	0.24	0.45	3.7	0.65		5.78[a]	1.19[b]	0.95[c]	0.79	0.30[d]

[a] $d = [0.7 + 0.35(\lambda_f - 0.15)]H_r = [0.7 + 0.35(0.24 - 0.15)]\ 7.9\ m = 5.78\ m$

[b] $z_o = 0.15H_r = 0.15*7.9\ m = 1.19\ m$

[c] $z_o = 0.5\lambda_f H_r = 0.5*0.24*7.9\ m = 0.95\ m$

[d] $z_o = (1 - d/H_r)\exp\{-[0.5(C_D/\kappa^2)(1 - d/H_r)\lambda_f]^{-0.5}\}H_r$, where d/H_r is given by formula (15), namely: $d/H_r = 1 + K^{-\lambda_p}(\lambda_p - 1)$. Recommended values for parameters: $C_D = 1.2$ and $K = 4$. $\kappa = 0.4$ is the von Karman constant.

$d/H_r = 1 + 4^{-0.45}(0.45 - 1) = 0.72$; $z_o = (1 - 0.72)\exp\{-[0.5(1.2/0.4^2)(1 - 0.72)0.24]^{-0.5}\}\ 7.9\ m = 0.30\ m$

5.5. Case 5: Industrial Plant (Case 3) in Chicago Urban Area

Case 5 concerns a medium-sized 400 m by 400 m industrial plant which is located near one corner of a small 894 m by 894 m urban area. The dimensions of the urban and industrial plant areas have been arbitrarily set so that the areas have a ratio of 4 : 1. To simplify the analysis, the urban area is assumed to have morphological parameters (e.g., H_r, λ_f and λ_p) as described for Chicago under Case 4. The industrial plant is assumed to have characteristics the same as the refinery in Case 3. A schematic diagram of the scenario is given in Figure 21.

As in Case 4, it is not possible to run the ROUGH software for this scenario, because no information is available for the individual obstacles in the urban area. Instead, two alternate ways of weighting the z_o results are presented. In one case, listed at the bottom of Table 12, the morphological parameters (λ_p and λ_f, and H_r) for the two areas (urban and industrial) are weighted by the areas, which have a 4 : 1 ratio. In

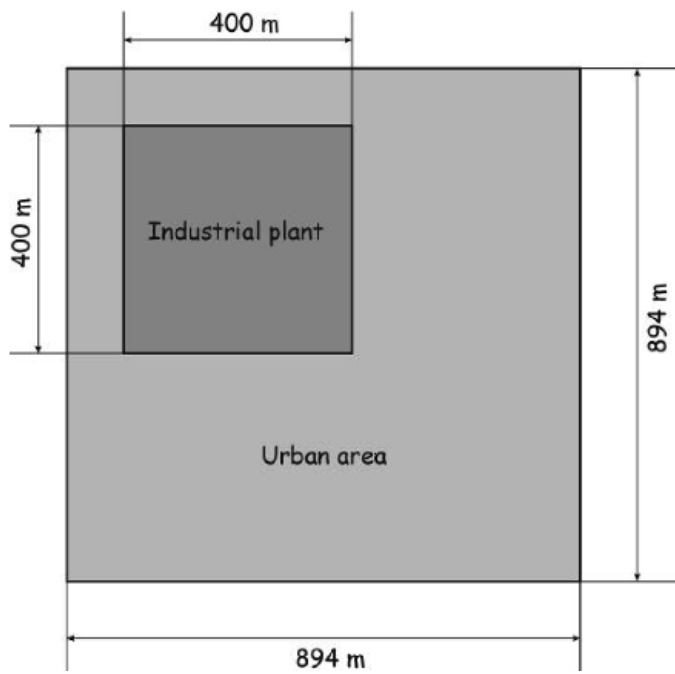

FIGURE 21. Case 5—An example of a 400 m by 400 m industrial plant (the refinery in Case 3) located within an 894 m by 894 m urban area with characteristics of the Chicago scenario discussed in Case 4.

TABLE 12. Estimates of Morphological Parameters and z_o for Case 5 (Refinery in Urban Area). The Top, Middle, and Bottom Panels Give the Results for the Urban, the Refinery, and the Combined Areas, Respectively. The steps in the calculations are shown in the footnotes.

	Estimates based on ROUGH software			Observations (from Petersen and Parce, 1994)		Estimates of d and z_o					Lot size and geometric characteristics				
Case 3 - Refinery	Average height H_r (m)	Ratio $\lambda_f=A_f/A_t$	Ratio $\lambda_p=A_p/A_t$	Observed d (m)	Observed z_o (m)	Eq. (18) d (m)	Eq. (17) z_o (m)	Lettau z_o (m) from eq. (14)	$z_o=0.1H_r$ (m)	Macdonald z_o (m) from eq. (16)	Lot width (m)	Lot length (m)	Total area A_t (m^2)	Frontal area A_f (m^2)	Plan area A_p (m^2)
	10	0.14	0.12	5.2 to 9.5	0.2 to 1.2	6.13	1.34	0.67	1	1.41	400	400	160000	22400	19200
Case 4 - Urban Area	Observations (from Grimmond and Oke, 1999)					Estimates of d and z_o					Lot size and geometric characteristics				
	Average height H_r (m)	Ratio $\lambda_f=A_f/A_t$	Ratio $\lambda_p=A_p/A_t$	Observed d (m)	Observed z_o (m)	Eq. (18) d (m)	Eq. (17) z_o (m)	Lettau z_o (m) from eq. (14)	$z_o=0.1H_r$ (m)	Macdonald z_o (m) from eq. (16)	Lot width (m)	Lot length (m)	Total area A_t (m^2)	Frontal area A_f (m^2)	Plan area A_p (m^2)
	7.9	0.24	0.45	3.7	0.65	5.78	1.19	0.95	0.79	0.28	800	800	640000	153600	288000
Case 5 - Refinery in Urban Area	Morphological characteristics					Estimates of d and z_o					Lot size and geometric characteristics				
	Average height H_r (m)	Ratio $\lambda_f=A_f/A_t$	Ratio $\lambda_p=A_p/A_t$			Eq. (18) d (m)	Eq. (17) z_o (m)	Lettau z_o (m) from eq. (14)	$z_o=0.1H_r$ (m)	Macdonald z_o (m) from eq. (16)	Lot width (m)	Lot length (m)	Total area A_t (m^2)	Frontal area A_f (m^2)	Plan area A_p (m^2)
	8.3[a]	0.22	0.38			6.01[b]	1.25[c]	0.91[d]	0.83	0.46[e]	800000	894[g]	894[g]	176000[h]	307200[i]

[a] This value of H_r is the average of H_r for case 3 and H_r for case 4, weighted over the respective total areas. $H_r = [H_r(\text{case 3})*A_t(\text{case 3}) + H_r(\text{case 4})*A_t(\text{case 4})]/[A_t(\text{case3}) + A_t(\text{case 4})] =$ $= (10\text{ m} * 160000\text{ m}^2 + 7.9\text{ m} * 640000\text{ m}^2)/(160000\text{ m}^2 + 640000\text{ m}^2) = 8.3\text{ m}$								
[b] $d = [0.7 + 0.35(\lambda_f - 0.15)]H_r = [0.7 + 0.35(0.22 - 0.15)]\ 8.3\text{ m} = 6.01\text{ m}$								
[c] $z_o = 0.15H_r = 0.15*8.3\text{ m} = 1.25\text{ m}$								
[d] $z_o = 0.5\lambda_f H_r = 0.5*0.22*8.3\text{ m} = 0.91\text{ m}$								
[e] $z_o = (1 - d/H_r)\exp\{-[0.5(C_D/\kappa^2)(1 - d/H_r)\lambda_p]^{-0.5}\}H_r$, where d/H_r is given by formula (15), namely: $d/H_r = 1 + K^{-\lambda p}(\lambda_p - 1)$. Recommended values for parameters: $C_D = 1.2$ and $K = 4$. $\kappa = 0.4$ is the von Karman constant. $d/H_r = 1 + 4^{-0.38}(0.38 - 1) = 0.65$; $z_o = (1 - 0.65)\exp\{-[0.5(1.2/0.4^2)(1 - 0.65)0.24]^{-0.5}\}\ 8.3\text{ m} = 0.46\text{ m}$								
[f] $A_t = A_t(\text{case 3}) + A_t(\text{case 4}) = 160000\text{ m}^2 + 640000\text{ m}^2 = 800000\text{ m}^2$								
[g] Lot length = Lot width = $(A_t)^{1/2} = (800000\text{ m}^2)^{1/2} = 894\text{ m}$								
[h] $A_f = A_f(\text{case 3}) + A_f(\text{case 4}) = 22400\text{ m}^2 + 153600\text{ m}^2 = 176000\text{ m}^2$								
[i] $A_p = A_p(\text{case 3}) + A_p(\text{case 4}) = 19200\text{ m}^2 + 288000\text{ m}^2 = 307200\text{ m}^2$								

another case, the appropriate z_o is estimated by weighting by the logarithm of the distance along a downwind trajectory, using Eq. (19a).

Table 12 is composed of three panels: the top panel summarizes the results for the urban area, the middle panel summarizes the results for the refinery averaged over all wind directions used for the simulations (eight wind directions from 0 to 360 degrees), and the bottom panel reports the final results obtained by calculating the area-weighted average of λ_p and λ_f. For example, the average height, H_r, in the bottom panel of Table 12 is the average of the Case 4 Chicago H_r and the Case 3 refinery H_r, weighted over the respective total areas: Average H_r = [1∗(10 m) + 4∗(7.9 m)]/5 = 41.6 m / 5 = 8.3 m.

Note that, no matter which z_o formula is used, there is not much difference between the estimated z_o for the refinery and the urban area. For example, for the recommended Eq. (17), z_o = 1.19 for the urban area and z_o = 1.34 m for the refinery. Consequently, the z_o for the combined refinery and urban areas, given in the bottom panel of Table 12, is not much different from the z_o for the individual cases. The combined z_o in Table 12 is closer to that for the urban area, since the area of the urban area in Figure 21 is four times the area of the refinery.

For Case 5, the four estimates of averaged z_o in Table 12 cover a relatively small range, from 0.46 to 1.25 m. These estimates also agree with the straightforward rules of thumb in Section 3.5.2.1, which would suggest a z_o in the range from 0.5 to 1.0 m.

As recommended in Section 3.5, an alternate way of estimating the combined z_o is to use Eq. (19a), which weights the z_o values by distance along a line rather than by area. To apply Eq. (19a), assume that a hypothetical pollutant source is located in the middle of the refinery, and a hypothetical receptor is located on the east edge of the urban area. Therefore, the pollutant plume would traverse 200 m of the refinery and 400 m of the urban area. Using the z_o values from our recommended Eq. (17) given in Table 12, a distance-weighted z_o is calculated to be 1.24 m using Eq. (19a):

$$\ln z_o = (200\text{m}/600\text{m}) \ln(1.34\text{m}) + (400\text{m}/600\text{m}) \ln(1.19\text{m}) = 0.214$$

or

$$z_o = 1.24 \text{ m}$$

These relatively small differences (10 or 20%) in z_o have little effect on the calculated transport and dispersion and the maximum C/Q

values. In this example, it would be appropriate to use an average z_o of about 1.27 m.

5.6. Case 6: Industrial Plant from Case 3 Located on a Peninsula

In Case 6, the industrial plant is assumed to be partly located on a peninsula, where the z_o for the water surface to the south is several orders of magnitude less than the z_o for the industrial plant or for the urban area. The industrial plant is assumed to have roughness characteristics identical to those for the refinery described in Case 3. An urban area is located on the mainland around the plant. A schematic diagram showing the orientation of the peninsula and the surrounding water and urban areas is given in Figure 22. Half of the 160,000 m^2 area of the industrial plant or refinery (which has the same total area and rough-

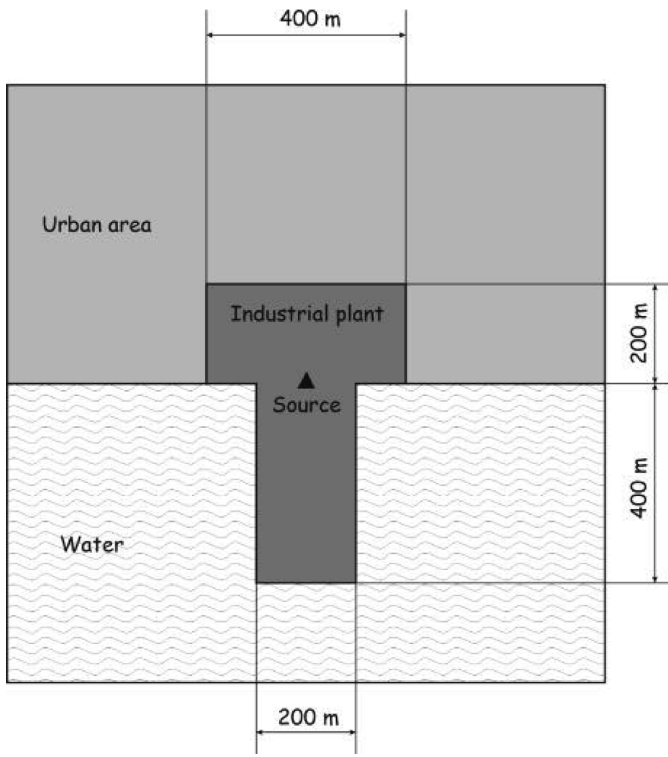

FIGURE 22. Schematic diagram of Case 6—a moderate-sized refinery on a peninsula, with an urban area to the north and water to the south.

ness characteristics as the refinery in Case 3) is on the peninsula, while the other half is embedded in the urban area. We assume that the roughness characteristics of the urban area are the same as for Case 4. The source release position is assumed to be at the center of the plant, in line with the primary shoreline, and Eq. (19a) is used to calculate the effective z_o values at several distances from the source for two plume directions—north and south. This is a case where the effective z_o varies strongly with wind direction, and an example is given of the application of Eq. (19c) for wind directions parallel to the shoreline, where one-half of the plume would be over the urban surface and one-half of the plume would be over the water.

As in Case 5, we use the results from the recommended Eq. (17) and assume that z_o for the industrial plant or refinery is 1.33 m and that z_o for the urban area is 1.19 m. Following the guidance in Table 5a, we assume that z_o for the water surface is 0.0001 m, which is valid for light winds. It is assumed that each roughness surface extends over a distance of more than 20% of the total distance from source to receptor. Also, for the initial estimates it is assumed that the roughness is constant across a 30 degree sector.

Table 13 contains the estimates of z_o, using Eq. (19a), for north and south wind directions and for five downwind receptor distances. For the north wind, blowing the plume or cloud out over the water, the effective z_o drops from 0.20 m to 0.0007 m as downwind receptor distance increases from 500 m to 2000 m. For the south wind, blowing the plume or cloud over the urban area, the effective z_o decreases slightly, from 1.3 to 1.22 m, at downwind receptor distances ranging from 250 m to 1000 m. The effects of these roughness variations on maximum normalized concentration, C/Q, can be estimated by the rough rules of thumb in Chapters 2 and 4, which showed that C/Q is proportional to $z_o^{-1/2}$. It can be inferred that, at the same downwind distance, the maximum C/Q at a distance of 1000 m to the north will be about $(0.0045 \text{ m}/1.22 \text{ m})^{1/2} = 0.061$ times the maximum C/Q at that distance to the south, over the water.

For the source location shown in Figure 22, it is clear that the calculations of z_o for a south wind would apply for any wind direction with a southerly component ranging from about 105 degrees to about 265 degrees (from north). This would assure that the criterion concerning the angle of 30 degrees would be satisfied, and the plume or cloud would travel over an urban surface after it passed out of the industrial

plant. Also, the distance traveled by the plume over the plant site is about the same for any southerly wind component. Similarly, for any wind direction with a northerly component ranging from about 285 degrees to about 75 degrees (from north), the plume or cloud would travel over the water surface after it passed out of the industrial plant. However, the distance traveled by the plume over the industrial area is about four times as large for a north wind (0 degrees) as for an east-north-east wind (68 degrees). Consequently, Eq. (19a) should be applied separately to each wind direction (in approximately 30-degree sectors) with a northerly component, to account for differing trajectories over the plant.

For this extreme example of different types of roughness obstacles to the north and to the south of the plant, the calculated effective z_o differs by several orders of magnitude with distance and also with direction from the source position. In cases with a less-marked difference in land-use, our decision concerning whether to account for the differences can be guided by the fact that the uncertainty in the z_o estimate (or the "observation" from a wind profile) is about a factor of 2 or 3. Therefore, we should account for land-use and wind direction effects on z_o only if the expected difference in z_o is more than a factor of 2 or 3.

This example also illustrates difficulties that may arise in the estimation of z_o for wind directions that would cause a plume or cloud to be advected parallel to the border between two roughness *z*ones. Recall that our criterion for accounting for a roughness surface has been set at an angle of 30 degrees. Consider an alternate case in Figure 22, where the wind direction might be from the east (a 30 degree sector including wind directions ranging from 75 to 105 degrees) or west (a 30 degree sector including wind directions ranging from 255 to 285 degrees). For a plume released at the source location and traveling a distance of at least 100 m in the west or east directions, part of one side of the plume would be over the urban area, with z_o = 1.19 m, and part of the other side of the plume would be over the water, with z_o = 0.0001 m. How should this difference be accounted for so that the resulting z_o will vary smoothly with wind direction rather than having a discontinuity? A discontinuity in modeled C/Q is undesirable because it could lead to very different pollutant control strategies or emergency response decisions over very small differences in positions. Our recommendation in Section 3 is that, if the z_o differs by more than a factor of 2 or 3 between the two *z*ones that occupy the 30 degree sector under a pollutant plume,

TABLE 13. Case 6—Industrial Plant on Peninsula—Effective z_o, Calculated from Eq. (19a) for North and South Wind Directions and Five Downwind Distances

	Total distance x_t from source to receptor (m)	Distance x_1 from source to water (m)	Distance x_2 from waterfront to receptor (m)	Plant z_o (m)	Water z_o (m)	Effective z_o (m) from eq. (19a)
North wind	500	400	100	1.33	0.0001	0.1991[a]
	750	400	350	1.33	0.0001	0.0158[a]
	1000	400	600	1.33	0.0001	0.0045[a]
	1500	400	1100	1.33	0.0001	0.0013[a]
	2000	400	1600	1.33	0.0001	0.0007[a]
	Total distance x_t from source to receptor (m)	Distance x_1 from source to north fence (m)	Distance x_2 from north fence to receptor (m)	Plant z_o (m)	Urban area z_o (m)	Effective z_o (m) from eq. (19a)
South wind	250	200	50	1.33	1.19	1.30[b]
	350	200	150	1.33	1.19	1.27[b]
	500	200	300	1.33	1.19	1.24[b]
	750	200	550	1.33	1.19	1.23[b]
	1000	200	800	1.33	1.19	1.22[b]

[a] $z_o = \exp[(1/x_t)\,\Sigma x_i \ln z_{oi}]$

For x_t = 500 m, $z_o = \exp\{[1/500\text{m}][400\text{m}\ln(1.33\text{m}) + 100\text{m}\ln(0.0001\text{m})]\} = 0.1991$ m

For x_t = 750 m, $z_o = \exp\{[1/750\text{m}][400\text{m}\ln(1.33\text{m}) + 350\text{m}\ln(0.0001\text{m})]\} = 0.0158$ m

For x_t = 1000 m, $z_o = \exp\{[1/1000\text{m}][400\text{m}\ln(1.33\text{m}) + 600\text{m}\ln(0.0001\text{m})]\} = 0.0045$ m

For x_t = 1500 m, $z_o = \exp\{[1/1500\text{m}][400\text{m}\ln(1.33\text{m}) + 1100\text{m}\ln(0.0001\text{m})]\} = 0.0013$ m

For x_t = 2000 m, $z_o = \exp\{[1/2000\text{m}][400\text{m}\ln(1.33\text{m}) + 1600\text{m}\ln(0.0001\text{m})]\} = 0.0007$ m

[b] $z_o = \exp[(1/x_t)\,\Sigma x_i \ln z_{oi}]$

For x_t = 250 m, $z_o = \exp\{[1/250\text{m}][200\text{m}\ln(1.33\text{m}) + 50\text{m}\ln(1.19\text{m})]\} = 1.30$ m

For x_t = 350 m, $z_o = \exp\{[1/350\text{m}][200\text{m}\ln(1.33\text{m}) + 150\text{m}\ln(1.19\text{m})]\} = 1.27$ m

For x_t = 500 m, $z_o = \exp\{[1/500\text{m}][200\text{m}\ln(1.33\text{m}) + 300\text{m}\ln(1.19\text{m})]\} = 1.24$ m

For x_t = 750 m, $z_o = \exp\{[1/750\text{m}][200\text{m}\ln(1.33\text{m}) + 550\text{m}\ln(1.19\text{m})]\} = 1.23$ m

For x_t = 1000 m, $z_o = \exp\{[1/1000\text{m}][200\text{m}\ln(1.33\text{m}) + 800\text{m}\ln(1.19\text{m})]\} = 1.22$ m

the geometric mean of the two z_o values should be estimated using Eq. (19c), with weighting by the angle sector covered by each z_o. As an example of the use of this method, consider a distance of 2000 m in Table 13, which shows that z_o = 0.0007 m for a trajectory from the north, and z_o = 1.22 m for a trajectory from the south. Now assume a

wind direction from the east (90 degrees), for which half of the plume would be over the land and half of the plume would be over the water at a distance of 2000 m. Then the geometric mean z_o over the width of the 30-degree plume sector would be calculated as follows:

$$\ln z_o = (15/30)\ln(0.0007\text{ m}) + (15/30)\ln(1.22\text{ m})$$
$$= 0.5\,(-7.26) + 0.5\,(0.199) = -3.53$$

or

$$z_o = 0.029\text{ m}$$

The advantage of this method is that the calculated z_o will vary continuously with wind direction with no step changes.

5.7. Case 7: Large 4 km by 4 km Refinery in a Desert

Case 7 concerns a large (4 km by 4 km) refinery in a desert. A schematic diagram of the site is given in Figure 23. It is assumed that z_o for this 4 × 4 km refinery is about 1 m, similar to that calculated for the 400 × 400 m refinery in Case 3. The value of z_o for the desert is assumed to be 0.03 m, typical of a flat desert with occasional rocks and small brush (see Table 5a). The effective z_o is calculated using Eq. (19a) for the case of hypothetical receptors located at distances of 4, 5, 6, 8, and 10 km from the center of the refinery (where the release is assumed to occur). The locations of the receptors have been chosen under the constraint that each roughness surface extends over a distance of more than 20% of the total distance from source to receptor.

Table 14 contains the results of the calculations of effective z_o. Note that at $x = 4$ km, where the trajectory passes over 2 km of refinery and 2 km of desert, the effective z_o is simply the geometric mean of the two z_o values (i.e., effective $z_o = (1.0\text{ m} * 0.03\text{ m})^{1/2} = 0.173$ m). At a distance of 10 km, where the trajectory has passed over four times as much desert surface as refinery surface, the effective z_o is two times the desert z_o.

If the z_o values in Table 14 were used as inputs to a dispersion model, it is expected that the maximum normalized concentrations, C/Q, at $x = 4$ km would be a factor of $(1.0/0.173)^{1/2} = 2.4$ higher than if the refinery z_o were used instead of the z_o from Eq. (19a). By a similar argument, the maximum normalized concentrations at $x = 4$ km would

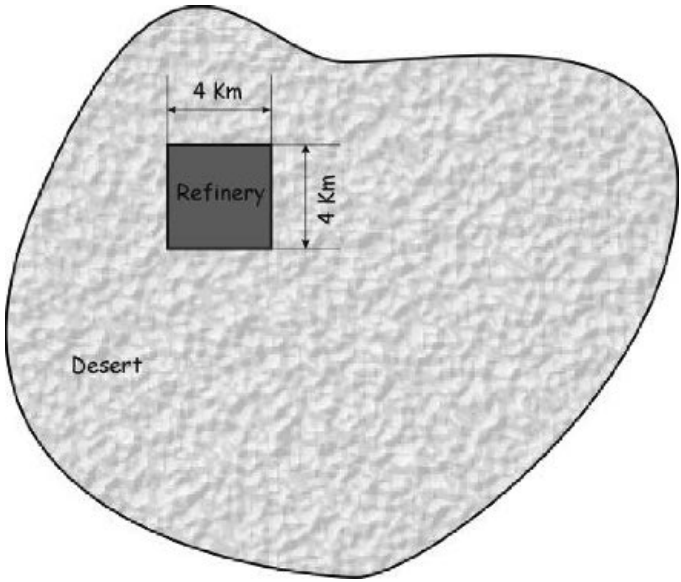

FIGURE 23. Schematic diagram of Case 7—a large (4 km by 4 km) refinery in a desert.

TABLE 14. Case 7—Large Refinery in Desert—Effective z_o, Calculated from Eq. (19a) for Five Distances Downwind of a Point Source at the Center of the Refinery

Total distance x_t from source to receptor (km)	Distance x_1 from source to fence (km)	Distance x_2 from fence to receptor (km)	Plant z_o (m)	Desert z_o (m)	Effective z_o (m) from eq. (19a)
4	2	2	1.00	0.03	0.173[a]
5	2	3	1.00	0.03	0.122[a]
6	2	4	1.00	0.03	0.097[a]
8	2	6	1.00	0.03	0.072[a]
10	2	8	1.00	0.03	0.060[a]

[a] $z_o = \exp[(1/x_t)\ \Sigma x_i \ln z_{oi}]$

For x_t = 4 km, $z_o = \exp\{[1/\ 4000\text{m}][2000\text{m ln}(1\text{m}) + 2000\text{m ln}(0.03\text{m})]\} = 0.173$ m

For x_t = 5 km, $z_o = \exp\{[1/\ 5000\text{m}][2000\text{m ln}(1\text{m}) + 3000\text{m ln}(0.03\text{m})]\} = 0.122$ m

For x_t = 6 km, $z_o = \exp\{[1/\ 6000\text{m}][2000\text{m ln}(1\text{m}) + 4000\text{m ln}(0.03\text{m})]\} = 0.097$ m

For x_t = 8 km, $z_o = \exp\{[1/\ 8000\text{m}][2000\text{m ln}(1\text{m}) + 6000\text{m ln}(0.03\text{m})]\} = 0.072$ m

For x_t = 10 km, $z_o = \exp\{[1/10000\text{m}][2000\text{m ln}(1\text{m}) + 8000\text{m ln}(0.03\text{m})]\} = 0.060$ m

be a factor of $(0.173/0.03)^{1/2} = 2.4$ lower than if the desert z_o were used instead of Eq. (19a).

5.8. Summary of Seven Cases Used for Worked Examples

The worked examples of the seven test cases have been described in detail in the previous sections. Table 15 contains a summary of the seven cases. The first case, the often-encountered small industrial processing plant, was included primarily to demonstrate the use of the methods. This is the only case of the seven in which the equilibrium atmospheric boundary layer has not developed to heights above the tops of the obstacles, H_r. The other six cases had boundary layer depths that extended to several times H_r.

Cases 2 through 5 represent typical extensive industrial, commercial, and/or urban sites. The estimated H_r, z_o, and d values are remarkably similar across the four test cases, with less than 20% variation in any of these parameters listed in Table 15. As an average over these four cases in the table, the mean H_r equals 8.8 m, the mean z_o equals 1.24 m, and the mean d equals 5.8 m. These results suggest that, for many applications, it may be sufficient to use the simple default recommendation that z_o is about 1 m for most industrial and urban sites, as found in the analysis of urban data reported by Grimmond et al. (1998) and shown in Table 3.

Cases 6 and 7 are included to show how the effective z_o can vary with distance from the industrial plant or with wind direction in some scenarios where the industrial plant is surrounded by water or by a desert. With the orders of magnitude differences between the z_o of the industrial plant and of the surrounding surface, it is important to calculate an effective z_o based on weighting the relative areas or distances of the two types of surfaces. Without these corrections there could be errors of a factor of two or more in concentrations predicted by a dispersion model making use of the z_o inputs, assuming that the maximum $C/Q \propto z_o^{-0.2}$ relation mentioned earlier is valid. As another example, since a factor of 10,000 difference exists between the z_o for the water surface and for the industrial plant in Case 6, there would be a factor of $(10{,}000)^{0.2} = 6.3$ difference in modeled maximum C/Q for the two surfaces.

TABLE 15
Summary of Seven Test Cases in Worked Examples

Description	Case 1 Small Industrial Site	Case 2 Warehouse Complex	Case 3 Refinery	Case 4 Urban (Chicago)	Case 5 Refinery in Urban Area	Case 6 Refinery on Peninsula	Case 7 Refinery in Desert
H_r (m)	2.9	8.4	10.0	7.9	8.3	depends on x and angle	
z_o (m)	0.44	1.15	1.33	1.19	1.25	1.2 (land) .0007 (water) at x = 2 km	.17(x = 4 km) .06 at x =10 km
d (m)	2.2	5.4	6.1	5.8	6.0	depends on x and angle	
ROUGH Software	Yes	Yes	No	No	No	No	No
Variation of z_o with x	No	No	No	No	Yes	Yes	Yes
Variation of z_o with wind direction	Small	Small	Small	No	Yes	Yes	Yes

Appendix

Text Files for CD-ROM with z_o Estimation Codes

Note that all section numbers, figure numbers, and table numbers in this Appendix, which contains exact copies of the text files on the CD-ROM, are not related to the numbering scheme in the main text of this book.

The CD-ROM, which includes these text files, was prepared by:

Pasquale Franzese
MS 5C3
George Mason University
Fairfax, VA 22030–4444
pfranzes@gmu.edu

The original program ROUGH, the databases SOURCE.R-3 and SOURCE.SML, and several other examples of the use of the ROUGH software were created by:

R.L. Petersen and D.K. Parce
Cermak Peterka Petersen, Inc.
1415 Blue Spruce Drive
Fort Collins, CO 80524
Ph. 303–221–3371 Fax 303–221–3124

for the American Petroleum Institute (API), 1220 L Street NW, Washington, DC, and are reported in:

Petersen, R.L. and D.K. Parce, 1994: Development and testing of methods for estimating surface roughness length at refineries. CCP Project 92–0890, CPP, Ft. Collins, CO 80524.

This CD-ROM contains the two programs and the databases that were used to calculate the roughness lengths and the displacement heights in some of the worked examples in the book by Hanna and Britter, *Wind Flow and Vapor Cloud Dispersion at Industrial and Urban Sites*, published in 2002 by the Center for Chemical Process Safety of the American Institute of Chemical Engineers (AIChE), 3 Park Avenue, New York, NY 10016.

The CD-ROM also contains the user's guides for these programs. The files on this CD-ROM are listed below:

README.TXT This file

ROUGH-GEOMETRY.FOR The Fortran 90 source code for the program ROUGH-GEOMETRY that calculates the geometric or morphological characteristics of a site. This program is essentially the program ROUGH.FOR created by Petersen and Parce (1994) for API, with a modified output and a few other minor changes. API has made the ROUGH program available to the Center for Chemical Process Safety to promote knowledge and enhance safety.

ROUGH-GEOMETRY.EXE The executable program that calculates the morphological characteristics of a site

ROUGH-GEOMETRY User's Guide.doc The ROUGH-GEOMETRY User's Guide in the form of a WORD 97 document.

SOURCE.SML The small industrial plant (18 m by 24 m) database to be used with ROUGH-GEOMETRY. This database was created by Petersen and Parce (1994), and is used as Test Case 1 in the book by Hanna and Britter (2002).

SOURCE.WRH The warehouses database to be used with ROUGH-GEOMETRY. This database is used as Test Case 2 in the book by Hanna and Britter (2002).

SOURCE.R-3 The (400 m by 400 m) refinery database to be used with ROUGH-GEOMETRY. This database was created by Petersen

and Parce (1994), and is used as Test Case 3 in the book by Hanna and Britter (2002).

ROUGH-ZO.FOR The Fortran 90 source code for the program ROUGH-ZO that calculates the surface roughness and the displacement length of a site.

ROUGH-ZO.EXE The executable program that calculates the surface roughness and the displacement length of a site.

ROUGH-ZO User's Guide.doc The ROUGH-ZO User's Guide in the form of a WORD 97 document.

Note that the three files, SOURCE.SML, SOURCE.WRH and SOURCE.R-3, are the databases for the sites used in Cases 1, 2 and 3 of the worked examples in the AIChE book by Hanna and Britter (2002). In order to use one of these files with ROUGH-GEOMETRY, the database must be copied in the same directory as ROUGH-GEOMETRY, and must be renamed SOURCE.DAT. Refer to Petersen and Parce (1994) for more details on the two cases for the 18 m by 24 m industrial plant and for the oil refinery (i.e., the SOURCE.SML and SOURCE.R-3 databases).

Questions can be directed to

Pasquale Franzese
MS 5C3
George Mason University
Fairfax, VA 22030–4444
Phone (703) 993–1992 Fax (703) 993–1980
pfranzes@gmu.edu

Steven R. Hanna
7 Crescent Ave.
Kennebunkport, ME 04046
hannaconsult@adelphia.net

The original program ROUGH, the databases SOURCE.R-3 and SOURCE.SML, and several other examples of the use of the ROUGH software were created by

R.L. Petersen and D.K. Parce
Cermak Peterka Petersen, Inc.
1415 Blue Spruce Drive
Fort Collins, CO 80524
Phone (303) 221–3371 Fax (303) 221–3124

for API, and are reported in:

Petersen, R.L. and D.K. Parce, 1994: Development and testing of methods for estimating surface roughness length at refineries. CCP Project 92–0890, CPP, Ft. Collins, CO 80524.

ROUGH-GEOMETRY User's Guide

The program ROUGH-GEOMETRY is a slightly modified version of the API program ROUGH (Petersen and Parce, 1994), that API has made available to the Center for Chemical Process Safety to promote knowledge and enhance safety.

The program ROUGH was designed to calculate the surface roughness length of a site using the Lettau or the Counihan methods, after calculating the geometrical or morphological characteristics of the site (i.e., the mean obstacles height, H_r, the ratio of frontal area to lot area, λ_f, and the ratio of plan area to lot area, λ_p). The program ROUGH-GEOMETRY consists of the portion of ROUGH that calculates the geometrical or morphological characteristics. ROUGH-GEOMETRY retains the structure and the algorithms used by ROUGH to calculate H_r, λ_f and λ_p, but does not calculate the surface roughness length.

ROUGH-GEOMETRY calculates the lot area, A_t, the frontal area, A_f, the plan area, A_p, the ratio of frontal area to lot area, λ_f, the ratio of plan area to lot area, λ_p, the mean obstacles height, H_r, and the number of obstacles included in the lot area. For a detailed explanation of the logic used by ROUGH (and therefore by ROUGH-GEOMETRY) in calculating these parameters, the reader is referred to the original report by Petersen and Parce (1994).

The surface roughness length of the site, z_o, can be subsequently calculated by either applying the equations recommended in the AIChE book by Hanna and Britter (2002), or by applying any other equation that is thought to be suitable for that site.

This user's guide was prepared by summarizing the information available from the report by Petersen and Parce (1994). This information should be sufficient to enable the reader to prepare the required databases and to run the ROUGH-GEOMETRY (or the ROUGH) software.

The inputs required by the program ROUGH-GEOMETRY include:

1. A database of the positions and characteristics of the obstacles for the entire site (see below for details on how to compile this database);
2. The width and length of the site (or of the portion of the site) that has to be analyzed;
3. The coordinates x and y of the center of the site with respect to the frame of reference used to compile the site database;
4. The wind direction. The angle of the wind direction is defined as the clockwise angle between the positive y-axis of the site's frame of reference and the direction of the wind.

The File SOURCE.DAT Includes the Site Database

The name of the database read by ROUGH-GEOMETRY must be SOURCE.DAT. It must be located in the same directory as ROUGH-GEOMETRY, and it must be written using the following FORTRAN format: (6f10.2, 2f4.3, 2i2).

Each line of the database provides the geometric characteristics of a specific obstacle, and includes ten variables in the following order: *X*-coordinate, *Y*-coordinate, Length, Width, Height, Theta, Horizontal Solidity, Vertical Solidity, Shape Factor, Stack Flag.

- *X- and Y- coordinates* (meters): the coordinates of the center of the obstacle relative to the origin of the frame of reference used in defining the database.
- *Length, Width and Height* (meters): the three dimensions of the obstacle. The Length is defined as the distance along the obstacle's centerline from the northern most to the southern most face of the obstacle. The Width is the distance along the obstacle's centerline from the western most to the eastern most face of the obstacle. For cylinders or spheres the Length and Width correspond to the diameter of the obstacle. The Height is the distance between ground level and the obstacle's top.
- *Theta* (degrees): the clockwise angle formed between the positive y-axis of the frame of reference and the obstacle's length centerline (i.e. the obstacle's local y-axis).
- *Horizontal Solidity and Vertical Solidity* (nondimensional parameters): the Horizontal Solidity *HS* is a measure of the lack of porosity of the element as it is viewed from the side. *HS* ranges from 0 to 1, where a value of 1 indicates that the element has no porosity

(i.e., it is solid). It corresponds roughly to the ratio of the amount of frontal area of the element that actually blocks the flow to the total frontal area of the element calculated as overall width by overall height. Similarly, the Vertical Solidity *VS* is a measure of the lack of porosity of the element as it is viewed from above. *VS* also ranges from 0 to 1.

- *Shape Factor*: defines the type of shape of the element. The program can evaluate only three types of shapes: rectangular boxes, vertical cylinders and spheres. Their shape factors are 0, 1, and 2, respectively. Shape factor "9" indicates that the shape is undefined and the program will ignore that element. The area of undefined shape elements can be manually calculated and inserted in the computational file COMPUT.DAT (see below).
- *Stack Flag*: indicates whether the element is located below or above another element. A value of 0 indicates that the element is not stacked, a value of 1 indicates that the element is stacked, and that the program will not calculate its plan area because it is included within a larger plan area of another element.

Numbers or notes written in the file SOURCE.DAT after the "Stack Flag" variable are not read by the program and may be inserted by the user for his or her own personal information. For example, the user can add a brief description of the element such as "Building," "Tank," "Pipe Rack," etc.

Example of preparation of the file SOURCE.DAT

To illustrate the preparation of the database SOURCE.DAT for a given site, we include as an example the case of a small portion (18 m by 24 m) of an industrial plant, as shown in Figure 1. This example, along with the database SOURCE.DAT, was given in the original report by Petersen and Parce (1994), and is also reported as one of the worked examples (i.e. case 1) included in the AIChE book by Hanna and Britter (2002).

Step 1. Prepare a plan view of the site, which includes also the height of each element. A plan view of the plant in Figure 1 is given in Figure 2.

Step 2. Set an arbitrary local frame of reference [indicated in Figure 2 as "Sector Origin (0,0)].

Step 3. The information can be summarized in the data entry table reproduced in Figure 3. The "Sector Offset" represents the coordinate of the origin of the local frame of reference relative to a global frame of reference. In this case it is assumed that the origin of the global frame of reference is 100 m east and 80 m south of the origin of the local frame of reference.

Step 4. Compile the file SOURCE.DAT using the FORTRAN format (6f10.2, 2f4.3, 2i2). This file is reproduced in Table 1 for the present case. Note that the first two columns are the x- and y-coordinates of the centers of the obstacles with respect to the absolute frame of reference.

The file COMPUT.DAT

COMPUT.DAT is an interim computational file generated by ROUGH-GEOMETRY. It contains the calculated individual frontal area, the plan area, the height and a character note for each obstacle. The user has the option of manually modifying this file, for example to add directly an obstacle's frontal and plan area that could not be included in the SOURCE.DAT file because of an anomalous obstacle shape. However

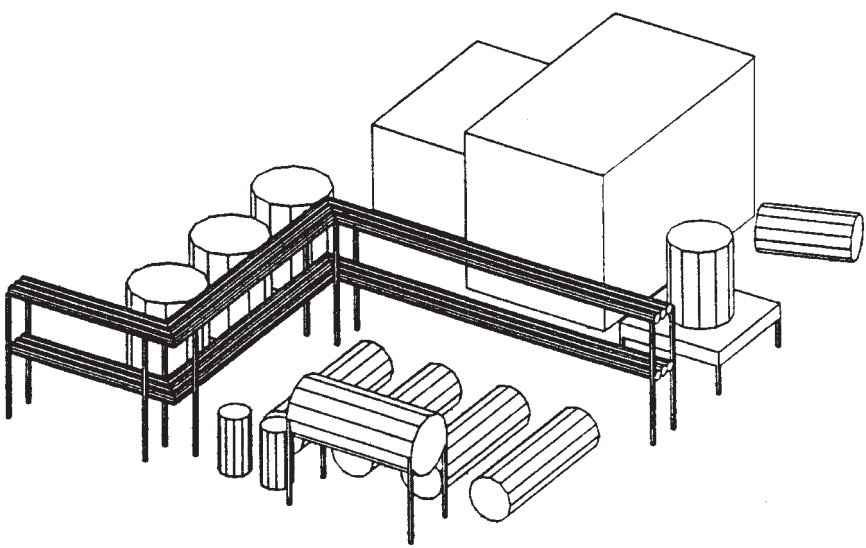

FIGURE 1: Three-dimensional view of portion of industrial plant (from Petersen and Parce, 1994).

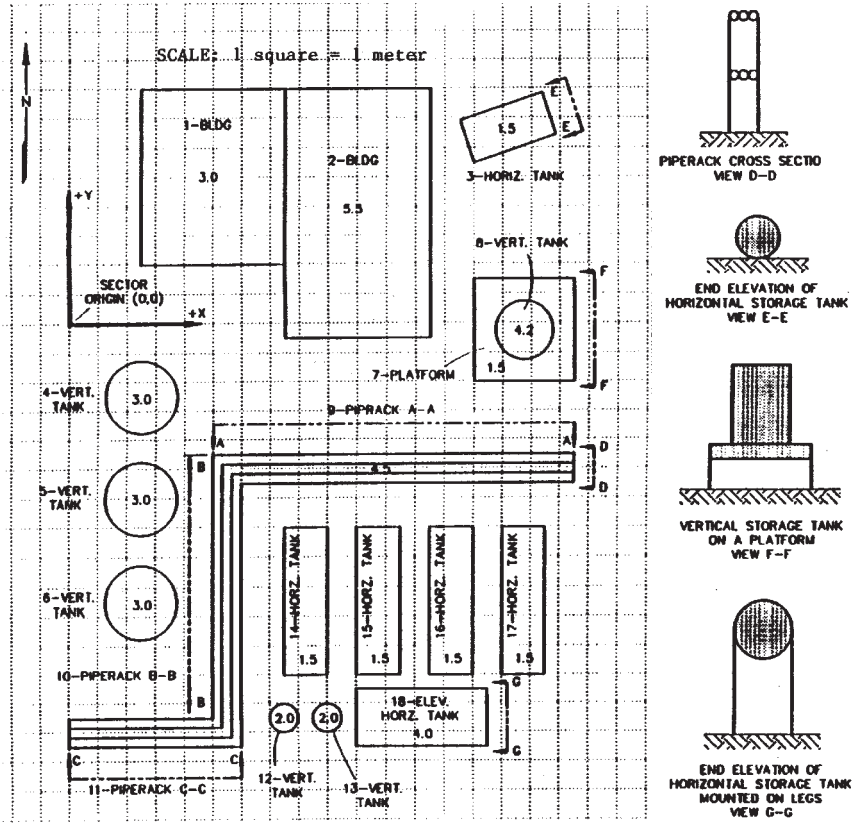

FIGURE 2. Plan view of a portion of the same industrial plant shown in Figure 1 (from Petersen and Parce, 1994)

API Surface Roughness
CPP Project 92-0890
REFINERY # EXAMPLE

Drawing Number / Name: FIGURE A-12 / A-13
Drawing Scale: 1 square = 1 meter
CW Angle from Plant to Magnetic North: 0°

Page: 1 of 1
Date: 05/20/94
By: DKP

No	Element Name / Description	Global X (+E/W-) meters	Global Y (+N/S-) meters	Sector X (+E/W-) meters	Sector Y (+N/S-) meters	Length (N / S) meters	Width (E / W) meters	Overall Height meters	CW Angle to North fm. C-L degrees	Horizontal (Side View) Solidity --	Vertical (Top View) Solidity --	Shape Factor n/a	Stacked Flag n/a
	SECTOR OFFSET	-100	80										
1	BLDG			5	5	6	5	3	0	1	1	0	0
2	BLDG			10	3.75	8.5	5	5.5	0	1	1	0	0
3	HORIZ. TANK			15.25	6.75	3	1.5	1.5	71.57	1	1	0	0
4	VERT. TANK			2.5	-2.5	2.5	2.5	3	0	1	1	1	0
5	VERT. TANK			2.5	-6.0	2.5	2.5	3	0	1	1	1	0
6	VERT. TANK			2.5	-9.5	2.5	2.5	3	0	1	1	1	0
7	PLATFORM			15.75	-0.25	3.5	3.5	1.5	0	0.333	1	0	0
8	VERT. TANK (on PLATFORM)			15.75	-0.25	2	2	4.2	0	0.643	1	1	1
9	PIPERACK A-A			11.25	-5	1	12.5	4.5	0	0.148	1	0	0
10	PIPERACK B-B			5.5	-9.5	8	1	4.5	0	0.148	1	0	0
11	PIPERACK C-C			3	-14	1	6	4.5	0	0.148	1	0	0
12	VERT. TANK			7.5	-13.5	1	1	2	0	1	1	1	0
13	VERT. TANK			9	-13.5	1	1	2	0	1	1	1	0
14	HORZ. TANK			8.25	-9.5	5	1.5	1.5	0	1	1	0	0
15	HORZ. TANK			10.75	-9.5	5	1.5	1.5	0	1	1	0	0
16	HORZ. TANK			13.25	-9.5	5	1.5	1.5	0	1	1	0	0
17	HORZ. TANK			15.75	-9.5	5	1.5	1.5	0	1	1	0	0
18	ELEV. HORZ. TANK			12.25	-13.5	2	4.5	4.0	0	0.5	1	0	0

FIGURE 3. Entry data table for the portion of the industrial plant represented in Figure 1 and 2 (from Petersen and Parce, 1994)

TABLE 1. File SOURCE.DAT for the Portion of Industrial Plant Shown in Figures 1 and 2

–95.00	85.00	6.00	5.00	3.00	0.0	1.0	1.0	0	0	1	Building
–90.00	83.75	8.50	5.00	5.50	0.0	1.0	1.0	0	0	2	Building
–84.75	86.75	3.00	1.50	1.50	71.57	1.0	1.0	0	0	3	Horz. Tank
–97.50	77.50	2.50	2.50	3.00	0.0	1.0	1.0	1	0	4	Vert. Tank
–97.50	74.00	2.50	2.50	3.00	0.0	1.0	1.0	1	0	5	Vert. Tank
–97.50	70.50	2.50	2.50	3.00	0.0	1.0	1.0	1	0	6	Vert. Tank
–84.25	79.75	3.50	3.50	1.50	0.0	.333	1.0	0	0	7	Platform
–84.25	79.75	2.00	2.00	4.20	0.0	0.64	1.0	1	1	8	Vert Tank (on Platform)
–88.75	75.00	1.00	12.50	4.50	0.0	.148	1.0	0	0	9	Piperack A-A
–94.50	70.50	8.00	1.00	4.50	0.0	.148	1.0	0	0	10	Piperack B-B
–97.00	66.00	1.00	6.00	4.50	0.0	.148	1.0	0	0	11	Piperack C-C
–92.50	66.50	1.00	1.00	2.00	0.0	1.0	1.0	1	0	12	Vert. Tank
–91.00	66.50	1.00	1.00	2.00	0.0	1.0	1.0	1	0	13	Vert. Tank
–91.75	70.50	5.00	1.50	1.50	0.0	1.0	1.0	0	0	14	Horz. Tank
–89.25	70.50	5.00	1.50	1.50	0.0	1.0	1.0	0	0	15	Horz. Tank
–86.75	70.50	5.00	1.50	1.50	0.0	1.0	1.0	0	0	16	Horz. Tank
–84.25	70.50	5.00	1.50	1.50	0.0	1.0	1.0	0	0	17	Horz. Tank
–87.75	66.50	2.00	4.50	4.00	0.0	0.5	1.0	0	0	18	Elev. Horz. Tank

if the user does not need to modify the file COMPUT.DAT, the content and structure of this file can be ignored.

- *Variables on the first line:* wind direction, lot width, lot length. FORTRAN format: (3f10.2).
- *Variables on the subsequent lines:* obstacle's frontal area, obstacle's plan area, obstacle's height, obstacle's character note. FORTRAN format: (3f10.2, a1).

The character note can be:

- R—indicates that the element is a rectangular box entirely within the lot bounds.
- C—indicates that the element is a vertical cylinder entirely within the lot bounds.
- S—indicates that the element is a sphere entirely within the lot bounds.
- Lowercase letters (i.e., r, c, and s) indicate that the element has the same shape as designated by the corresponding capital letters above, but it is only partially within the lot bounds.

- B—indicates that the element is entirely outside of the lot bounds.
- U—indicates that the element shape factor designated it as undefined.
- X—indicates that a shape factor other than 0, 1, 2 or 9 was used in SOURCE.DAT and that as a result the program ignored the element.

An example of the file COMPUT.DAT created by ROUGH-GEOMETRY is given in Table 2.

TABLE 2. The file COMPUT.DAT created by ROUGH-GEOMETRY for the small industrial plant represented in Figures 1 and 2, for a wind direction of 0 degrees (i.e. wind coming from south)

0.00	18.00	24.00
15.00	30.00	3.00R
27.50	42.50	5.50R
4.98	4.50	1.50R
7.50	4.91	3.00C
7.50	4.91	3.00C
7.50	4.91	3.00C
1.75	12.25	1.50R
5.38	0.00	4.20C
8.32	12.50	4.50R
0.67	8.00	4.50R
4.00	6.00	4.50R
2.00	0.79	2.00C
2.00	0.79	2.00C
2.25	7.50	1.50R
2.25	7.50	1.50R

Example of a ROUGH-GEOMETRY Run

We reproduce here the sequence of prompts and responses that are obtained when running ROUGH-GEOMETRY for the example of the small industrial plant shown in Figures 1 and 2, using the database SOURCE.DAT listed in Table1.

```
C:> rough-geometry  [enter]
ROUGH-GEOMETRY - Version 1.1 - Released March 2001
Should the results be displayed on the Screen, saved in a File
or Both? (S/F/B)  b [enter]
Will the data be obtained as previously computed areas,from the
file COMPUT.DAT or as raw element dimensions from the file
SOURCE.DAT ? (C/S)  s [enter]
Reading element number: 18
Enter the width and length of the region (respectively--
separated by a comma) to be considered:  18,24 [enter]
Enter the x and y displacements (separated by a comma)from the
origin used to locate the elements to the center of the region
to be considered:  -91,77 [enter]
Input the wind direction to be evaluated (in degrees): 0
[enter]
Working on element number: 18
Finished making computational file.
Do you want to exit to edit it? (Y,<N>)    N [enter]
Computing surface characteristics... Please Wait.
** The results are stored in the file: ROUGH.OUT **
Region Width (m): 18.00 No. of Elements: 18
Region Fetch (m): 24.00 Frontal Area (m^2): 112.10
Total Area (m^2): 432.00 Plan Area (m^2): 171.06
X-Displacement (m): -91.00 Ave. Height (m): 2.90
Y-Displacement (m): 77.00 Lambda_f: 0.26
Wind Dir. (Deg): 0.00 Lambda_p: 0.40
Caution: The height of one element accounted for 10.5% of the
mean height.
Caution: The silhouette area of one element accounted for 24.5%
of the mean silhouette area.
Caution: The plan area of one element accounted for 24.8% of
the total plan area.
Caution: The total element plan area accounts for 39.6% of the
area of the evaluated region.
```

Technical details of differences between ROUGH and ROUGH-GEOMETRY

The program ROUGH-GEOMETRY was derived from the program ROUGH (Petersen and Parce, 1994) by making the following changes:

- The input formats from the keyboard have been changed to free format, i.e. the responses to the ROUGH-GEOMETRY prompt can be simply written as integers.
- The ROUGH subroutines "Lettau" and "Counihan" have been eliminated, as ROUGH-GEOMETRY does not perform roughness estimations.

- The output of ROUGH-GEOMETRY includes the lot area, A_t, the frontal area, A_f, the plan area, A_p, the ratio of frontal area to lot area, λ_f, the ratio of plan area to lot area, λ_p, the mean obstacle height, H_r, and the number of obstacles included in the lot area.
- The ROUGH subroutine "Trapazoid" has been replaced. This subroutine calculates the area of the trapezoid formed by the portion of a rectangular obstacle that is outside of the boundary of the lot area. However this subroutine causes ROUGH to give an unrealistic plan area A_p for wind directions close to 90 or 270 degrees, although the results for wind directions equal to 90 and 270 degrees are correct. The new subroutine implemented in ROUGH-GEOMETRY minimizes the error in the computation of the trapezoids outside of the boundaries, resulting in a negligible error in the calculation of A_p.
- Several minor changes were made that were needed to convert the programming language from the original Microsoft FORTRAN version 5.0 to Lahey FORTRAN 90, version 4.50i. These changes did not affect the logic of ROUGH.

References

Petersen, R.L. and D.K. Parce, 1994: Development and testing of methods for estimating surface roughness length at refineries. CCP Project 92–0890, CPP, Ft. Collins, CO 80524.

Hanna, S.R. and Britter, R.E., 2002: *Wind Flow and Vapor Cloud Dispersion at Industrial and Urban Sites*. AIChE/CCPS, 3 Park Avenue, New York, NY 10016.

ROUGH-ZO User's Guide

The program ROUGH-ZO calculates the surface roughness length, z_o, and the displacement length, d, of an industrial or urban site using equations presented in the AIChE book by Hanna and Britter (2002). The inputs required by the program are the site's ratio of frontal area to lot area, λ_f, the ratio of plan area to lot area, λ_p, and the mean obstacle height, H_r. These input parameters have to be previously estimated by the user, who can calculate them directly from the geometric characteristics of the roughness elements, or using approximate estimates found in textbooks (e.g., Hanna and Britter, 2002), or using software such as

the programs ROUGH-GEOMETRY (distributed with ROUGH-ZO) or ROUGH (Petersen and Parce, 1994).

Equations Used by ROUGH-ZO

The program ROUGH-ZO has four alternate equations for estimating z_o:

1. The equations recommended by Hanna and Britter (2002):

$$z_o = \lambda_f H_r \qquad \text{for } \lambda_f < 0.15$$

$$z_o = 0.15\, H_r \qquad \text{for } \lambda_f > 0.15$$

2. The equation recommended by Macdonald et al. (1998):

$$z_o = [1 - (d/H_r)] \exp\{-[0.5\beta(C_D/\kappa^2)][1 - (d/H_r)\lambda_f]^{-0.5}\} H_r,$$

with $d/H_r = 1 + K^{-\lambda p}(\lambda_p - 1)$, with the following values for the parameters: $\beta = 1$, $C_D = 1.2$, $\kappa = 0.4$, and $K = 4$ (tuned for staggered arrays of identical cubes).

3. The equation recommended by Hanna and Britter (2002) as a rule of thumb, in case no information is available on the frontal area and the plan area:

$$z_o = 0.1\, H_r$$

4. The Lettau (1969) equation:

$$z_o = 0.5\, \lambda_f H_r$$

The program also calculates two alternate estimates of the displacement length, d, as given in the following equations:

1. The equations recommended by Hanna and Britter (2002):

$d = 3\lambda_f H_r$ for $\lambda_f < 0.05$

$d = [0.15 + 5.5(\lambda_f - 0.05)]H_r$ for $0.05 < \lambda_f < 0.15$

$d = [0.7 + 0.35(\lambda_f - 0.15)]H_r$ for $0.15 < \lambda_f < 1.0$

$d = [0.7 + 0.35(1 - 0.15)]H_r$ for $\lambda_f > 1$

5. The equation recommended by Macdonald et al. (1998):

$$d = [1 + K^{-\lambda p}(\lambda_p - 1)]H_r, \qquad \text{with } K = 4.$$

Example of a ROUGH-ZO run

We reproduce here the sequence of prompts and responses that are obtained when running ROUGH-ZO. In this example, the user wants to

estimate the roughness length, z_o, and the displacement length, d, of a site with average obstacle height H_r = 9 meters, ratio of frontal area to lot area λ_f = 0.12, and ratio of plan area to lot area λ_p = 0.22.

```
C:> rough-zo [enter]
Input average obstacles height Hr (m) : 9 [enter]
Input normalized frontal area lambda_f: 0.12 [enter]
Input normalized plan area lambda_p : 0.22 [enter]
Hanna and Britter (2002) Zo = 1.08 meters
Macdonald et al. (1998) Zo = 0.69 meters
Zo = 0.1 Hr = 0.90 meters
Lettau (1969) Zo = 0.54 meters
Hanna and Britter (2002) d = 4.82 meters
Macdonald et al. (1998) d = 3.94 meters
```

References

Hanna, S.R. and Britter, R.E., 2002: *Wind Flow and Vapor Cloud Dispersion at Industrial and Urban Sites*. AIChE/CCPS, 3 Park Avenue, New York, NY 10016.

Lettau, H., 1969: Note on aerodynamic roughness parameter estimation on the basis of roughness element description. *J. Appl. Meteorol.*, **8**, 828–832.

Macdonald, R.W., R.F. Griffiths, and D.J. Hall, 1998: An improved method for the estimation of surface roughness of obstacle arrays. *Atmos. Environ.*, **32**, 1857–1864.

Petersen, R.L. and D.K. Parce, 1994: Development and testing of methods for estimating surface roughness length at refineries. CCP Project 92–0890, CPP, Ft. Collins, CO 80524.

References

AIChE/CCPS, 1989: *Guidelines for Chemical Process Quantitative Risk Analysis*. AIChE, 3 Park Avenue, New York, 585 pp.

Arya, P.A., 1999: *Atmospheric Transport and Dispersion*. Oxford University Press, New York, 310 pp.

Auer, A.H., 1978: Correlation of land use and cover with meteorological anomalies. *J. Appl. Meteorol.*, **17**, 636–643.

Bentham, T. and R.E. Britter, 2001: Spatially averaged flow velocity within large groups of obstacles. To appear in *Atmos. Environ.*

Bottema, M., 1997: Urban roughness modeling in relation to pollutant dispersal. *Atmos. Environ.*, **31**, 3059–3075.

Briggs, G.A., 1973: Diffusion Estimation for Small Emissions. ATDL Report 79, Atmospheric Turbulence and Diffusion Laboratory, NOAA/ARL, Oak Ridge TN 37830.

Briggs, G.A., R.E. Britter, S.R. Hanna, J.A. Havens, A.G. Robins and W.H. Snyder, 2001: Dense gas vertical diffusion over rough surfaces: results of wind tunnel studies. *Atmos. Environ.,* **35***,* 2265–2284.

Brighton, P.W., 1989: *The Effects of Natural and Man-Made Obstacles on Heavy Gas Dispersion*. UK Atomic Energy Authority, SRD/091/WP1.

Britter R.E., 1982: Modelling flow over complex terrain and implications for determining the extent of adjacent terrain to be modelled. In *Wind Tunnel Modelling for Civil Engineering Applications* (ed. Reinhold), Cambridge University Press.

Britter, R.E., 1989: Atmospheric dispersion of dense gases. *Ann. Rev. of Fluid Mech.*, **21**, 317–344.

Britter, R.E., G.A. Briggs, S.R. Hanna and A.G. Robins, 2001: The passive limit of short-range vertical dispersion of dense gases in a turbulent boundary layer, To appear in *Atmos. Env.*

Britter, R.E., R.P. Cleaver, and M.G. Cooper, 1991: Development of a Simple Model for Denser-than-Air Vapour Clouds over Real Terrain. British Gas MRS E 622.

Britter, R.E. and J.C.R. Hunt, 1978: Velocity measurements and theoretical estimates of the flow between buildings in a simulated atmospheric boundary layer. *J. Ind. Aero.*, **4**, 165–182.

Britter, R.E. and McQuaid, J.M., 1988: *Workbook on the Dispersion of Dense Gases*. HSE Report No. 17/1988, Health and Safety Executive, Sheffield, UK, 158 pages.

Brown, M.J., 2000: Urban parameterizations for mesoscale meteorological models, Chapter 5 in *Mesoscale Atmospheric Dispersion* (ed., Z. Boybeyi), WIT Press, Ashurst Lodge, Ashurst, Southhampton S0407AA UK, pp. 193–255.

Businger, J.A., 1975: Aerodynamics of vegetated surfaces. In *Heat and Mass Transfer in the Biosphere* (eds. De Vries and Afgan), 139–165.

CERC, Ltd., 1998: ADMS Technical Specification. CERC, 3 Kings Parade, Cambridge, UK, CB2 1SJ.

Cimorelli, A.J., S.G. Perry, A. Venkatram, J.C. Weil, R.J. Paine, R.B. Wilson, R.F. Lee and W.D. Peters, 1998: AERMOD—Description of Model Formulation, USEPA, Research Triangle Park, NC, 27711, 113 pages.

Cionco, R.M., 1965: Mathematical model for air flow in a vegetative canopy. *J. Appl. Meteorol.*, **4**, 517–522.

Cionco, R.M. and R. Ellefsen, 1998: High resolution urban morphology data for urban wind flow modeling. *Atmos. Environ.*, **32**, 7–17.

Clarke, J.F., J.K.S. Ching, F.S. Binkowski and J.M. Godowitch, 1978: Turbulent structure of the urban surface boundary layer. *Proc. 9th Internat. Tech. Meeting on Air Pollution Modeling and Its Appication*, NATO/ CCMS.

Counihan, J., 1971: Wind tunnel determination of the roughness length as a function of the fetch and roughness density of three-dimensional roughness elements. *Atmos. Environ.*, **5**, 637–642.

Davenport, A.G., C.S.B. Grimmond, T.R. Oke and J. Weiranga, 2000: Estimating the roughness of cities and scattered country. 12th Conf. on Applied Climatology, 8–11 May 2000, Asheville NC, Amer. Meteorol. Soc., 45 Beacon St., Boston, MA 02105, 96–99.

Davidson, M.J., 1997: The influences of an array of obstacles on plume dispersion. U. Cambridge.

Davidson, M.J., K.R. Mylne, C.D. Jones, J.C. Phillips, R.J. Perkins, J.C.H. Fung and J.C.R. Hunt, 1995: Plume dispersion through large groups of obstacles—a field investigation. *Atmos. Environ.*, **29**, 3245–3256.

Davidson, M.J., W.H. Snyder, R.E. Lawson, and J.C.R. Hunt, 1996: Plume dispersion from point sources upwind of groups of obstacles—wind tunnel simulations, *Atmos. Environ.*, **30**, 3715–3725.

Deardorff, J.W., 1970: Convective velocity and temperature scales for the unstable planetray boundary layer and for Rayleigh convection. *J. Atmos. Sci.*, **27**, 1211–1213.

DeBruin, H.A.R. and C.J. Moore, 1985: Zero-plane displacement and roughness length for tall vegetation, derived from a simple mass conservation hypothesis. *Bound.-Lay. Meteorol.*, **31**, 39–49.

DeVaull, G.E., J.A. King, R.J. Lantzy, and D.J. Fontaine, 1995: *Understanding Atmospheric Dispersion of Accidental Releases*. AIChE/CCPS, 3 Park Avenue, New York, NY 10016.

Dirkmaat, J.J., 1981: Experimental studies on the dispersion of heavy gases in the vicinity of structures and buildings. Symp. on Designing with the Wind, Nantes, France, Paper III-3.

EPA, 1986: *Guideline on Air Quality Models* (Revised). EPA-450/2–78–027R, USEPA/OAQPS, RTP, NC 27711.

EPA, 1995: User's Guide for the Industrial Source Complex (ISC3) Dispersion Model. Vol. II—Description of Model Algorithms. EPA-454/b-95–0036, EPA/OAQPS, Research triangle Park, NC 27711.

Ermak, D.L., 1990: User's Manual for SLAB, an Atmospheric Dispersion Model for Denser-than-Air Releases. UCRL-MA-105607, Lawrence Livermore National Laboratory, Livermore, CA.

Garratt, J.R., 1977: Review of drag coefficients over oceans and continents. *Mon. Wea. Rev.,* **105**, 915–929.

Garratt, J.R., 1992: *The Atmospheric Boundary Layer*. Cambridge Univ. Press.

Goode, K. and S.E. Belcher, 1999: On the parameterisation of the effective roughness length for momentum transfer over heterogeneous terrain. *Bound.-Lay. Meteorol.*, **93**, 133–154.

Grimmond., C.S.B., T.S. King, M. Roth, and T.R. Oke, 1998: Aerodynamic roughness of urban areas derived from wind observations. *Bound.-Lay. Meteorol.*, **89**, 1–24.

Grimmond, C.S.B. and T.R. Oke, 1999: Aerodynamic properties of urban areas derived from analysis of surface form. *J. Appl. Meteorol.*, **38**, 1261–1292.

Hall, D.J., R. Macdonald, S. Walker, and A.M. Spanton, 1998: Measurements of dispersion within simulated urban arrays—a small scale wind tunnel study. BRE Client Report CR 244/98, Building Research Establishment, Garston, Watford WD2 7JR, UK, 71 pages.

Hall, D.J., R.W. Macdonald, S. Walker, and R.F. Griffiths, 2001: Measurements of dispersion and wind speed within simulated urban arrays—a small scale wind tunnel study. Part I—Dispersion. To appear in *Atmos. Environ.*

Hall, D.J., A.M. Spanton, R. Macdonald, and S. Walker, 1997: A Simple Model for Estimating Dispersion in Urban Areas. BRE Client Report CR 169/97, Building Research Establishment, Garston, Watford WD2 7JR, UK, 91 pages.

Hanna, S.R., 1970: *Turbulence and Diffusion in the Atmospheric Boundary Layer over Urban Areas*. ATDL Report 70–2, NOAA/ATDL, Oak Ridge, TN, 77 pages.

Hanna, S.R., 1971: Simple methods of calculating dispersion from urban area sources. *J. Air Poll. Control Assn.*, **21**, 774–777.

Hanna, S.R., 1992: Effects of surface roughness on short range dispersion. Proceedings, AMS 10th Symposium on Turbulence and Diffusion. Am. Meteorol. Soc., 45 Beacon St., Boston, MA 02105, 102–105.

Hanna, S.R., G.A Briggs, and R.P. Hosker, 1982: *Handbook on Atmospheric Diffusion*. DOE/TIC-11223 (DE82–002045). NTIS/USDOC, Springfield, VA.

Hanna, S.R. and R.E. Britter, 2000: Effects of Urban and Industrial Roughness Obstacles on Maximum Pollutant Concentrations. Proceedings, NATO/CCMS Internat. Tech. Meeting on Air Pollution Modeling and Its Applications, 15–19 May 2000, Boulder, CO.

Hanna, S.R. and J.C. Chang, 1992: Boundary layer parameterizations for applied dispersion modeling over urban areas. *Bound.- Lay. Meteorology*, **58**, 229–259.

Hanna, S.R. and J.C. Chang, 2001: Use of the Kit Fox field data to analyze dense gas dispersion modeling issues. *Atmos. Environ.,* **35**, 2231–2242.

Hanna, S.R., J.C. Chang, and D.G. Strimaitis, 1990: Uncertainties in source emission rate estimates using dispersion models. *Atmos. Environ.*, **24A**, 2971–2980.

Hanna, S.R., P.J. Drivas, and J.C. Chang, 1996: *Guidelines for Use of Vapor Cloud Dispersion Models*. AIChE/CCPS, 3 Park Avenue, New York, NY 10016, 285 pages.

Hanna, S.R. and P. Franzese, 2000: Along wind dispersion—a simple similarity formula compared with observations at 13 field sites and in one wind tunnel. *J. Applied Meteor.* **39**, 1700–1714.

Hanna, S.R. and K.W. Steinberg, 2001: Overview of Petroleum Environmental Research Forum (PERF) dense gas dispersion modeling project. *Atmos. Environ.*, **35**, 2223–2230.

Havens, J.A. and T.O. Spicer, 1985: Development of an Atmospheric Dispersion Model for Heavier-than-Air Mixtures. Final report to U.S. Coast Guard, USCGHQ, Washington, DC.

Havens, J.A., H. Walker and T. Spicer, 2001: Wind tunnel study of air entrainment into two-dimensional dense gas plumes at the Chemical Hazards Research Center. *Atmos. Environ.,* **35**, 2305–2318.

Holtslag, A.A.M. and M. Ek, 1996: Simulation of surface fluxes and boundary layer development over the pine forest in HAPEX-MOBILHY. *J. Appl. Meteorol.*, **35**, 202–213.

Horst, T.M., 1999: The footprint for estimation of atmosphere-surface exchange fluxes by profile techniques. *Bound.-Layer Meteor.*, **90**, 171–188.

Horst, T.W. and J.C. Weil, 1992: Footprint estimation for scalar flux measurements in the atmospheric surface layer. *Bound.-Layer Meteor.*, **59**, 279–296.

Horst, T.W. and J.C. Weil, 1994: How far is far enough? The fetch requirements for micrometeorological measurements of surface fluxes. *J. Atmos. Oceanic Tech.*, **11**, 1018–1025.

Hosker, R.P., 1984: Flow and diffusion near obstacles. *Atmospheric Science and Power Production* (ed. D. Randerson), Chapter 7, USDOE/TIC-27601, 241–326.

Hussein, M. and B.L. Lee, 1980: A wind tunnel study of the mean pressure forces acting on large groups of low-rise buildings. *J. Wind Eng. Ind. Aero.*, **6**, 207–225.

Jackson, P.S., 1981: On the displacement height in the logarithmic velocity profile. *J. Fluid Mech.*, **111**, 15–25.

Jerram, N., R.J. Perkins, J.C.H. Fung, M.J. Davidson, S.E. Belcher, and J.C.R. Hunt, 1994: Atmospheric flow through groups of buildings and dispersion from localised sources. *Proc. NATO Advanced Study Institute,* Karlsruhe (ed. Plate E.J. and Cermak J.E.). Kluwer, Dordrecht.

Johnson, W.B., R.C. Sklarew, and D.B. Turner, 1976: Urban air quality simulation modeling, in *Air Pollution* (3rd edition) (A.C. Stern ed), Vol. 1, Ch. 10, Academic Press, New York, 503–562.

Kondo, J. and H. Yamazawa, 1986: Aerodynamic roughness over an inhomogeneous ground surface. *Bound-Lay. Meteorol.,* **35**, 331–348.

Kutzbach, J., 1961: Investigations of the modification of wind profiles by artificially controlled surface roughness. Studies of the three dimensional

structure of the planetary boundary layer. Annual Report 1963: Dept. of Meteorol., University of Wisconsin, Madison, 37–96.

Lettau, H., 1969: Note on aerodynamic roughness parameter estimation on the basis of roughness element description. *J. Appl. Meteorol.*, **8**, 828–832.

Lo, A.K., 1990: On the determination of zero-plane displacement height and roughness for flow over forest canopies. *Bound.-Lay. Meteorol.*, **51**, 225–268.

Macdonald, R.W., 2000: Modelling the mean velocity profile in the urban canopy layer. *Bound.-Lay. Meteorol.* **97**, 25–45.

Macdonald, R.W., S. Carter, and P.R. Slawson, 2000: Measurements of Mean Velocity and Turbulence Statistics in Simple Obstacle Arrays at 1:200 Scale. Thermal Fluids Report 2000–1, Mechanical Engineering, University of Waterloo, 200 University Ave. West, Waterloo, Ontario, Canada N2L 3G1.

Macdonald, R.W., R.F. Griffiths, and S.C. Cheah, 1997: Field experiments of dispersion through regular arrays of cubic structures. *Atmos. Environ.*, **31**, 783–795.

Macdonald, R.W., R.F. Griffiths, and D.J. Hall, 1998: A comparison of results from scaled field and wind tunnel modelling of dispersion in arrays of obstacles. *Atmos. Environ.*, **32**, 3845–3862.

Macdonald, R.W., R.F. Griffiths, and D.J. Hall, 1998: An improved method for the estimation of surface roughness of obstacle arrays. *Atmos. Environ.*, **32**, 1857–1864.

Macdonald, R.W., D.J. Hall, S. Walker, and R.F. Griffiths, 2001: Measurements of dispersion and wind speed within simulated urban arrays—a small scale wind tunnel study. Part II—Wind speed profiles. Submitted to *Atmos. Environ.*

Macdonald, R.W., D.J. Hall, S. Walker, and A.M. Spanton, 1998: Wind Tunnel Measurements of Windspeed within Simulated Urban Arrays, BRE Client Report C 243/98, Building Research Establishment, Garston, Watford WD2 7JR, UK, 68 pages.

Masson, V., 2000: A physically based scheme for the urban energy budget in atmospheric models. *Bound. Lay. Meteorol.*, **94**, 357–397.

Marshall, J.K., 1971: Drag measurements in roughness arrays of varying density and distribution. *Agric. Meteorol.*, **8**, 269–292.

Mason, P.J., 1988: The formation of aerially averaged roughness lengths. *Quart. J. Roy. Meteorol. Soc.*, **114**, 399–420.

Mavroidis, I, R.F. Griffiths, C.D. Jones, and C.A. Biltoft, 1999: Experimental investigation of the residence of contaminants in the wake of an obstacle under different stability conditions. *Atmos. Environ.*, **33**, 939–949.

McElroy, J.L. and F. Pooler, 1968: St. Louis Dispersion Study Volume II—Analysis, US Dept. HEW, Arlington, VA.

Melia, J., 1991: The dispersion of dense fluids through arrays of obstacles, Ph.D. Thesis, University of Cambridge.

Melia, J. and R.E. Britter, 1990: The dispersion of dense gases through an obstacle array. *Waves and Turbulence in Stratified Flows*, Oxford Univ Press.

Meroney, R.N., 1982: Turbulent diffusion near buildings. *Engineering Meteorology* (E.J. Plate,ed.), Chapter 11, Elsevier.

Oke, T.R., 1987: *Boundary Layer Climates*, Routledge, London.

Oke, T.R., 1987: Street design and urban canopy climate. *Energy and Buildings*, **11**, 103–113.

Pasquill, F., 1961: The estimation of the dispersion of windborne material. *Meteorol. Mag.*, **90**, 33–49.

Pasquill, F. and F.B. Smith, 1983: *Atmospheric Diffusion* (3rd edition), John Wiley and Sons, New York.

Pavageau, M., S. Rafailidas, and M. Schatzmann, 1997: A comprehensive experimental data bank for the verification of urban car emission dispersion models. *Int. J. Env. Poll.* **8**.

Petersen, R.L., 1989: Effect of homogeneous and heterogeneous surface roughness on heavier-than-air dispersion. 6th US Nat. Conf. On Wind Engin., Houston (same title also with M.A. Ratcliffe as API Publication No. 4491).

Petersen, R.L., 1997: A wind tunnel evaluation of methods for estimating surface roughness length at industrial facilities. *Atmos. Environ.*, **31**, 45–57.

Petersen, R.L. and B.C. Cochran, 1998: Development and testing of methods for estimating surface roughness length at refineries and other industrial facilities. CCP Project 95–1214, CPP, Ft. Collins, CO 80524.

Petersen, R.L. and D.K. Parce, 1994: Development and testing of methods for estimating surface roughness length at refineries. CCP Project 92–0890, CPP, Ft. Collins, CO 80524.

Petersen, R.L. and M.A. Ratcliff, 1989: Effect of homogeneous and heterogeneous surface roughness on heavier-than-air gas dispersion, Vols I and II, API Pubs No. 4491 and 4492, API, Washington, DC.

Puttock, J.S. and J.C. Hunt, 1979: Turbulent diffusion from sources near obstacles with separated wakes—I. An eddy diffusivity model. *Atmos. Environ.*, **13**, 1–13.

Ramsdell, J.V., S.R. Hanna, and H.E. Cramer, 1982: Turbulent diffusion coefficients within and above the urban domain. Final Report, Contract No. 23111 05480, U.S. Army ASL, WSMR, NM 88002.

Ratti, C., S. Sabatino, R. Britter, M. Brown, F. Caton, and S. Burian, 2001: Analysis of urban databases with respect to pollutant dispersion for a number of European and American cities. *Proc. 3rd Int. Conf. on Urban Air Quality,* Loutraki, Greece, 19–23 March.

Raupach, M.R., R.A. Antonia, and S. Rajagopalan, 1991: Rough-wall turbulent boundary layers. *Applied Mechanics Reviews*, **44**, 1–25.

Raupach, M.R., 1992: Drag and drag partition on rough surfaces. *Bound.-Lay. Meteorol.,* **60**, 375–395.

Raupach, M.R., A.S. Thom, and I. Edwards, 1980: A wind-tunnel study of turbulent flow close to regularly arrayed rough surfaces. *Bound.-Lay. Meteorol.*, **18**, 373–397.

Raupach, M.R., J.J. Finnigan, and Y. Brunet, 1996: Coherent eddies and turbulence in vegetative canopies: the mixing layer analogy. *Bound.-Lay. Meteorol.*, **78**, 351–382.

Riethmuller, M.L., 1986: Effect of distributed obstacles on the dispersion of a heavy gas cloud. Von Karman Institute for Fluid Dynamics Report EAR 8208.

Roberts, P.T., R.E. Fryer-Taylor, and D.J. Hall, 1994: Wind-tunnel studies of roughness effects on gas dispersion. *Atmos. Environ.*, **28**, 1861–1870.

Roberts, P.T. and D.J. Hall, 1994: Wind tunnel simulation. Boundary layer effects on dense gas dispersion experiments. *J. Loss Prev. Process Ind.*, **7**, 106–117.

Robins, A., D. J. Carruthers, and C.A. McHugh, 1997: The ADMS building effects module. *Int. J. Environ. and Poll.*, **8**, 708–717.

Robins, A., P. Hayden, and I. Teasdale, 1999: Dispersion from elevated sources above obstacle arrays—modelling requirements. *Atmos. Environ.*

Robins A. and R. Macdonald, 1999: A Review of Flow and Dispersion in the Vicinity of Groups of Buildings. Report No. ME-FD/99.93 University of Surrey.

Rotach, M.W., 1995: Profiles of turbulence statistics in and above an urban street canyon. *Atmos. Environ.*, **29**, 1473–1486.

Rotach, M.W., 1999: On the influence of the urban roughness sublayer on turbulence and dispersion. *Atmos. Environ.*, **33**, 4001–4008.

Rotach, M.W., 2001: Simulation of urban-scale dispersion using a Lagrangian stochastic dispersion model. *Bound-Lay. Meteorol.*, **99**, 379–410.

Roth, M., 2000: Review of atmospheric turbulence over cities. *Quart. J. Roy. Meteorol. Soc.,* **126**, 941–990.

Schlichting, H., 1968: *Boundary Layer Theory* (6th edition), McGraw-Hill, New York, 748 pages.

Schmid, H.P., 1994: Source areas for scalars and scalar fluxes. *Bound.-Lay. Meteorol.*, **67**, 293–318.

Scire, J.S., D.G. Strimaitis, and R.J. Yamartino, 1998: A User's Guide for the CALPUFF Dispersion Model (Version 5.0). EPA/OAQPS, Research Triangle Park, NC 27711.

Snyder, W.H., 2001: Wind tunnel study of entrainment in two-dimensional dense-gas plumes at the EPA's fluid modeling facility. *Atmos. Environ.*, **35**, 2285–2304.

Stull, R.B., 1997: *An Introduction to Boundary Layer Meteorology*. Kluwer Atmospheric Publishers, 101 Philip Drive, Norwell, MA 02061, 670 pages.

Sykes, I., 1997: PC-SCIPUFF 1.0 Technical Documentation. Titan Research & Technology Division, Titan Corp., P.O. Box 2229, Princeton, NJ 08543–2229.

Theurer, W., 1999: Typical building arrangements for urban air pollution modelling. *Atmos. Environ.*, **33**, 4057–4066.

Thom, A., 1971: Momentum absorption by vegetation. *Quart. J. Roy. Meteorol. Soc.,* **97**, 414–428.

Weiringa, J., 1993: Representative roughness parameters for homogeneous terrain. *Bound.-Lay. Meteorol.*, **63**, 323–363.

Wilson, D.J., 1995: *Concentration Fluctuations and Averaging Times in Vapor Clouds*. CCPS project No. 73, AIChE/CCPS, 3 Park Avenue, New York, NY, 10016, 181 pages.

Wilson, D.J. and R.E. Britter, 1982: Estimates of building surface concentrations from nearby emissions. *Atmos. Environ.*, **16**, 2631–2646.

Wilson, D.J. and E.H. Chui, 1987: Effect of turbulence from upwind buildings on dilution of exhaust gases. *ASHRAE Trans.*, **93**, 2186–2197.

Witlox, H.W.M. and K. McFarlane, 1994: Interfacing dispersion models in the HGSYSTEM hazard-assessment package. *Atmos. Environ.*, **28**, 2947–2962.

Wooding, R.A., E.F. Bradley and J.K. Marshall, 1973: Drag due to regular arrays of roughness elements of varying geometry. *Bound.-Lay. Meteorol.*, **5**, 285–308.

Woodward, J. L., 1998: *Estimating the Flammable Mass of a Vapor Cloud*. AIChE, 3 Park Ave., New York, NY 10016–5901.

Glossary

ADMS Atmospheric Dispersion Modeling System (CERC, 1998)

AERMOD American Meteorological Society/EPA Regulatory Model (Cimorelli et al., 1998)

AIChE American Institute of Chemical Engineers

Atmospheric boundary layer The layer about 1000 m deep next to the ground that is strongly affected by diurnal variations in surface conditions such as ground temperature.

Atmospheric transport and dispersion model A model that follows the movement and dilution of a pollutant after it is released into the atmosphere (Hanna et al., 1982).

Atmospheric turbulence Random and rapid fluctuations in wind components, which determine the rate of turbulent dispersion or spread of the cloud. Typically expressed by the *turbulent velocity* (averaging about 1 m/s), which is the standard deviation of rapid fluctuations in wind speed (σ_u refers to fluctuations in the along-wind (x) direction, σ_v refers to fluctuations in the lateral (y) horizontal direction, and σ_w refers to fluctuations in the vertical (z) direction).

Average concentration The concentration averaged over time and/or space.

Building downwash models Models used for estimating the flow and dispersion in and near the recirculating cavity behind buildings, where plumes may "downwash" to the ground.

Buoyant cloud The in-cloud density is less than the ambient density, due to the emissions of hot gases or materials with low molecular weight. Buoyant cloud and light cloud are synonymous.

Buoyant turbulence Generated by heating of the ground surface by the sun and is suppressed by cooling of the ground surface at night. Surface heating leads to the formation of buoyant thermal bubbles from the warm ground surface on sunny afternoons. The opposite effect happens during clear nights, when the surface cooling causes the suppression of turbulence.

CALMET/CALPUFF California Meteorological and California Puff Models (Scire et al., 1998)

CCPS Center for Chemical Process Safety of the American Institute of Chemical Engineers

Centerline height Elevation of plume centerline above ground after plume rise is completed.

Centroid height Mass-weighted mean height of plume, as defined by Eq. (1).

Characteristic velocity, u_c The typical wind speed in the obstacle array.

Chemical reactions Removal of pollutants from the air by reactions with other chemicals. However, although one pollutant may be removed by the chemical reaction, another pollutant may be generated. Recent research has expanded this concern to heterogeneous reactions involving both gases and particles.

Cloud Any type of pollutant mass moving through the atmosphere.

Cloud mass-weighted mean height The concentration mass-weighted mean height of a pollutant cloud.

Computational fluid dynamics (*CFD)* A class of models that can simulate very highly resolved three-dimensional time-dependent distributions of wind flows and material concentrations. These models generally solve the basic equations of motion and conservation using very small grid spacings and time steps and are computer-intensive.

Constant stress layer The layer near the ground (about 50 m to 100 m deep) where the stress, τ, decreases by only about 10%, leading to the assumption of a constant u^* layer near the ground

Continuous stability categorization method Based on the Monin–Obukhov length, L

Convective scaling velocity, w^* A scaling velocity important during light-wind daytime conditions with strong surface heating. w^* is proportional to the cube root of the product of the heat flux, H_s, and the mixing depth, z_i.

DEGADIS Dense Gas Dispersion Model (Havens et al., 2001)

Dense cloud Cloud density is greater than ambient air density, due to the high molecular weight, the cold temperature, and/or the presence of aerosols in the emissions. Dense cloud and heavy cloud are synonymous.

Deposition The rate at which material accumulates on a surface.

DERA UK Defence and Evaluation Research Agency, developers of urban dispersion model (UDM).

Dilution Reduction in concentration due to effect of wind.

Dispersion coefficients σ_y (lateral component), σ_z (vertical component), and σ_x (along-wind component)

Displacement length, d A scaling length that becomes important for describing the wind profile at elevations close to the average roughness obstacle height, H_r, for densely packed roughness obstacles. It describes the vertical displacement (from the ground surface) of the effective ground level and is approximately equal to 0.5 H_r for obstacle types such as urban centers, tall crops, and forests.

Displacement zones Recirculation zones adjacent to buildings or other obstacles where the flow has separated from the obstacle and reattached downwind.

Dose Time-integrated concentration

Drag force The surface stress, τ_o, arises through direct viscous stress and through the pressure asymmetry around roughness elements on the surface (sometimes called form or pressure drag). In atmospheric flows the pressure asymmetry dominates over direct viscous stresses and it produces a drag force, commonly called the drag, on the roughness elements.

Dry deposition Effective downward vertical velocity of small aerosols and gases if they are chemically reactive with the ground surface. In many cases, this process is a function of the ability of a vegetative leaf to absorb the substance once the substance passes through the openings in the leaf surface. For most materials, a dry deposition velocity of about 0.01 m/s can be assumed.

Effective transport speed, u_e Defined as the vertical integral of the concentration-weighted wind speed,

$$u_e = \frac{\int u(z)C(z)\,dz}{\int C(z)\,dz}$$

where z is the height above ground, $C(z)$ is the height-variable concentration of pollutant in the cloud, and $u(z)$ is the height-variable wind speed. u_e is also known as the cloud advective speed.

Elevated clouds or plumes Pollutant releases at elevations above about 10 or 20 m.

EPA Environmental Protection Agency (U.S.)

ERP Equivalent Roughness Pattern used in the Kit Fox experiments, consisting of square plywood boards with $W = H_r = 2.4$ m.

Exponential wind profile Formula proposed for vegetative canopies that is also valid for other types of surface obstacles (Cionco, 1965).

Far-field The area beyond the influence of local structures and plume buoyancy effects. Typically the far-field begins at about 1000 m from the source.

Fluid model experiments Experiments carried out at small scale in wind tunnels and water channels.

Free stream or geostrophic wind speed, G Wind speed at the top of the boundary layer.

*friction velocity, u** The fundamental scaling velocity, equal to the square root of the surface stress, τ_o, divided by the air density. The surface stress can be observed by special instruments that directly observe the drag at the surface, or by fast response turbulence instruments using the definition: $\tau_o = \rho\langle -u'w'\rangle = \rho u^{*2}$ where u' is the longitudinal wind speed fluctuation, w' is the vertical wind speed fluctuation, and the average is over about a one-hour time period. The variable u^* can also be estimated from wind observa-

tions. A rough rule of thumb is that the ratio u^*/u is about 0.05 to 0.1, where u is the wind speed at a height of about 10 m, which is the standard measurement height at airports around the world. u^* has typical values ranging from about 0.05 m/s in light winds to about 1 m/s in strong winds.

Full-scale field experiments Field experiments of flow and dispersion around full sized obstacles (e.g., buildings, storage tanks, nuclear reactor structures, street canyons, isolated hills).

Fully developed flow Flow in a long, constant area pipe in which the mean velocity profiles are independent of position along the pipe. In the pipe the surface shear stress is balanced by the longitudinal gradient of static pressure in the pipe (the "pressure gradient").

Gaussian models A class of transport and dispersion model which assumes that the distribution of pollutant concentration has a Gaussian or normal shape [e.g., $\exp(-y^2/2\sigma_y^2)$, where y is the lateral crosswind distance from the center of the plume or puff and σ_y is the lateral dispersion component].

Gradient transport or K theory The eddy diffusivity coefficient K is used to solve the mass conservation equation for the pollutant. The solution can be obtained analytically for some simple cases but must be solved numerically for more general cases. This model is most useful when the size of the cloud is greater than the dominant turbulent length scales.

Gravitational settling velocities Downward velocity of particles due to gravity (about 10 cm/s for an aerosol diameter of about 50 μm and about 100 cm/s for an aerosol diameter of about 200 μm, assuming an aerosol density approximately equal to the density of water, or about 1000 kg/m^3).

Ground-level releases Source emissions from near ground level.

Heavy gas A gas whose density is greater than that of the ambient air. Synonymous with dense gas.

HEGADAS Heavy Gas Dispersion Model

HGSYSTEM Heavy Gas System Model (Witlox and McFarlane, 1985)

HPDM Hybrid Plume Dispersion Model

Internal boundary layer A transition layer rising downwind of a change of surface roughness, which separates the air below, which has

adjusted to the new surface, from the air above, which is still influenced by the old upwind surface. The internal boundary layer has an average slope of about 1/100 to 1/10.

Inversion In the air quality literature, the term inversion refers to a situation when the actual temperature gradient is positive (i.e., the temperature increases with height).

Inversion, capping A type of inversion that occurs aloft, at an elevation of about 1000 m, and marks the top of the layer of air subjected to strong vertical mixing during the day. The height of this layer is often referred to as the *mixing depth,* z_i.

Inversion, ground-based During calm and clear nights, the inversion can be as much as 100 or 200 m deep, causing inhibition of vertical growth of pollutant clouds.

Inversion, synoptic A persistent elevated inversion caused by subsiding air associated with a large-scale weather system such as a stagnant high pressure system.

ISC3 Industrial Source Complex—Version 3 model recommended by the EPA (1995) for many types of industrial sources.

Kit Fox Field experiments at the Nevada Test Site involved ground-level area source releases of CO_2 gas within a large array of roughness obstacles (Hanna and Steinberg 2001 and Hanna and Chang 2001).

Law of the wall Formula describing the profile of mean velocity close to the surface, given by a mathematically derived (using a classical asymptote matching approach) and experimentally confirmed relation. This has two forms depending upon whether the surface is aerodynamically (or hydraulically if you are a civil engineer) smooth or rough.

Light cloud A cloud with density less than that of the ambient air. Synonymous with buoyant cloud.

Local friction velocity, u^*_{local} Friction velocity measured at a local position (height) based on the local wind shear at some height, z, or the local square root of the average of $\langle u'w' \rangle$.

Local thermal circulations Circulation caused by the sun's heating of one side of a street canyon or obstacle, while the other side remains in the shade. The thermal effects would drive local flow circula-

tions since the flow would tend to be upward on the heated side of a street and downward on the shaded side of a street.

LPDM (*Lagrangian Particle Dispersion Model)* A model in which the individual trajectories of thousands of "particles" are tracked by the computer and the particle's motion is determined by a mean flow velocity plus a correlated turbulent velocity and a random turbulent velocity.

Mechanical turbulence Turbulence caused by the wind speed variations and the surface roughness elements, and can be thought of as simple mechanical mixing or stirring of the air.

Mesoscale The distance scales ranging from about 1 to 100 km.

Mesoscale puff models Used for estimating transport and dispersion at distances ranging from a few kilometers to 100 km, intermediate-scale. The pollutant release is modeled as a series of puffs, which are allowed to have curved trajectories to account for space and time variations in meteorology.

Mixing depth, z_i Maximum elevation of mixing in a typical daytime boundary layer.

Monin–Obukhov length, L Accounts for the effects of stability and is proportional to u^{*3} divided by the surface turbulent heat flux, H_s, to or from the ground surface:

$$L = -\frac{u^{*3}/\kappa}{gH_s/c_p\rho T}$$

where $g = 9.8\ \mathrm{m/s^2}$ is the acceleration of gravity, $c_p = 1005\ \mathrm{J\,kg^{-1}K^{-1}}$ is the specific heat of air at constant pressure, and T is the air temperature (in K). The friction velocity, u^*, in this formula is based on the surface stress, τ_o. H_s (in Watts/$\mathrm{m^2}$) is positive during the day and negative at night.

Monin–Obukhov similarity theory Used in many boundary layer and transport and dispersion models to estimate winds, temperatures, and turbulence in the atmospheric boundary layer. This theory states that the mean wind and temperature profiles and turbulent velocities in the boundary layer are completely determined by three scaling lengths (z_o, d, and L) and a scaling velocity (u^*).

NAAQS National Ambient Air Quality Standards

Near-field The area within a few hundred meters downwind of the source where there is possible influence of local structures, source geometry, and initial plume momentum and buoyancy effects.

Neutral cloud The in-cloud density is equal to the ambient density. Neutral cloud and passive cloud are synonymous.

Neutral stability The ambient boundary layer is well-mixed, with Pasquill stability class D, $Ri = 0$, and $1/L = 0$. Usually occurs with high winds and/or small surface heat fluxes.

NRC Nuclear Regulatory Commission

Passive gas A gas whose density is equal to that of the ambient air. Synonymous with neutral.

PHA Process hazards analysis

Plume A cloud of pollutants resulting from a continuous but not necessarily steady release.

Plume rise Rise of plume in elevation above source due to buoyancy or momentum.

Potential temperature θ The temperature that a parcel of air at height z at temperature T would have if it were brought adiabatically to mean sea level. The gradient, $d\theta/dz$, is defined such that it equals the vertical gradient of actual temperature, dT/dz, plus 1 C/100 m. Therefore, in a neutral atmosphere, the vertical gradient of potential temperature is 0.0 C/100 m.

Puff A cloud of pollutants resulting from a nearly instantaneous or short duration release.

Receptor An instrument, person, or hypothetical location where the pollutant concentration is observed or calculated.

Recirculation cavity A volume downwind of an obstacle where the flow recirculates.

Removal by settling, deposition, washout, and chemical reactions Material can be removed from the atmosphere by a variety of processes.

Ri (Richardson Number) Measure of atmospheric stability proportional to the vertical gradient of potential temperature, $\partial\theta/\partial z$, divided by the square of the vertical gradient of wind speed, $\partial u/\partial z$.

Roughness sublayer The lower part of the boundary layer, typically of depth a few H_r, where the flow depends explicitly on the presence of the obstacles, their size, and their geometry.

SCIPUFF Second Order Closure Puff model (Sykes et al., 1998)

Similarity model A model of flow or dispersion where the key variables are scaled by similarity variables such as u^*, L, or z_o. The resulting scaled dimensionless variables may follow "similar" curves and relationships.

Skin friction coefficient $2(u^*/u_{ref})^2$, or the nondimensional local surface shear stress coefficient. The engineering "skin friction coefficient," c_f, is traditionally tabulated in engineering texts. It is sometimes given as a function of surface type and ratio of roughness element height to pipe or boundary layer thickness. Often it is implicitly presented through the classic Moody diagram (Schlichting, 1955) which covers aerodynamically smooth and rough surfaces over a comprehensive range of Reynolds numbers including laminar, transitional, and turbulent flows.

SLAB A dense gas dispersion model based on the slab solutions (Ermak, 1990).

Solidity (ranges from 0 to 1) Measure of lack of porosity of an object. For example, a solid building has a solidity of 1.0, while a pipe rack at a refinery has a solidity of 0.5.

Stability Refers to the ratio of the suppression of turbulence by thermal effects to the generation of turbulence by mechanical effects such as wind shears. Transport and dispersion models characterize the effect of stability through use of one or more dimensionless stability parameters, such as the Richardson number, *Ri*, the Monin–Obukhov length, L, or the Pasquill stability class.

Stability class The Pasquill stability class scheme is based on time of day, wind speed, cloudiness, and sun's intensity. The six stability classes are denoted by the letters A through F, with A being very unstable, D being neutral, and F being very stable.

Street canyons and tunnel entrances Special situations for which models are developed based on empirical analysis of field data, simplified scaling models, or CFD models.

Surface boundary layer Layer of depth 50 to 100 m where the friction velocity u^* can be assumed constant.

Surface heat flux, H_s Turbulent heat flux upward from the surface, measured by fast response turbulence instruments using the identity $H_s = c_p\rho\langle w'T'\rangle$, where w' is the fluctuation in vertical wind

speed and T' is the fluctuation in temperature, and the average is taken over about one hour. A typical value of H_s in the daytime is about 200 w/m^2 (J/sm^2) and at night is about –20 W/m^2.

Surface roughness length, z_o A measure of the amount of mechanical mixing introduced by the surface roughness elements and, as a rough rule of thumb, is equal to about 0.1 times the average height, H_r, of the roughness elements.

Transition region Any region marking the area where one formula is used at smaller values of the independent variable (say, x, or z) and another formula is used at larger values of the independent variable. In this book, transition or interpolation formulas are suggested so the solution varies smoothly across the transition region.

Turbulence intensity The ratio of the turbulent velocity to the mean wind speed (e.g., σ_u/u).

Turbulent dispersion Rate of spread in the vertical (z), lateral (y), or downwind (x) directions of the pollutant cloud about its center of mass due to atmospheric turbulence in the atmosphere.

Turbulent velocities Components of turbulent speed fluctuations. For example, the lateral, longitudinal, and vertical turbulent velocities in the boundary layer are equal to about σ_u (m/s) = $1.9u^*$, σ_v (m/s) = $2.4u^*$, and σ_w (m/s) = $1.25u^*$.

URA Uniform Roughness Array used at the Kit Fox experiments, consisting of rectangular plywood boards with width, W = 0.8 m, and with height, H_r = 0.2 m.

Urban/industrial heat island Because of heat generated by man's activities and by industrial processes, an urban or industrial area is often several degrees warmer than its surroundings. This is called a heat island. The thermal input from home heating or from industrial processes are typically of order 10 to 100 W/m^2, or the same order as the natural boundary layer daytime heat flux, H_s

Vent models A group of specialized models for expressing the concentration on the roof or side of a building resulting from emissions from a short vent on the building.

Very near-field The area very close to the source where the specific geometry of one or two individual obstacles influence the flow and dispersion.

Virtual source method This method is applied when there is a change in dispersion conditions at some point along a plume trajectory due to changes in underlying surface, stability, wind speed, or other effects. In order that the calculated plume dispersion coefficient has no discontinuities, a virtual distance is calculated upwind of the position of interest so that the dispersion coefficient is the same at that point for the upstream conditions and the downstream conditions.

Wet deposition Removal of gas and aerosol pollutants by rain or cloud droplets.

Wind tunnel Used for fluid modeling experiments at small scale.

Index

T

U